CRANFIELD UNIVERSITY

BAPTISTE BONNET

MATCHING OF INTERNAL COMBUSTION ENGINE CHARACTERISTICS FOR CONTINUOUSLY VARIABLE TRANSMISSIONS

SCHOOL OF ENGINEERING

PHD THESIS

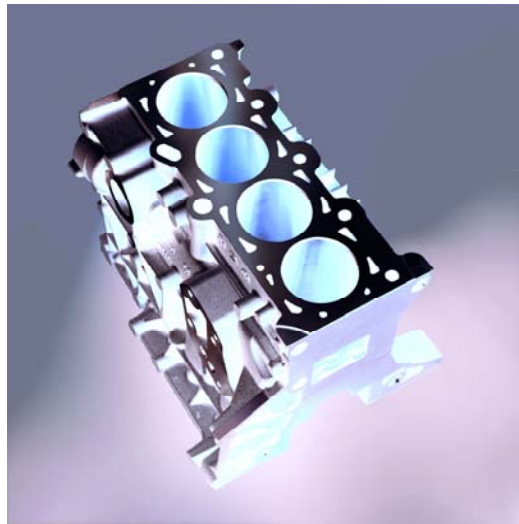CRANFIELD UNIVERSITY

SCHOOL OF ENGINEERING, AUTOMOTIVE DEPARTMENT

PHD THESIS

BAPTISTE BONNET

MATCHING OF INTERNAL COMBUSTION ENGINE CHARACTERISTICS FOR CONTINUOUSLY VARIABLE TRANSMISSIONS

SUPERVISOR: PROF. NICHOLAS VAUGHAN

2007

This thesis is submitted in partial fulfilment of the requirements
for the Degree of Doctor in Philosophy.

ABSTRACT

This work proposes to match the engine characteristics to the requirements of the Continuously Variable Transmission [CVT] powertrain. The normal process is to pair the transmission to the engine and modify its calibration without considering the full potential to modify the engine. On the one hand continuously variable transmissions offer the possibility to operate the engine closer to its best efficiency. They benefit from the high versatility of the effective speed ratio between the wheel and the engine to match a driver requested power. On the other hand, this concept demands slightly different qualities from the gasoline or diesel engine. For instance, a torque margin is necessary in most cases to allow for engine speed controllability and transients often involve speed and torque together. The necessity for an appropriate engine matching approach to the CVT powertrain is justified in this thesis and supported by a survey of the current engineering trends with particular emphasis on CVT prospects. The trends towards a more integrated powertrain control system are highlighted, as well as the requirements on the engine behaviour itself.

Two separate research axes are taken to investigate low Brake Specific Fuel Consumption [BSFC] in the low speed region and torque transient respectively for a large V8 gasoline engine and a turbocharged diesel V6 engine. This work is based on suitable simulation environments established for both engines in the powertrain. The modelling exercises are aimed at supplying appropriate models that can be validated against experimental data. The simulation platforms developed then allow the investigation of CVT powertrain biased engine characteristics.

The V8 engine model in particular benefited from engine and vehicle dynamometer data to validate the model behaviour and the accuracy of the prediction. It

benefited from the parallel work conducted on the Electrically Assisted Infinitely Variable Transmission [EASIVT] project in Cranfield University. The EASIVT vehicle is a parallel mild hybrid aimed at demonstrating the combined fuel economy benefits of a CVT technology and hybridisation. From the CVT powertrain requirements for fuel economy, BSFC operation can be further promoted in the low speed region if Noise Vibration and Harshness [NVH] counter-measures are developed. A study of the combustion torque oscillations at the crankshaft led to the elaboration of an Active Vibration Control [AVC] strategy for the hybrid Integrated Motor Generator [IMG]. Successful implementation of the strategy in both simulation and in-vehicle helped quantify the benefits and short comings of engine operation for best fuel economy. The development in parallel of the hybrid control functions for torque assist and regenerative braking made it possible to implement the low speed AVC in the vehicle without a driveability penalty.

The V6 TDI model yielded a realistic and representative simulation for the transient torque response improvement research to be undertaken. For that purpose, the model was tuned against full-load data and the air path control sub-systems were designed and calibrated similarly to a real application. The model was able to highlight the turbocharger lag issue associated with a large combined speed and torque transient inevitable in the fuel economy biased CVT powertrain. This study proposes a Manifold Air Injection [MAI] system in the intake of the engine to help breathing when the VGT operating conditions cannot be shifted rapidly enough for a manoeuvre. The system design constraints were analysed and a suitable strategy was elaborated and calibrated. A sensitivity analysis was also conducted to demonstrate the influence of the MAI design and control variables on the engine performance in the CVT powertrain

In conclusion, the benefits of the engine characteristic matching were highlighted in both cases. A review of the work achieved is available in the last chapter, including prospects for further improvements and investigations. The ideal engine characteristics for gasoline and diesel engine technologies integrated in a CVT powertrain are derived from the experience gathered in the research and the results obtained from the tests in low speed operation and transient torque control respectively

for the gasoline and the diesel engines. The engine characteristics can be altered toward a better match with a CVT by the use of specific hardware and control strategy.

This work recommends that a direct injected, variable valve actuated gasoline engine provides the ideal starting point for low fuel consumption powertrain. When integrated within a mild hybrid CVT powertrain, the full benefits are obtained with the use of low speed operation and AVC. If no electrical machine is available to torque assist the engine, then existing supercharging concepts for a downsized engine can be applied.

Diesel engines can also be downsized because of their high torque density. Increased turbocharging boost levels allow steady state torque levels to be maintained in the downsizing process. The CVT powertrain can optimise the fuel consumption and emission levels by appropriate selection of the engine steady state operating points. The torque response lag then becomes critical for the CVT to control the engine speed. This can be improved by the use of Manifold air Injection to assist the turbocharger.

TABLE OF CONTENTS

NOTATION

Acronyms

AFR	Air Fuel Ratio [lambda]
AMT	Automated Manual Transmission
APID	Adaptive Proportional Integrator Derivative
AVC	Active Vibration Control
BAS	Belt Alternator Starter
BSFC	Brake Specific Fuel Consumption
CA	Crank Angle
CAN	Common Area Network
CCP	CAN Calibration Protocol
CO	Carbon Monoxide
CPEMS	Cylinder Pressure Based Engine Management System
CR	Compression Ratio
CVT	Continuously Variable Transmission
DegCA	Degrees Crank Angle
DSP	Digital Signal Processing
EASIVT	Electrically Assisted Infinitely Variable Transmission
EBD	Electrical Boosting Device
ECT	Engine Coolant Temperature
ECU	Engine Control Unit
EGR	Exhaust Gas Recirculation
EMAP	Exhaust Manifold Absolute Pressure
EMS	Engine Management System
ESP	Electronic Stability Program
ETB	Electronic Throttle Body
ETC	Electronic Throttle Control
EVC	Exhaust Valve Opening
FE	Fuel Economy
HC	Hydro-Carbons
HCCI	Homogeneous Charge Combustion Ignition

HCU	Hydraulic Control Unit
HSDI	High Speed Direct Injection
IAT	Intake Air Temperature
IC	Internal Combustion
ICE	Internal Combustion Engine
IMAP	Intake Manifold Absolute Pressure
IMG	Integrated Motor Generator
IOL	Ideal Operating Line
ISAD	Integrated Starter Alternator Device
ISG	Integrated Starter Generator
IVC	Inlet Valve Closure
IVT	Infinitely Variable Transmission
LSHT	Low Speed High Torque
LUT	Look-Up Table
MAF	Mass Air Flow
MAI	Manifold Air Injection
MAP	Manifold Absolute Pressure
MBT	Maximum for Best Torque
NOx	Nitrogen Oxides
NVH	Noise Vibration and Harshness
PE	Power Electronics
PI	Proportional Integrator
PID	Proportional Integrator Derivative
PM	Particulate Matter [soot]
PMEP	Pumping Mean Effective Pressure
RadCA	Radians Crank Angle
ROFI	Rate Of Fuel Increase
ROHR	Rate Of Heat Release
SFC	Specific Fuel Consumption
SITO	Single Input Two Outputs
SOC	State Of Charge
SPL	Sound Power Level
TDC	Top Dead Centre
TITO	Two Inputs Two Outputs
TRD	Transmission Ratio Derivative
VGT	Variable Geometry Turbocharger
VNT	Variable Nozzle Turbine
VTES	Visteon Torque Enhancement System
VVA	Variable Valve Actuation

WOT	Wide-Open Throttle	
ZEV	Zero Emissions Vehicle	

Variables

A	Residual burned gas heat release coefficient	n/a
AccImg	IMG acceleration	rad/s²
$A_{FFT}x1$	Engine side vibration level FFT	g
$A_{FFT}x2$	Body side vibration level FFT	g
AMAP	Accumulator Manifold Absolute Pressure	mbar
EMAP	Exhaust Manifold Absolute Pressure	mbar
F_{aero}	Aerodynamic drag force on vehicle	N
FMEP	Friction Mean Effective Pressure	bar
IAT	Intake Air Temperature	K
Ibat	Battery current	A
IImg	Equivalent DC model current to IMG	A
IMAP	Intake Manifold Absolute Pressure	mbar
IMAP_req	Target IMAP	mbar
Inj1Dur	Fuel injection No. 1 duration	s
Inj1Dur_req	Required fuel injection No. 1 duration	s
Inj1SOI	Start of injection No. 1	degCA bef. TDC
InjDur	Fuel injection duration	s
InjMass	Fuel mass injected per hub	mg
InjMass_req	Required fuel mass to inject per hub	mg
InjSOI	Start of injection	degCA bef. TDC
k	Combustion chamber gas kinetic energy	J
K_D	APID derivative coefficient	Nm/(rad/s²))
K_I	APID integrator coefficient	Nm/rad
K_P	APID proportional coefficient	Nm/(rad/s))
MAF_eng	Estimated cycle air charge	g/s
MAF_error	VGT compressor mass air flow error	g/s
MAF_man	Derivative of air mass in manifold	g/s
MAF_req	Target engine fresh air charge	g/s
MAF_thr	Throttle mass air flow	g/s
m_f	Mass of fuel in combustion chamber	g
MFF_des	Desired equivalent injection mass fuel flow	g/s
PhaseAct	4th order AVC sinewave phase [φ]	degCA bef. TDC
Phi	Fuel to air ratio	n/a
PosEGR	EGR valve opening	%
PosImg	IMG position [high resolution]	degCA
PosMAI	MAI valve opening	%
PosPedal	Driver accelerator pedal position	%

PosRack	VGT actuator position	%
PosThr	Throttle position	%
PwrDriverReq	Equivalent driver power request	kW
Q$_{comb}$	Heat released by combustion	J
RatControl	Required CVT ratio	n/a
SpdDyn	Dynamometer speed	rev/min
SpdEng	Engine speed	rev/min
SpdEngNVH	Minimum engine speed for NVH	rev/min
SpdError	Engine speed error	rev/min
SpdImg	IMG speed	rev/min
SpdVeh	Vehicle speed	km/h
SpdWhl	Driving wheel speed	rev/min
SpkAdv	Spark advance	degCA bef. TDC
T$_{gas}$	Local gas temperature	K
TrqAct	4th order AVC sinewave amplitude [A]	Nm
TrqDyn_req	Requested dynamometer torque	Nm
TrqEng	Engine torque	Nm
TrqEngDriverReq	Equivalent driver requested engine torque	Nm
TrqEngEst	Estimated engine torque	Nm
TrqEngSFC	BSFC IOL engine torque	Nm
TrqImg	IMG output torque	Nm
TrqImg_AVC	AVC 4th order sinewave torque	Nm
TrqImgMax	Maximum IMG torque request	Nm
TrqImgMin	Minimum IMG torque request	Nm
TrqImgReq	Requested IMG torque	Nm
TrqWhl	Driving wheel torque	Nm
TrqWhlReq	Driver requested wheel torque	Nm
VoltsBat	Battery voltage	V
VoltsImg	Equivalent DC model IMG voltage	V
WeightDriver	Driver set-point weight	n/a
WeightSFC	BSFC set-point weight	n/a
X	Mass fraction of liquid fuel	n/a
X$_{BGR}$	Fraction of burned gas before combustion	n/a
Y$_{D}$	Derivative signal	rad/s²
Y$_{I}$	Integrator signal	rad
Y$_{P}$	Proportional signal	rad/s

Constants

AVC_PHASE	Calibrated AVC phase [2D LUT]	degCA bef. TDC
AVC_SPLIT	Calibrated split ratio between AVC_TRQ_ENGVIB & AVC_TRQ_BODYVIB	n/a
AVC_TRQ_BODYVIB	Calibrated AVC amplitude for body vibration [2D LUT]	Nm
AVC_TRQ_ENGVIB	Calibrated AVC amplitude for engine vibration [2D LUT]	Nm
AVC_TRQ_FINAL	Calibrated AVC final amplitude [2D LUT]	Nm
C_{diss}	Kinetic energy dissipation factor	Hz
C_{mode}	Heat release coefficient	kJ/(kg.K)
C_{rate}	Heat release coefficient	s
C_{turb}	Turbulent kinetic energy coefficient	n/a
ENG_MAI_GAIN	Calibrated MAI closed-loop proportional control gain	%/(g/s)
ENG_MAI_IMAP_THLD	Calibrated threshold value on IMAP error to trigger MAI	mbar
ENG_MAI_TC1	Calibrated digital filter 1 time constant [T_{c1}]	s
ENG_MAI_TC1	Calibrated digital filter 2 time constant [T_{c2}]	s
ENG_STOICH_AFR	Stoichiometric AFR	n/a
InjMFR	Rated injector mass flow rate	Kg/s
R	Perfect Gas Constant	J/(kg.K)
TRQ_IMG_MAX	Maximum IMG torque	Nm
TRQ_IMG_MIN	Minimum IMG torque	Nm
Tumble_fact	Tumble value coefficient	n/a
V_{man}	Intake manifold volume	m³
α	Weighting factor for APID error function	n/a
α_R	Residual burned gas effect on heat release	n/a
β	Frechet approximation for APID	Nm/(rev/min)
τ	Liquid fuel evaporation time constant	s

Chapter 1: INTRODUCTION

1.1 Background

Automobiles have long been the most popular method of personal transportation. Although it is a relatively recent invention, improvements are continually carried out on the original concepts. They were first driven by cost reduction and the necessity to let a larger part of potential customers gain access to car purchase. As customer expectation rose, vehicle refinement has become an issue, with a continuing cost reduction effort. The various petroleum crises led some car manufacturers to consider fuel consumption as one of the important features in order to sell cars. More recently, the demand for environmentally friendly vehicles has raised and legislation is becoming tougher in order to force the automotive industry to provide the market with low emission vehicles.

The architecture of modern cars tends to offer multiple options in order to improve fuel efficiency and emissions. The engine is the obvious part to focus on, but recent emission and fuel consumption priorities do not necessarily converge towards the same solutions. Major improvements of the mechanical efficiencies within the engine are limited by the requirements for mass production cost targets. The combustion process does offer another way to improve the fuel efficiency. In the last decade the diesel engine fuel consumption advantage resulted in larger sales [1] and became a real alternative to gasoline engines. This was achieved with major technology development toward more refinement for customers and cheaper costs for manufacturer.

It is worth noting that fuel consumption is strongly influenced by the vehicle mass and both rolling resistance and aerodynamic drag to a lesser extent because of the low speed nature of most legal drive cycles. Aerodynamics plays a leading part in the overall energy losses at cruise speed. However, it is mostly influenced by style and design as well as functional requirements like doors, cabin layout. Rolling resistance is particularly dealt with by tyre manufacturers which recently developed materials and construction patterns that improve the rolling resistance without compromising the cornering abilities.

Increasing weight has compromised the fuel consumption of the modern vehicle bringing equipment like climate control, electric seats, electronic stability control, satellite navigation, and on board entertainment over a large part of the automotive market. Customer expectations in terms of passenger room also rose at the same time as crashworthiness standards were improved by the generalisation of very demanding tests.

The policy seems to rely more on a controlled increase rather than a significant but costly weight reduction.

The remaining parameter influencing the fuel efficiency of road vehicles is the transmission. The integration of this aspect within the powertrain optimisation process has been investigated in the present thesis. The most common transmission layout in Europe is the manual gearbox [2] or Manual Transmission [MT], consisting in the driver selected discrete ratios. The Automatic Transmission [AT] is common place in the North American and Japanese markets, although it is understood as less efficient from a mechanical power transmission point of view. Indeed manual transmissions generally have a peak efficiency of 95% whereas the current best automatics are stuck at 86 % mainly because of the torque converter losses [3].

Recent continuously variable transmissions proved efficiencies between automatics and manuals. Furthermore, they allow the engine to be constantly used at its best Brake Specific Fuel Consumption [BSFC] where a manual or an automatic transmission will be able to provide only a limited number of gear ratio [up to seven]. Hence the overall efficiency of the powertrain and transmission can be improved over a driving cycle. The strategy behind the CVT controller can therefore allow significant fuel consumption improvements of up to 22% [4].
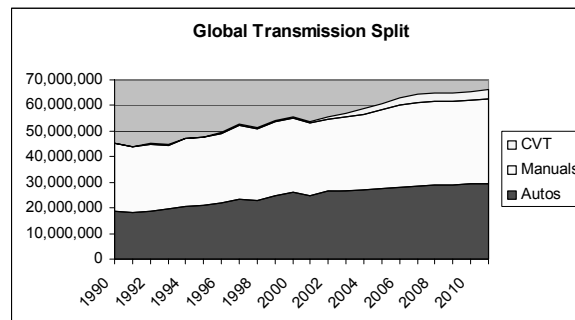
Figure 1.1 – Worldwide vehicle transmissions split. Projected sales for CVT transmissions in 2004 are 2 millions units to compare to 1.4 millions in the year 2003. [Source Torotrak PLC]

The significant but not always realised fuel economy gains of CVT have not however been followed by an equally important growth in the market shares [Figure 1.1]. Unlike AT's vs. MT's, current CVT do not represent a significant share in the markets [2], particularly in North America where automatics offer a similar driving feel but without the fuel efficiency. The CVT penetration in Japan is better, with 15 to 20% of the market. Considering the ever increasing fuel prices worldwide, the CVT advantage should justify the manufacturer's costs involved in bringing a new type of transmission in the market. Marketing considerations aside, there are a number for reasons to this slow growth. Most of them lay on the fact that customers are not prepared to sacrifice their market specific driving styles. Hence CVT vehicles still have to match rather different driveability expectations. These are addressed by compromising the best fuel economy operation of the powertrain as developed in Section 1.2 and 1.3 below.

1.2 Principles of CVT Operation

Continuously variable transmissions feature a radically different approach to power transmission compared with well-established manual and automatic gearboxes. They rely on the possibility to adjust the speed ratio across the powertrain to any value within the ratio span. This very much affects the need for the powertrain controller to select the most appropriate gear ratio depending mostly on the driver's pedal input and the vehicle speed. The second chapter of this thesis provides an insight into the design of the CVT hardware. As for now, the continuously variable transmission can be considered as a simple variator hence allowing the operation of the engine within a large speed range at any given vehicle speed.

1.2.1 Control Strategies

The engine in the CVT powertrain is operated at a speed and torque formulated by the transmission controller. This changes the established concept of a driver to engine interaction where the transmission is a relatively passive component. With a CVT, the engine and transmission have to be controlled in an integrated way.

There are a number of CVT technologies available. The Infinitely Variable Transmission [IVT] is a type of CVT that allows an infinite gear ratio between the engine and the wheel, i.e. engine running and vehicle stopped. Further information about these can be found about these in Appendix A. Some CVT's are speed ratio controlled, some are torque controlled. The latter differs from the former only in the fact that the low level control strategy acts on the torque transmitted by the CVT rather than its effective ratio. This does not change the higher level strategy which operates the engine independently of the wheel speed.

The CVT also offers the possibility to be operated like a fixed ratio gearbox if this is a requirement. The control software would purposely hold a constant speed ratio through the transmission to suit the driver's demand of a familiar feel. However, a manual automated gearbox [sequential, dual shaft] complies with this sort of requirement much better and the point of a CVT resides more in its considerable fuel saving potential and driveability qualities for smooth driving. Indeed driveability and fuel economy is a trade-off which the CVT transmission makes possible to solve. These two objectives are discussed in Section 1.2.1.1 and 1.2.1.2.

1.2.1.1 Fuel Saving Principles

If an internal combustion engine is to be considered like a mere power production plant, then like any other power source it has operating conditions where its efficiency is best, i.e. with minimum fuel consumption. However these properties are not used at their full potential with fixed ratio transmissions and adequate operation of the engine is left to the driver's appreciation.

With a CVT the control algorithm decides which engine operating condition of speed and torque is the best match to the request from the driver in steady state and transient manoeuvre. The desired ratio is then achieved as described in Chapter 2 by accurate control of the transmission hydraulic actuation pressure. The scope of possible

powertrain behaviour and driving feel is entirely dependant on the control strategy and subsequent calibration. The ideal compromise therefore lies between the fuel efficiency priority and the driveability of the vehicle.

Some CVT behaviours however keep close to conventional fixed ratio transmissions and aim at providing a controlled speed ratio between engine and vehicle. A straight forward speed ratio controlled CVT is described in [5]. The GM VT25-E belt CVT utilizes a torque converter and is closed-loop ratio controlled such as to minimize fuel consumption while maintaining quick response under transients. To achieve this, a slightly higher than necessary variator pressure is maintained in some cases so that sudden torque rise through the transmission does not have to be hydraulically compensated for. An alternative study on ratio control by Lee *et al.* [6] demonstrates the benefits of control algorithms on this hydraulic pressure. He maximises the efficiency of the transmission by keeping the pressure as low as possible.

Murray [7] describes a method to work out appropriate steady-state operating points of the Torotrak Infinitely Variable Transmission [IVT][Chapter 2]. An Ideal Operating Line [IOL] was established for fuel economy and another one for driver performance requests. The final speed / torque set point is then calculated using weighting functions based on the present accelerator pedal position. For a given engine power request there could be one [or two] ideal operating point where the BSFC [g/kWh] is minimal. Figure 1.2 shows the engine map featuring the trace curves of engine power and BSFC. Then for each engine power request, an ideal SFC operating line can be worked out. This is also called the optimum operating line.
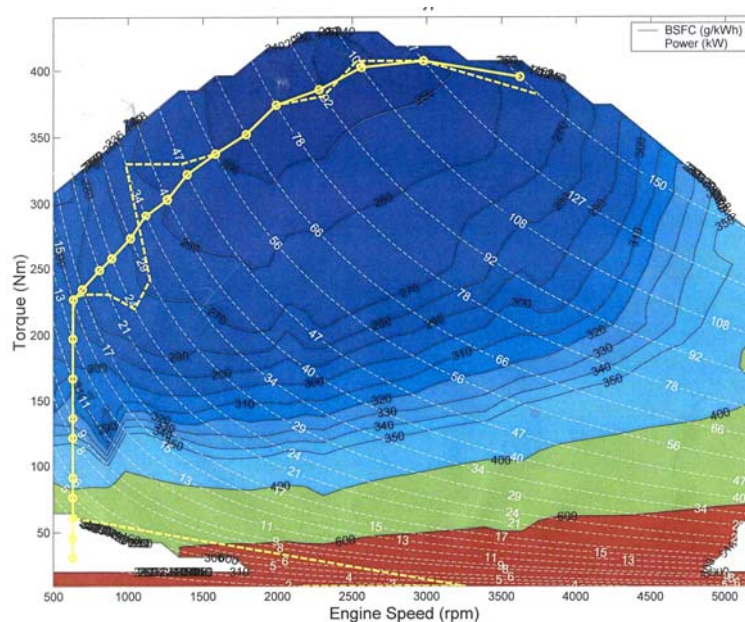
Figure 1.2 – Ford V8 5.4L Triton BSFC Map & Control Line. In a Torque over speed reference frame, lines of constant power are superimposed on iso BSFC curves resulting in an extensive map of the engine. An operating line was also drawn to complete the example. [Source Torotrak Plc]

Lee *et al.* [8] highlight an interesting feature to be taken into account during CVT controller design which is the powertrain response lag. This is due to throttle response, engine torque dynamics, and CVT shift dynamics. In the CVT speed ratio control, the desired ratio is determined from the engine optimal operating point and the current vehicle speed. Then ideally the ratio control effectively moves the engine operating point along the IOL for best fuel consumption. In reality powertrain response lags imply a systematic deviation from the line.

As a consequence, the desired ratio during a vehicle speed transient is calculated from the vehicle speed and accounts for the powertrain response lag. This causes a transmission speed ratio overshoot and subsequent engine speed rise. Repeatedly the fuel consumption is affected and the driver feels the pedal as very sensitive which compromises driveability. These concerns are addressed in [8] with a control strategy which evaluates the vehicle velocity *after* the powertrain lag and modifies the optimal transmission ratio to a desired ratio [Figure 1.3].
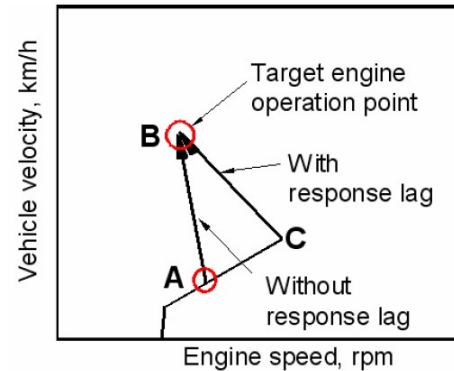
Figure 1.3 – Effect of response lag on engine performance [8]. The engine speed overshoot during transient is created by an instantaneously inappropriate transmission ratio.

1.2.1.2 Driveability Issues

As previously mentioned, driveability standards have always been set by conventional manuals and advanced automatics. The potential for driveability improvement is significant with CVT altogether with fuel economy benefits but most drivers will be not be ready to reconsider their long established driving habit and style.
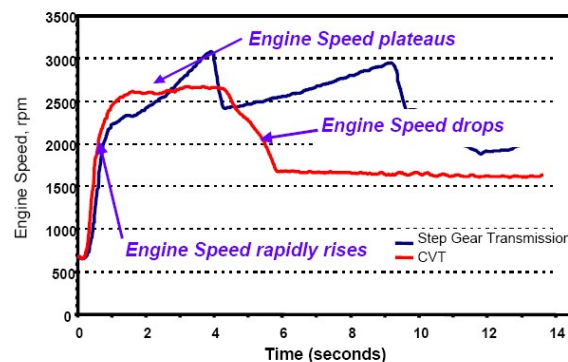
Figure 1.4 – Engine speed "motor-boat feel" profile during transient [5]. As the driver depresses the accelerator pedal the engine speed quickly rises to match torque demand and then is maintained constant during the tip in manoeuvre. The lack of motoring torque during engine acceleration followed by a constant thrust feel is similar to the propeller effect in a motor boat.

One of the most undesirable features CVT controllers are designed to avoid is the motor boat feel as shown in Figure 1.4. This happens when an excessive "on-demand power" control strategy is implemented to keep the fuel consumption low by maintaining engine revs as low as possible under partial pedal inputs. The direct drawback is that higher engine speeds are required each time the pedal position increases, causing a delay in vehicle response. The GM powertrain engineers [5] got around the problem using fuzzy logic to determine driver intention during transients.

Consequently there is a lot of work carried out by powertrain, Noise Vibration & Harshness [NVH] and road test engineers in order to develop pieces of control software that combine the driveability and fuel economy strategies rather than dissociate them. The difficulty is taken even further by the controversial subjectivity of driveability qualities. A rather extensive study has been achieved by Deacon [9] and Wicke [10] in order to match subjective assessment with repeatable, objective tests. Similar approach was adopted by Dorey and Martin [11] from Ricardo. Their respective studies demonstrate how a set of key benchmark tests can reflect the subjective feedback from a number of test drivers.

However each car manufacturer had grown an established idea of what their customers are expecting for longitudinal response and feel to pedal inputs. The "character" components has therefore to be taken into account to match customers requirements and one same transmission hardware can be controller and calibrated so it provides very different responses but keeps fuel efficiency and performance similar.

Jantos [12] presents the relationship between the Transmission Ratio Derivative [TRD] and the drive properties. His work indeed highlights the fact that CVT introduce this additional degree of freedom which never exists with competing automatics and manuals. The relationship between the transmission ratio derivative ψ and driving power P_d available at the wheel is derived from moment equilibriums in the driveline using simplified road load torque expression.

$$P_d = \omega_1 \cdot \frac{T_e - J_1 \cdot \omega_1 \frac{\psi}{i} + \frac{J_1 \cdot r_d \cdot i}{J_2}\left[c_1 + c_2\left(\frac{\omega_1}{i} \cdot r_d\right)^2\right]}{\frac{J_1}{J_2}i^2 + 1}$$

Equation 1.1 – r_d is the tyre rolling radius, c_1 and c_2 are road load coefficients. Other notations are presented in Figure 1.5.
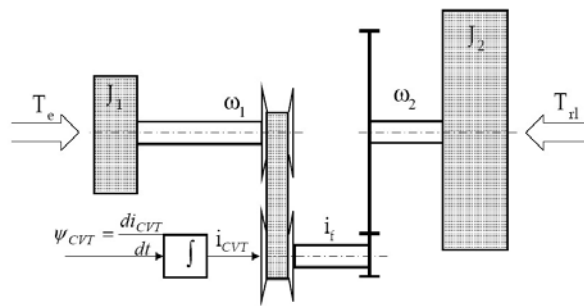
Figure 1.5 – Physical model of the car powertrain with CVT [12]. This is a simplified inertia model of the entire vehicle powertrain from engine to road. J_1 is the engine and transmission input shaft equivalent inertia. J_2 is the equivalent driveshaft, wheels and vehicle inertia.

From this parameterized equation, Jantos explains how the TRD influences the longitudinal dynamics using iso-parametric characteristics as shown in Figure 1.6. Indeed under transient condition resulting from an increase of the accelerator pedal deflection, an inappropriate control of the transmission ratio would result in a decrease of vehicle speed which is totally unacceptable. Therefore a maximum transmission ratio derivative map was established using numerical simulation [Figure 1.6]. Jantos also further demonstrates the importance of a TRD control strategy by detailing that P_d not only depends on the torque produced by the engine but also on the key ψ values.
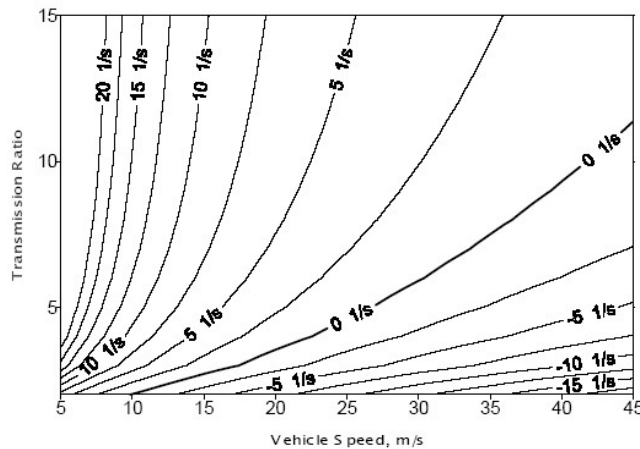
Figure 1.6 – Maximum transmission ratio derivative [12] was computed to cancel out any vehicle speed decrease when the accelerator pedal position increases. Negative values can be observed in the high speed region when an excessive downshift would mean all the extra available torque should be used up to accelerate the different rotating parts.

In order not to compromise driveability with fuel efficiency Murray [7] presented a way of designing a CVT controller that is easy to calibrate. The relative importance of SFC, performance and emissions is weighted and depends on the driver input mainly. This indeed is part of a transmission controller design far different from most of the others. The Torotrak IVT is torque controlled as opposed to speed ratio controlled meaning that demand is on a highly integrated powertrain control together with the transmission control.

The variator described in Section 2.1 of the next chapter reacts to an input torque and the speed ratio is set by subsequently by the torque balance with the engine. As a direct consequence any controller decision to modify the reaction torque in the variator in order to increase the wheel torque has to be accompanied by an identical change of engine output torque. If this condition was not to be fulfilled then very undesirable rev dropping such as described by Jantos [12] would occur under accelerator pedal deflection. Hence a significant amount of work [13] [14] had to be carried out in order to make the two systems work in a synchronised manner. Functionality such as hill climb / descent control [TORC®] or geared neutral [4] are exclusivity to this kind of transmission.

This sort of transmission and associated control method described in Chapter 2 set an increased demand to more controllable IC engines. The effects of the control structure on the powertrain performance are explored by Liu *et al.* [15] who showed that too much emphasis laid on electronic throttle control to maintain low levels of fuel consumption [on the IOL] inevitably lead to poor wheel speed response, i.e. poor longitudinal performance response. Therefore the Single Input Two Output [SITO] architecture is best replaced by a Two Input Two Output [TITO] architecture where both throttle and transmission ratio derivative [12] are the controlled variables.
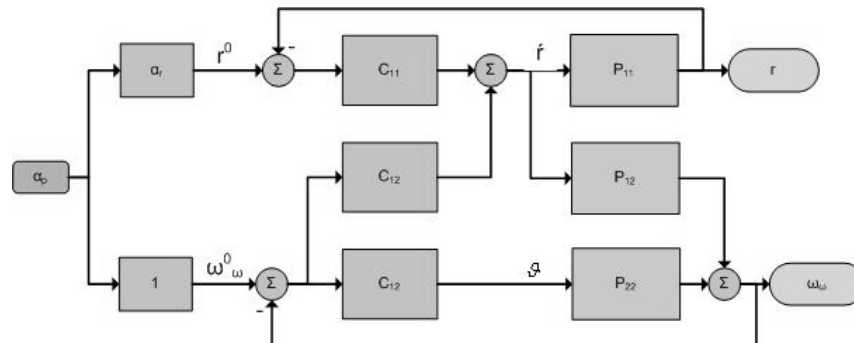
Figure 1.7 – Reduced multivariable controller with TITO system [15].

Where α_p is the scaled driver pedal position; r is the transmission speed ratio; ω_w is the wheel speed; ϑ is the throttle command.

The multivariable control architecture shown in Figure 1.7 allows the phase of the wheel speed response to be largely improved, i.e. no undershoot as explained by Jantos [12] without slowing down the speed ratio controller.

Finally it is clear that satisfactory driveability performance with CVT can be achieved by adequate control provided that the engine can the used as an actuator in the same way as the toroidal variator is for example. This is the reason why CVT transmissions did not break through in the automotive market until the appearance of powerful control units in vehicle during the 1990. The pressure is now also on the powertrain engineer to provide flexible, cost effective solutions to integrate the powertrain and the transmission.

1.2.2 Limitations & Challenges

The compromise to be obtained between fuel economy, emission levels and vehicle driveability is a known challenge which already exists with automatic and Automated Manual Transmission [AMT] during the calibration of the shift strategy. Crewe *et al.* [16] demonstrate the benefits of a holistic approach for the optimisation of the hybrid powertrain. Calibrating engine, automated manual transmission and hybrid electrical machine all together shows clear advantages by reducing the iterative process of a separate calibration stage for each component, and it also provides opportunities to reach a much more optimised solution. CVTs rarely operate in fixed ratio strategy thus they present a more complicated task to reach an optimised engine – transmission match.

In most cases, CVT's are paired with existing engines which will carry over their calibration for evident cost benefits. Thus before any calibration work has started with the CVT, the final result is already compromised by the inadequacy of the engine within its operating envelope. The CVT operation is so far removed from fixed step AT and AMT that specific requirements must be set on the engine operation. As established previously, CVT true fuel economy benefits are obtained by optimised steady state operation in regions where conventional powertrains rarely venture. For most drive cycles, the low power requirements mean an untypical Low Speed High Torque [LSHT] region of engine operation which poses two major problems developed in 1.2.2.1 and 1.2.2.2:

- Engine operating envelope limits

- Torque margin and response lag

1.2.2.1 Engine Operating Envelope

Standard engine calibrations are biased toward manual transmission operation in order to yield good emissions levels in the part load operation. For example these objectives are achieved with use of Exhaust Gas Recirculation [EGR], or Rate of Heat Release [ROHR] control in the case of diesel engines. Engine warm-up phases are of the upper most importance in drive cycles involving cold start, leading to calibrations of spark-advance, injection timing or fuel mixture which promote exhaust after-treatment in cold conditions. Brace *et al.* [17] demonstrate how IOL strategies can improve on both of these aspects during CVT steady-state or quasi steady state conditions. He therefore shifts the engine operating envelope where better fuel economy and emission levels can be obtained.

Figure 1.8 shows a set of IOL computed from engine data for a 1.0l gasoline engine. Each IOL will optimise a particular parameter, e.g. fuel consumption, CO, HC or NOx emissions during steady state operation as in Murray [7]. However, operating the engine low in the speed range at higher torque levels can become problematic. Firstly, because the engine operating condition is closer to the boundaries of the performance envelope, the torque margin necessary to change the engine speed and provide wheel torque response during tip-ins is smaller. This affects the steady state

operation as discussed in the next chapter. Secondly, high overdrive ratio can be detrimental to the driver comfort. NVH issues arise when combustion torque fluctuations at low frequency are transmitted to the vehicle body through the engine mounts. Effectively, the LSHT region will be perceived as under revving because the firing frequency vibrations and noise are normally not present in the cabin at these low engine speeds.
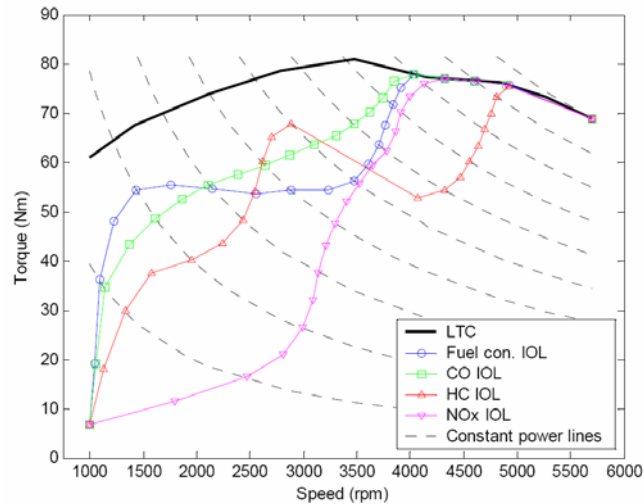
Figure 1.8 – IOLs for various emission optimisation aspects [17] for a 1.0l Geo SI engine with equivalent engine power curves

When IOLs overlap with regions of bad NVH, a compromise has to be reached by moving away from the IOL in order to provide a smooth running feel of the engine. The holistic approach suggested for a hybrid vehicle by Crewe *et al.* [16] helps prevent large operating incompatibilities between the transmission and the engine. In this particular case, the performance envelope for transmission, electrical machine and engine are defined simultaneously. By identifying the key factors early on, design parameters such as gear ratios, electrical machine rating or engine calibration variables such as injection timing or boost pressure can be optimised for best fuel economy whilst keeping NOx emissions below the legislative limit. A similar approach could be adopted with the inclusion of NVH aspects in the study. By measuring the levels of engine-born vibrations and the subsequent energy cost of NVH reduction, the engine operating envelope can be altered for the benefit of the powertrain overall fuel economy. This is undertaken in this thesis in the case of the EASIVT hybrid vehicle control strategy discussed in Chapter 5.

1.2.2.2 Torque Margin and Response Lag

The previous section explains how the optimisation of the steady state operation is part of the CVT powertrain integration challenge. Transient operation is another part that is closely related to the disadvantages IOL operation.

Most IOLs shift the engine operation in the LSHT region where little torque margin is left in order to respond to transient demands. The torque margin is indeed the only available way to change the engine speed without reducing the wheel torque. On top of that, the LSHT is characterised by relatively long response time to torque commands, due to throttle actuation, fuelling and principally manifold dynamics delays. Figure 1.9 shows an example of the time constant used by a CVT controller to model the manifold filling and emptying effects with a first order lag.
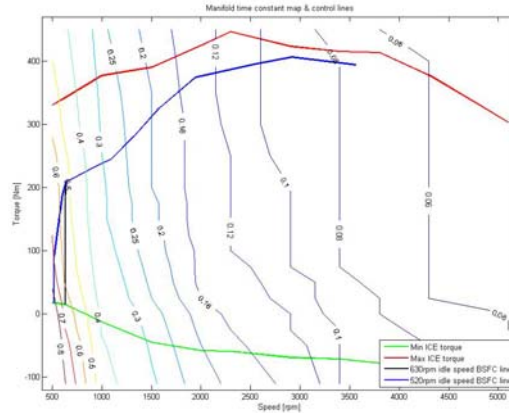
Figure 1.9 – Manifold time constant for a Ford V8 5.4L Triton [19] with best BSFC control lines for 520 [black] and 630 rev/min [blue] idle speeds. The manifold time constant increases with lowering speeds to reach 0.8s at idle.

Vaughan *et al.* [18] suggest the use of torque dilution to shift the best BSFC and best NOx regions of the engine map down to lower torque values for a small gasoline engine as shown in Figure 1.10 and Figure 1.11. This technique provides an increased torque margin and both external EGR and lean operation offer quicker response time than conventional throttling.
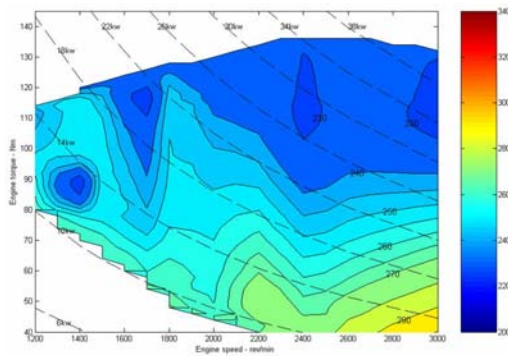
Figure 1.10 – Standard Stoichiometric BSFC map [18] for a Ford Zetec SE 1.7l engine, i.e. without the use of torque dilution techniques
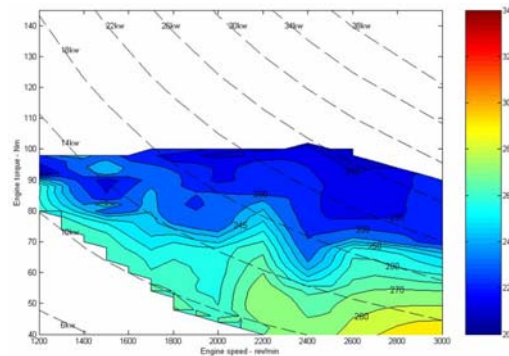
Figure 1.11 – Combined lean mixture and EGR dilution BSFC map [18] for same engine as Figure 1.10, showing lower torque at similar BSFC

A CVT specific engine operating envelope similar to Vaughan [18] often can not be achieved with a simple alteration of the engine calibration. Effectively it is the steady state strategy which is modified from the IOL to ensure adequate acceleration feel. This prevents full use of the CVT powertrain potential for fuel economy and emission levels.

1.2.2.3 Closing Comments

The considerations in the previous paragraphs suggest the necessity to establish the desirable engine features for a CVT early on in the powertrain integration process. An adequately matched vehicle – CVT – engine system will offer a superior compromise of driveability, fuel consumption and emission.

Figure 1.12 summarises on top of the engine map the various aspects of CVT powertrain operation discussed previously; the torque margin area is delimited by the WOT torque, the maximum power, the IOL [only the BSFC is represented here] and the NVH curves. These boundaries are those within which the CVT operation strategy must find an optimised calibration. The term engine characteristics therefore encompasses the afore mentioned boundaries or limiting factors, as well as the BSFC, HC, CO, NOx, or Particle Matter [PM] specifics within the engine map. The following section will explain how a number of these engine characteristics can be optimised specifically for CVT operation.
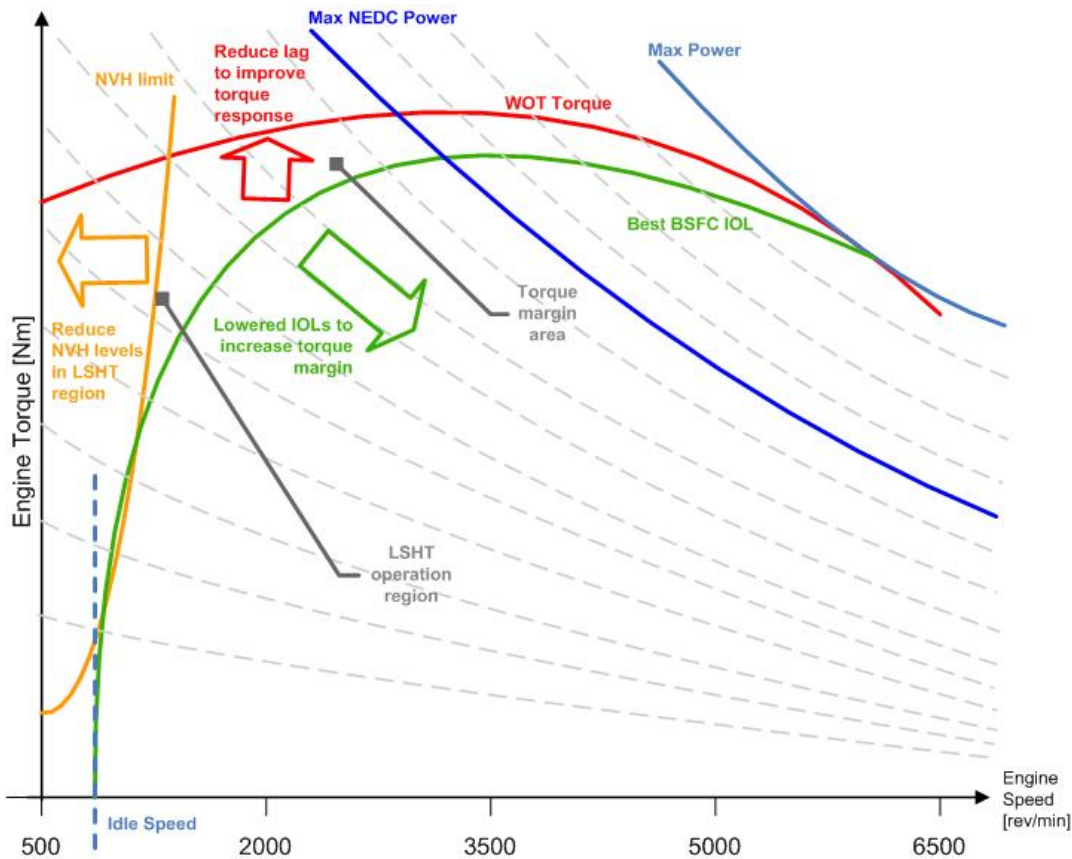
Figure 1.12 – Summary of engine performance envelope for an ad-hoc engine. The torque margin existing between the BSFC IOL [or any IOL previously mentioned] and the WOT torque is the key factor to good CVT driveability. The torque response lag following an increased demand from the IOL also has to be kept minimal. NVH issues arising in the LSHT region can limit the acceptable use of the torque margin, therefore affecting IOL operation near the idle speed.

1.3 Matching of Engine Characteristics

Designing and calibrating a CVT powertrain involves as with any other type of transmission a number of early choices regarding the torque and speed ratings of both engine and CVT. The engine power and speed range would normally determine a number of CVT specifics such as ratio span and rated input torque. Engines are never specifically developed for CVT application and it is not the intention of the study to suggest so. However, there are clear incentives to properly match the engine and the CVT during the early stages of the integration process. The suggested benefits in terms of driveability, fuel economy and emissions are drawn from a better compromise regarding the operating conditions of the powertrain.

1.3.1 Aim

This study will aim at developing engine design and control features which are particularly desirable for pairing with a CVT. Because hybrid powertrains also offer combined benefits with CVTs [19][20][21], they are included within the scope of this study as potentially part of the system. Both gasoline and diesel engine technologies will be considered because both have different characteristics which are compatible with CVT [17].

1.3.2 Research Axis

1.3.2.1 Powertrain Integration and Matching

A significant amount of effort has been put into the development of CVT control strategies and associated calibration in order to overcome some of the difficulties related to engine operation. The literature referred to in this study will reflect this fact and show how powertrain lag, torque margin, fuel consumption and emission have been taken into account in the delivery of new CVT powertrains. This has been achieved by a significantly raised level of powertrain control coordination [22].
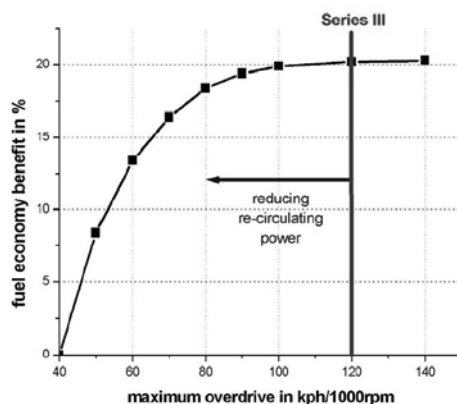
Figure 1.13 – Overdrive ratio optimisation [4] for Torotrak's Series III IVT. A reduction in maximum ratio will reduce the low-regime re-circulating power, hence benefiting powertrain efficiency

The CVT design itself has been refined to provide a better solution, yet internal combustion engine characteristics are seldom questioned during powertrain integration. Figure 1.13 shows an example of Torotrak's IVT maximum overdrive ratio optimisation for fuel economy.

The development of simulation techniques as well as the emergence of new engine technologies has however promoted investigations towards a better engine – CVT match. For example Honda has successfully transferred their VTEC-E lean-burn engine technology into a CVT hybrid powertrain [22].

Other research activities have been demonstrating that adequately altering some of the engine characteristics will benefit overall powertrain fuel efficiency and emissions. Brace *et al.* [17][18], Crewe *et al.* [16] have shown the relevance of such an approach, mostly avoiding taking engine characteristics for a fixed starting point.

This study will investigate two aspects of engine operation related to CVT powertrain integration as introduced in Section 1.2. Each investigation path is applied to a different engine technology to demonstrate that characteristics matching benefits both gasoline and diesel engine in the CVT powertrain. The following aspects are therefore studied:

- LSHT operation of a gasoline engine [Section 1.3.2.2]

- Torque response lag of a turbocharged diesel engine [Section 1.3.2.3]

1.3.2.2 Gasoline Engine LSHT Operation

During the course of the Electrically Assisted Infinitely Variable Transmission [EASIVT] project involving Cranfield University, Torotrak Development Ltd. and Cummins Generator Technologies [formerly Newage AVK SEG], a number of CVT powertrain integration aspects have been covered [23]. Based on an existing IVT demonstration vehicle and simulation platform, the project aimed at demonstrating the combined fuel economy benefits of the IVT and a mild hybrid powertrain. This task was carried out both in simulation and with a prototype vehicle, the latter giving the opportunity to show that driveability could also benefit from such a layout.

The baseline IVT demonstrator vehicle is based on the standard 1999 4-speed AT Ford Expedition. During the changeover to IVT, the V8 engine was fitted with an Electronic Throttle Body [ETC] and a custom Engine Control Unit [ECU] to provide a suitable interface with the new IVT vehicle controller. Although a high level of powertrain integration was already reached on Torotrak's IVT demonstrator, the engine characteristics were not altered at all in the process in order to benchmark for fuel economy, emissions and driveability solely based on direct IVT benefits.

The installation of an Integrated Motor Generator [IMG] in place of the flywheel during the hybrid conversion allows a number of new opportunities regarding the operation of the engine, especially in the LSHT region. The IMG provides a means to overcome the torque margin challenge and implement a more aggressive use of the best BSFC IOL. The high bandwidth response of the IMG also makes it possible to implement a strategy that controls the combustion torque fluctuations which can cause undesirable vibrations, hence extending the effective LSHT area of operation. The implementation of this strategy which allows the reduction of the engine idle speed for increased fuel economy is investigated in a first research activity.

1.3.2.3 Diesel Engine Torque Response Lag

Direct injected, turbocharged diesel technology has recently benefited from advances in high pressure injection systems; relatively high torque values can be obtained at low engine speeds whilst maintaining a fuel economy advantage compared with similar gasoline engines. Multiple injections in High Speed Direct Injected [HSDI]

diesels also help keep NVH levels within acceptable levels. Also diesel specific exhaust after-treatment technology was developed to avoid undesirable PM smoke emissions around full load operation transients.

The diesel engine therefore seems to feature a number of advantages for integration into a CVT powertrain. The abundance of torque helps avoiding shift busyness while covering most of the power band in normal driving condition. There are however two main challenges with diesel-CVT pairing:

- NOx levels – they are the main downside of HSDI diesel compared with gasoline technology. Osamura *et al.* [24] from Nissan identified this and showed how a NOx specific IOL can help address the problem to give CVT an edge over fixed-step transmission diesels. A similar approach was adopted by Deacon [9] and Brace *et al.* [17].

- Engine inertia – generally higher than gasoline engines; the engine mechanical inertia poses an increased difficulty to provide good wheel torque response [24] because the shift in engine operation condition is intrinsically slower than gasoline. Moreover, the turbocharger lag during an engine torque transient makes good diesel – CVT powertrain driveability a bigger challenge.

This study will investigate a potential solution to improve the torque response of a turbocharged HSDI diesel engine during a driver tip-in. Variable Geometry Turbocharger [VGT] and EGR control are two existing technologies which have to be incorporated into the investigations. Early studies conducted by Rohrbacher [25] indicate that air injection in the engine air path would improve the torque response. This concept called Manifold Air Injection [MAI] is therefore at the heart of the second research activity presented in this thesis.

1.3.3 Objectives & Methodology

Two challenges related the matching of engines for CVT powertrain are clearly identified. The solutions suggested will be evaluated making use of computer simulations specifically set-up for this purpose and within the scope of this thesis.

1.3.3.1 Investigation Path

LSHT operation of the engine to promote fuel economy in a CVT powertrain poses a number of problems related to torque margin, NVH levels and driveability. The objective of the first research activity is to analyse with experiments and in simulation how NVH related issues prevent IOL operation in this region; a strategy for the high frequency control of the IMG is developed based on this analysis to reduce the amplitude of the undesirable torque fluctuations when appropriate. This Active Vibration Controller [AVC] is then incorporated within the hybrid controller which addresses torque margin concerns. The EASIVT project provides a valuable opportunity to implement the AVC strategy as part of the hybrid control in a real vehicle and demonstrate how LSHT operation is beneficial to fuel economy without compromising driveability.

The second research activity is carried out in simulation only. An engine model for an Audi 3.0L V6 TDI was established, enabling all relevant phenomena to be reproduced within the simulation platform. The plant model and its controller in Simulink are validated against experimental full load data in order to ensure a satisfy degree of confidence and realism to the study. Simple models for CVT and vehicle were integrated to that simulation to reproduce driving manoeuvres which exhibit poor vehicle response due to the torque response lag. The MAI system is then implemented in the models and the control options are explored.

Once a satisfying behaviour for the MAI is reached for the most demanding power-on downshift manoeuvre, the various aspects of the benefits to the engine combustion mixture, the turbocharger and the air path are analysed. In both research activities, improvements as much as possible are quantified and compared against potential alternative solutions.

1.3.3.2 Reporting Format

Having established the requirements for a higher degree of prime mover matching during the powertrain design and integration process in this first chapter, a review of existing powertrain state-of-the-art including CVT, engine and hybrid technologies will set the background to this study. The third chapter introduces the simulation tools used for both research activities.

For each of the two research activities carried out in parallel, two chapters are dedicated: Chapters 4 and 6 focus on establishing suitable simulation platforms using AMESim modelling software. Chapters 5 and 7 provide a detailed examination of the method employed, the results obtained and their implications.

The concluding chapter of this report analyses the findings of both investigations, provides performance metrics when appropriate, and suggest further investigation paths. CVT mechanical design explanations can be found in Appendix A. Appendix B presents the potential application of the engine matching to alternative transmission systems. Appendix C details the modelling technique on which the models are based.

Chapter 2: A MODERN APPROACH TO POWERTRAIN DESIGN

The research presented in this report focuses on the matching of the engine characteristics for CVT powertrains as proposed in the previous chapter. There are different CVT concepts available including toroidal and variable pulley layouts which are described in Appendix A. This chapter studies in detail the design of the IVT torque control to highlight the requirements on the engine from a powertrain integration perspective. The potential contribution of a hybrid system is presented. The current trends in engine control systems are introduced and their relevance to the investigation is subsequently highlighted. Alternative transmission system find an application in the powertrain matching investigations presented, they are discussed in Appendix B.

2.1 IVT Controller Case Study

The control of the IVT is particularly interesting in the light of the work presented in the following chapters. The operation of the powertrain can be decomposed into steady state and transient operation for the purpose of the case study below as shown in Figure 2.14.
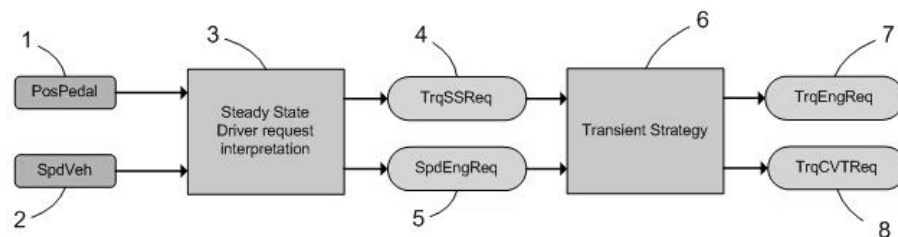
Figure 2.14 – Simplified torque control operation strategy. The driver pedal① and vehicle speed② are interpreted③ into a steady state engine torque request④ and a speed request⑤. The transient strategy⑥ computes the appropriate engine torque request⑦ and CVT reaction⑧.

2.1.1 Steady-State Operation

As explained previously with Murray [7], steady state operation of a CVT is achieved at an ideal operating point of engine speed and torque. These ideal operating conditions form an ideal operating line which depends on the engine power request. The wheel power is indeed a straight forward calculation from the vehicle speed and a calibrated wheel torque request as shown in Figure 2.15. The driver feel of the vehicle response to a pedal input is also very much associated with the engine speed response as demonstrated by Wicke [10]; Figure 2.16 shows the calibrated look-up table for driver requested engine speed depending on vehicle speed.
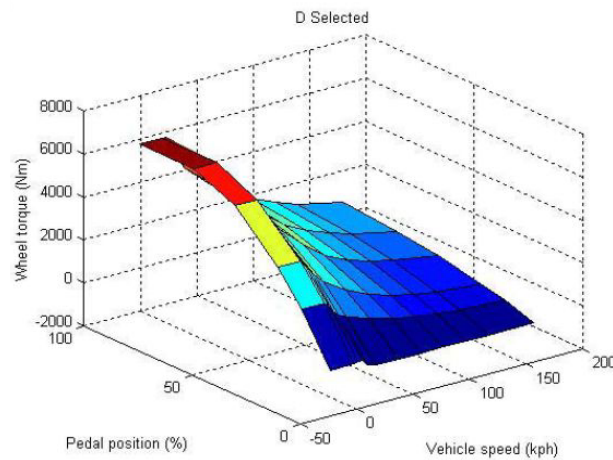
Figure 2.15 – Steady-state wheel torque in Drive [26] depending on driver's pedal request and vehicle speed
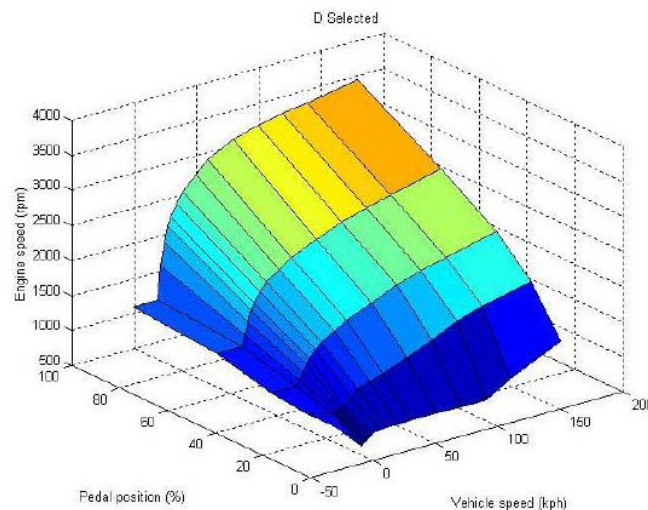
Figure 2.16 – Steady-state engine speed in Drive [26] depending on driver's pedal request and vehicle speed

The powertrain controller uses a built-in transmission model to determine the required IVT input torque from the requested wheel torque and engine speed. However, this driver requested operating point is rarely the most efficient in terms of BSFC [see Figure 1.2]. So a more efficient engine operating point can be determined for the same engine power using the IOL. There are actually many ways to optimize the engine operating point for a requested power, e.g. for BSFC, NOx, HC or even NVH. Brace *et al.* [17] demonstrate the impact of the chosen operating line on tail-pipe emissions. Figure 2.17 demonstrates how the IOL is used for the purpose of best SFC.
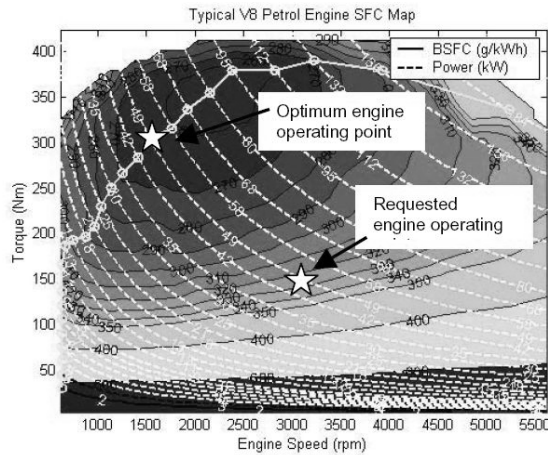
Figure 2.17 – Optimisation of the engine operating point [26] from a driver requested engine speed and torque to an equivalent power best SFC point
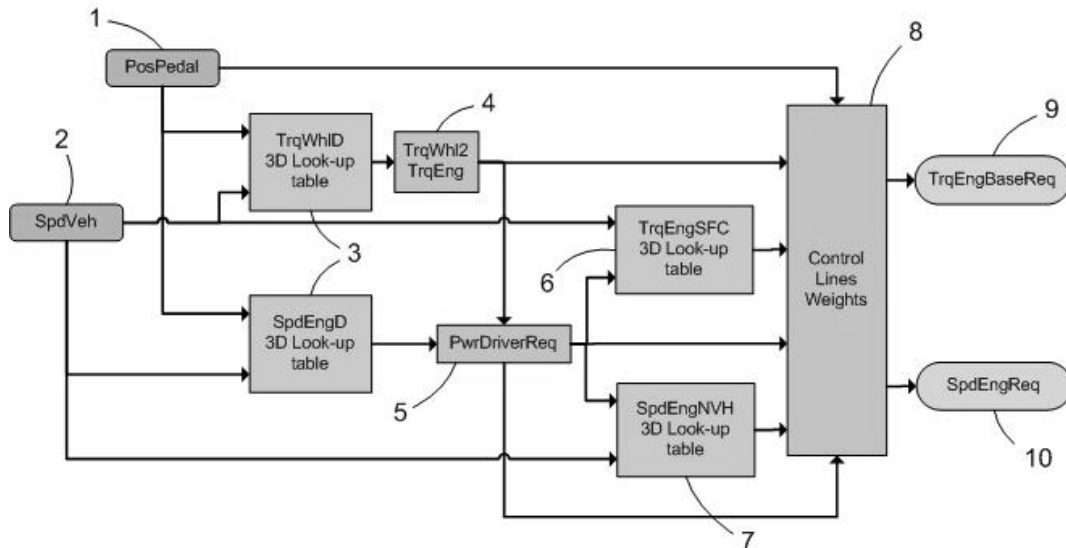
Figure 2.18 – Simplified Torotrak IVT steady state operation strategy. The driver pedal① is interpreted using the vehicle speed② to obtain the required wheel torque and engine speed③. A backward transmission model④ establishes the resulting engine torque request. The best SFC⑥ and best NVH operating condition is calculated from the equivalent engine power request. Weights⑧ are then applied to find the best compromise for the steady state engine torque⑨ and speed⑩.

Figure 2.18 shows a simplified version of the steady state operating strategy for the IVT control. This shows how the driver demand is interpreted into a wheel torque request and a desired engine speed. The IOL are then used to optimise the engine operation for the same engine power. Between steady state operating periods, the transient strategy described in the next section modifies the speed and torque set point to match the driver power requirement.

2.1.2 Transient Strategy

The steady state control strategy described in the previous paragraph is very generic and can be found in most CVT controllers, but it is also modified by the transient control strategy which responds to changing driver inputs for most of real life driving and a majority of drive cycles. The transient control strategy is crucial for the driveability and the performance feel of the powertrain because it very much affects the longitudinal response of the vehicle following a change in the pedal position by the driver.

The role played by the transient control strategy is to move the engine operating point from one position on the IOL to another. This cannot be executed by moving along the IOL because of the slow and poor vehicle acceleration response this would produce. The fuel economy and driveability compromise resides precisely on which strategy to adopt when it is necessary to operate the engine away from the IOL. Torotrak's IVT has the slight advantage to be operated in a torque control mode, meaning that the hydraulic pressure applied to the variator directly influences the torque output at the wheel rather than the transmission ratio.
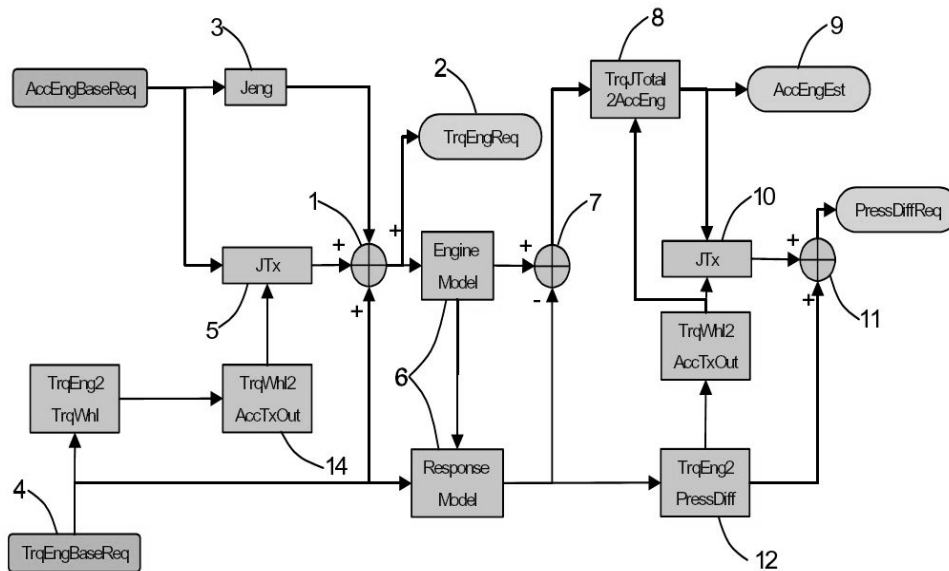
Figure 2.19 – Simplified Torotrak IVT transient torque strategy [26]. The required engine torque *TrqEngReq* ② is formulated from the sum① of engine③ and transmission⑤ inertial requirements plus a base engine torque *TrqEngBaseReq*④ from the steady state strategy. An engine model⑥ is used to estimate the actual torque available. The transmission inertia⑩ is once again taken into account to compute the variator reaction torque and associated hydraulic pressure *PressDiffReq*.

The driver interpreted desired wheel torque and engine speed are again taken into account, only this time to formulate an engine acceleration value. In the case of an increase in pedal position requiring more power and an associated transmission ratio downshift, the subsequent driveline acceleration torques are calculated; the necessary engine torque will be produced by the engine, but a fraction of it will not be reacted by the transmission hydraulic control. So the balance between engine output torque and transmission input reaction torque will cause the engine speed to vary, therefore allowing a change in the operating conditions along the speed axis. This inertial torque can be positive or negative respectively for downshifts and upshifts.

The simplified transient control strategy for the IVT is presented in Figure 2.19. Ratio-controlled transmissions operate in a slightly different way, but will hit the same challenges to offer good response without compromising overall fuel efficiency. The principles remain similar in achieving down or upshift but the detailed implementation is different. Because the necessary excursion out of the IOL very much depends on the current vehicle speed, engine speed and torque operating condition as well as the actual demand from the driver it is rather difficult to devise pre-established transient operating conditions to move from one steady state condition to another.

After having presented the key issues related to CVT operation, Sections 2.2 and 2.3 will introduce and comment on the possibilities to match the engine characteristics for the CVT powertrain.

2.2 Hybrid Powertrains

In the following paragraphs some of the possibilities offered by the integration of an electrical machine on the crankshaft will be introduced. As explained above CVT operation on IOL can cause powertrain vibrations due to the engine firing frequency which creates crankshaft torsional vibrations [27]. It is within the scope of the present research to seek improvements to these eventual NVH problems. Furthermore, NVH are increasingly regarded as one of the key features the overall performance of current powertrains [28][29]. Hybridization provides one of the solutions adopted in the industry [30], and therefore it will be introduced in the following paragraphs to set the background on hybrid vehicles.

2.2.1 The Parallel Hybrid Layout

There are a number of different hybrid layouts under development or currently in production and available to customers. It is not the objective of this review to cover all of them extensively, so the following sections focus on the parallel hybrid layout which is the architecture most closely related to conventional powertrains. Walters *et al.* [31] provides an early review of both series and parallel hybrid powertrain layouts.

The definition of a parallel layout is that both the electrical machine and the ICE are mechanically connected to the driving wheels. In most cases this means that the vehicle cannot run in electric only mode, also known as Zero Emission Vehicle [ZEV] mode. Figure 2.20 illustrates a typical parallel hybrid layout where an Integrated Starter Generator [ISG] is installed on the engine flywheel, effectively replacing the conventional ring gear starter motor and the alternator.
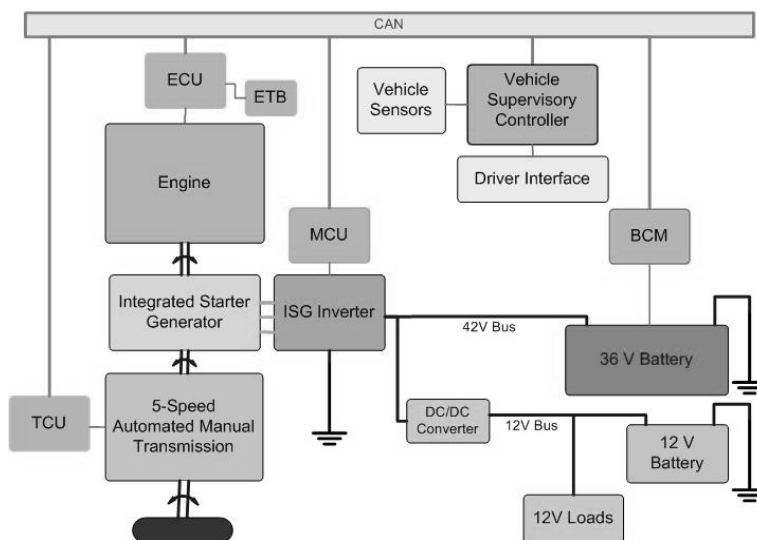
Figure 2.20 – Mild parallel hybrid vehicle architecture [32] in a 1.6l gasoline engined Ford Focus, with an 8kW crankshaft mounted integrated starter generator. This type of layout typically offers stop/start, power assist and regenerative braking functionalities

The IMG is capable of powertrain torque assist but does not necessarily have the engine cranking capability of an ISG. Micro, mini, mild or full hybrids are adjectives that subjectively describe the power ratio of IMG versus ICE. The parallel hybrid configuration offers a number of possibilities regarding the operation of the two power sources.

First the engine can be stopped and restarted on demand without using a conventional starter motor acting on a gear ring. The ISG is sometimes positioned on the side of the engine block instead of the crankshaft, and takes the name Belt Alternator Starter [BAS]. A BAS allows fast and quiet engine starts through a belt with no gearing noise characteristic of the starter motor. The same device can operate as a generator, subsequently making the alternator redundant and cutting costs. Walters *et al.* [33] and Okuda *et al.* [34] provide detailed considerations for such applications. The implementation of a stop start strategy yields between 2.6% [35] and 14% [36] depending on the application and the drive cycle. The stop / start at idle is generally the only functionality of micro-hybrids.

The IMG can be used to assist the engine to improve the response to a driver acceleration request as discussed in Section 2.2.3. This torque split strategy can involve steady state operation too, providing opportunities to generate electrical power and re-charge the battery [19]. Mini and mild hybrids usually have this functionality at various levels of power split. However, the most efficient way to store energy into the battery is during braking events; the negative torque produced by the IMG in generation mode is partially or totally substituted for the mechanical brakes action, consequently storing some of the energy otherwise wasted in heat generation [20]. Full hybrids make maximum use of this available energy, benefiting from a high power rated IMG.

2.2.2 Crankshaft Torsional Vibration Damping

Beyond the output torque produced by a reciprocating engine there exist large torque fluctuations at the engine firing frequency. These fluctuations are induced by the different phases of the Otto and Diesel cycles where power is produced by the combustion events during the expansion stroke. For the rest of the time torque is produced by the reciprocating forces and inertias which can be positive or negative. The torque fluctuations are then smoothened by the inertia of the flywheel, driveline and vehicle. However, at low engine speeds it is shown [37] that the firing frequency component of the output torque signal is significant compared to the average torque as illustrated in Figure 2.21.
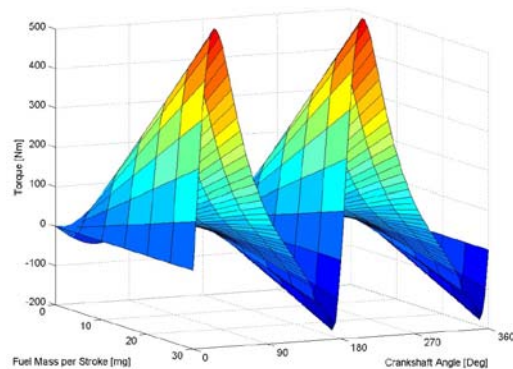
Figure 2.21 – Torque Pulsation of a 4-cylinder SI Engine [38]. The compression strokes are associated with the negative torque values, causing torsional load fluctuations on the engine output shaft

Some hybrid powertrains feature the functionality to actively counteract the aforementioned vibrations using the IMG, among other strategies like regenerative braking or stop / start [39]. A crankshaft mounted machine achieves this by being controlled as generator in the high torque periods and as a motor in the low torque periods. An example of a layout for such application is shown in Figure 2.22.
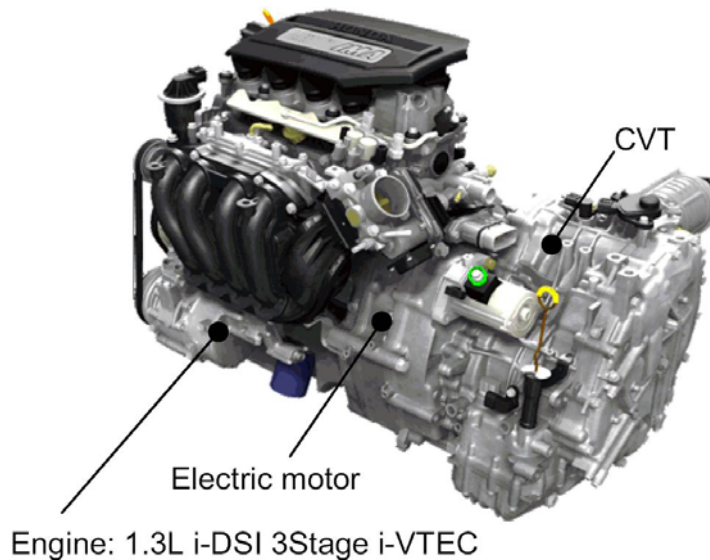
Figure 2.22 – Honda Civic hybrid powertrain [40][41] with electrical
machine in-between a downsized engine and CVT

If the mechanical design requirements for an electrical machine for Active Vibration Control [AVC] are reasonably straight forward [42] the optimum control is not. An engine torque sensor would provide the ideal feedback signal for closed loop control. However, the cost and installation difficulties make the design of a solution with torque feedback control very difficult. Indeed, none of the published papers features such a set-up. Instead of this, solutions have been developed in order for the controller to be provided with a prediction of the engine output. Davis [43] describes an observer based control system. A disturbance input decoupling signal is generated to command the motor using an engine model. The model based observer estimates the cylinder pressure from crank angle, engine speed and throttle position. An engine dynamics model is then used to predict the AC torque component decoupled from the DC torque output. The ISG is then controlled to produce the inverse of the torque ripple estimation.

Badreddine [44] focuses more on the control of speed oscillations. These oscillations of the crankshaft speed within the engine cycle are directly linked to the torque oscillations causing the vibration. Therefore a high bandwidth speed feed back signal can be used by the AVC strategy. The torque balancing signal is computed by an adaptive Proportional Integrator Derivative [PID] controller which minimizes the speed error around its average value. The adaptation algorithm changes the PID coefficients as engine operating conditions change. The tuning of the PID speed controller is carried

out by an error minimizing algorithm. The error function is a weighted combination of plant-states [engine speed] and control effort.

AVC offers an opportunity to extend the engine operation towards LSHT when beneficial to the CVT powertrain fuel economy. It therefore provides a way to match the engine operation envelope. A specific application of AVC integration in a hybrid powertrain is proposed in Chapter 5 of this thesis.

2.2.3 Driveline Motor Assist

As stated before, continuously variable transmissions and hybrid powertrains are compatible technologies [45] but integration within existing car packages can prove problematic. Fortunately aggressive hybridizations allow engine downsizing not to compromise performance when compared with the original vehicle, i.e. a smaller engine can be chosen which together with the IMG will meet target performance. Figure 2.23 illustrates an aggressive packaging arrangement that integrates the IMG and a downsized torque converter. The additional boost offered by the IMG indeed reduces necessary torque multiplication from the torque converter.

The strategy behind driveline motor assist is to help maintain high driveability levels, i.e. keep the ratio shifting smooth and shorten response times for downsized engines [see also Sections 2.3.2.2 and 2.3.2.3]. The IMG torque can be used by the CVT speed control strategy as additional torque margin and therefore increase its ability to operate on the IOL where little engine torque margin would normally be available.

The additional IMG torque can also be used to compensate for a lower ratio torque converter that would potentially penalise the CVT shift in engine speed.

Figure 2.23 – ISAD asynchronous induction machine [46] spread out view with apparent packaging cavity saved for a downsized torque converter

Ortmann [47] describes a shift strategy that is helped by using the excess engine torque to charge the battery instead of wasting it with spark retard. It illustrates the demand on the engine for better controllability in order to obtain energy consumption optimised powertrains and the opportunity offered by a CVT integrable hybridisation concept. A concept study in simulation by Frijlink, *et al.* [48] further demonstrates the interest of implementing an ISG into the CVT powertrain. The electrically powered torque boost capability can enhance the driveability of the CVT powertrain by increasing the combined ISG and ICE torque margin temporarily. This enables using a ratio control strategy that is more fuel economy biased.

2.3 Engine Control & Operation

The demand for new levels of engine torque controllability has been established in the previous sections. This is part of a global trend towards highly integrated powertrains as introduced in Chapter 1. The following paragraphs illustrate the effects on the development of engine control and operation and highlight the possibilities opened to the matching of engine characteristics for CVT powertrain.

2.3.1 Powertrain Control Architectures
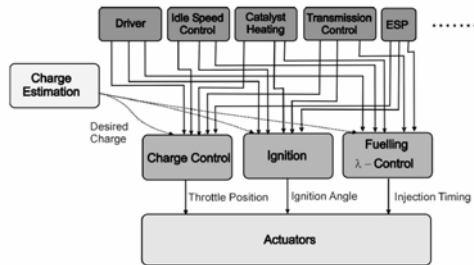
Figure 2.24 – Conventional vehicle control systems [49]. Each sub function is carried out independently from one another.
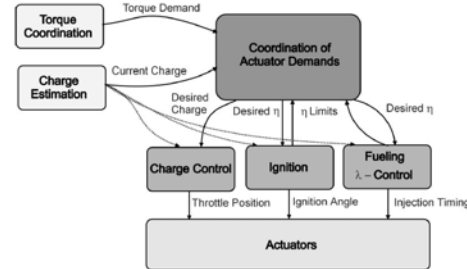
Figure 2.25 – Torque-based gasoline engine control structure [49] where a torque coordinator ensures each sub function is achieved in harmony.

The requirement for enhanced controllability of the engine has not only been driven by the development and production of CVT transmissions. Similar conclusions were drawn by most transmission engineers who progressively became powertrain engineers. Heintz *et al*. [49] present this new approach to torque based engine management systems and highlight the gains in terms of decoupling of vehicle control systems as well as the significant simplification the overall vehicle control architecture. This rationalisation is shown in Figure 2.24 and Figure 2.25.
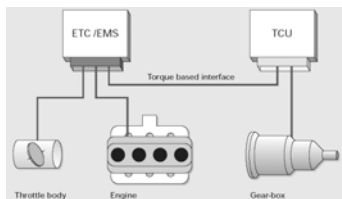
Figure 2.26 – Stand alone control architecture [50]. A separate ECU for each component
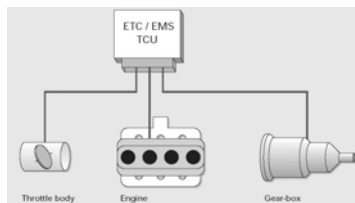
Figure 2.27 – Full powertrain control architecture [50]. One single ECU supervises all components.

The torque demand to the engine takes into account the request from the driver, the friction losses, the ancillaries, the internal sub-functions [e.g. idle speed], the external sub-functions [e.g. ESP]. For each of these torque demands, the coordination controller establishes priorities and coordinates the engine torque demand with engine and vehicle speed. This engineering driven mutation is also clearly highlighted by Helmut *et al*. [50]. Working for Siemens AG they witness the worldwide trends in powertrain development and they had to supply adequate, advanced control hardware architecture as well as maintaining cost effective powertrain control design modularity. This is illustrated in Figure 2.26, Figure 2.27 and Figure 2.28.
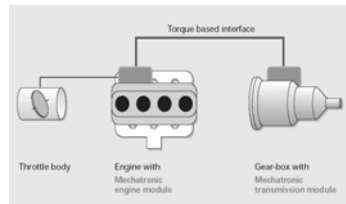
Figure 2.28 – The mechatronic control module architecture [50]. ECU and actuator are integrated to minimize information exchanges.

Very similar concepts for current and future vehicle are applied to the Bosch CarTronic [51] open architecture for structuring the entire vehicle control systems.

These developments in vehicle control architecture and communication are driven by increasing demands for powertrain control complexity to which this thesis contributes.

2.3.2 Advanced Engine Technologies

2.3.2.1 Cylinder Pressure Based Engine Management

The idea of using cylinder pressure as a main feedback variable for engine management system is not new. It is difficult to use the concept on production vehicle largely due to the high cost of the cylinder pressure sensors [52]. Indeed the expensive technology that allows life-long reliability prevented implementation on large scale production engines. Therefore in-cycle cylinder pressure feedback is essentially used for engine mapping purposes on test beds. Most pressure sensors mounted on engines are only used for knock detection or peak cylinder pressure which does not demand high frequency response or being installed in the combustion chamber.

Figure 2.29 – Kistler combustion chamber sensor prototype [53]. A very compact, rugged and temperature proof sensor is mounted in the cylinder chamber wall for direct sensing and minimal calibration. The sensor is exposed to a rough environment.
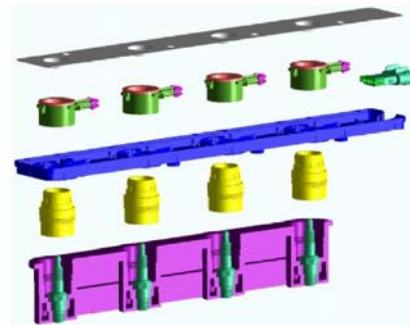
Figure 2.30 – Delphi Packard modular non intrusive pressure sensing system [54]. The sleeves in yellow mounted in the spark plug boss measure the material stress using thin walled strain gauges. Calibration is required and temperature influences the mechanical behaviour of the cylinder head.

However, the recent development of low cost, bespoke sensors made the idea of a Cylinder Pressure Based Engine Management Systems [CPEMS] realistic and work has been carried out by some of the big car manufacturers. DaimlerChrysler [53] was involved in such program with Ricardo and Kistler [Figure 2.29]. General Motors [54] together with Delphi [Figure 2.30] has made public similar development work.
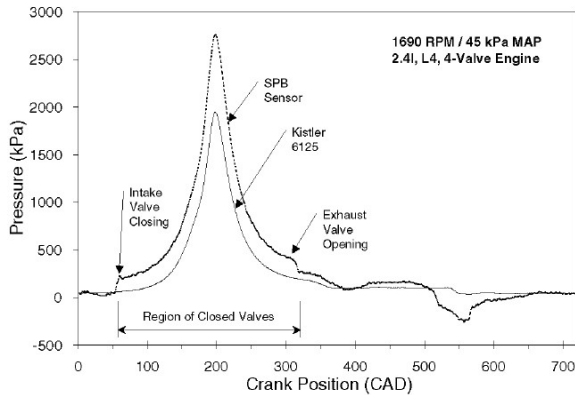
Figure 2.31 – Part throttle sensor signal comparison [54]. Spark Plug Boss Sensor and Kistler sensor signals are compared over an engine cycle.

The benefits of such systems are mainly on the fuel economy and emissions side. They allow increased EGR and optimized spark advance which reduces the fuel economy loss from spark retard. HC emissions are kept minimal by optimising the catalyst converter operation with better air-fuel ratio control. The multiple advantages found by the GM powertrain engineers are presented in Table 2.1.

Primary Benefits	Description
Fuel Economy	Increased EGR reduces pumping work and improves gas properties; individual cylinder spark timing optimizes each cylinder; MBT spark advance avoid fuel economy loss from spark retard
NOx Emissions	Increased EGR levels beyond normally practical levels with MBT spark timing
Hot HC Emissions	Hot HC emissions may be reduced by lean exhaust biasing and the associated catalyst HC conversion efficiency
Cold HC Emissions	Air fuel ratio control during the cold start enable AFR for reduced HC emissions. Precise retard control improves catalyst heating
Secondary Benefits	**Description**
Misfire Dectection	Cylinder pressure provides outstanding misfire detection and partial burn detection for full engine operating range
Knock and Pre-Ignition Detection	Improved knock detection and pre-ignition detection enables aggressive MBT spark calibrations for improved engine torque and efficiency. Eliminates 'false retard'. Replaces knock sensors
Air Fuel Balancing	Improves dilution limit and yields improved AFR control, reducing fleet emissions, and emissions dispersion & deterioration
Calibration Assist	Simplifies and reduces calibration requirements for 'fast to market' and 'niche' markets
Service Diagnostic	Detect and diagnose a variety of component failures on-board. Improves service effectiveness. Improves customer satisfaction
Warranty Reduction	Compensation for component degradation. Accurately detect component failure; reduce 'no trouble found' occurences
Camshaft Phasing	Determines active cylinder [cylinder ID] immediately upon cranking. Replaces cam sensor

Table 2.1 – Benefits for CPEMS [54] as described by GM Powertrain.

CPEMS systems show a clear trend in engine control systems aimed at optimising emissions and fuel economy. The benefits detailed in Table 2.1 are applicable to all types of transmissions. The higher EGR dilution achievable may contribute to a slightly lower torque IOL but CPEMS cannot be regarded as a means to specifically match the engine characteristics for a CVT application.

2.3.2.2 Variable Valve Actuation and Throttle-less Engine Control

The pumping losses play a major role in the fuel economy penalty of part load operation of a gasoline engine. These losses are mainly due to the throttle body pressure drop used to control the engine output torque, effectively modulating the breathing efficiency of the engine. Variable Valve Actuation [VVA] has been developed to control the valve lift and /or timing and reduce the pumping losses in part load. A number of car manufacturers and suppliers have developed such system in an effort to reduce emission levels and fuel consumption.

Pierik *et al.* [55] document the Delphi VVA technology which is capable of varying the valve lift using a mechanical system, shown in Figure 2.33. BMW promoted their successive generations of variable valve train systems across their model range. The Vanos technology allowed variation of the cam phasing to optimise engine breathing efficiency and internal EGR.

Flierl *et al*. [56] describe the evolution to the Valvetronic technology, which allows fully variable control of valve lift and timing over the engine operating range. The throttle was redundant and the system [Figure 2.32] subsequently controls the engine load. Pierik [55] achieved a reduction of the Pumping Mean Effective Pressure [PMEP] by up to *80%* compared to the baseline engine set-up using a similar throttle-less strategy.
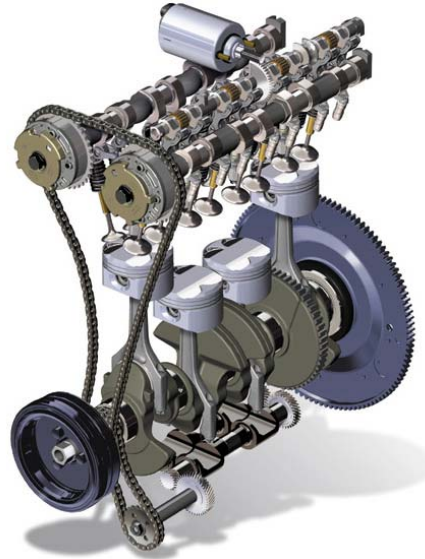
Figure 2.32 – BMW Valvetronic System [57] in 1.6L engine with double-VANOS technology to control intake and exhaust cam phasing
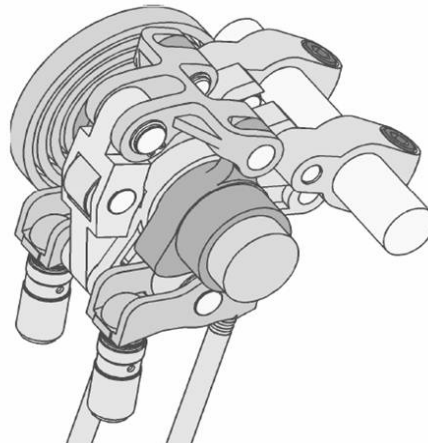
Figure 2.33 – Delphi VVA mechanism configuration [55]. An input cam similar to a conventional cam profile actuates a roller mounted on the rocker. The rocker therefore oscillates and leverages on the output cam which oscillates 40 degrees

Inlet valve throttling is not the only application for VVA systems. Stokes *et al.* [58] experimentally demonstrate how a mechanical variable lift on both inlet and exhaust valves enables the operation of the engine in Controlled Auto Ignition [CAI], also known as Homogeneous Charge Compression Ignition [HCCI]. Auto-Ignition is a combustion mode where the air-fuel mixture is brought to such a high temperature that it self ignites, without the need for sparking. The combustion does not involve flame propagation as in a gasoline engine and therefore the chemical kinetics are much faster even compared to diesel combustion. The combustion at quasi-constant volume yields high efficiencies [low BSFC] and low NOx emissions. Controlled Auto-Ignition therefore consists in:

- Obtaining repeatable temperature rise during the compression stroke of the cycle so that auto-ignition occurs at the same time during each cycle

- Limiting the rate of pressure increase to protect the ICE components

These objectives can be achieved with a full VVA system by trapping large amounts of exhaust gas in the combustion chamber with an early Exhaust Valve Closure [EVC]. Figure 2.34 shows the effect of the early EVC and early Intake Valve Closure [IVC] with the HCCI re-compression stroke. This negative valve overlap limits the amount of exhaust gases pumped out of the chamber during the exhaust stroke as well as the fresh air intake during the intake stroke. The high level of internal EGR from the valve lift strategy yields the required high temperature and the air-fuel dilution necessary to reduce the rate of pressure increase. The drawback is that these conditions can only be achieved in the low speed part load engine operating region.
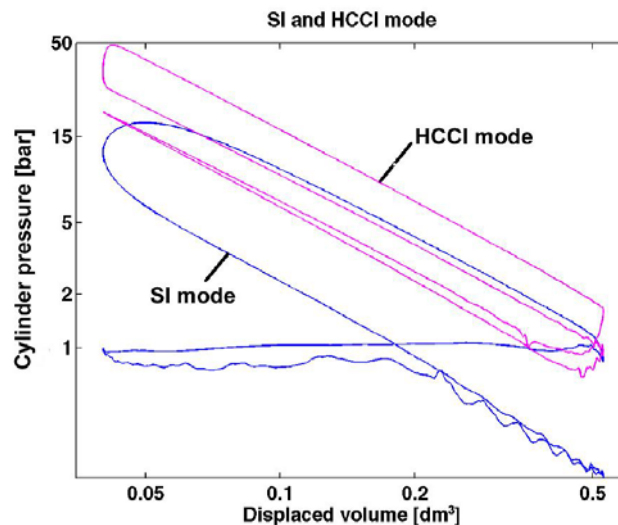
Figure 2.34 – SI and HCCI engine cycle in PV diagram [59]. The SI cycle shows early Intake Valve Closure [IVC]. The HCCI cycle shows the characteristic re-compression stroke achieved with a 'negative' valve overlap.

Stokes *et al.* [58] implemented the variable valve lift to an existing independent exhaust and intake phaser. The modified engine shows a *4.4%* fuel consumption gain at *2000 rev/min, 2.0 bar* Brake Mean Effective Pressure [BMEP]. Stoichiometric CAI shows reductions of *13.8 %* in BSFC and *94 %* in NOx at the same operating point with the CAI envelope covering most of the NEDC drive cycle loads. The low load gains in fuel economy are comparable with the state of the art lean burning stratified direct injected engines without the need for a specific lean NOx trap.

The potential for VVA in diesel engines seems to be in exhaust temperature control for cold start after-treatment efficiency, and HCCI combustion control based on the capability to adjust the effective Compression Ratio [CR] and the level of internal EGR. Lancefield [60] investigated in simulation the potential benefits of VVA control on modern diesel engines equipped with cooled EGR and VGT. Low load BSFC levels can be reduced by up to *19%* when retarding the Inlet Valve Closure [IVC]. Minimizing the mass flow through the engine at light load generally proves beneficial to the BSFC. However, Exhaust Valve Opening [EVO] changes very much affected the EGR and VGT systems without yielding significant improvement in BSFC. Fessler *et al.* [61] confirm these tendencies experimentally, exhibiting the trade-off between lower BSFC values obtained by aggressive IVC advance and lower BSNOx values obtained by cooled external EGR. The latter indeed requires late IVC, which affects the turbocharger efficiency as found by Lancefield.

These efforts must be put in the perspective of the demonstration by Vaughan *et al.* [18] that adequate engine control strategy can significantly benefit the CVT powertrain overall fuel economy. HCCI and EGR dilution are engine operation modes enabled by VVA which can be used to modify an IOL position in a CVT application. The alteration of the IOL for an increased torque margin is particularly beneficial to CVT's. Furthermore, the CVT powertrain is potentially capable of maximising the benefits obtained in the load region by deliberately operating there under low power conditions. Throttle-less engine load control benefits fuel economy for all transmissions but the faster response time is also highly desirable in the CVT powertrain.

2.3.2.3 EGR and Turbocharger Control in Diesel Engines

The torque margin necessary to control the engine speed is critical to the driveability characteristic of the CVT powertrain as explained in the first chapter. Moreover, the time delay associated with the engine torque response to load change is also critical because it defines how much of the existing torque margin can be delivered at an instant *t* after the torque request has changed. In naturally aspirated engines, intake manifold filling [and emptying] is the largest contributor to response lag. This is due to the throttling effect combined with the pumping effect of the engine, which change the mass of air in the intake. Adequate design of the intake system and Electronic Throttle Control [ETC] can minimize this lag, and the naturally aspirated engine effectively sets the benchmark for torque response.

Diesel engines however are now systematically turbocharged in order to provide power densities equivalent to gasoline engine. The turbocharging systems have a large response lag. The exhaust gases energy is increased when the engine load is increased, effectively accelerating the turbine. The mechanical inertia of the turbocharger limits this acceleration and causes a slow response on the compressor side which provides the fresh air charge to the engine. A typical turbocharged diesel engine with Variable Geometry Turbine [VGT] and EGR is shown in Figure 2.35.
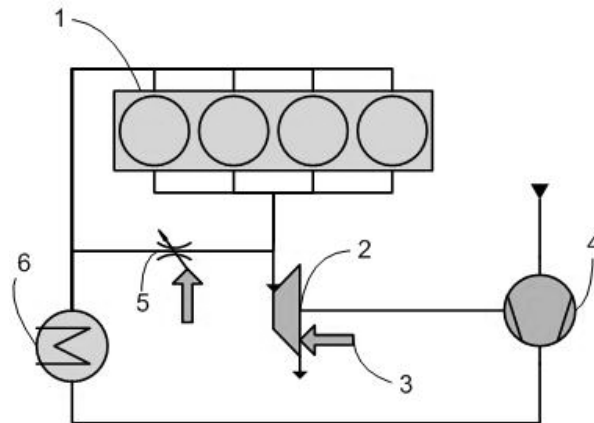
Figure 2.35 – Typical turbocharged engine layout with VGT and EGR. The engine ① exhaust gases drive a turbine ② with a variable geometry. The VGT is controlled ③ by the EMS as well as the EGR valve ⑤. The intercooler ⑥ increases the density of the intake air from the compressor ④.

As highlighted in Figure 2.35, the control of the VGT is made more complicated by the EGR system which effectively bypasses the turbine. It is therefore important for the engine control system to adjust EGR valve opening and VGT actuator position in a coordinated way. Typically the strategy is to control the Mass Air Flow [MAF] entering the cylinder and Intake Manifold Absolute Pressure [IMAP]. This is achieved by regulating the EGR flow around a target valve opening set-point to obtain a desired fresh air MAF. The VGT is also controlled around a target position set-point to produce a desired IMAP. This conventional method based on close loop Proportional Integrator [PI] control yields acceptable results and is implemented in most existing engines.

Van Nieuwstadt *et al.* [62] from Ford present the various control alternatives available and their consequences at the implementation stage. Two particularly interesting options are described in details by Witejunge [63]. One is to feed the EGR MAF error signal to the VGT IMAP controller. This enables the VGT control signal to be corrected at the source, before loss of exhaust gas power. Effectively the blade position will be increased for a higher motoring power to the turbine before the exhaust pressure decreases due to the higher EGR flow. Figure 2.36 shows the MAF error improvement from this control architecture improvement. This shows reduced MAF error but does not directly improve the torque delivery during a load command increase.
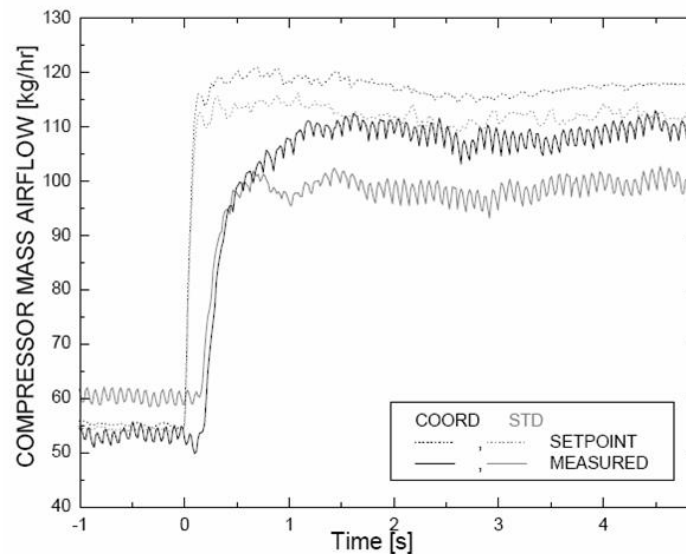
Figure 2.36 – Effect of coordinated VGT and EGR control on MAF response [63]
during tip-in transient. The MAF error is rapidly minimised but with no real gain on
response time.

A second suggestion is to control the Exhaust Manifold Absolute Pressure [EMAP] rather than the IMAP. The direct effect is to maximise the performance of the PI closed-loop VGT position control and therefore improve the turbocharger speed response [Figure 2.37]. This control arrangement yields a faster torque response during high load transient as demonstrated in Figure 2.38. The standard controller shows a response time to 90% of 0.68s and the EMAP control reduces this to 0.32s. Witejunge [63] highlights limitation of this control strategy to large load transient. Smaller changes in the torque request indeed require a finer control of the engine IMAP that the EMAP cannot give.

The findings above highlight the control issues related to VGT and EGR control. In a CVT powertrain, the management of the torque response lag in the largest transient will be critical. The time delay will cause poor vehicle initial acceleration compared to a MT where the engine speed varies much slower. A solution for the improvement of the turbocharged diesel engine response time is investigated in Chapter 7 of this Thesis.
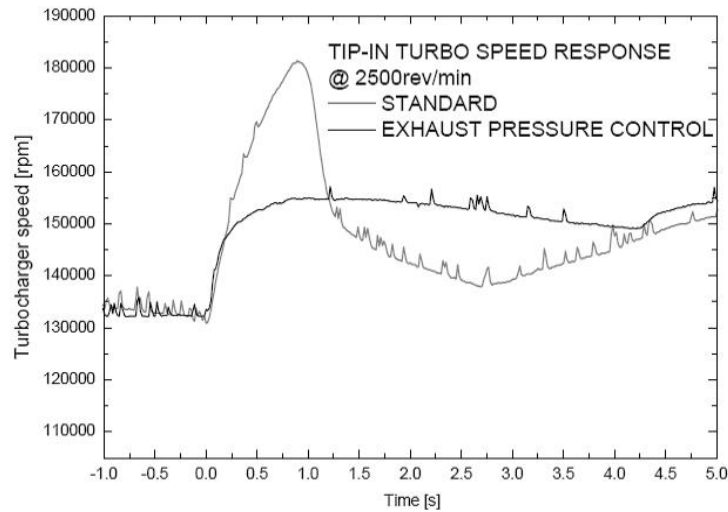
Figure 2.37 – Effect of EMAP control on VGT speed [63] compared to standard IMAP control during tip-in transient. The control of the exhaust pressure minimizes the turbocharger speed oscillations.
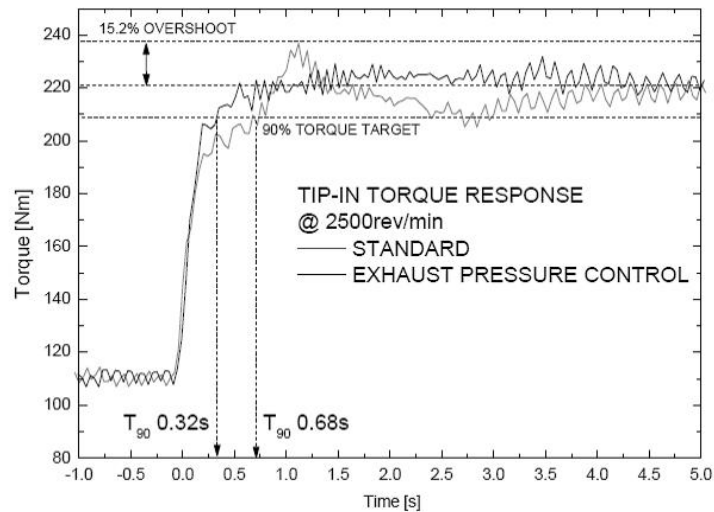
Figure 2.38 – Effect of EMAP control on engine torque [63] compared to standard IMAP control during tip-in transient. The response time to 90% is halved.

2.3.3 Torque Assist and Boosting Technologies

Torque assistance consists in temporarily adding torque to the engine output to compensate for its natural response lag or lack of efficiency. Torque boosting refers to more powerful devices that increase the overall torque of the engine. These technologies have been recently developed to enable aggressive engine downsizing, which consists in reducing the engine displacement and increasing is specific power output. The lower displacement yields lower frictional losses for improved fuel economy and an optimisation of the specific power output allows steady state performance comparable to a larger displacement engine. The specific power output is often increased by means of turbocharging and / or supercharging.
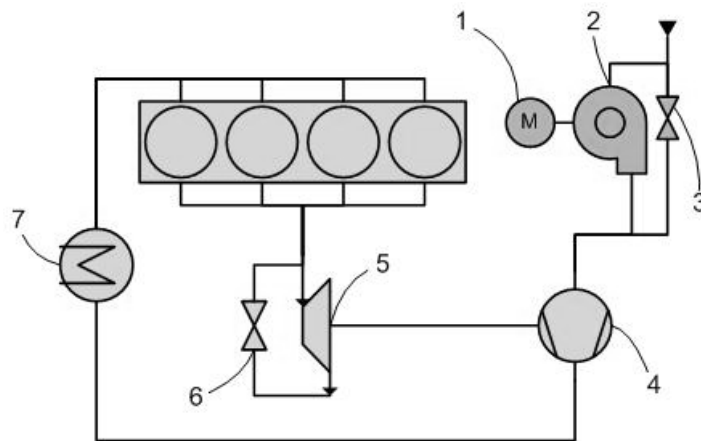
Figure 2.39 – Electrical boosting device assisting turbocharged engine [64]. An electrical motor ① drives the centrifugal compressor ② to produce a desired pressure and air-flow upstream of the conventional compressor ④. A valve ③ is used to disengage the EBD when desired. The turbine ⑤, associated waste-gate ⑥ and the intercooler ⑦ are part of the baseline set-up.

George, et al. [64] acknowledge the lack of low end torque in both naturally aspirated and turbocharged downsized engine and suggest the use of an Electrical Boosting Device [EBD]. The Visteon Torque Enhancement System [VTES] is an electrically powered supercharger which can be implemented in both naturally aspirated and supercharged gasoline engines. The EBD control system receives a target Manifold Absolute Pressure [MAP] and MAF set-point that increases the volumetric efficiency of the engine.

When paired with a turbocharger [Figure 2.39], the device is controlled to eliminate the response lag associated with the low exhaust gas energy. The electrical energy cost of the EBD is minimized by appropriate State of Charge [SOC] control of the vehicle *12V* battery and integration of the control strategy within the powertrain control system. When the engine torque margin is reduced and torque assist becomes insufficient, this device would provide an opportunity to the CVT powertrain control to require a torque boost.

The torque boosting capability of the VTES is shown in Figure 2.40 and Figure 2.41. However, systematic use of the EBD for CVT shifts will put higher demand on the vehicle battery and inevitably result in torque losses due to the higher currents required from the alternator. This would have to be taken into account by the CVT shift strategy to avoid a large fuel economy penalty caused by torque boosting.
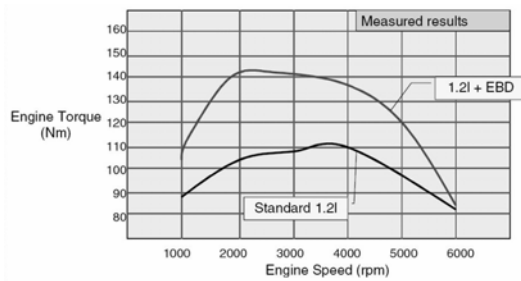
Figure 2.40 – EBD Performance with a naturally aspirated application [64] showing increased torque levels for a small size gasoline engine
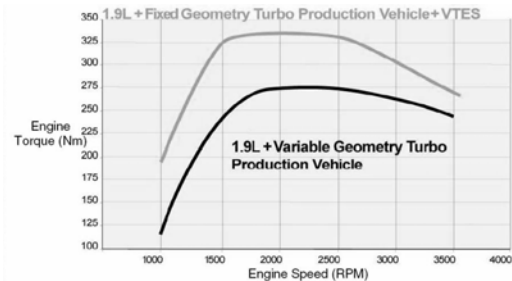
Figure 2.41 – EBD Performance with a turbocharged application [64] showing increased torque levels for with fixed geometry turbocharger compared to a VGT version

An alternative to EBD for torque assist and boosting is a small, mechanical drive supercharger placed also upstream of the compressor as shown in Figure 2.43. Kleeberg, et al. [65] provide in depth analysis of the advantages of the supercharging techniques applied to turbocharged engines. In the part load operation, the baseline turbocharged direct injected gasoline engine features lower BSFC values than a comparable, bigger displacement naturally aspirated engine. This is particularly interesting for CVT powertrain because the lower torque IOL offers an increased torque margin. The torque assist during transient offered with a mechanical supercharger or electrical device could address concerns of degraded CVT driveability compared to a standard MT application.
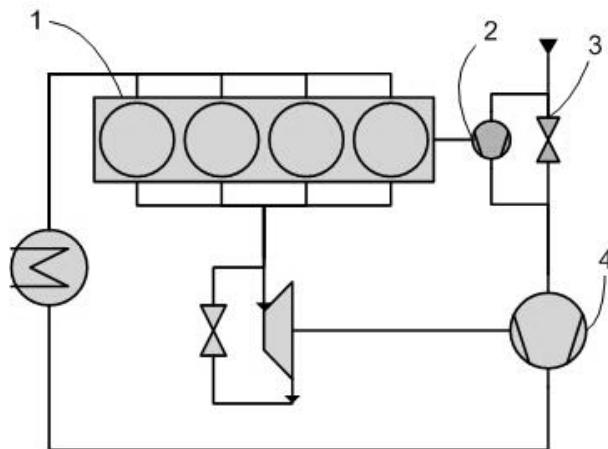
Figure 2.42 – Mechanical supercharger assisting turbocharged engine [65]. A small supercharger ② driven by the engine ① is activated by a valve ③ for the initial boosting. Then the conventional compressor ④ driven by the turbine ⑤ produces the target IMAP.

Figure 2.43 shows how the mechanical supercharger can compensate for the lag otherwise unavoidable in the baseline turbocharged engine. The response lag exhibited in 3rd gear with a MT would be a great disadvantage to the CVT powertrain when engine speed changes are required. The benefits of the mechanical booster shown below are clear with the MT, showing better driveability thanks to a quicker vehicle speed response.
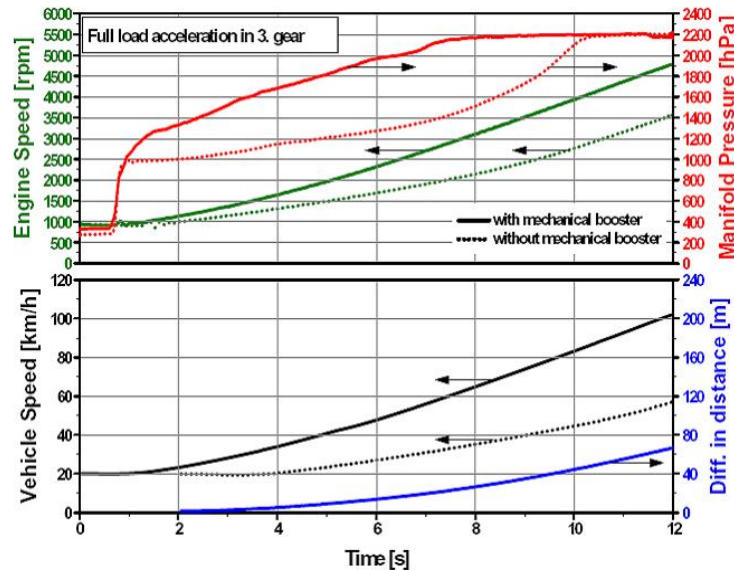
Figure 2.43 – Transient improvement with mechanical supercharging
[65] in a turbocharged gasoline engine application with MT. The higher boost pressure enables a faster pull-away in 3rd gear.

Comparatively, CVT driveability would be more sensitive to lag cancellation than with any type of fixed ratio gearbox like a MT in the case of Figure 2.43. This again is due to the speed changes controlled in the CVT powertrain with the engine torque margin. This enables a more systematic operation of the engine on the IOL for greater fuel economy, without any compromise on the vehicle acceleration response. The CVT powertrain is therefore closer to its true fuel economy potential with the use of the torque assist technology.

2.4 Closing Comments

The method of setting the engine speed operating point was explained with the presentation of the IVT torque control as an example. This shows how the engine torque and speed are chosen independently of the vehicle speed in order to achieve better fuel economy than a fixed ratio gearbox. As explained in Chapter 1 the CVT speed ratio control which enables the aforementioned IOL strategy relies on the torque margin available between a current operating condition and the maximum torque available at that speed.

Hybrid vehicles can provide an additional source of torque for the CVT to achieve quick engine speed control for best driveability. Moreover, the potential for Active Vibration Control with the IMG allows operating in the LSHT region where engine vibration is normally too high. This is investigated in Chapter 5.

The recent developments in engine design and control features were analysed in the light of the CVT powertrain requirements explained in Chapter 1. The vehicle control systems architecture has evolved to match the increased level of complexity within the powertrain. This benefits powertrain design efforts such as the matching of the engine characteristics to the CVT powertrain in this thesis. VVA systems enable CAI engine operating mode under low load conditions and a faster load change response than conventional valvetrains. These are clearly attributes which the CVT can capitalise on better than other transmissions. However, in turbocharged applications the response lag which is critical already with MT and AT becomes a bigger issue with CVT. Appropriate control of VGT and EGR systems can improve the response times in some cases but torque assist represents a more attractive alternative. Chapter 7 of this thesis will investigate a potential solution to the diesel engine turbocharger lag.

Chapter 3: CREATING A SIMULATION ENVIRONMENT WITH AMESIM

Most of the investigations presented in this study are based on simulation models. This short chapter introduces the requirements on the modelling and simulation platform and subsequently justify the adoption of AMESim and Simulink respectively for plant and controller model development. Additional descriptions of the models can be found in Appendix C.

3.1 Requirements & Objectives

There are a number of commercially available software packages which allow modelling of engine and powertrain for both transient and steady state behaviour. Because of the nature of the plant to be emulated, very high degrees of complexity can be achieved. The limiting factor is often the amount of effort to obtain sufficient data to parameterize a model and validate it with real-life. When dealing with high fidelity models, another issue comes into play. Considering the size of the plant, the size of the model can increase to such an extent that performing simulations can prove very demanding on computational resources.

Models are made of equations describing a physical phenomenon locally. The more accurate the model, the more parameters have to be sensibly adjusted. It can be significantly time consuming to tune a complicated model covering a number of physical domains such as mechanics, thermo-fluids, chemistry and electronics. There is therefore a compromise to be found between the level of details required for each part of the system and the amount of real-life data which will be required to successfully run the simulation of the overall plant. This might not be such a concern for studies which are focused on a particular area, i.e. combustion or injection; but the requirement in the present case is for a complete plant model.

Furthermore, simulation times often become of importance. Although the local models can be individually run in simulation rather quickly, once coupled with a

number of other models sharing inputs and output the simulation may become unexpectedly slow. The reason for that is that solving equations that are coupled takes up more computational resources than they would independently. A stiff model is known as a model where small time steps need to be used in order for the solvers to converge towards sufficiently accurate values of the state variables. Further explanation on solvers and integration algorithm is given in Appendix C.

The objective of each modelling exercise was therefore to build a simulation environment capable of reproducing the behaviours presented in Table 3.2, within minimum time scales.

Manoeuvre and Operating Condition	Function Involved	Frequency Range
Steady State Engine Operation	Steady-state AFR control Frictional losses Spark advance Fuelling EGR strategy	Less than 1 Hz
Engine Torque Transient	Manifold filling effects Transient AFR control Emissions control Turbocharger transient EGR transient Mechanical inertias	Between 1 and 10 Hz
Combustion Torque Fluctuations	Cylinder pressure profile Torsional compliances	Between 10 and 100 Hz
Powertrain Ratio Shift	Engine speed transient Transmission actuator response	Less than 100 Hz
Fuelling and Combustion Processes	Injection timing Fuel vaporization Wall-wetting effect Rate of heat release Emissions	Less than 1 kHz

Table 3.2 – Modelling requirements for engine and powertrain matching investigation. The involvement of a number of physical domains and the variety of frequency ranges make up for most of the modelling challenge.

Table 3.2 summarizes the various engine and powertrain operating conditions and behaviours which have direct implications on the complexity of the simulations. Those phenomena could be looked at separately and this is often a necessity in order to perform in-depth investigations of a particular system. However, the point of the present investigation is precisely to consider a more global approach of the engine and powertrain match. It is therefore important to be able to reproduce most of those systems in simulation to a degree of accuracy which enables weak points to be identified in the architecture.

Each and every item in Table 3.2 does not have to be modelled to the same level of detail, but it is important to highlight their role in the plant. It is the task of the modelling and simulation engineer to assess these roles and accordingly model each subsystem. Chapter 4 & 6 will explain those choices and justify them.

3.2 AMESim Simulation Package

AMESim [66] is a 1D lumped parameter, multi-port simulation package [67] which is being used widely in the automotive industry. The 1D lumped parameter approach is not exclusive to AMESim; a number of software suites such as WAVE by Ricardo Software [68], BOOST by AVL [69] or GT-Power by Gamma Technologies [70] boast the same approach to engine modelling. Most of those software offer interfaces with the industry's standard Matlab & Simulink package [71] for mathematical computing. Simulink in particular is extensively used to develop control strategies thanks to its block diagram based interface for Matlab [72]. The usefulness of Simulink for engine and powertrain modelling will be discussed in Section 3.3.

The key advantage of AMESim lays in its ability to integrate in one model a number of very different physical domains via its extensive array of libraries as shown in Figure 3.44. These features prove very useful to model a plant that include intake and exhaust systems, combustion chambers, fuelling system, crankshaft assembly, electric motor, transmission, driveline and vehicle. Moreover, the capacity of the AMESim algorithm to deal with each sub-model computing requirement is the key to reliable and time effective simulations.
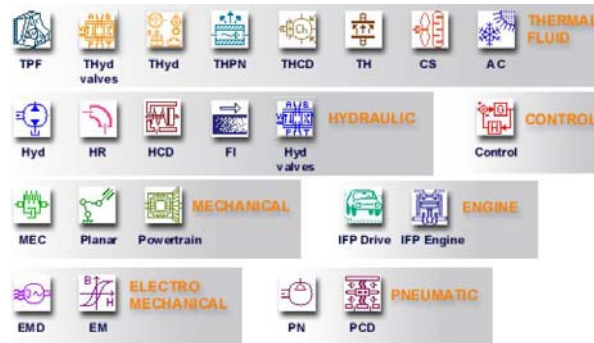
Figure 3.44 – The AMESim standard and additional libraries [66] cover a large range of engineering domain from thermo-fluids to mechanical systems. IFP Drive and Engine are additional libraries.

In fact, there are a number of different algorithms included in the AMESim solver that help it switch to the best method at each integration step to satisfy the user requested accuracy demands. For example, hydraulic systems such as fuelling rails are very demanding because they are very stiff. Some systems require modelling equations that contain discontinuities [see Section C.1.3] – typically mechanical problems. The fact is that algorithms that are good at handling discontinuities are rarely as good with stiff equations. The AMESim solver has the particularity that it adapts the integration time step to the current stiffness of the system and it switches solver as necessary to optimize run times.

3.3 MATLAB & SIMULINK Package

Matlab is a high-level mathematical language which allows rapidly performing tasks that are computationally intensive, like mathematical analysis, control development, signal and image processing, or system modelling. This proved to be particularly useful for the automotive industry to reduce their product development time while advancing the degree of functionality. The rapid raise of customer expectation and the ever more stringent emission and fuel economy regulation has motivated increasingly complex systems which could no longer be dealt with empirically.

Simulink is an interface to the Matlab language that creates a graphic interface to create time based simulations using blocks instead of code. Each block containing user defined equations is part of a network of signals which is interpreted into Matlab language. Simulink and Matlab have now become a standard to develop controllers for vehicle, engine, powertrain, or chassis systems.

A plant can be modelled in Simulink, therefore allowing the simulation of a complete system in one single software environment. However, it is also possible to interface a Simulink model with a plant model established with another software package [see Section 3.2]. The exact implications of a split environment are discussed in appendix C, but it is important to understand the convenience of such a layout where the most appropriate tool can be used to model the plant and the controller. Such implementations have been successful; Garcia *et al.* [73] explain how such a simulation tool has assisted Renault engineers in reducing their transmission system design time and budget. He [74] demonstrates how his Simulink controller model reproduces production like engine management algorithms for a turbocharged V6 diesel engine model established with the GT-Power suite [75] in both steady state and transient conditions.

Chapter 4: V8 GASOLINE ENGINE MODEL

This chapter presents the modelling of the Ford Triton 5.4L V8 gasoline engine for combustion torque oscillation, speed and torque transients in order to investigate LSHT operation with a hybrid CVT powertrain environment as introduced in Chapter 1.

4.1 Requirements

Establishing the performance requirements for a model is a necessity which was highlighted in the beginning of this study. Only with clear functionality and accuracy levels objectives can a model be built and run within reasonable time scale and yet successfully reproduce real life behaviour and characteristics. It is intended to use this engine plant and controller model to develop a strategy enabling the optimisation of the powertrain fuel economy by operating the engine in the LSHT region. This strategy is based on reduced idle speed, active vibration control of the combustion torque fluctuations using an IMG, and CVT controlled best BSFC operation. The model performance requirements subsequent to LSHT operation simulation cover most of the conditions introduced in Table 3.2 and developed in Section 4.1.2.

4.1.1 Engine Description

Figure 4.45 – Ford Triton 5.4 V8 gasoline engine cut-away. Shown here in its 3 valve per cylinder configuration the engine is a naturally aspirated.

The Ford Triton V8 is a large displacement gasoline engine used mostly for light truck or Sport Utility Vehicle applications in North America. Designed in the nineties, it does not feature any advanced technology in its original form [Figure 4.45]. Torotrak replaced the mechanical throttle with an Electronic Throttle Control [ETC] during the replacement of the transmission for an IVT.

The injection and sparking are controlled by a custom Zytek EMS calibrated to replicate the performance of the engine with its original control unit. The injection system is of the port-injected, sequential type.

4.1.2 Operating Conditions

4.1.2.1 Steady State

The exact reproduction of the engine fuel consumption and torque is paradoxically not a prime objective. Mean value models provide a more suitable way of simulating these conditions. Indeed, the level of detail required for this V8 model to reproduce phenomena such as combustion torque ripples or engine load transient implies that a number of higher frequency systems have to be modelled. These high frequency sub-models such as combustion or friction also have an influence on the steady state performance. It would consequently be difficult to model to high degree of fidelity for both steady state and short transient. The steady state torque and BSFC predictions have limited influence on the strategy to be developed, so predictions within ±*20 %* are acceptable at a given engine speed. Moreover, it will be demonstrated in Chapter 5 that the LSHT control strategy is best calibrated with the real plant because of the implications on the vehicle driveability.

4.1.2.2 Engine Load Transient

These torque transients are here differentiated from the combustion torque oscillations. Torque transient due to load changes can play a significant role in the definition of the active vibration controller input signals frequency range. Such signals are potentially engine speed, actual torque, or spark advance. It is consequently important to obtain a model with a relatively high level of fidelity in the throttle response characteristics. Less than ±*10%* error is the order of magnitude for the accuracy target.

4.1.2.3 Combustion Related Torque Oscillations

This phenomenon is at the core of the LSHT operation strategy because it is one of the limiting factors to how far the strategy can go in reducing the idle speed and how costly the subsequent active vibration control strategy will be in electrical energy. Obtaining accurate prediction of the engine torque output shape during an engine cycle is crucial in designing the active vibration controller for the IMG. The requirement in this frequency range is mostly qualitative, but less than ±*5%* error on the torque fluctuation phase is regarded as a target. Dynamometer data will be employed mostly for the purpose of ensuring this requirement is met.

4.1.2.4 Powertrain Shifting

In the case of CVT powertrain, engine speed changes due to external engine load changes e.g. hydraulic pressure in belt drive or variator reaction torque. Together with the engine load changes, the effective ratio changes within the powertrain have a direct influence on the current speed and torque operating conditions therefore they have the similar influence on the AVC input signal frequency range. Because of the potentially

much faster response of hydraulics compared to the throttle, the powertrain shifts represent the highest input frequency to the LSHT strategy. However, only the engine inertia and torsional compliance are expected to be influential as the transmission model is not included in the scope of the model described in this section.

4.1.2.5 Fuelling and Ignition Processes

Fuelling and ignition have very low time constant but because they occur in a discrete way during the engine cycle they can have an influence in lower frequency bands and therefore cannot be disregarded. Thus a low level of accuracy in the fuel mixing and ignition process models is an acceptable requirement for the model. They are both combined with other processes such as combustion or load transient and can consequently be validated together with the dynamometer data introduced in Section 4.2.
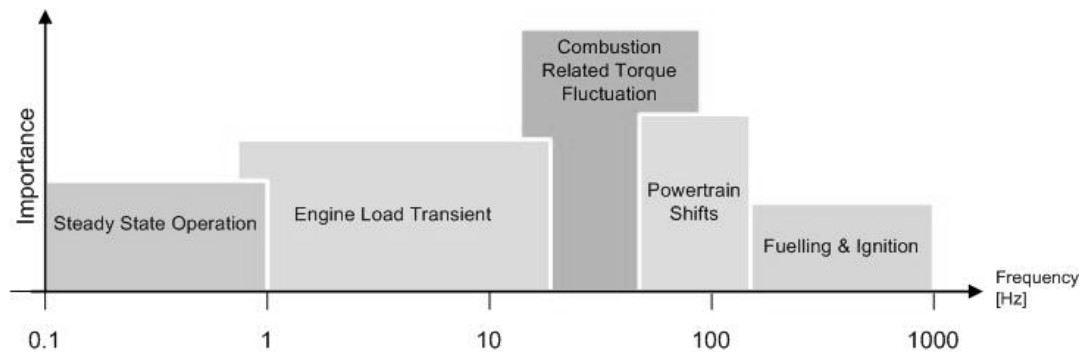
Figure 4.46 – Relative importance of phenomena for V8 engine model established to develop LSHT control strategies. Each frequency band identified previously is represented by a bar which height is arbitrarily set to represent its level of importance in the modelling objectives.

The relative importance of the phenomena mentioned above are summarised in Figure 4.46. It clearly highlights the distribution around the engine firing frequency band which is the area of concern for active vibration control.

4.2 Dynamometer Data

Experimental data when available is a great help to design the model and validate it. One option would be to measure and test each of the engine sub-components in order to validate each sub-model independently. Another option is to parameterise the sub-model with known data and then tune the unknown parameters in order to validate the performance of the complete model. The latter was more appropriate within the time constraints, and because the engine uses a relatively generic technology, most of the sub-components parameters contribution to the overall performance was identifiable.

4.2.1 Instrumentation

A relatively extensive test plan was devised for engine dynamometer testing of the V8 Triton engine at the Torotrak Development Ltd's facility. The aim was to collect data to calibrate the model for the plant and the controller as well as validating the performance of the simulation environment subsequently established. Table 4.3 shows the list of EMS variable monitored and recorded during each test point.

A cylinder pressure sensor [Figure 4.47] was mounted to one of the cylinders for the purpose of model matching and a 3-axis accelerometer was installed on the engine mount to correlate the vibration with the engine torque. These 4 signals were sampled at a high sampling rate together with the unprocessed crankshaft encoder pulses in order to relate each signal to the engine position over the cycle. Table 4.4 provides a summary of the additional data sampled via a National Instruments data acquisition set-up.

Particular attention was paid to the synchronicity of the data logging in order to ensure that pressure, torque and acceleration levels could be evaluated against crank angle for the purpose of model validation.
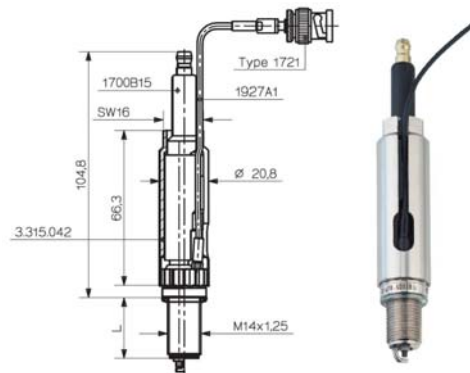
Figure 4.47 – Kistler 6117B measuring spark plug with integrated pressure sensor [52]. Its design allows a non-intrusive pressure measurement inside the combustion chamber up to *200 bar* at *±0.6 %* accuracy.

EMS Variable Name	Physical Name	Units
brake_torque_actual_ch01	Dynamometer brake torque	Nm
cem_trq_eng_est	Estimated engine torque	Nm
mbe_cylinder_trigger	Active cylinder	n/a
mbs_mbt_spark_advance	MBT spark advance	deg
mff_inj_pwr_elec_cyl1	Fuel injection duration	s
mip_afr_average	Average AFR	n/a
mip_ect	Engine Coolant Temperature [ECT]	degC
mip_engine_oil_temperature	Engine oil temperature	degC
mip_engine_rpm	Engine speed	rev/min
mip_iat	Inlet Air Temperature [IAT]	degC
mip_map	Inlet Manifold Absolute Pressure [IMAP]	kPa
moi_maf_cyl_mgst	Mass Air Flow [MAF] estimate in cylinder	mg/stroke
moi_meas_mgst	Measured MAF	mg/stroke
moi_maf_throttle_mgst	Throttle MAF	mg/stroke
mpc_pos_pedal	Virtual pedal position	%
msa_spark_eng_act	Actual spark advance	deg
mtc_cmd_pos_thr_final	Actual throttle position	%
mtc_trq_brake_req	Required engine brake torque	Nm
mtc_trq_eng_fric	Estimated engine friction torque	Nm
mtc_trq_ind_req	Required engine indicated torque	Nm
mtc_trq_loss_final	Estimated total engine torque losses	Nm

Table 4.3 – EMS data collection. All relevant EMS variable were collected at 100Hz sampling rate via CAN link from the Pi OpenECU G800 EMS to a laptop based ATI Vision calibration and data acquisition tool. Most variables should remain static during steady state conditions.

Variable Name	Comments	Units
Position encoder pulse signal	36 teeth - missing tooth 40 deg before TDC	V
Torque sensor analogue signal	LP filtered at 500Hz for torque fluctuations	Nm
Pressure sensor signal	Charge amplified	bar
X-axis accelerometer signal	Filtered at 5 kHz to avoid aliasing	g
X-axis accelerometer signal	Filtered at 5 kHz to avoid aliasing	g
X-axis accelerometer signal	Filtered at 5 kHz to avoid aliasing	g

Table 4.4 – Dynamometer data collection. Sampled at *20 kHz* independently from the variables in Table 4.3, the addition of the encoder pulses signal allows referencing each of the 5 other measured channels to the crank position

4.2.2 Data Collected

A large amount of data were collected across the engine speed and load spectrum. A first set of measurement focused on LSHT operation with emphasis on in-cycle torque fluctuation measurement. This covered speeds between *500* and *1200 rev/min* and loads between *600 mbar* Intake Manifold Absolute Pressure [IMAP] and WOT [approximately *1013 mbar* at test conditions]. Figure 4.48 shows an example of the post processed data for a given engine operating point. These results later allowed tuning the plant model to match the cylinder pressure profiles observed on the dynamometer.
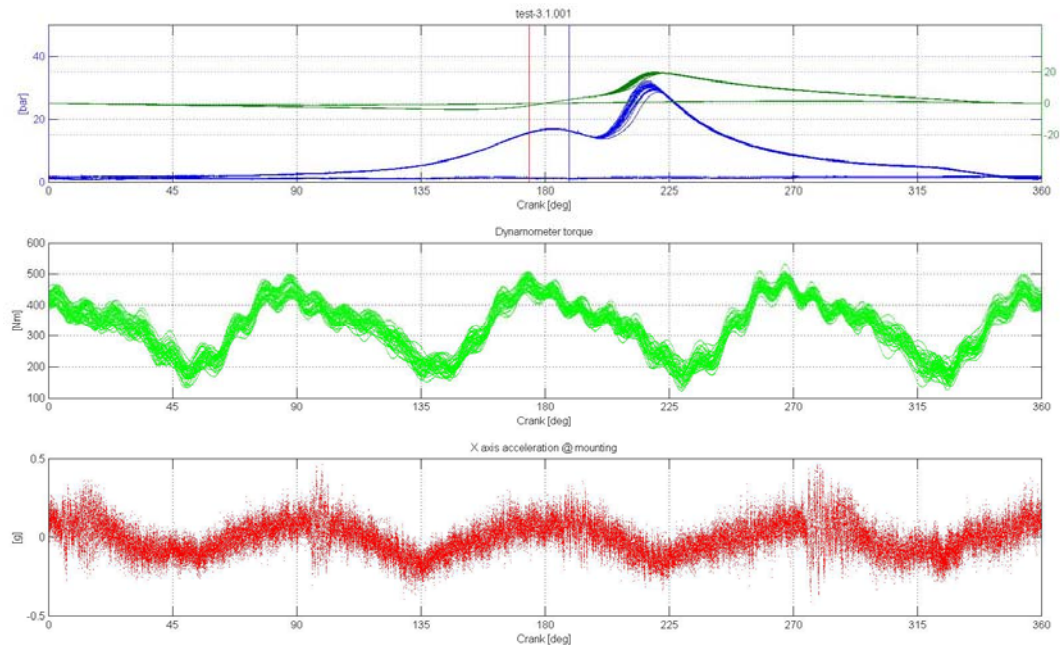
Figure 4.48 – Typical data sample. At a given engine speed and load operating point, the data are plotted against the crank angle derived from the position encoder signal for a large number of consecutive cycles. The quality of the data is demonstrated by repeatability of the trace. The cylinder pressure [blue] can then be converted to a crankshaft torque in bar.m [dark green].

A second set of data collection covered the complete engine range from *1000* to *5000 rev/min* and load from *300 mbar* IMAP to WOT. The aim of this exercise was to gather valuable information on the engine control strategy for sparking and fuelling. The spark advance calibration used in the engine model was directly sampled on the engine dynamometer as presented in Figure 4.49. The targeted AFR for the controller model was obtained similarly.
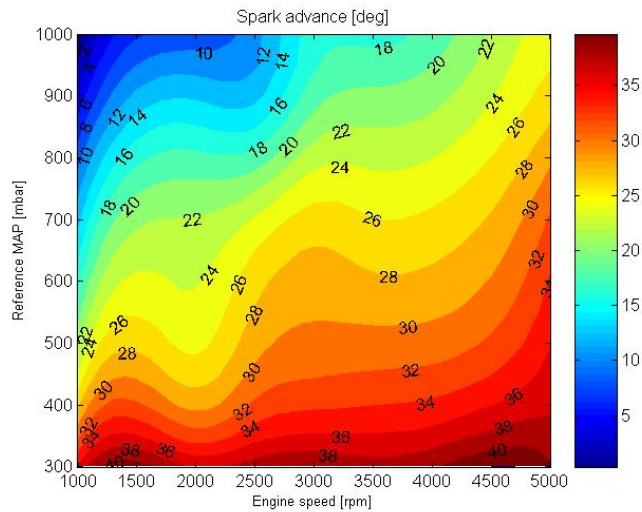
Figure 4.49 – Spark advance calibration sampled on the engine dynamometer for direct use in the controller model calibration.

The pressure measurements which importance was previously highlighted [Figure 4.46] were particularly critical in the LSHT region where the model will be finely tuned to match the real life data collected. Figure 4.50 shows the evolution of the pressure profile with the engine load at each of the 16 engine speed set-points in the first batch of tests. The data in Figure 4.50 clearly shows how little correlation can be found between the sparking strategy and the peak cylinder pressure magnitude and timing. This is partly due to the fact that MBT spark is not systematically employed.
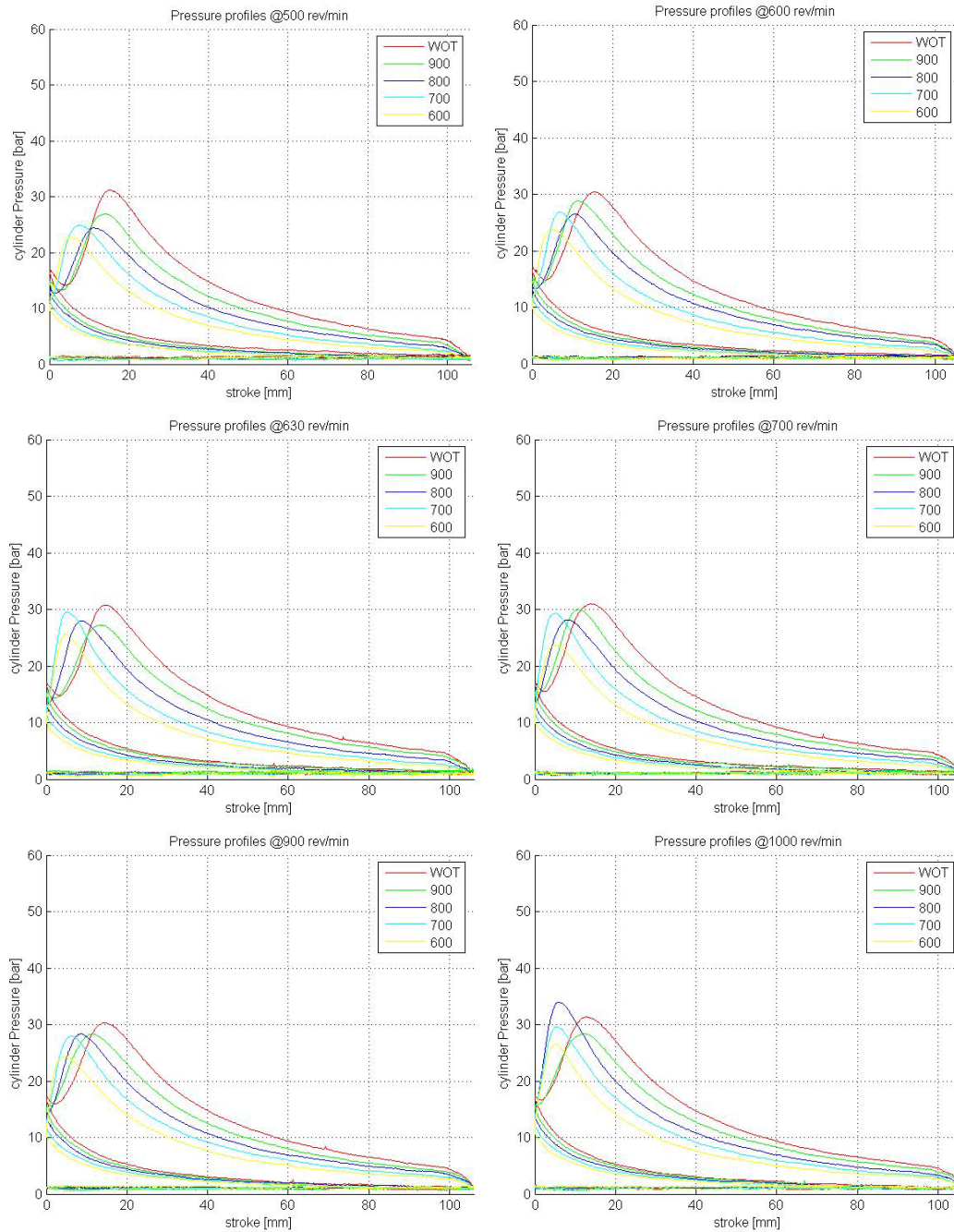
Figure 4.50 – Cylinder pressure profiles measured in one cylinder between *500* and *1000* *rev/min* for various engine loads. The load set-points are 5 IMAP values in mbar adjusted with the throttle. A set manifold pressure is preferable to a set throttle position to ensure a consistent engine load at different engine speeds

4.3 Description

This section describes the model for the engine hardware in AMESim and the associated controller model executed in Simulink. Additional details on the 1D modelling techniques applied in AMESim can be found in Appendix C.

4.3.1 Plant Model

At the core of the engine model lie validated submodels specifically developed for engine applications by IFP [76] in a dedicated 'engine' library. They are merged with conventional mechanical, control, or fluid modelling elements in one graphical layer as illustrated in Figure 4.51.

4.3.1.1 Injection and Combustion
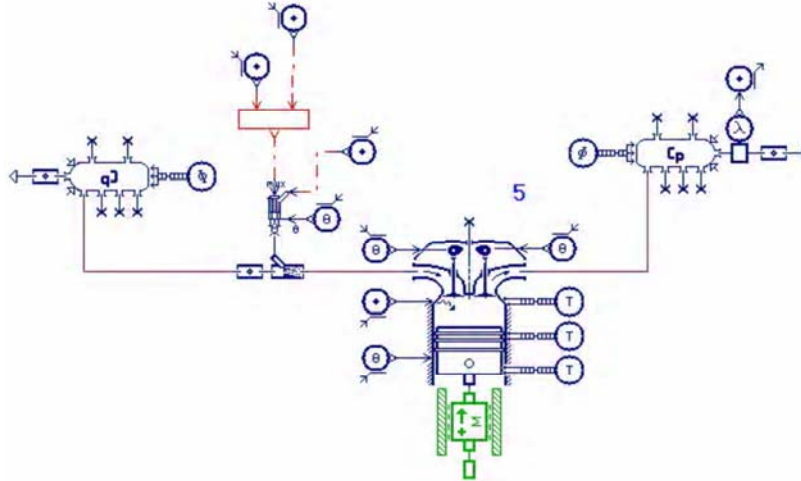
Figure 4.51 – Gasoline engine intake, combustion and exhaust models in AMESim. Intake and Exhaust are modelled by pneumatic chambers. The injector model interfaces between control variables and intake port, while the lambda sensor interfaces between exhaust and controller. The piston included in the cylinder model is the interface with the crankshaft model [Figure 4.52].

The submodel assembly in the centre of Figure 4.51 was replicated 8 times into 2 banks of cylinders. The details associated with the air path submodel parameters are discussed below [see Figure 4.53]. Table 4.5 specifies the globally declared parameters used by each duplication of the chamber and head sub-model, which were indexed with a cylinder number. Constant temperature sources are associated by the thermal exchange sub-models within the combustion chamber. The pistons interact with the crankshaft model assembly presented below [Figure 4.52]. They are masses with viscous friction, to replicate the work losses of the piston rings on the walls.

Variable Name	Title	Value	Units
Cyl_block_temp	Cylinder wall temperature	273+150	K
Cyl_head_temp	Cylinder head temperature	273+150	K
Piston_mass	Piston and con-rod small end mass	0.4	kg
Piston_temp	Piston head temperature	273+250	K
Piston_friction_stiction	Piston stiction force	0	N
Piston_friction_coulomb	Piston Coulomb force	0	N
Piston_friction_viscous	Piston viscous friction coefficient	2.3	N/(m/s)
Piston_friction_windage	Piston windage friction coefficient	0	N/(m/s)²
Stoech_AFR	Stoichiometric air fuel ratio	14.6	n/a
Injection_pressure	Fuel ramp constant pressure	5	bar
Injection_temp	Fuel temperature in ramp	273+40	K
Injection_vol	Port injection runner volume	0.5	L
Injection_X	Liquid fuel film mass to injected fuel ratio	0.1	n/a
Cturb	Turbulent kinetic energy coefficient	5	n/a
Cdiss	Kinetic energy dissipation parameter	24	Hz
Vflame	Flame initial volume	10^{-6}	m³
Fwrink	Flame winkling coefficient	1	n/a
Tumble_fact	Tumble value coefficient (% of vol. efficiency)	0.77	n/a

Table 4.5 – Global parameters for engine combustion chamber. All parameters related to the sub-assembly shown in Figure 4.51 are declared once for each of the 8 duplicates.

Figure 4.51 provides a view of the fluid flows within the engine. AMESim accounts for three types of gases – i.e. fresh air, vaporised fuel and burnt fuel – and one liquid, i.e. liquid fuel. The mixing in this multi-port injected engine occurs sequentially in the intake runners modelled by a dedicated element. In this volume, the liquid fuel is injected into advanced chamber model. Vaporisation is modelled with a τ-X approach, where X is the mass fraction of liquid fuel wetting the walls of the cavity and a time constant characterises the evaporation phenomenon for the liquid fuel from both the volume and the walls [Equation 4.2]. This wall-wetting and evaporation 1D model is relatively simple and yields a realistic and thermodynamically representative simulation of the fuel injection delays and poor mixing at low engine speed.

$$\tau = 0.0001 + \frac{0.0001}{T_{gas}}$$

**Equation 4.2** – Evaporation time constant [s] function of T_{gas}, the local gas temperature. Both evaporation phenomena are described by the same function for simplicity.

The combustion model selected is a 1D flame propagation model [1D CFM, by IFP]. Known to be more predictive than the generic Wiebe model, it accounts for two zones in the chamber – i.e. burned and unburned gases – and simulated the premixed

flame. Appendix C provides details on the two alternative combustion models available. The CFM code was preferred for its ability to predict flame propagation delays in the LSHT region where Wiebe assumes the heat release is a function of crank angle after sparking. The parameters C_{turb}, C_{diss} and *Tumble_fact* where tuned so that the simulated pressure profiles match the experimental measurements presented in Section 4.2.2.

4.3.1.2 Crankshaft

Figure 4.52 shows the crankshaft sub-model assembly interfacing with the combustion chambers via the pistons, also represented in Figure 4.51. The engine inertia is effectively split between the 5 sections of the crankshaft and the piston. The timing end on the right hand side of the diagram assumes 3 times as much inertia as the other sections and adopts its own friction properties to model the belt mechanism added inertia and its contribution to the engine friction. The associated parameters are specified in Table 4.6.
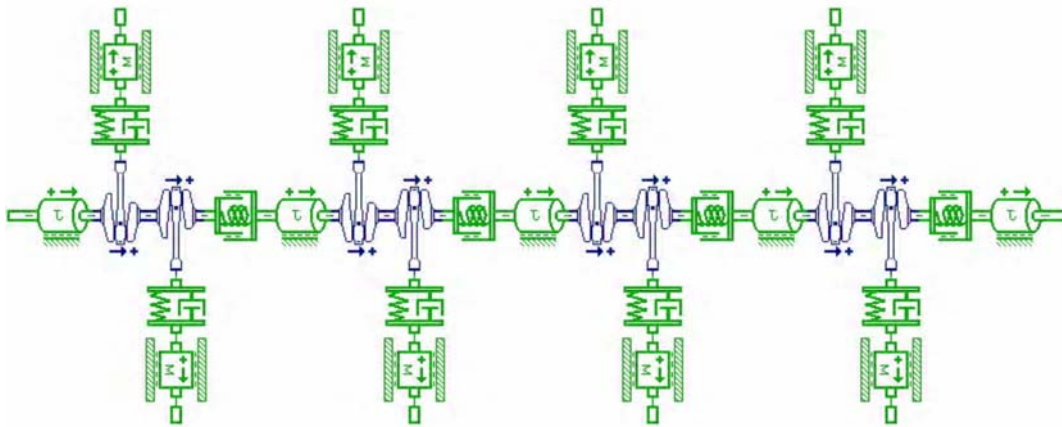
Figure 4.52 – Crankshaft and connecting rods models assembly for torsional vibration modelling. The connecting rods are modelled with a stiffness and a damping characteristic. Their big-end is merged into the associated crank inertia and their small-end is merged with the piston mass [Figure 4.51]. Each facing crank pair is linked to the others with a torsional stiffness and damping model.

Each inertia / crank element is linked to its side equivalent with a combined stiffness and damping sub-model aimed at replicating the torsional dynamics of the crankshaft. The mechanical properties were selected empirically but the Eigen frequencies of the system proved to be well beyond the frequency range of the torque fluctuations of interest, therefore minimizing the impact of the parameter. However, the small compliance offered by this layout is necessary for smooth running of the solver. The damping indeed eliminated high frequency vibrations excited by the potential discontinuities in the combustion models. The bearing friction properties were tuned so that the combined piston, bearing and ancillaries torque losses match the engine WOT frictional torque data obtained from Torotrak. This was achieved with a low accuracy level which influences the steady state performance of the model as mentioned in Section 4.1.1.

Variable Name	Title	Value	Units
Initial_speed	Engine initial crankshaft speed	630	rev/min
Flywheel_inertia	Input coupling and IVT input shaft inertias	0.173+0.04	kg.m²
Coupling_stiffness	Engine coupling stiffness	22	Nm/deg
Coupling_damping	Engine coupling damping coef.	0.22	Nm.s/deg
Anc_friction_coulomb	Ancillaries and camshaft engine drag torque	11	Nm
Anc_friction_viscous	Ancillaries and camshaft viscous torque	0.002	Nm/(rev/min)
Bearing_inertia	Crankshaft bearing inertia	0.17/7	kg.m²
Bearing_friction_stiction	Crankshaft bearing stiction torque	0	Nm
Bearing_friction_coulomb	Crankshaft bearing coulomb torque	0	Nm
Bearing_friction_viscous	Crankshaft bearing viscous coefficient	0.001	Nm/(rev/min)
Bearing_stiffness	Crankshaft bearing torsional stiffness	8700	Nm/deg
Bearing_damping	Crankshaft bearing torsional damping coef.	0.05	Nm/(rev/min)
Piston_conrod_stiffness	Connecting rod stiffness	10^7	N/m
Piston_conrod_damping	Connecting rod damping coefficient	10000	N/(m/s)

Table 4.6 – Global parameters for engine crankshaft. The mechanical parameters of for the submodels [Figure 4.52] are either from real-data, e.g. coupling properties or tuned to match a higher level overall value, e.g. friction parameters tuned to replicate the torque losses over the engine speed range

4.3.1.3 Air Path

The intake and exhaust volumes previously introduced are pneumatic chambers with heat exchange which are connected to the cylinder head models of each cylinder. Figure 4.53 shows the layout of chambers and pipe sub-model assembly forming the air path. A heat flux of *1000W* at the intake provided a realistic temperature increase of the intake air in the chamber of around *50 degC* depending on the airflow through the chambers. Throttling is achieved with an advanced pipe sub-model accounting for the butterfly angle. The actuation delay on the real-life Electronic Throttle Control [ETC] was modelled by a first order filter.
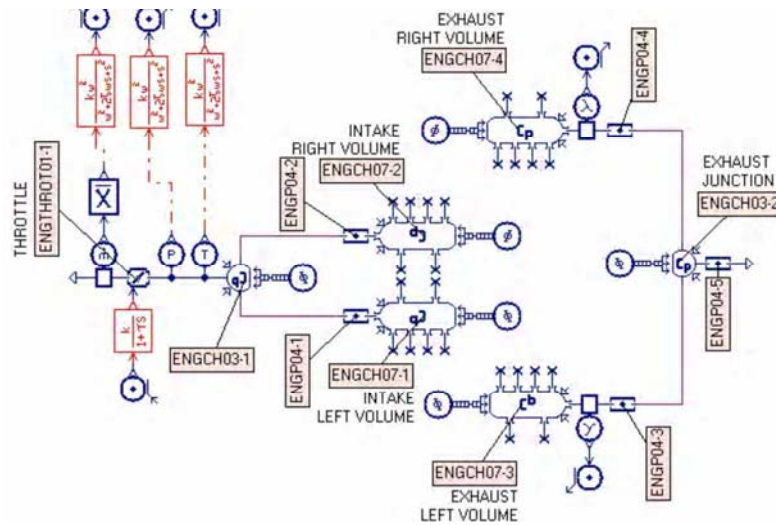
Figure 4.53 – Air path model assembly with throttle body and sensors [cylinders not represented]. Each sensor's raw signal is scaled and filtered. Both intake and exhaust manifold chambers can also be seen in Figure 4.51

A plenum type chamber models the intake volume for each bank. These volumes are fed from the throttle via two large diameter runs. During torque and speed transients, the volumes fill and empty depending on the engine air-charge and the throttle position. The capacities were set to match the manifold filling effects observed on the average engine torque output during drive cycles. The total capacity of the intake submodels is *14 L* with the throttle accounting for most of the pumping losses. The exhaust is modelled in much the same way. The V8 exhaust manifolds are modelled with volumes feeding a junction via two pipes. This set-up is only aimed at providing the head sub-models with a representative back pressure on the exhaust valves. The contribution of the exhaust gases pumping to the engine's losses is even smaller than the intake losses therefore no particular tuning was carried out on the exhaust sub-model parameters.

The throttle body model includes Mass Air Flow [MAF], IMAP and IAT sensors for engine control purposes. The signals are filtered with 2nd order Butterworth filters to eliminate noise from the controller inputs to Simulink.

Variable Name		Title	Value	Units
Fc	[global]	Cut-off frequency for Butterworth filters	20	Hz
ENGTHROT01_D		Throttle bore diameter	80	mm
ENGCHR03-1_total_volume		Throttle & 1st Intake chamber volume	5	L
ENGCHR07-1&2_total_volume		Intake plenum L & R volume	2	L
ENGP04-1&2_pipe_length		Intake run L & R length	100	mm
ENGP04-1&2_pipe_diameter		Intake run L & R diameter	100	mm
ENGCHR07-3_total_volume		Exhaust manifold L & R volume	4	L
ENGP04-3&4_pipe_length		Exhaust tube L & R length	700	mm
ENGP04-3&4_pipe_diameter		Exhaust tube L & R diameter	65	mm
ENGCHR03-2_total_volume		Exhaust junction volume	3	L
ENGP04-5_pipe_length		Exhaust tube length	1000	mm
ENGP04-5_pipe_diameter		Exhaust tube diameter	70	mm
Td_thr		Throttle actuation time constant	0.032	s

Table 4.7 – Local parameters for the air path sub-models. The intake and exhaust sub-models shown in Figure 4.53 are parameterised using real data or equivalences.

4.3.1.4 Environment and Controller Interface

With AMESim Engine library, a number of specific environment properties have to be set for application across the whole model. They cover the engine fluid specification for all thermo-dynamic sub-models, mechanical specification for combustion and valvetrain / head sub-models as shown on the left hand side in Figure 4.54.
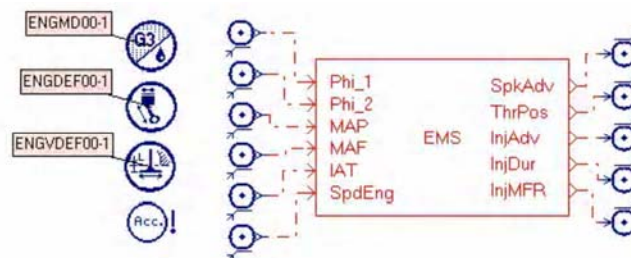
Figure 4.54 – EMS interface block for Simulink in AMESim with environment definition icons. In this co-simulation set-up, the sensor signals on the left are passed on discreetly to the Simulink EMS model which communicates the actuator commands on the right.

An interface block sends and receives global variables from the controller model in Simulink. These are exchanged between the two simulation environments at a fixed communication interval of *100 μs*, well below the loop-time of the controller presented in the next section.

Table 4.8 shows the environment properties definition for the engine model in AMESim. They mostly cover physical dimensions and architecture specific parameters that are central to all Engine library sub-components.

Variable Name	Title	Value	Units
ENGMD00-1_coefficient_x	Fuel x coefficient in C_xH_y	8	n/a
ENGMD00-1_coefficient_y	Fuel x coefficient in C_xH_y	18	n/a
ENGMD00-1_heating_value	Fuel heating value	44109	kJ/kg
ENGMD00-1_density	Fuel constant density	824	Kg/m^3
ENGDEF00-1_number	Number of cylinders for firing model	8	n/a
ENGDEF00-1_architecture	Engine architecture	'V'	n/a
ENGDEF00-1_angle	Engine 'V' angle	90	deg
ENGDEF00-1_bore	Engine cylinder bore	90.2	mm
ENGDEF00-1_stroke	Engine cylinder stroke	105.9	mm
ENGDEF00-1_length	Connecting rod length	160	mm
ENGDEF00-1_ratio	Engine cylinder compression ratio	10	n/a
ENGDEF00-1_order	Engine firing order	1-3-7-2-6-5-4-8	n/a
ENGVDEF00-1_intake_no	Number of intake valves per cylinder	1	n/a
ENGVDEF00-1_exhaust_no	Number of exhaust valves per cylinder	1	n/a
ENGVDEF00-1_intake_d	Intake valve equivalent diameter at max lift	41	mm
ENGVDEF00-1_exhaust_d	Exhaust valve equivalent diameter at max lift	39	mm
ENGVDEF00-1_intake_l	Intake valve max lift	9	mm
ENGVDEF00-1_exhaust_l	Exhaust valve max lift	9	mm
ENGVDEF00-1_intake_in	Intake valve in-flow coefficient at max lift	0.6	n/a
ENGVDEF00-1_intake_back	Intake valve back-flow coefficient at max lift	0.4	n/a
ENGVDEF00-1_exhaust_out	Exhaust valve out-flow coefficient at max lift	0.6	n/a
ENGVDEF00-1_exhaust_back	Exhaust valve back-flow coef. at max lift	0.3	n/a

Table 4.8 – Properties for engine environment definitions. They are associated with the environment definition icons shown in Figure 4.54
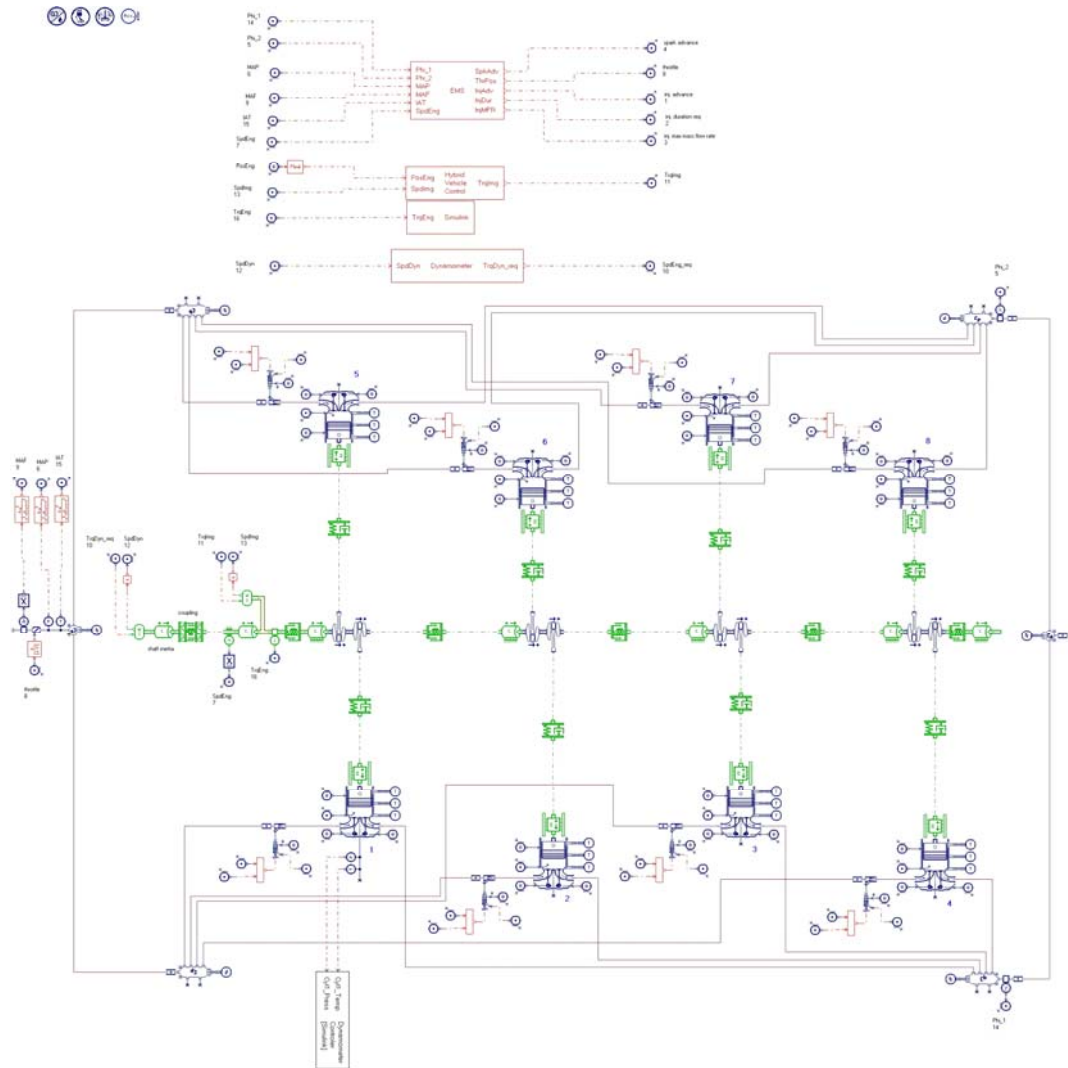
Figure 4.55 – Complete AMESim model of the Ford Triton 5.4l V8
gasoline engine with interface to Simulink for EMS controller model

Figure 4.55 shows a complete view of the graphical layer for the engine plant model described above. It includes the intake sub-assembly on the left hand side, the exhaust sub-assembly on the right hand side, the crankshaft in the centre and the EMS Simulink interface at the top. A number of additional blocks related to the integration of the model within a powertrain simulation environment appear on the left end of the crankshaft and will be discussed in the next chapter.

4.3.2 Controller Model

The controller for the AMESim plant model is executed in Simulink and runs co-simulated between the two modelling environments. Simulink offers a controller design environment facilitating later integration with other powertrain control strategies during this research effort.

The architecture of EMS model illustrated in Figure 4.56 is not extensively representing a complete application because there is no need for torque controllability. Moreover, the output requirements for the EMS are set by the input requirements of the engine model presented Figure 4.54 which eliminates the need for low level layer of control strategy for the actuators.
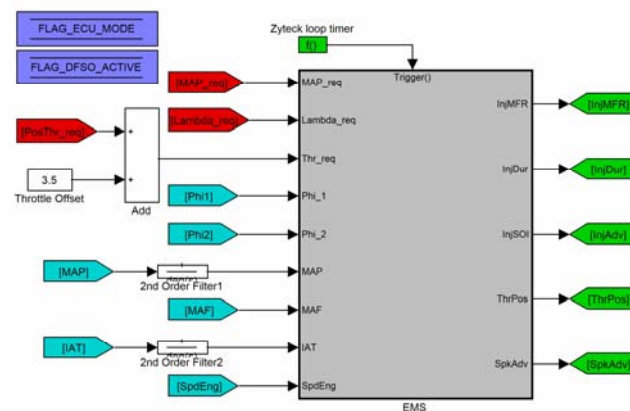
Figure 4.56 – EMS model block in Simulink. A trigger function simulates the loop time in a real ECU and the inputs and outputs correspond to these illustrated in Figure 4.54

Closed-loop throttle control for the engine torque output is not an important requirement for the current modelling task. However critical such a strategy is in this research effort, the objective of the simulation is to develop the Active Vibration Controller and verify LSHT operability of the system. Consequently the throttle is a direct feed forward control signal. A first order filter at *32 ms* time constant simulates the actuation delay in the ETC as mentioned above.

Sparking is controlled from a look-up table using the data gathered from a real engine as previously detailed. The spark advance is therefore defined for warm engine condition at the test conditions of *1.013 bar* atmospheric pressure and *19 degC* ambient air temperature. The look-up table [Figure 4.57] is based on the engine speed and the load indicating manifold pressure sampled in AMESim.
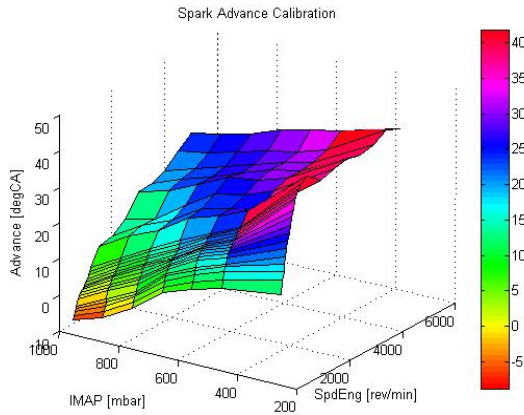
Figure 4.57 – Spark advance calibration in degCA as from the dynamometer measurements presented in Section 4.2.2
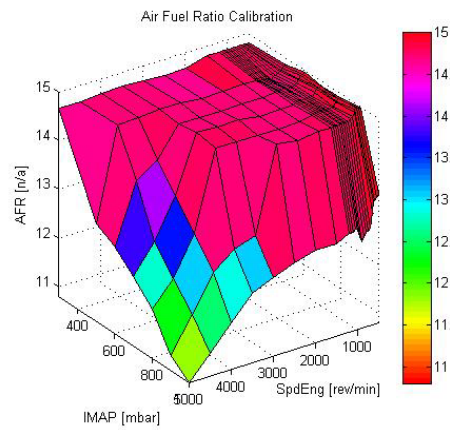
Figure 4.58 – Air fuel ratio calibration as from dynamometer measurements presented in Section 4.2.2

4.3.2.1 Fuel Injection Control

The fuelling strategy illustrated in Figure 4.59 is the core functionality of the EMS model. To ensure an accurate recreation of the engine torque fluctuations according to the requ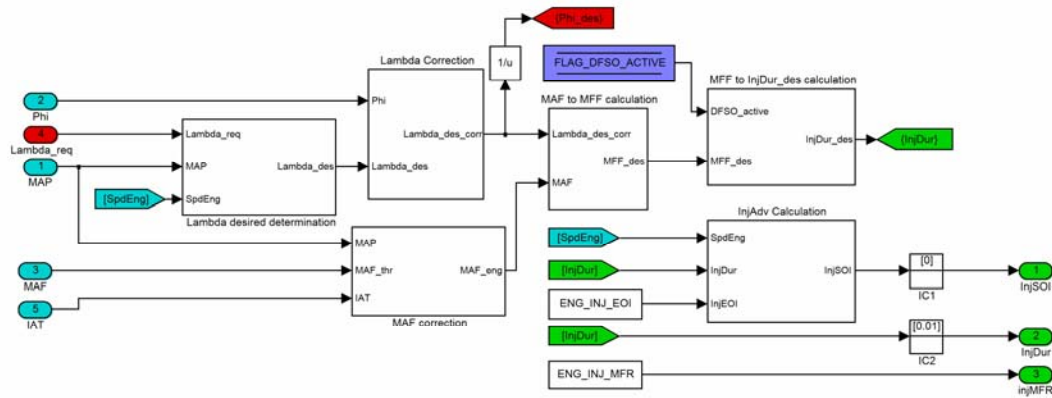irements of Section 4.1, the control signals sent to the injector sub-model have to be based on realistic sensing in the plant model rather than setting-up a stoichiometric supply to the combustion models and eliminate injectors. This ensures the contribution of fuelling delays to the torque transients.

Figure 4.59 – EMS fuelling strategy model. Based on the engine load and speed, the model derives the desired lambda value according to a look-up table. The actual engine air charge *MAF_eng* is derived from the throttle MAF, the IMAP, and the charge temperature. The model then established the subsequent injector opening time *InjDur*, and adapts the start of injection to maintain a constant end of injection crank timing

The Mass Fuel Flow [MFF] desired is calculated from the estimated engine MAF, i.e. the air charge effectively entering the cylinders past the injectors. Equation 4.3 shows the relation between the two depending on the desired lambda value [λ]. The target lambda is itself defined from a look-up table [Figure 4.58] similar to the sparking strategy and defined from the dynamometer tests.

$$MFF\_des = \frac{MAF\_eng}{Lambda\_des \cdot ENG\_STOECH\_AFR}$$

Equation 4.3 – where *MFF_des* is the desired mass fuel flow per cycle, *MAF_eng* is the estimated cycle air charge and *ENG_STOECH_AFR* is the stoichiometric AFR constant

The engine MAF is estimated using a manifold filling and emptying model as shown in Equation 4.4.

$$MAF\_eng = MAF\_thr - MAF\_man$$

Equation 4.4 – where *MAF_thr* is the measured mass air flow through the throttle, *MAF_man* is the derivative of the mass of air inside the manifold

The throttle MAF is measured by a sensor sub-model in AMESim and the change of air mass inside the manifold *MAF_man* is defined with Equation 4.5.

$$MAF\_man = \frac{V_{man}}{R} \cdot \frac{d}{dt}\left(\frac{IMAP}{IAT}\right)$$

Equation 4.5 – where *V_man* is the intake manifold volume and *R* is the perfect gas constant

The injection duration is finally set in [s] using the desired *MFF* and the rated injector mass flow rate [Equation 4.5]. The injector mass flow rate constant was adjusted so that the controller model matches the real EMS injection duration at a given *MAF*.

$$InjDur = \frac{MFF\_des}{\frac{4}{60} \cdot SpdEng \cdot InjMFR}$$

Equation 4.6 – where *InjDur* is the target injection duration, and *SpdEng* is the engine speed and *InjMFR* is the injector mass flow rate

4.3.2.2 EMS Model Inputs and Plant Model Outputs

The engine controller described above receives a throttle command from the Simulink environment. The engine speed is set in AMESim for the purpose of this modelling exercise. In the next chapter, the engine and controller created are integrated into a powertrain simulation. The engine speed and throttle position command will then become the interface between the engine / controller model and the rest of the other models within the Simulink environment.

There are a large number of outputs from the model. The port interfacing of the submodel allows sampling of any physical variable exchanged between the sub-models described previously. However, engine output torque, manifold pressure [IMAP] or cylinder pressure were of particular interest therefore sampled in AMESim and fed back into Simulink for logging purposes.

For the purpose of model validation and performance analysis, the controller was run with direct user inputs in a first instance to replicate both steady state operation and transient. The following paragraphs present and discuss the simulation of the model under these conditions.

4.4 Performance Analysis

The aspects of model validation and tuning discussed above were executed at various stages of the simulation platform development. They were based on the experimental data gathered on the dynamometer then later in the EASIVT project during the implementation phase of the hybrid controller and its subsequent calibration. This section highlights the quality of the predictions offered by the model in view of the requirements previously highlighted. The limitations of the model are also emphasised in order to justify the integration of the engine and associated EMS into the powertrain simulation environment presented in the next chapter.

4.4.1 Combustion Related Torque Oscillations

This was set to be the main objective of the modelling exercise and was therefore at the core of the modelling exercise. The following actions were subsequently taken:

- All known physical dimensions were implemented in the plant model [bore, stroke and valve train parameters]

- Sparking and fuelling calibrations were carried over to the controller model [Figure 4.57 and Figure 4.58]

- Engine model combustion parameters were tuned to match the pressure profiles [Table 4.5]

- Engine inertial values were carried over; reciprocating masses were estimated; friction characteristics [Table 4.6] were tuned to match available engine friction data.

Figure 4.60 and Figure 4.61 show the level of accuracy reached by the engine head and combustion models at full load.
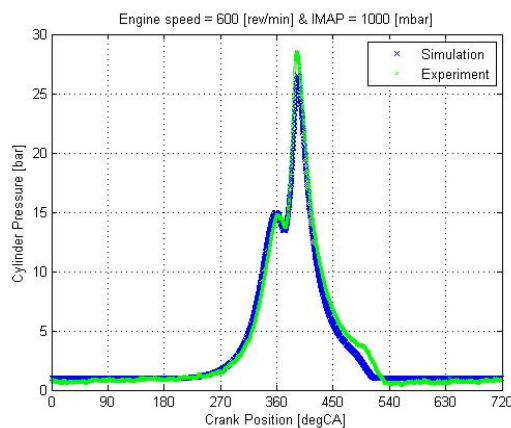
Figure 4.60 – Model correlation of cylinder pressure at *600 rev/min* and *1000 mbar* IMAP.
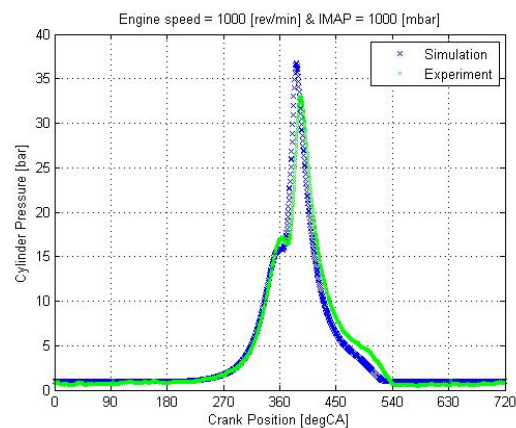
Figure 4.61 – Model correlation of cylinder pressure at *1000 rev/min* and *1000 mbar* IMAP.

Due to time constraints and limitations to the number of calibration parameters within the sub-models, the combustion model is tuned mostly in full load. The high degree of correlation obtained between experimental and simulated pressure measurements within LSHT region [*500* to *1200 rev/min*] is the pre-requisite to obtain satisfying torque oscillation power-on transient torque predictions.
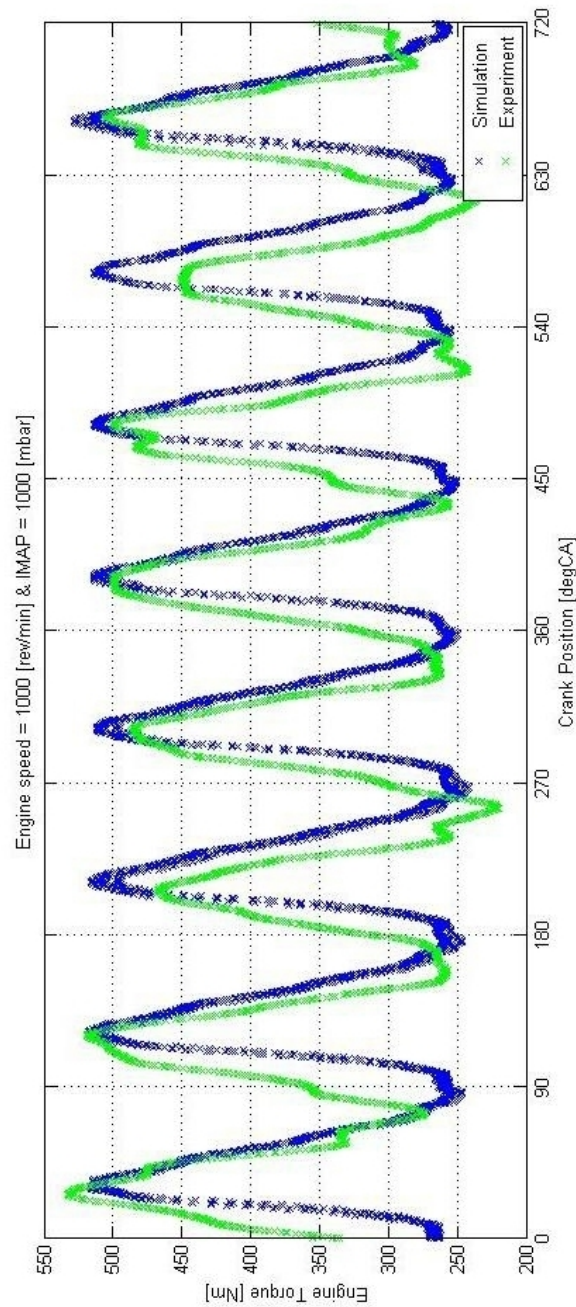
Figure 4.62 – Model correlation of torque output at *1000 rev/min* and *1000 mbar* IMAP over a number of engine cycles. This shows the satisfying level of accuracy obtained with the model. *15 Nm* is the average torque difference and the phase of the oscillations differs by less than *5 degCA*

Figure 4.62 shows the comparison of the real engine torque output as measured on the dynamometer against the model output in steady state operation at *1000 rev/min* full load. The following observations can be made:

- Both signals exhibit an offset sine wave shape at 4 times the engine rotational frequency – the firing frequency.

- The average torque, i.e. steady state value – is very similar with less than *15 Nm* [*4.2 %*] difference on this particular operation point.

- The amplitude of the combustion related torque oscillations is well predicted, but the model is unable to predict the cylinder to cylinder variations characteristic of poor combustion repeatability at low speed.

- The phase of the torque output main frequency component is predicted within a few crank angle degrees [less than *5 degCA*]. This is observed at the peak values of torque; however the experimental torque is a more distorted sine wave which can be observed in the bottom lumps between the combustion events. This is largely due to inaccuracies in the reciprocating masses and valve train models.

In conclusion, the model established meets the requirements set at the start of the exercise for the combustion torque oscillations predictability. The following section examines the simulation of load and speed transients.

4.4.2 Engine Load Transients and Powertrain Shifts

Another important aspect of the engine model performance is the engine load transient and transmission controlled speed variation, i.e. powertrain shifts. Although accuracy levels are not as critical as the torque fluctuation prediction, this aspect of the model operation will allow the testing of the AVC controller during transients in LSHT region in simulation.

The model torque output was compared against the IVT controller torque estimation during an FTP74 drive cycle carried out of the vehicle dynamometer. Because the model does not have the torque control functionality of the real EMS, a throttle position log was taken to control the engine model instead of a torque request. This effectively tests the engine model independently of a torque controller performance. The model is controlled during the simulation at the same engine speed and subsequently throttled in the exactly same conditions as during the experiment.

Figure 4.63 shows a comparison of simulated and experimental torque during the first *100 s* of the drive cycle. The simulated torque was filtered to eliminate the torque fluctuation and allow a graphical correlation of the average value with the experimental data. The top graph shows the exact speed correlation executed by the simulation set-up. The bottom graph shows how closely the model can predict the engine torque output. Differences are mainly in the steady state operation where the simulation systematically under estimates. The speed and torque transients show a very good correlation between model and experiment, therefore satisfying the requirement previously established.
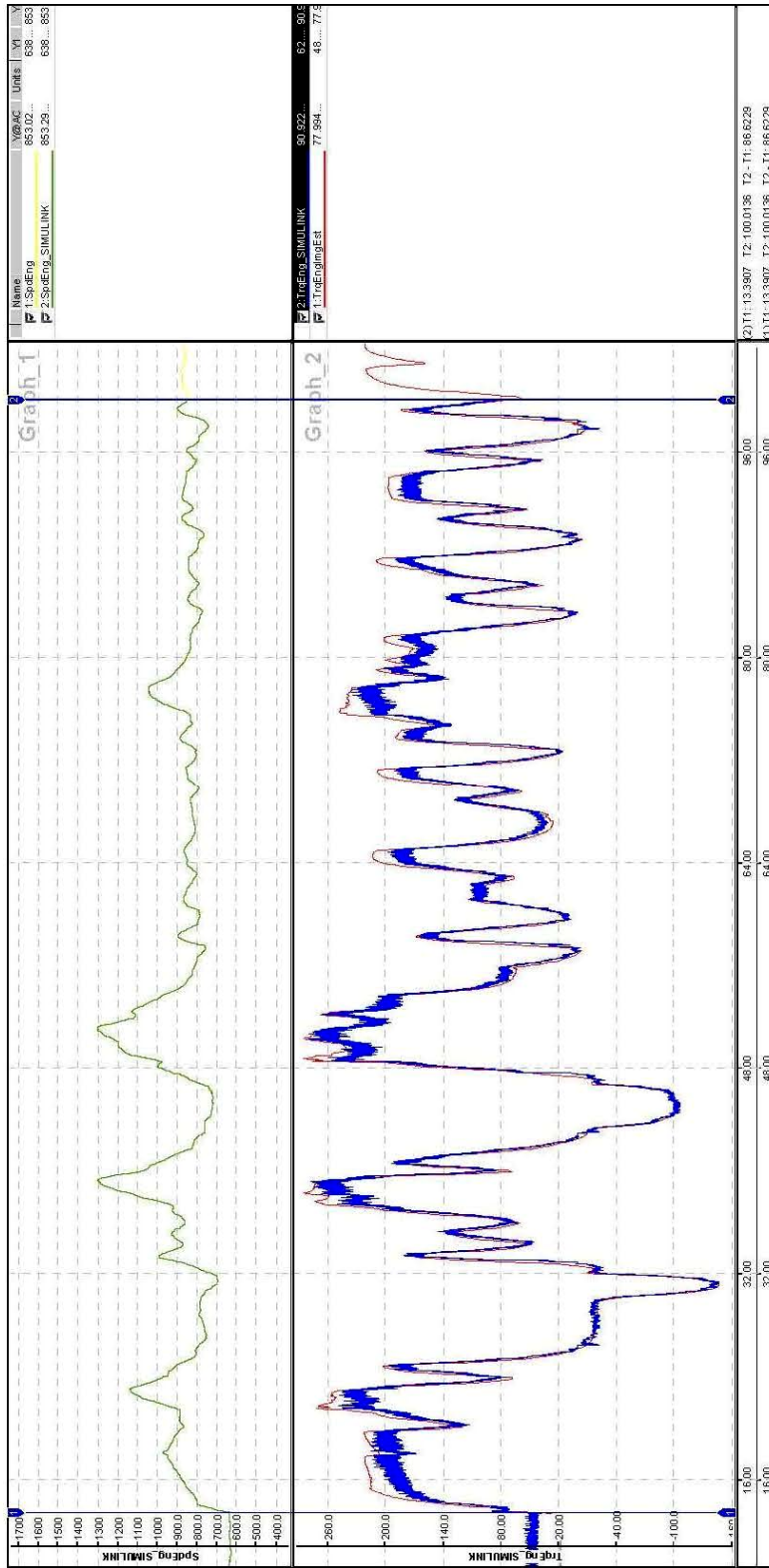
Figure 4.63 – Comparative run over first 100s of FTP74 drive cycle. The engine model is compared to vehicle data with the same throttle command log and a controlled engine speed to replicate the same operating conditions. The engine speed is displayed on the top graph in green. On the bottom graph, the vehicle engine torque is in red and the simulated torque is in blue. The engine model torque fluctuations are filtered for clarity.

4.4.3 Limitations

There are inevitably a number of limitations within the engine model and controller. A number of these were set from the start when the modelling requirements were specified. The following conditions were excluded or had no particular accuracy requirement:

- Cold starts are not investigated. Although some rather straight forward modifications could be implemented in the AMESim plant model for that purpose, the development of an appropriate and representative cold start strategy in the EMS model would involve major upgrades in the sparking and fuelling strategy. The combustion models employed would also reach the limits of their capability. Cold starts could however be of interest for any NVH biased controller.

- Fuelling, sparking and combustion related cylinder to cylinder torque fluctuations. Due to uneven air charge, fuel injection & mixing hysteresis, poor sparking repeatability or combustion instability, the engine torque output is never completely even, especially at low speed. The frequencies characterizing these phenomena are logically lower than the firing frequency.

- High speed engine operation is of no interest for a LSHT strategy therefore no model tuning effort was carried out above *2000 rev/min*

Within the scope of the modelling exercise, mid to low engine load operation shows the lowest levels of accuracy. Figure 4.64 shows the difference in cylinder combustion profiles between experiment and simulation at *1000 rev/min* and *700 mbar* IMAP, corresponding to *16 %* throttle.

Although there is no particular divergence between experimental and simulation results observed in the low load operation of the engine, the effects of a model tuning exercise in the full load region are visible. This does not compromise the quality of the work achievable using the models, but introduces a lower level of confidence in the prediction accuracy out of the LSHT region.
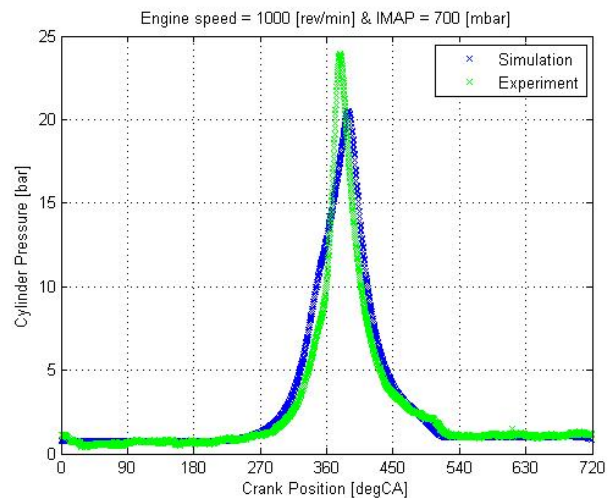
Figure 4.64 – Model correlation of cylinder pressure at *1000 rev/min* and *700 mbar* IMAP showing poor accuracy.

4.5 Closing comments

A V8 engine model and controller were established and simulation can now be run from the Simulink environment. The level of modelling details in both plant and controller are chosen to match the operation requirements set at the beginning of the chapter. These focus on the torque oscillation due to the combustion events at a 4th order of the engine rotational frequency.

The model has been tuned and validated using in-cylinder pressure measured on an engine dynamometer at various speeds and loads of the engine LSHT region. The engine mean output torque was validated against vehicle dynamometer data to ensure acceptable levels of accuracy are reached during speed and torque transients.

This engine model is the starting point of the powertrain simulation created in the next chapter for AVC strategy development purposes.

Chapter 5: BEST BSFC AND NVH CONTROL IN HYBRID CVT POWERTRAIN

Following the development of the V8 engine model, simulations were established to develop a control strategy for the IMG in the EASIVT vehicle capable of reducing the amount of vibrations in the LSHT region. This enabled a modified engine operation that matches the hybrid IVT powertrain requirements for fuel economy. The hybrid control strategy developed in parallel also ensured that driveability standards are maintained if not increased in the hybridisation process.

5.1 EASIVT Hybrid Powertrain

5.1.1 Baseline IVT Strategy & Compromises

The following paragraphs develop the analysis of the IVT operation initiated in Chapter 2 to explain how the CVT controller ideal strategy is altered to work around engine operation limitations highlighted in Chapter 1.

5.1.1.1 Engine Operation Control

The engine operating conditions are determined from the vehicle speed and the driver pedal demand. A wheel torque request and a driver requested engine speed are set from a calibrated look-up table. In turn vehicle speed and wheel torque request determine the engine requested power using a transmission efficiency model. The engine operating condition strategy inputs are therefore requested engine power and driver requested engine speed. The latter reflects the driveability requirement for an engine speed that matches the vehicle acceleration feel.

The IVT is a torque controlled transmission that benefits from a high overdrive ratio [Appendix A] allowing virtually any engine operating condition to be used for most vehicle speeds. The maximum ratio enables overdrive down to *1000 rev/min* engine speed at *119 km/h* vehicle speed. However, a number of constraints are taken

into account to formulate the actual steady state operating condition from the power request into the IVT.

- ▪ The ideal operating torque [*TrqEngSFC*] for the given power request [*PwrDriverReq*] which gives an engine speed for best BSFC, i.e. on the fuel economy IOL.

- ▪ The weight of the aforementioned SFC point depending on *PwrDriverReq* and the accelerator pedal position *PosPedal*.

- ▪ The engine torque *TrqEngDriverReq* derived from *SpdEngDriverReq*. This is the driveability biased engine operating condition.

- ▪ The weight of the aforementioned driver set-point depending on *PwrDriverReq* and PosPedal.

- ▪ The minimum engine speed [*SpdEngNVH*] which ensures that undesirable engine vibrations are avoided in the LSHT region. This varies with vehicle speed *SpdVeh* and *PwrDriverReq*.

Consequently, the engine steady state torque request which will be reacted by the IVT to produce the required wheel torque is a weighted average of *TrqEngSFC* and *TrqEngDriverReq*, which is altered to ensure that the *SpdEngNVH* minimum is achieved. This limit can have detrimental effects to the actual position of the engine operation set-point, as developed in the following paragraphs.

5.1.1.2 Effects of NVH minimum speed

Figure 5.65 presents the NVH related minimum target speed which effectively shifts the best SFC operation of the engine. Only the low power speed operation is modified by thislook-up table because higher power requires greater engine speeds.
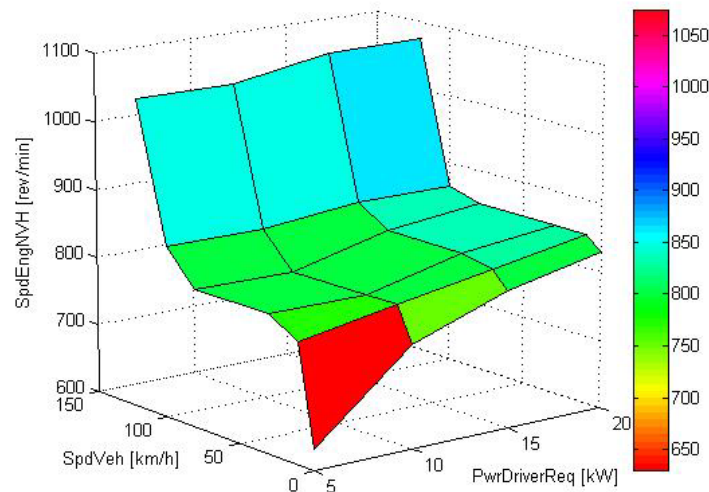
Figure 5.65 – Minimum engine speed for NVH strategy depending on vehicle speed and driver power request on engine. The speed is maintained above *800 rev/min* apart from back-out pedal position at low vehicle speed.

Incidentally, in these low engine power conditions, the SFC operation is preferred to driver requested engine speed. For most of the small pedal inputs, the driver requested operating point is indeed less important and SFC operation has no direct effect on the driveability attributes of the powertrain. Figure 5.66 and Figure 5.67 show the calibration tables containing the aforementioned weights.
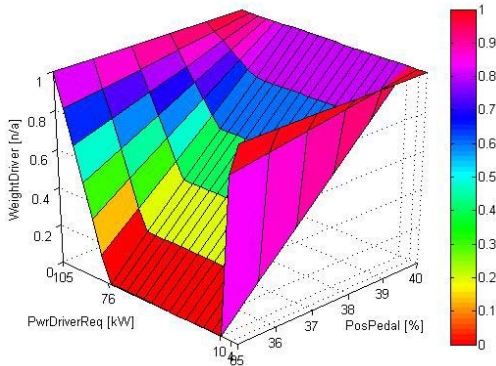
Figure 5.66 – Driver request weight in baseline IVT calibration. All pedal inputs above *40 %* will results in driver biased engine speed operation. Figure 5.67 shows the complements.

Figure 5.67 – SFC operation weight in baseline IVT calibration. At pedal position below *35 %*, SFC operation prevails, apart from power requests below *10 kW*

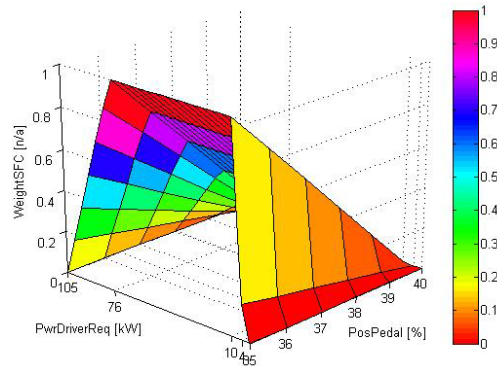There is however a subtlety in this calibration where power requests less than *10 kW*, i.e. back-out situations see the driver weight maintained at *1* and effectively ensures that the NVH minimum speed limit is always achieved. This shows how the IVT high overdrive and fuel saving potential is compromised in order to avoid LSHT operation and its associated NVH problems. Effectively, the BSFC obtainable from the 630 rev/min idle speed is never used and the engine speed is kept above the minimum speeds shown in Figure 5.65. Table 5.9 shows the potential fuel economy predicted in simulation if LSHT operation was permitted, and then if lower engine speeds were used in the lowest end of the engine power spectrum by reducing the idle speed.

Vehicle Configuration	Baseline IVT			
Environment	Backward model simulation			
Test weight	2495			kg
Crankshaft inertia	0.2473			kg.m²
FUEL ECONOMY				mpUSg
	Engine operation strategy			
Drive Cycle	Standard	No NVH IOL	No NVH IOL & 520 idle	
FTP 75 city cycle	16.96 REF	17.56 -3.49 %	18.28 -7.78 %	
HWFET highway cycle	22.77 REF	22.99 -0.97 %	23.05 -1.24 %	

Table 5.9 – Fuel economy predictions for baseline IVT vehicle from backward model simulations [19][77]. The penalty of the NVH IOL is particularly sensitive in the low power city cycle. The potential benefit of a reduced idle speed is therefore *7.78 %* and *1.24 %* for city and highway cycles respectively.

The engine operation strategies investigated in simulation [19] against the baseline calibration in Table 5.9 are illustrated in Figure 5.68.
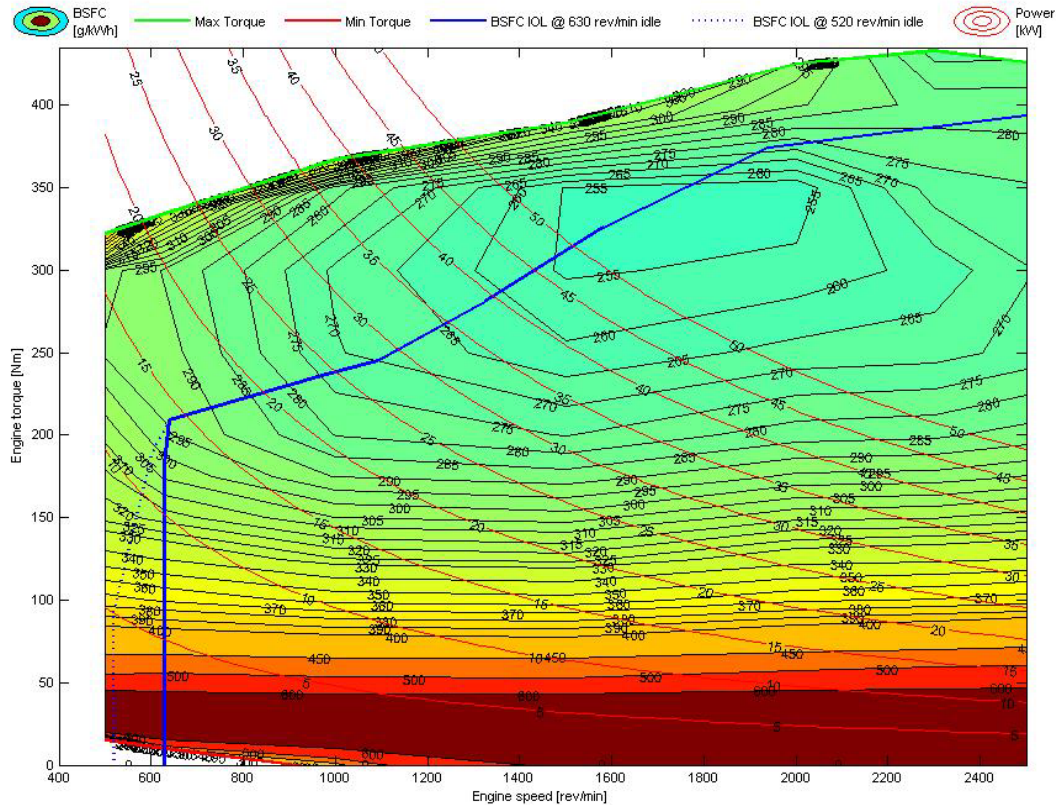
Figure 5.68 – BSFC Ideal operating lines for Ford 5.4L V8 engine. The blue IOL is where the engine would be operated in steady state in the LSHT region if NVH restrictions were ignored. The dotted blue line suggests further improvement in the BSFC IOL by reducing the idle speed from *630* to *520 rev/min*. Both strategies were evaluated in simulation [Table 5.9]

The NVH minimum engine speed has a predicted impact of *3.5 %* fuel economy in the EPA 75 drive cycle. The EPA highway cycle at higher power requests is less sensitive to the LSHT operation. Furthermore, if the low speed torque qualities of the V8 engine could be matched to the IVT high overdrive, the idle speed could be reduced to *520 rev/min* and an estimated *7.8 %* fuel economy could be gained over the baseline figures. These initial considerations are the starting point to an engine operation matching exercise including the hybridisation of the powertrain.

5.1.2 Hybridisation & Engine Characteristics Matching

5.1.2.1 Driveability Requirements

The calibration implemented in the baseline vehicle is not entirely based on fuel economy optimisation. Driveability is a very important aspect, even in the low power, low pedal demand situations where the engine speed transient control of the engine is critical. The previous paragraphs present the baseline steady state strategy and its sensitivity to fuel economy over a drive cycle. The transient operation of the engine introduced in Chapter 2 poses yet more challenges, especially in the LSHT region. Figure 5.69 shows the time constants employed by the transmission to estimate the manifold response lag to throttle control. The manifold dynamics are particularly slow in the LSHT region, causing large torque response delays.
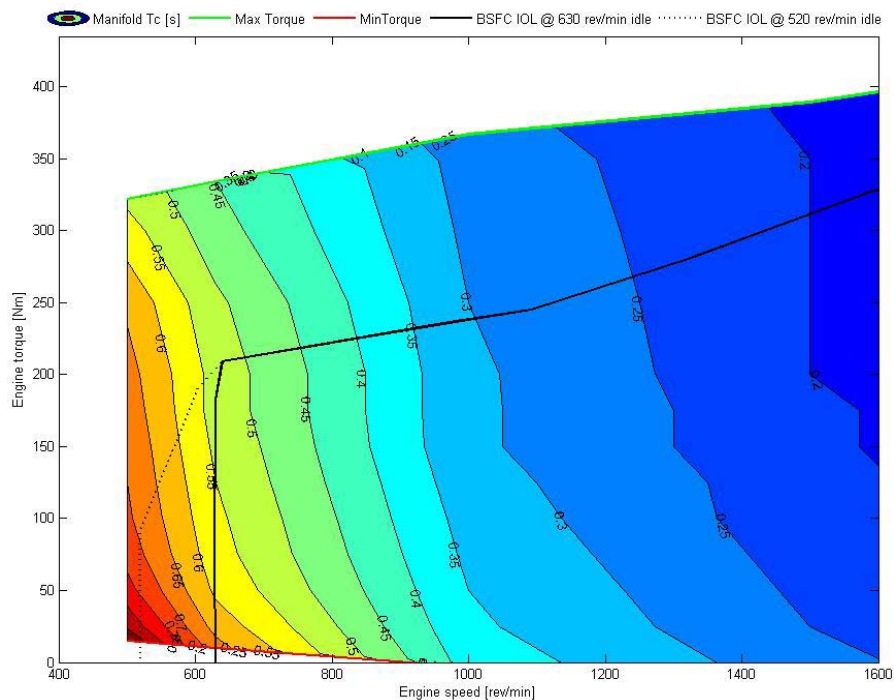
Figure 5.69 – Manifold dynamics model for Ford 5.4L V8 engine, time constant.
The smaller the engine speed the bigger the manifold delay, causing larger torque response lag.

The engine operation in the LSHT region poses the problems mentioned in the first chapter in relation to the torque margin available from steady state operation on the IOL to the maximum torque. Enforcing lower engine speeds on the IOL means that the torque response to throttle inputs will be slower. On the IOL at *800 rev/min*, the manifold lag is estimated at *0.42 s*. This time constant is up at *0.53 s* and *0.7 s* respectively at *630* and *520 rev/min*.

The engine speed control achieved by controlling the balance of torque output and reaction torque at the IVT input is directly affected by the manifold lag. Aggressive

LSHT operation results in slower powertrain dynamics and ultimately slower vehicle longitudinal response to pedal tip-in. The compromise between maximum fuel economy and driveability requirements is hereby highlighted.

5.1.2.2 EASIVT Hybrid Layout

The Electrically Assisted Infinitely Variable Transmission is the integration of parallel hybrid architecture to the IVT powertrain. The project demonstrates the fuel economy and driveability benefits offered by this hybrid IVT. The IMG is a crankshaft mounted electrical machine packaged between the engine and the transmission. Figure 5.70 illustrates the EASIVT hybrid architecture.
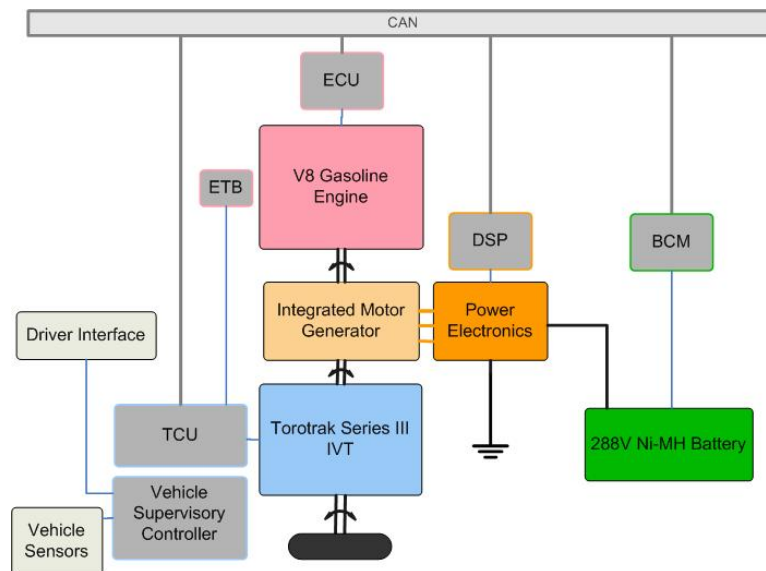
Figure 5.70 – EASIVT parallel hybrid powertrain architecture. The IMG is mounted on the crankshaft between engine and transmission, enabling direct torque assist. The power electronics inverter controlled via CAN is DC linked to a 288V 6.5Ah battery

The potential improvements to the powertrain are based on the following functions.

- Torque Assist [21][48]. By adding positive or negative torque at the transmission input shaft, the IMG can be used to control the engine speed and reduce throttle activity for that purpose. Appropriate control strategy of the IMG torque request should result in greater engine operation efficiency.

- Regenerative Braking [20]. During braking events, extra negative torque can be produced by the IMG to recover some of the deceleration energy otherwise dissipated by the conventional brakes. The energy stored can then be used for positive torque assist.

Moreover, the IMG can be used to reduce the torque fluctuation in the LSHT region which creates undesirable NVH levels. The engine and IMG power source would subsequently offer a better match for the IVT operation requirements for both fuel economy and driveability.

5.2 Noise Vibration and Harshness Study

To investigate the NVH problems associated with LSHT operation of the engine in the IVT baseline vehicle, the calibration of the vehicle controller was altered to force engine operation at constant torque and / or constant speed. The following paragraphs describe the information gathered during the tests carried out with the objective of LSHT operation in the EASIVT vehicle.

5.2.1 Test Plan

Figure 5.71 shows the instrumentation installed in the baseline vehicle for the purpose of the NVH study. The objective is to map the vibration and noise caused by the engine in the LSHT region using:

- Steady state operation and engine speed sweep at constant torque

- Vibration measurements on both sides of one engine mount with two tri-axial B&K 4506 accelerometers.

- Cabin noise measured using a Larson-Davis 2559 microphone and NVH levels assessed by driver and passenger during steady state operation.
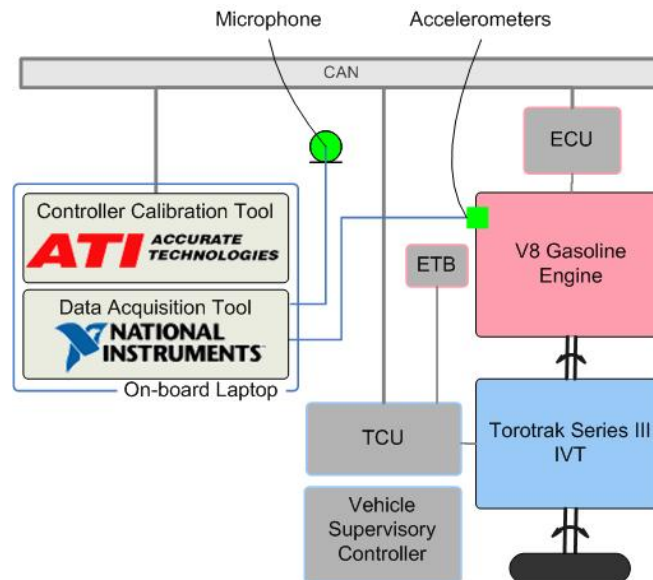
Figure 5.71 – Vehicle NVH Test Set-up. The accelerometers are installed on the engine mount and the microphone is inside the vehicle. LSHT torque operation is forced with a CAN calibration tool.

Assuming symmetry of the engine, transmission and chassis assembly, only one side of the engine was investigated and considered sufficient without cross checking with the other side. The two accelerometers were installed as shown in Figure 5.72 with definition of the relevant axis system. The same axis system was used for both accelerometers. Accelerometer 1 and 2 will be respectively referred to as engine side and body side. The y axis is the vehicle longitudinal axis.
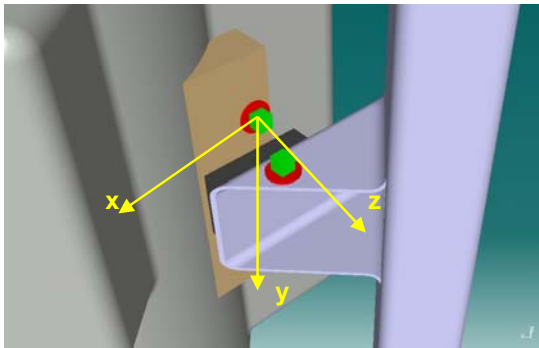
Figure 5.72 – Accelerometer setup. The sensors in green are located on each side of one engine mount.

| Accelerometer Type		Brüel & Kjaer 4506
Axes	n/a	3
Sensitivity	mV/g	100 (at 159.2 Hz)
Measuring range	'g'	±70
Temperature range	degC	-54 to +100
Frequency range	Hz	X: 0.3 to 5500 Y & Z: 0.6 to 3000
Dimensions [H x W x L]	mm	17 x 17 x 14.5
Weight	g	15
Min. sampling rate	kHz	10 (after LP filter)

Table 5.10 – Accelerometers specification, High sensitivity and wide dynamic range.

5.2.1.1 Scope & Method

Both steady state and transient tests were executed at a constant torque [apart from the full load tests] by means of flattening the engine look-up tables in the IVT controller. The vehicle acceleration during the steady state tests was kept to a minimum by starting the test from a reasonably high speed so as to offer the maximum frictional resistance. Transients were kept as slow as possible by increasing the total weight of the vehicle.
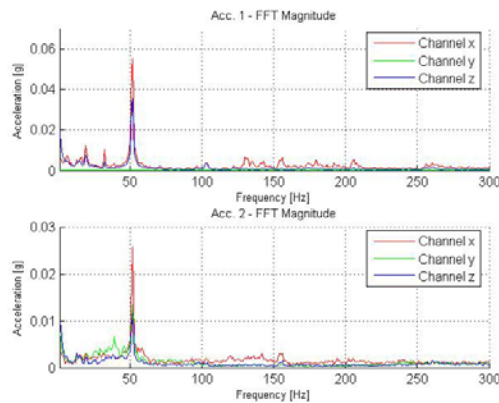
Figure 5.73 – Acceleration FFT plots for all 6 channels – one steady state test
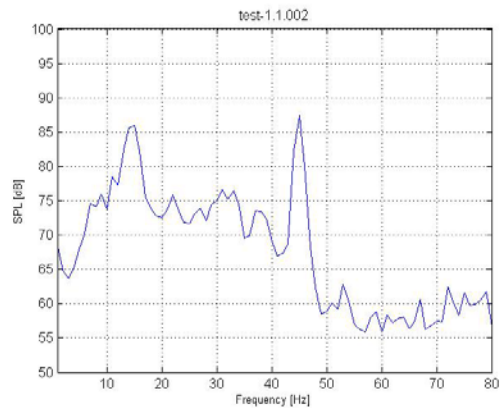
Figure 5.74 – Sound Power Level spectrum – one steady state test

The steady state test signals were post processed using Fast Fourier Transforms [FFT] of the 6 accelerometer signals averaged over a period of *5 s* at a resolution of *1 Hz* as shown in Figure 5.73. An FFT of the microphone signal using Hanning windowing characterised the Sound Power Level [SPL] spectrum expressed in dB as shown in Figure 5.74.The FFT spectra were then used to measure the 4th order peak value which then populated a table covering the speed range [*650 – 1000 rev/min*] at different torque levels *[200 Nm to WOT]*.

The transient tests were post processed one manoeuvre at a time and the data are presented by means of Campbell plots and waterfall displays. The engine speed

recording was used as the second dimension for the representation of the results. These tests do not exhibit the same accuracy as the steady state data for a particular torque and speed operating point. However they provide a broad picture of the sampled signals logged at once, hence eliminating repeatability problems such as sensor drift or temperature changes. Both Figure 5.75 and Figure 5.76 highlight the *order lines,* making the reading quick and clear.
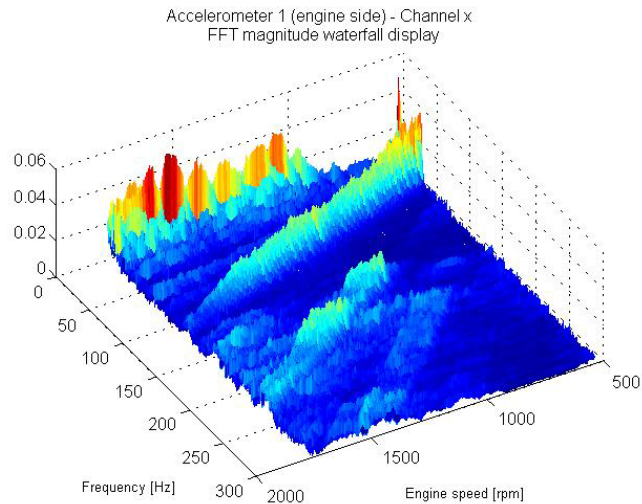
Figure 5.75 – Waterfall display of engine side x-acceleration. Typical transient test post processed data based on incremental FFT at *1Hz* resolution.
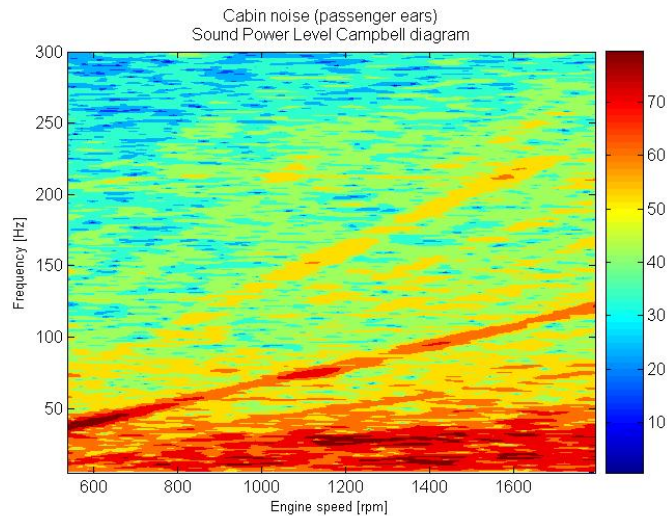
Figure 5.76 – Campbell plot of cabin Sound Power Level [SPL]. Post processed sound measurement during speed transient.

5.2.1.2 Noise assessment method

The noise present in the cabin was compared to the engine vibration frequencies. The sound was evaluated in three different ways:

- Driver and passenger subjective assessment [human ear]

- Steady state measurements [microphone]

- Transient measurements [microphone]

The microphone was placed in the most convenient position next to the driver's ear in between the two front seat headrests. The signal was pre-amplified and logged together with the acceleration levels. It was then converted into a SPL value in dB with reference to 20.10^{-6} Pa using a calibration signal [Equation 5.7]. The microphone specification can be found in Table 5.11.

Microphone Type		Larson Davis 2559
Sensitivity	mV/Pa	12.9 (-37.8$^{\pm 1.1}$ dB re: 1V/Pa)
Measuring range (±2dB)	Hz	4 to 25,000
Lower limiting frequency	Hz	1
Resonant frequency	kHz	23
Influence of vibration	n/a	65 dB re: 20µPa @ 0.1g
Diameter	mm	13.2

Table 5.11 – Microphone specification. The sensor is then associated to a PRM 902 pre-amplifier

$$L_P = 20 \cdot \log_{10}\left(\frac{p}{p_0}\right) \text{ where } p_0 = 20 \cdot 10^{-6}\,Pa$$

Equation 5.7 – where L_p is the SPL value in dB of the pressure p

In-vehicle sound measurements offer poor repeatability because of the road noise and the weather conditions. Consequently, the subjective assessment by the passengers is a way of confirming the information supplied by objective measurements. These were first meant to be only steady state conditions. Because of the extended period of time necessary to carry out the steady state test, transient sound measurements were a more appropriate solution to a meaningful correlation of the vibration levels with the cabin noise.

5.2.2 Results & Analysis

5.2.2.1 Vibration Source Identification

As expected the main frequency component of both acceleration and sound signals was coinciding with the engine 4th order frequency, i.e. the firing frequency as previously mentioned. Figure 5.77 illustrates this phenomenon, with large vibration components at the engine firing frequency in the plane perpendicular to the crankshaft. This confirms the main source of engine vibration is its roll response to the combustion related torque fluctuations. The body side vibration levels are expectedly lower due to the rubber mounts energy absorption properties but they exhibit the same characteristics as on the engine side.
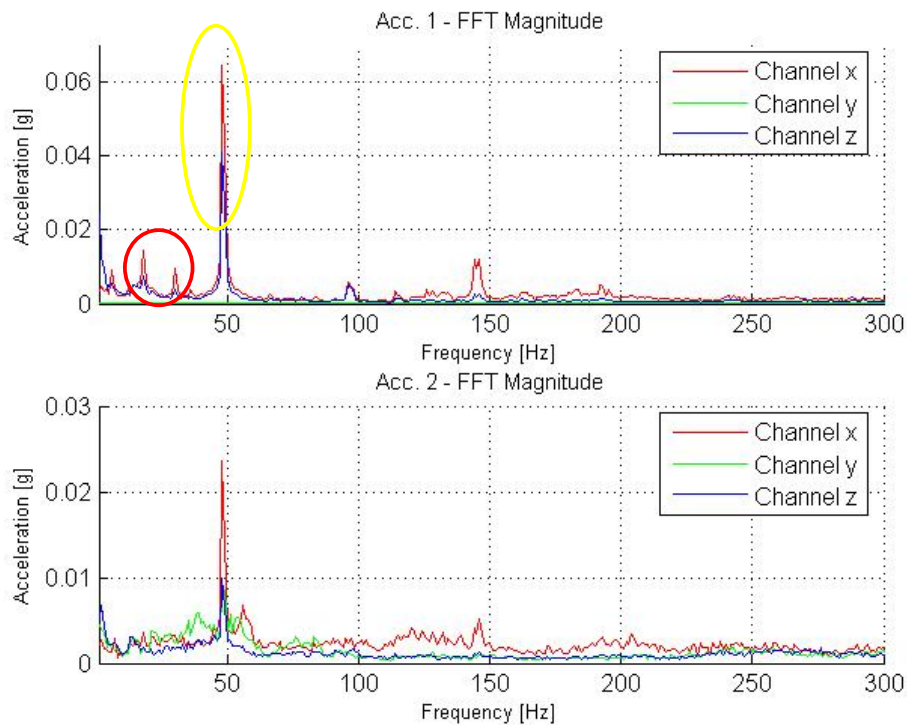
Figure 5.77 – Steady state data FFT @ *725 rev/min* [*12 Hz*] & full load. The x & z axis clearly show the highest level of vibration at the firing frequency [yellow circle]. Accelerometer 1 and 2 are respectively on the engine and body sides. 2nd and 3rd order engine frequencies [red circle] are absorbed by the engine mount.

Once identified for each 4th order peak, the steady state tests can be collated into a general table as explained previously. The engine side x axis – tangent to roll motion, consistently showed the highest levels at firing frequency, confirming that the engine roll motion provoked by its torque fluctuations is the main source of vibration in the speed range of interest. Figure 5.78 displays all the data collected during the steady state tests for the x axis on the engine side and body side and cabin.

The peak engine vibration clearly occurs below *725 rev/min*. Above this speed the engine vibration levels remain almost constant all the way through the speed range with exception of the *200 Nm* curve which is closer to a constant negative slope line. This is confirmed by the transient data in Figure 5.79 and Figure 5.80, which feature the same decreasing shapes of the 4th order line.

Cabin SPL and engine vibration are correlated; however, the highest vibration levels on the body side are not observed in the same region. This is clearly important information regarding the AVC control strategy calibration, indicating that the magnitude of vibration going through the chassis are not necessarily as important as the frequency.
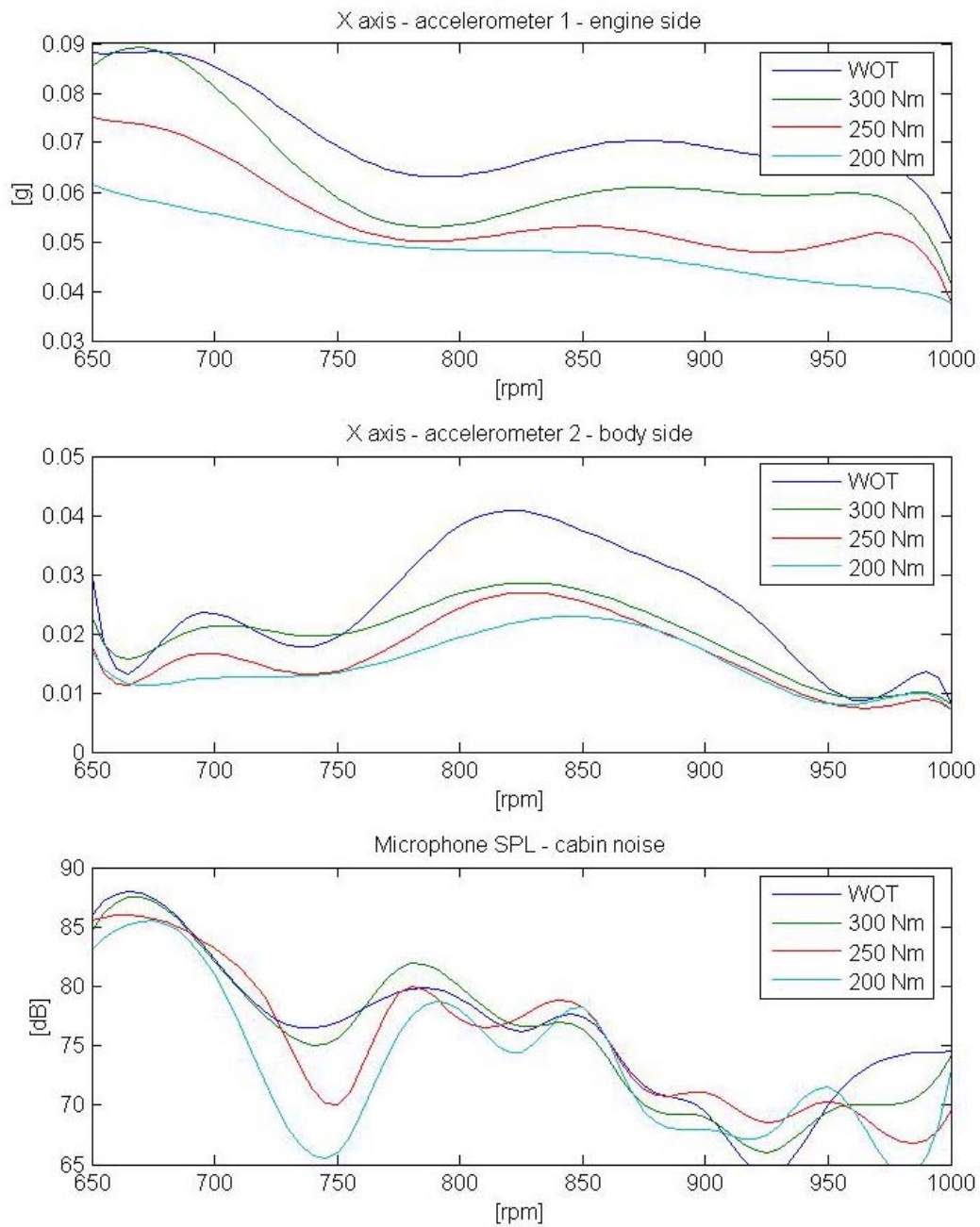
Figure 5.78 – Engine acceleration, body acceleration and sound correlation at various torque levels. The data are interpolated. The highest vibration values occur on the engine side and a satisfying correlation can be observed between engine torque and vibration level
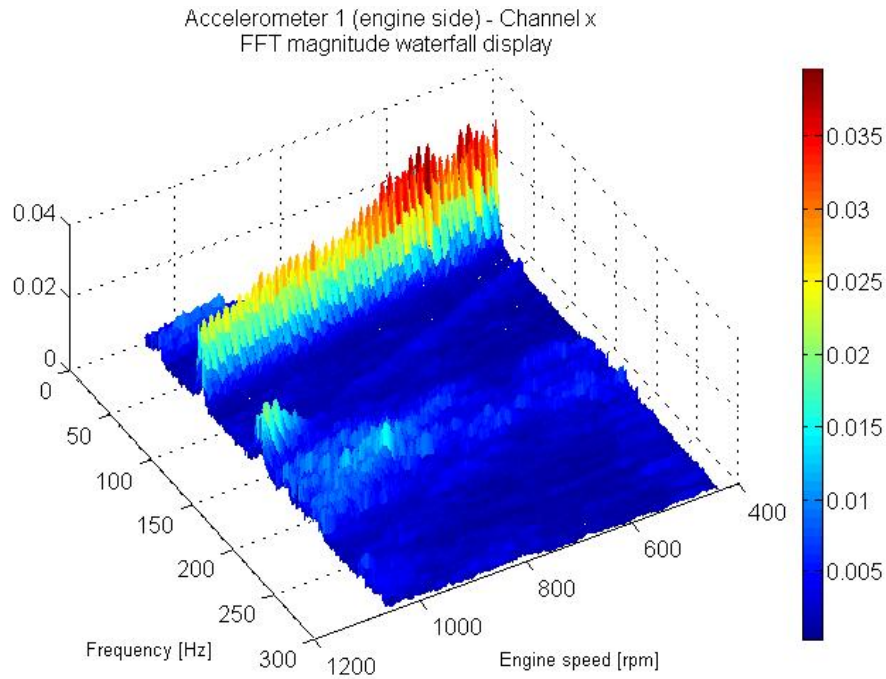
Figure 5.79 – Engine side x axis vibration during speed transient test at *200 Nm* constant torque. The highest levels occur below *700 rev/min*.
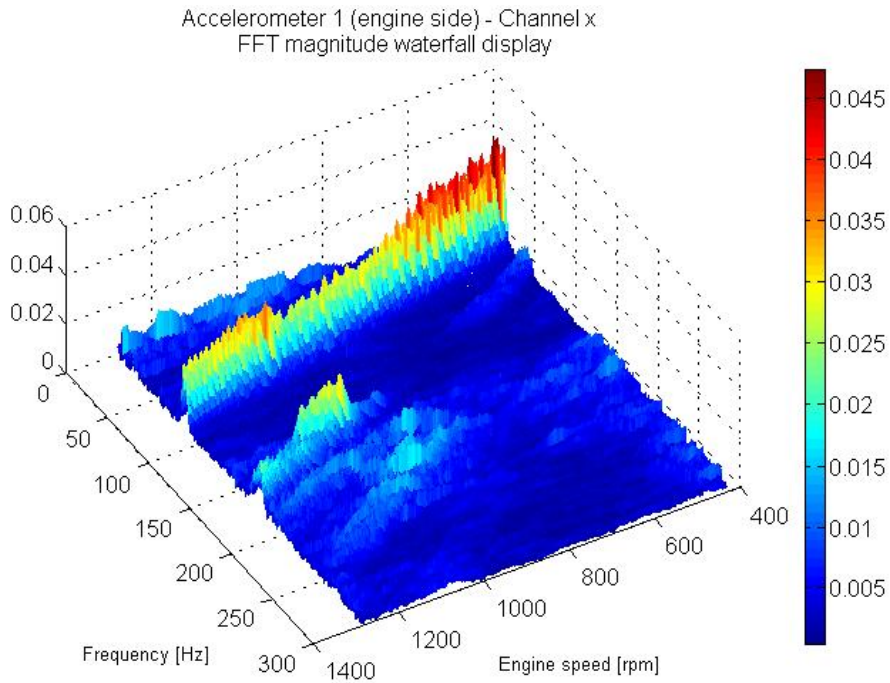
Figure 5.80 – Engine side x axis vibration during speed transient test at *300 Nm*. Constant torque. The highest levels occur below *700 rev/min*.

The effect of the engine mount compliance on the frequencies transmitted from the engine to the vehicle body is shown by comparing Figure 5.81 and Figure 5.82. The cut –off frequency of the engine mount appears at *900 rev/min*.
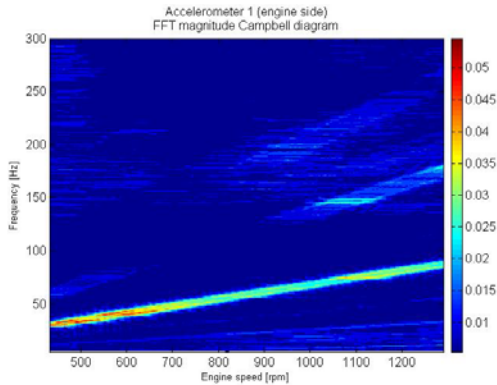
Figure 5.81 – Engine side x axis vibration during transient test at *300 Nm*. The highest levels occur below *700 rev/min* [data identical to Figure 5.80]
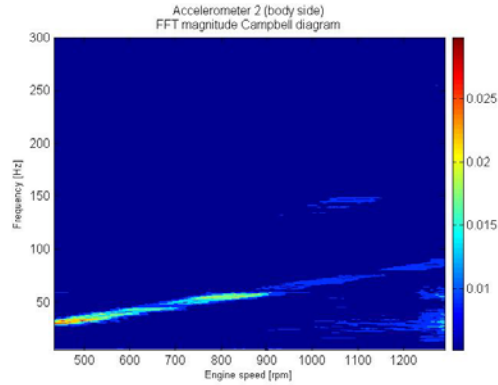
Figure 5.82 – Body side x axis vibration during transient test at *300 Nm* for comparison with engine side in Figure 5.81

The steady state data actually allows plotting a transfer function [Equation 5.8] for the engine mount in both x and z directions, shown in Figure 5.83. A maximum can be observed on both axes between *800* and *850 rev/min*, i.e. 4th order frequency between *53* and *56 Hz*. This confirms the observations made with the transient data above.

$$T_f{}^x(\omega) = \frac{A_{FFT}{}^{x2}(\omega)}{A_{FFT}{}^{x1}(\omega)}$$

Equation 5.8 – where $A_{FFT}{}^{x1}$ and $A_{FFT}{}^{x2}$ are the FFT of the vibration levels from accelerometer 1 and 2 respectively.
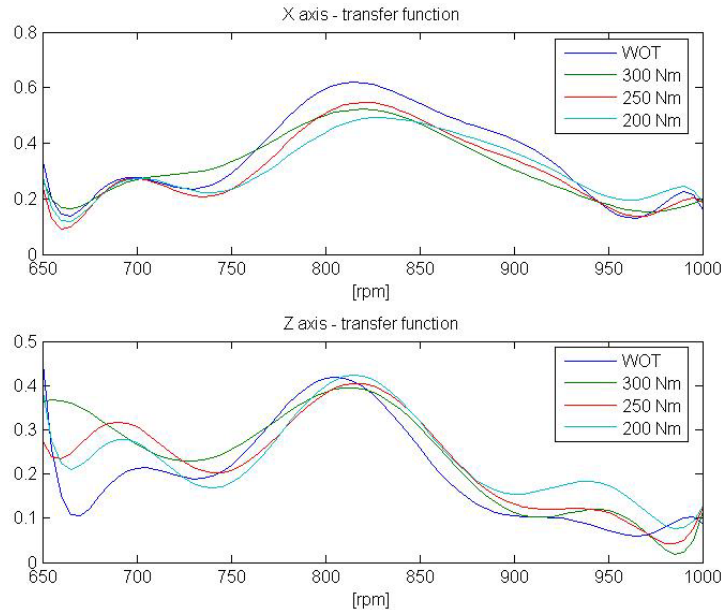
Figure 5.83 – Vibration transfer function of the engine mount in the cross plane, perpendicular to the crankshaft with polynomial interpolation

5.2.2.2 Vibration & Noise Mapping

Figure 5.84 and Figure 5.85 summarize the information presented so far, showing 4th order vibration levels measured during a succession of steady state runs of both sides of the engine mounting.
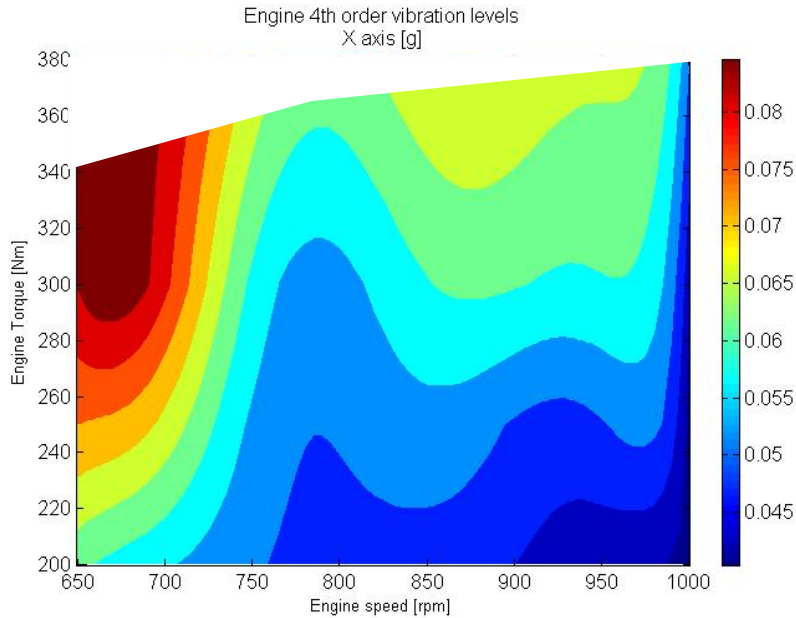
Figure 5.84 – 4th order engine vibration map extrapolated from steady state data as introduced in Figure 5.78
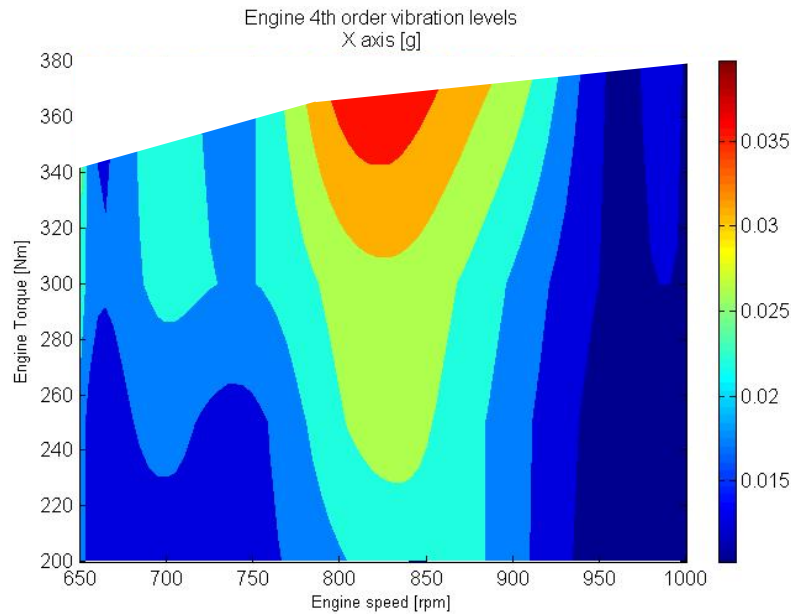
Figure 5.85 – 4th order body vibration map extrapolated from steady state data as introduced in Figure 5.78

The sound measurements during both steady state operation and transient manoeuvres bring another component to the previous deductions. From the passengers point of view the engine firing frequency vibration was clearly present in the cabin around *700 rev/min* and below in the form of abnormal 'growling' noise and a vibration felt at the passenger's feet through the floor panel. This is further confirmed by the data presented in Figure 5.86.
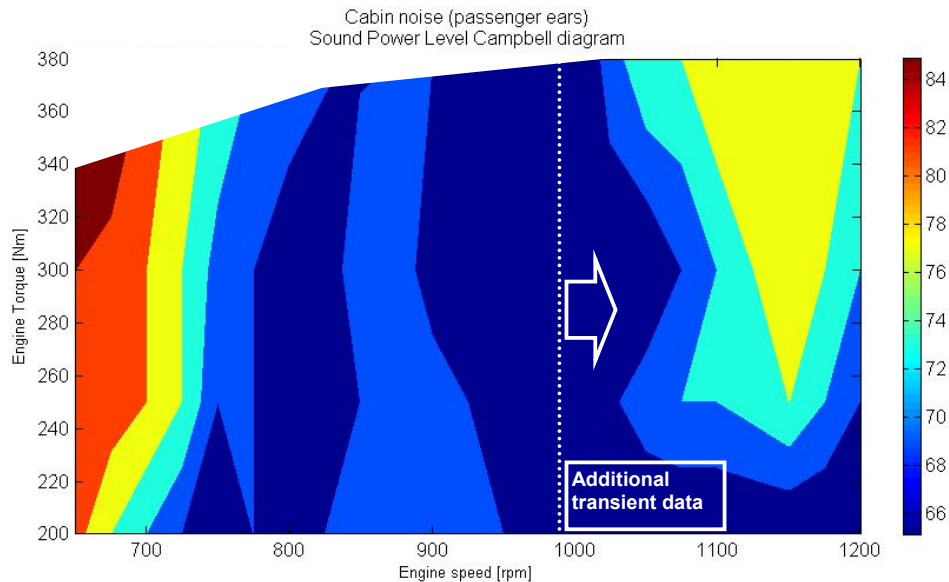
Figure 5.86 – 4th order cabin noise extrapolated from transient measurements.
The contours show the noise detected by the ear below *700 rev/min* and does not reflect the large transmission of vibration through the mount previously highlighted

5.2.3 Summary and teachings

- Vibration data are very coherent between steady state and transients in shape and magnitude.

- Among the three possible noise assessment methods, the steady state measurement was the most direct in order to quantify 4th order frequency noise. This should inform later development and calibration of engine borne NVH reduction strategy

- Vibration transfer to the cabin and noise radiation is worse at the lower end of the speed range than it is where the engine mount transfer function is peaking. This indicates that NVH counter-measures should focus on reducing the source noise at its worst – i.e. below *725 rev/min*, rather than where chassis excitation peaks [see Figure 5.83 and Figure 5.85].

5.3 Active Vibration Controller Design

The NVH investigations in the LSHT region presented above yielded maps of the engine and body vibration levels to inform the development of the AVC strategy. The model established in the previous chapter is designed to reproduce the torque oscillations identified and is integrated in a simulation environment including an IMG model for AVC testing.

5.3.1 Investigations in Simulation

The Ford Triton 5.4l V8 engine model established previously in AMESim is integrated into a Simulink powertrain model including the IMG and its associated power electronics. This is achieved in an effort to offer a test environment for the AVC strategy that is similar to a test bed. The specification for the IMG is shown in Table 5.12.

Cummins Power Generation IMG & PE Specification		
Topology	n/a	Dual stage axial flux
Number of poles per stage	n/a	12
Type	n/a	Permanent magnet
Maximum torque	Nm	±300 Nm
Rated torque [speed]	Nm	80 Nm [600 rev/min]
Maximum speed	rev/min	2500
Inertia	kg.m^2	0.3
Rated temperature [max]	degC	90 [160]
Cooling	n/a	forced air

Table 5.12 – IMG and PE specifications. The motor generator is a dual stage cascaded axial flux machine rated at 80 Nm. The peak 300 Nm is determined by regenerative braking capacity requirements.

The design of the IMG early in the EASIVT project aimed at providing sufficient peak torque to maximise regenerative braking energy over the EPA city cycle. The cascaded layout met the requirement for torque in the LSHT region. A model of the machine was developed for hybrid functionality development in simulation, using a quasi-empirical engine model and an IVT model developed by Torotrak [13]. The DC brushless model was subsequently associated with the V8 model specifically for AVC strategy investigations.

5.3.1.1 Powertrain Models Integration

The engine model is associated to a DC motor model of the IMG by Cacciatori [77] in Simulink as presented in Figure 5.87. The mechanical model estimates the torque output *TrqImg* and equivalent DC current *IImg*. The thermal model estimates copper, iron, stray, windage and convection losses to determine the motor temperature.
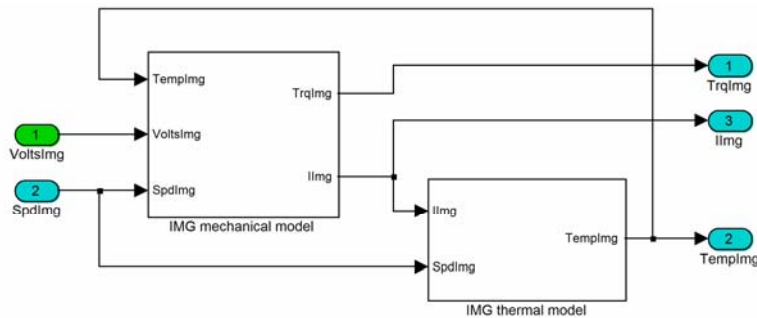
Figure 5.87 – IMG DC model in Simulink [77]. The crankshaft speed *SpdImg* is a non-filtered value of *SpdEng*. *VoltsImg* is an input from the PE model. The outputs are fed to the AMESim IMG inertia model

The power electronics model [77] associated with the IMG is presented in Figure 5.88. It exchanges current *IImg* and *VoltsImg* with the IMG DC model above. The power electronics receive a torque demand *TrqImgReq* from the environment. Both PE and IMG models obtain the speed *SpdImg* from the mechanical interface in AMESim [Figure 5.89]
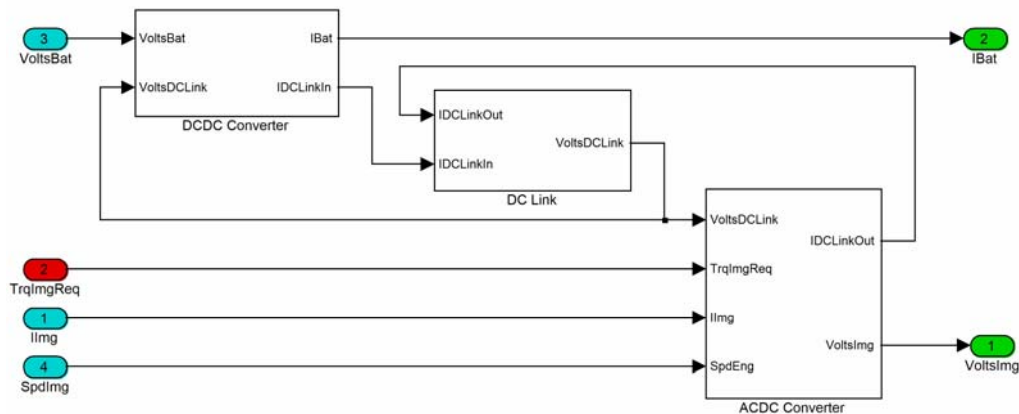
Figure 5.88 – Power electronics model in Simulink [77]. The DC-DC converter and DC link models feed the AC/DC converter model. The inputs are battery voltage *VoltsBat*, IMG model current *IImg*, the requested torque *TrqImgReq* and the current speed *SpdImg*.

The torque signal computed by the IMG model is sent to the AMESim environment through the co-simulation interface. The motor speed is communicated back to Simulink via the same interface. The nature of the model does not necessarily require exchanging additional state variables other than the speed in this case. Figure 5.89 presents the modifications implemented in the engine model environment in AMESim to interface the IMG model with the engine output shaft.
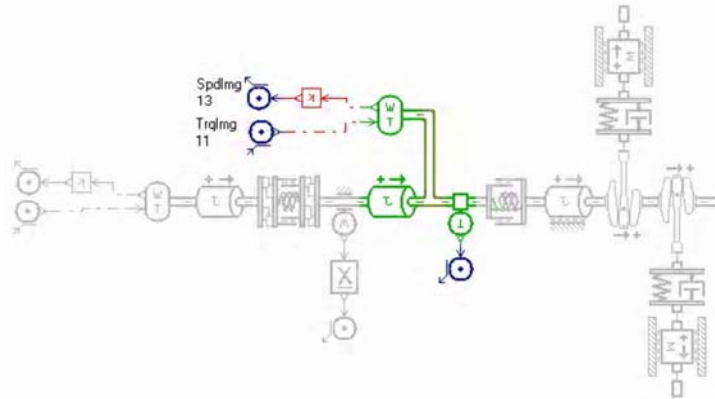
Figure 5.89 – IMG mechanical interface in AMESim. The IMG inertia is inserted on the output shaft of the V8 model [on the right, in grey] described in the previous chapter. The torque from the DC model *TrqImg* is added to the engine torque, the speed from the inertia model *SpdImg* is fed back to Simulink

In addition to the IMG models, a battery model is necessary to run the power electronics model. Although the simple empirical model [77] of the battery is not directly relevant to the current application, it was implemented for simulation purposes but will not be discussed in this report.

The engine and IMG pair can be simulated in the upgraded environment established for the engine alone simulation. A simple high bandwidth dynamometer type model was implemented in AMESim and speed controlled from Simulink to follow any requested speed profile. The model illustrated in Figure 5.90 was previously used to validate the engine model dynamic performance in conclusion of the previous chapter.
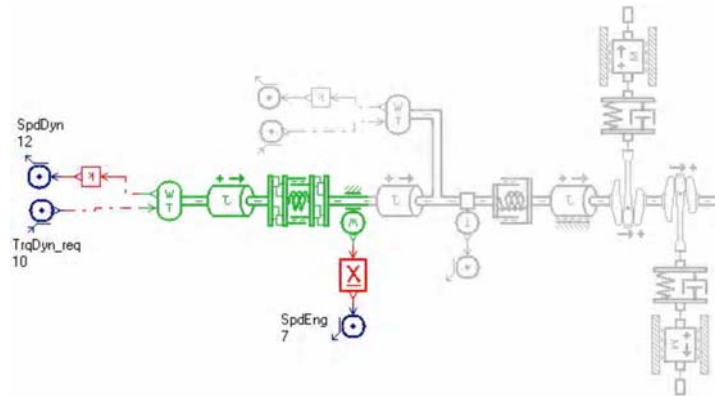
Figure 5.90 – Dynamometer mechanical interface in AMESim. The control torque *TrqDyn_req* is an input from the Simulink environment whilst the speed *SpdDyn* is fed back to the controller. The engine coupling model is carried over.

The powertrain model used in the following investigations is illustrated in Figure 5.91. The engine model exchanges torque and speed signals with IMG and dynamometer models in Simulink.
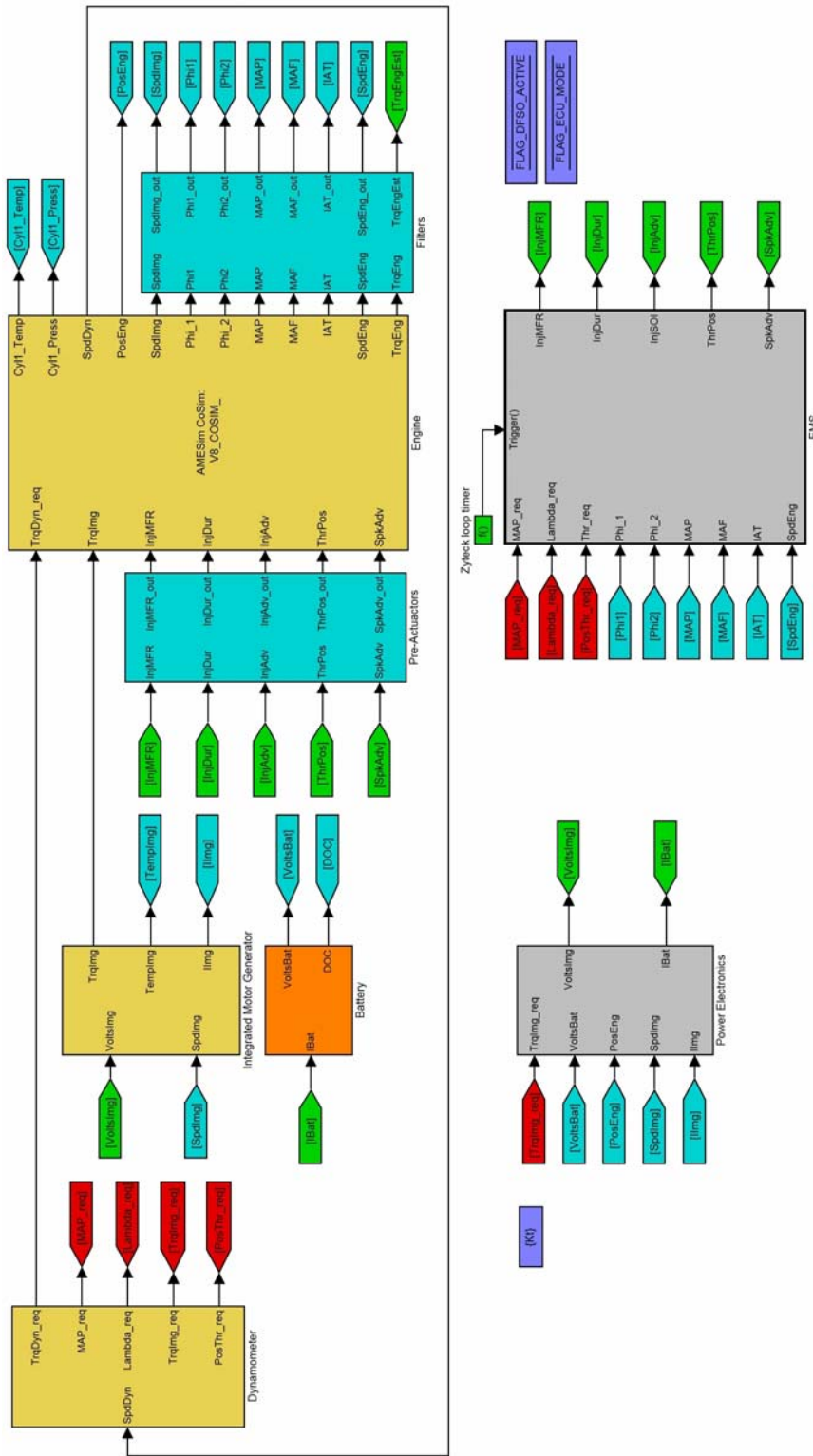
Figure 5.91 – Powertrain models integration in Simulink. Each sub-system presented previously appears as a block [yellow], exchanging physical signals with each other and control variables with the controller models [grey]. The command signals are in red, sensor signals in blue, control signals in green as per the convention used throughout this document.

5.3.1.2 Control Architectures

The effects of the firing frequency torque oscillations simulated by the engine model were highlighted previously in the NVH study. They create engine roll vibrations which excite body frequencies and ultimately panel vibrations and noise [Figure 5.92]. The requirement for LSHT operation was explained in the beginning of this chapter. Therefore the AVC strategy objective is to reduce the amount of engine vibration by damping the torque oscillations.
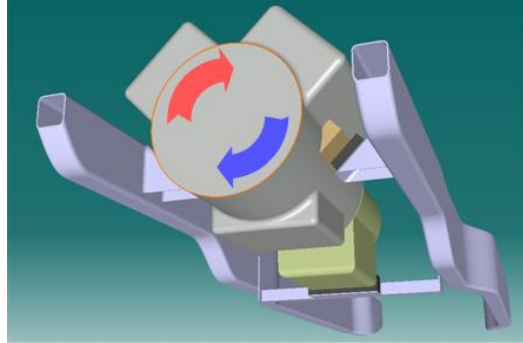
Figure 5.92 – Engine roll motion on chassis. Created by the torque oscillations, the vibrations on the chassis have detrimental effect on the vehicle NVH.

Bradreddine [44] suggests speed oscillations can be minimised on the crankshaft output at speeds close to idle using an Adaptive PID [APID] control of the IMG. The APID control technique is particularly attractive in the context of AVC for LSHT because it is based on an error function to minimise. The performance index of the system can be formulated as shown in Equation 5.9.

$$E = SpdError^2 + \alpha \cdot TrqIMG^2$$

Equation 5.9 – where *SpdError* is the difference between target speed and measured speed, and *TrqIMG* is the torque counter-measure signal. α is a weighting factor

This error function could also account for battery current for example which is ideal for hybrid powertrain calibration optimisation. Then the modified Frechet approximation tuning algorithm is derived from Equation 5.9 and defined by:

$$\dot{K}_P = \lambda \cdot Y_P \left[SpdError - \frac{\alpha}{\beta} \cdot TrqIMG \right]$$

Equation 5.10 – where *λ* is the adaptation gain and *ß* is the Frechet approximation constant, $Y_P = SpdError$

$$\dot{K}_D = \lambda \cdot Y_D \left[SpdError - \frac{\alpha}{\beta} \cdot TrqIMG \right]$$

Equation 5.11 – where $Y_D = \dfrac{d(SpdError)}{dt}$

This technique was successfully implemented in a 4 cylinder version of the V8 engine model in order to investigate the potential application of LSHT strategy with a small displacement engine. The APID controller based on the tuning algorithm presented by Badreddine [44] was set-up in simulation and is presented in Figure 5.93.
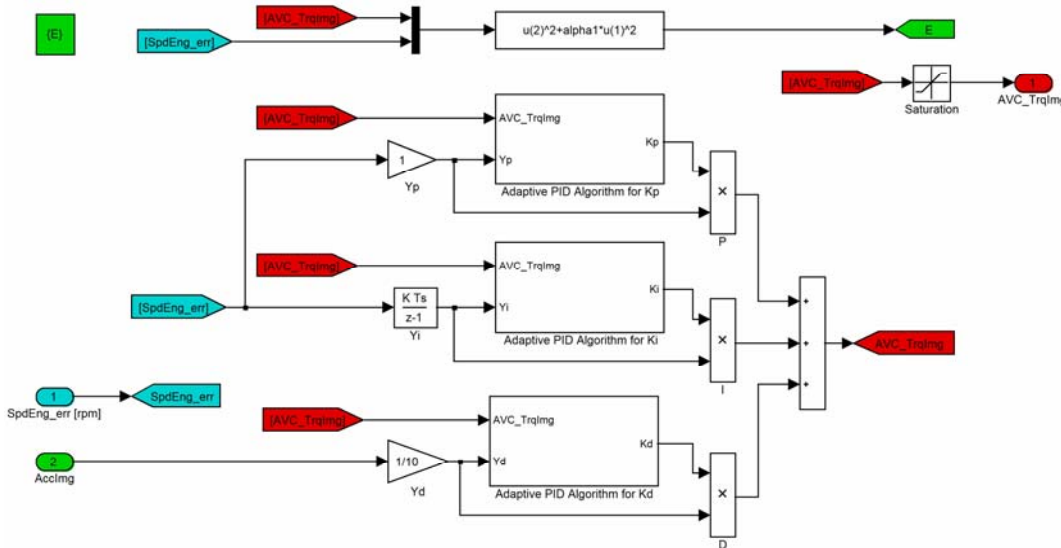
Figure 5.93 – Adaptive PID control structure for speed error control. The speed oscillation error [blue] is used as a feed-back signal to the PID torque controller.

The tuning algorithm requires an estimation of the approximation constant β followed by calibration of the adaptation gain λ and weighting factor α. The calibration variables will determine the capacity of the algorithm to self-tune and minimise the performance index presented in Equation 5.9. The advantage of this AVC strategy focussed on speed oscillations is that is does not require extensive calibration work across the range of operation. However, the requirement for a high bandwidth engine speed signal could not be fulfilled within the EASIVT scope. Such a set-up is preferably integrated in the IMG power electronics control running at much faster loop-times than the vehicle control units.

The performance of the APID control is shown in Figure 5.94 and Figure 5.95. Figure 5.94 shows the engine speed error and torque oscillations created by the 4 cylinder engine without any control. At $t = 1.7s$ [not shown], the proportional gain K_P is set to *5 Nm / (rad/s)* and the adaptive tuning is triggered for the derivative coefficient K_D. The derivative coefficient rapidly converges to 0.43 and the IMG control and engine variables are sampled from $t = 9s$. Ideal coefficients could be obtained in simulation and implemented in the real controller, or a simple adaptive tuning strategy could be implemented to let the coefficients self-tune on-line.

The *TrqImg* control signal in Figure 5.95 shows a high frequency component [approximately *300Hz*] created by the derivation of the speed signal [*AccImg*] for the Y_D component [Figure 5.93]. The engine speed signal derivation r amplifies the noise from the discrete crank position reading and therefore relies on the resolution of the

position encoder. This further emphasises the requirement for a high resolution speed encoder on the crankshaft. However, this high frequency in the control signal may be above the frequency response range of the IMG and PE package.
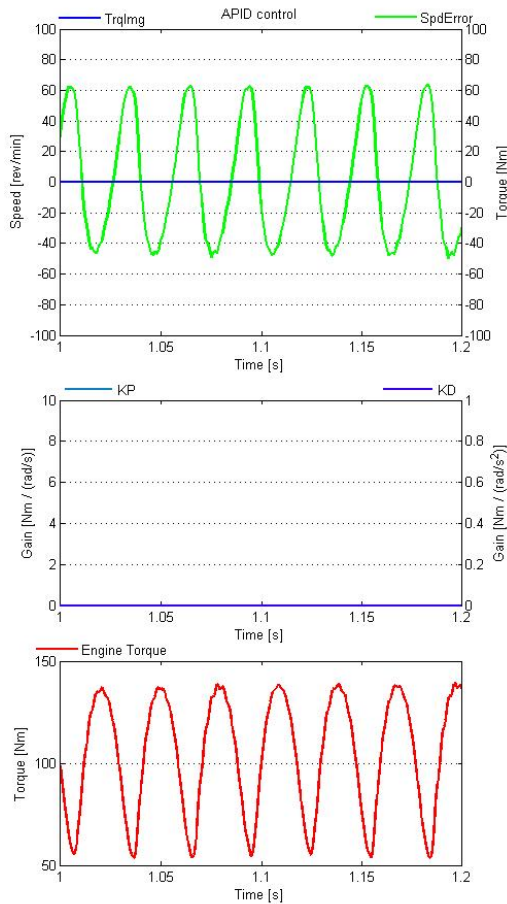
Figure 5.94 – Engine speed oscillations in I4 engine without control. The speed and torque amplitudes are respectively *109 rev/min* and *83 Nm* at *1000 rev/min*
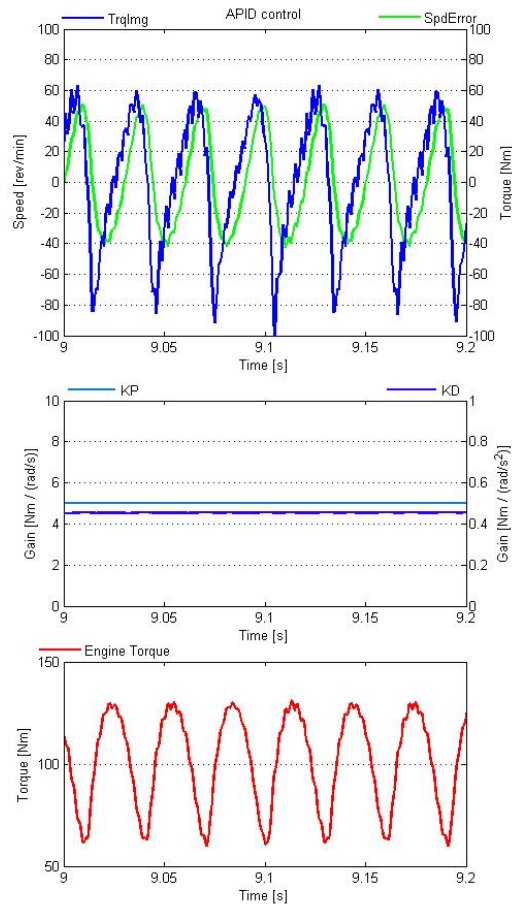
Figure 5.95 – Engine speed oscillations in I4 engine with control. The speed and torque amplitudes are respectively *88 rev/min* and *65 Nm* at *1000 rev/min*

The AVC strategy to develop and implement for the EASIVT LSHT operation could not benefit from the high sampling frequency speed sensor necessary to the feedback PID control. Therefore a feed forward strategy had to be developed. The model and the dynamometer data suggested that the V8 benefits from even running characteristics in the LSHT region. Indeed the torque output is a slightly distorted sine wave offset by the average torque. This means in the computation of the Fourier power spectrum for the engine torque output, most of the power above the rotational frequency [1st order] is at the 4th order component. The AVC makes the most use of this property, as detailed below.

5.3.1.3 AVC Strategy

Early simulations suggested that a 4th order frequency IMG torque sine wave reduces the peak to peak torque output of the engine & IMG combination. This is achieved by adjusting the phase of the counter-measure torque to be in opposite phase with the firing frequency torque oscillations. Equation 5.12 describes the torque counter measure suggested for the IMG request. This strategy is implemented in the EASIVT simulation environment as explained below.

$$TrqIMG = A \cdot \sin(4\alpha - \varphi)$$
Equation 5.12 – where *TrqIMG* is the torque counter-measure signal. α is the crank angle in *radCA* and φ is the phase offset to obtain opposite phase with 4th order engine torque oscillation.

The effect of the AVC torque counter measure to the 4th order engine torque oscillation in simulation is shown in Figure 5.96. The speed oscillations associated with the IMG & engine torque oscillation is reduced when the phase of the AVC command matches the combustion events 4th order sine wave approximation. The ideal phase obtained here at 700 rev/min WOT is *62.5 degCA* before TDC.
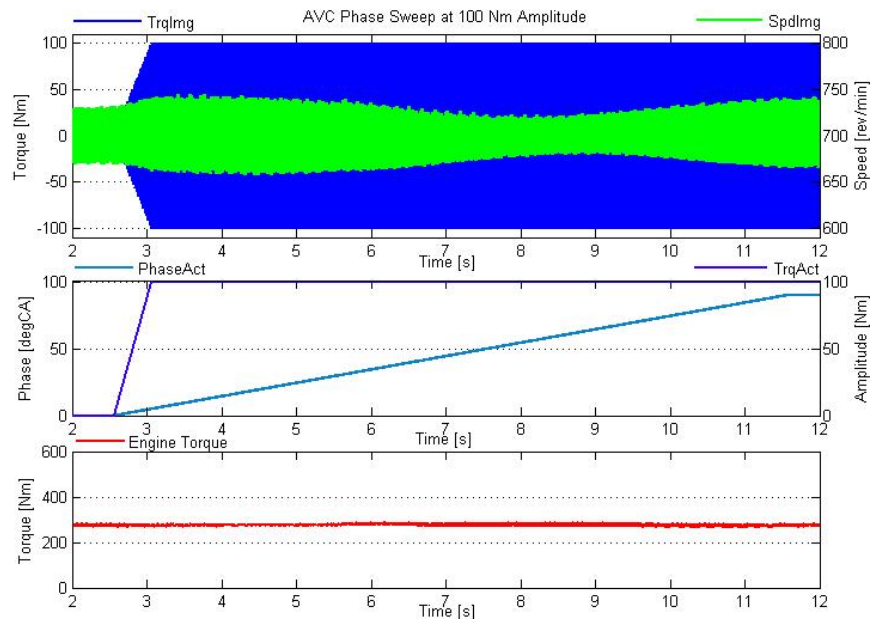
Figure 5.96 – AVC phase sweep at constant engine speed and AVC amplitude in Simulation. The engine speed [green] oscillations increase at the beginning of the simulation as the AVC is switch on and the phase sweep starts. When the phase *PhaseAct* reaches the appropriate crank angle, then the *SpdImg* oscillations reach a minimum.

The AVC amplitude required to reduce the 4th order engine related vibration depends on the engine operating conditions of speed and torque. It is difficult to calibrate *TrqAct* in simulation as its impact on the vibration levels in the vehicle cannot be assessed. However, the NVH investigations conducted conclude that the level of vibrations itself depends engine operating point therefore provision was made for a look-up table determining the *TrqAct* command from engine speed and estimated torque. Figure 5.97 shows the impact of *TrqAct* on the engine & IMG output torque in steady state conditions.
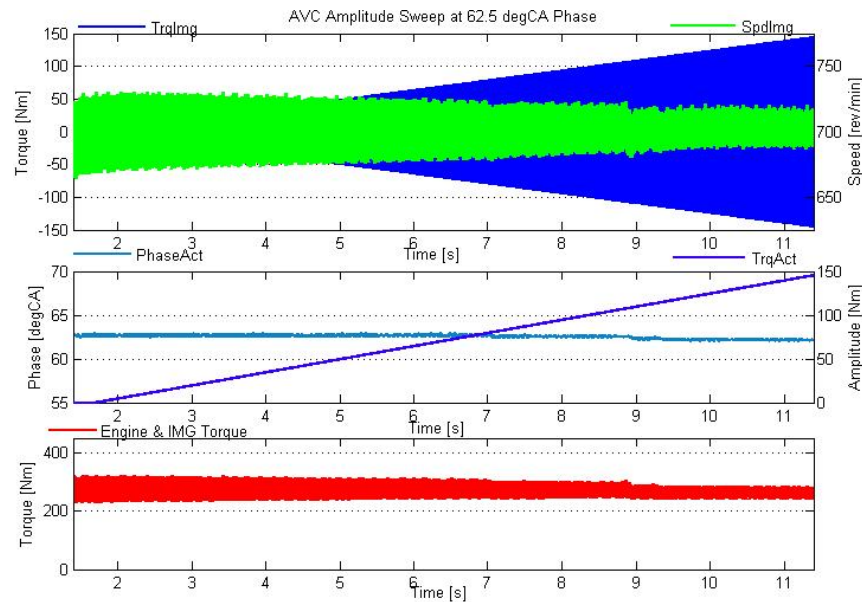
Figure 5.97 – AVC amplitude sweep at constant engine speed and AVC phase in Simulation.
As the AVC sine wave amplitude increases, the engine speed oscillation reduce and the torque output generated by the engine and IMG see the level of oscillations reduce accordingly.

There are subsequently two signals for the AVC strategy to adjust during LSHT operation, being *TrqAct* and *PhaseAct*:

▪ The phase depends on the engine characteristics and does not depend on the level of engine vibration nor does it impact the current consumption of the AVC. A basic calibration can therefore be achieved with the model using engine speed and estimated torque as inputs to a look-up table. It seems however that the phase of the engine torque 4th order oscillation can be related to the spark advance *SpkAdv*, so provision was made to use this EMS variable as an input to the AVC strategy.

▪ The torque amplitude requirement was mapped in two look-up tables established with the results from the NVH study. The engine and body vibration level maps from the NVH study were respectively converted into engine and body related AVC amplitude look-up tables. An equivalence ratio was adjusted to scale the vibration levels in *g* to amplitude in *Nm* so that the maximum AVC amplitude in the table was *120 Nm*. This effectively makes *TrqAct* proportional to the 4th order vibration magnitude measured experimentally. The basic calibration obtained could then be used during the strategy development in simulation and later tuned once implemented in the vehicle.

The battery power required by the AVC strategy varies with the efficiency of the power electronics. This efficiency depends mostly on the engine speed and the low frequency torque request from the hybrid controller to the IMG. The latter shifts the average value of the IMG torque and therefore it has the same effect on the DC current from the battery. The worse case occurs at low speed and with AVC only where the power drawn from the battery is less than *1 kW* RMS at *100 N*m TrqAct.

5.3.2 Controller Design & Calibration

5.3.2.1 Simulink Models

The AVC control block [Figure 5.98] implemented is split into a high level layer [Figure 5.99] and a low level layer [Figure 5.100]. The former is embedded in the powertrain controller and sets the appropriate amplitude *TrqAct* and phase *PhaseAct* depending on the engine operating condition. The latter is built in the DSP platform of the PE and calculates the AVC torque request *TrqImg_AVC* using the top layer commands and the high resolution position signal also used by the IMG inverter control.
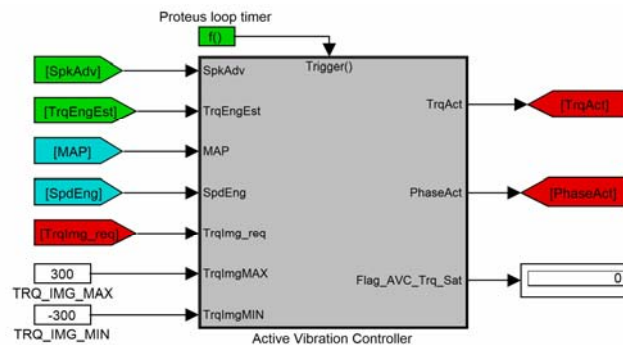
Figure 5.98 – AVC high level block in Simulink. The trigger function [top] runs the block in discreet mode. The IMG torque request is used to saturate the AVC amplitude request with respect to *TRQ_IMG_MAX* and *TRQ_IMG_MIN*

The high level strategy [Figure 5.99] is to be implemented in a rapid prototyping ECU with the rest of the vehicle and powertrain control, running at *8 ms* loop time. Therefore the AVC block model [Figure 5.98] runs in discrete mode. It reads engine speed *SpdEng*, estimated torque *TrqEngEst*, the alternative LUT input *MAP*, and the spark advance *SpkAdv*. The later allows using an alternative strategy to set *PhaseAct* as a function of the spark timing rather than a calibrated LUT. This strategy was not adopted in the vehicle implementation.

In Figure 5.99, two LUT set target amplitudes [top left] to cancel out engine and body vibrations. The weighted average of the two steers the calibration towards engine or body vibration AVC cancellation. The third LUT [bottom left] sets the phase. The overriding stage [centre] allows the calibration engineer to set his own demand to the control signals. The safety stage [right] limits the rate of change for both amplitude and phase to prevent large step demands to the low level layer, which will create discontinuities in the IMG torque output component *TrqImg_AVC*. This potentially could cause driveline bumps.
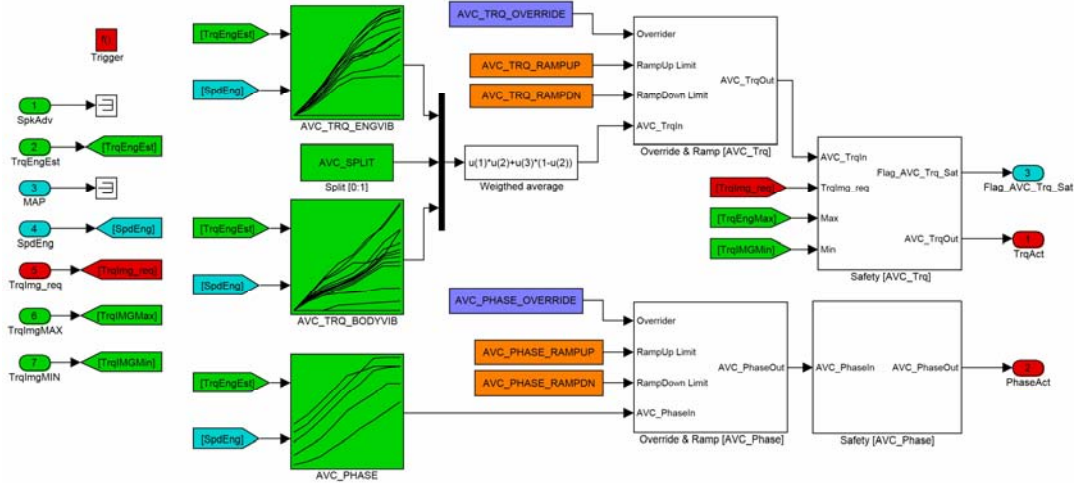
Figure 5.99 – High level AVC strategy imbedded in the AVC block. IVT estimated engine torque *TrqEngEst* and engine speed *SpdEng* are the inputs to the look-up tables [green]. There are two AVC amplitude maps for the engine and the body vibration respectively. The amplitude target is a weighted average of the two.

The safety block for *TrqAct* also accounts for the IMG torque request *TrqImg_req* from the hybrid controller [not implemented in this simulation] to ensure that the maximum and minimum torque *TrqImgMax* and *TrqImgMin* are never exceeded when the low level controller [Figure 5.100] formulates the AVC sine wave. These boundary variables are set by the hybrid control strategy [77] based on the IMG performance envelope and the battery limits. *TrqAct* is interactively read by the hybrid strategy which assigns priorities to the various components of the final IMG torque requests.
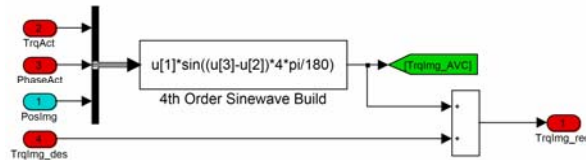
Figure 5.100 – Low level AVC strategy imbedded in the power electronics block. The high angle resolution *PosImg* is referenced to the engine TDC position and used to create the variable frequency sine wave. The amplitude and phase in *degCA* are set in the high level strategy.

The low level layer is the part of the AVC strategy which cannot be implemented in the 8 ms loop time control environment. The 4th order counter-measure formulation [Equation 5.12] is based on the crankshaft position *PosEng*, which is a TDC referenced version of the high resolution speed sensor signal used by the power electronics for IMG torque control. The *PosImg* signal is read from a 164-tooth plate with two magnetic sensors and a missing tooth for position reference. The signal is interpolated to yield *0.24 degCA* resolution and the missing tooth is referenced to cylinder 1 TDC. This is achieved in the IMG DSP controller at *16 μs* loop-time.

Figure 5.101 shows the phase LUT obtained in simulation by tuning the *PhaseAct* manually at various steady-state operating points of the LSHT region. This baseline calibration will then be verified in the EASIVT vehicle. Figure 5.102 and Figure 5.103 respectively show the engine and body vibration cancellation *TrqAct* LUT previously mentioned.
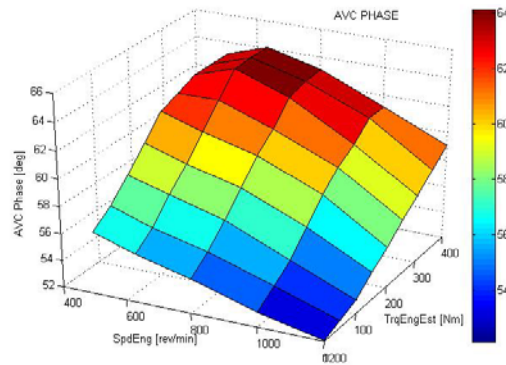
Figure 5.101 – AVC phase map calibrated in the simulation environment for each steady state operating point. The values are tuned to minimize the torque oscillations with *100 Nm TrqAct* amplitude.
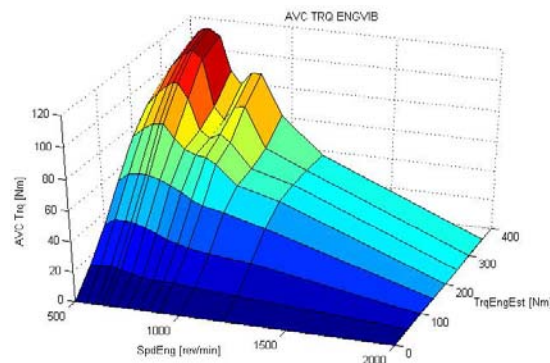
Figure 5.102 – Engine AVC amplitude map calibrated proportional to engine vibration levels measured in the baseline IVT vehicle. The surface obtained was smoothened and sloped down to zero at *0 Nm* and *2000 rev/min*.
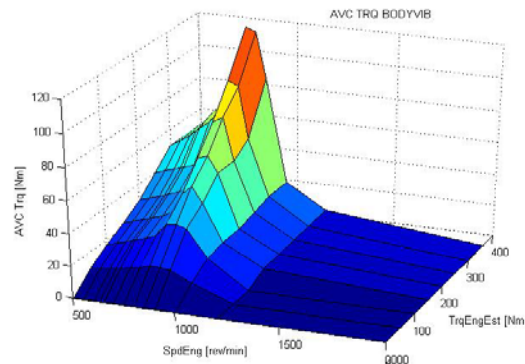
Figure 5.103 – Body AVC amplitude map calibrated proportional to body vibration levels measured in the baseline IVT vehicle. The surface obtained was smoothened and sloped down to zero at *0 Nm* and *2000 rev/min*.

Figure 5.104 shows the average combination *AVC_TRQ_ENGVIB* and *AVC_TRQ_BODYVIB* for *TrqAct* obtained from the NVH measurements. Additional data shows where the engine speed strategies mentioned previously [Section 5.1.1] operate in the LSHT map.
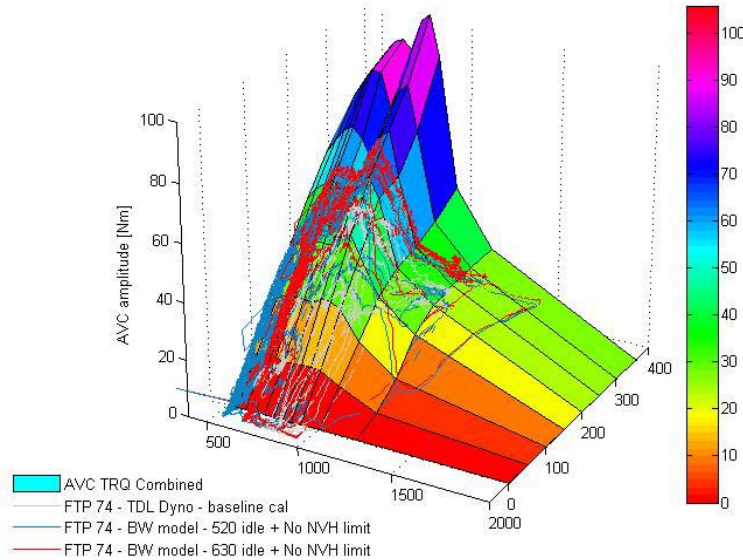
Figure 5.104 – Combined AVC map and engine operation during the FTP74 city cycle for the baseline IVT calibration [vehicle dynamometer], the NVH limit free *630 rev/min* idle strategy, and the *520 rev/min* reduced idle LSHT strategy [both backward model simulation].

The data from the drive cycle simulations plotted over the AVC amplitude map in Figure 5.104 shows how the cancellation of the NVH limit promotes operation in the LSHT region compared to the baseline calibration. The backward simulation data for a *520 rev/min* idle speed demonstrates that the FTP cycle involves a significant amount of low power conditions where the better BSFC of the reduced idle speed will contribute toward improved fuel econmomy.

5.3.2.2 AVC Transient Operation

The simulation environment was used to validate the AVC control architecture and its integration within the hybrid IVT controller. Figure 5.105 shows the simulation of the first *100 s* of the EPA city cycle using experimental data to command the model controllers. Throttle position *PosThr* and engine speed *SpdEng* from vehicle dynamometer testing feed respectively the engine controller model and the dynamometer model. The LSHT operation is limited above *800 rev/min* by the baseline NVH strategy as explained in the beginning of the chapter.

These simulation results are used to confirm the satisfying transient behaviour of the AVC strategy which is calibrated in steady state only. The rate limiters implemented are tuned [Table 5.13] based on the analysis of the transient requirements for phase and amplitude changes so that they do not intervene during normal operation.

Variable Name	Title	Value	Units
AVC_PHASE_MAXRATE	PhaseAct maximal rate of change	degCA/s	100
AVC_PHASE_RAMPUP	PhaseAct override ramp up rate	degCA/s	20
AVC_PHASE_RAMPDN	PhaseAct override ramp down rate	degCA/s	-20
AVC_TRQ_MAXRATE	TrqAct maximal rate of change	Nm/s	500
AVC_TRQ_RAMPUP	TrqAct override ramp up rate	Nm/s	100
AVC_TRQ_RAMPDN	TrqAct override ramp down rate	Nm/s	100
AVC_SPLIT	Engine to body TrqAct calibration weight	n/a	1

Table 5.13 – Additional AVC calibration parameters related to transient operation. The rate limiters prevent large step changes from the discreet reading of the LUT; the ramp parameters are for calibration purposes only.
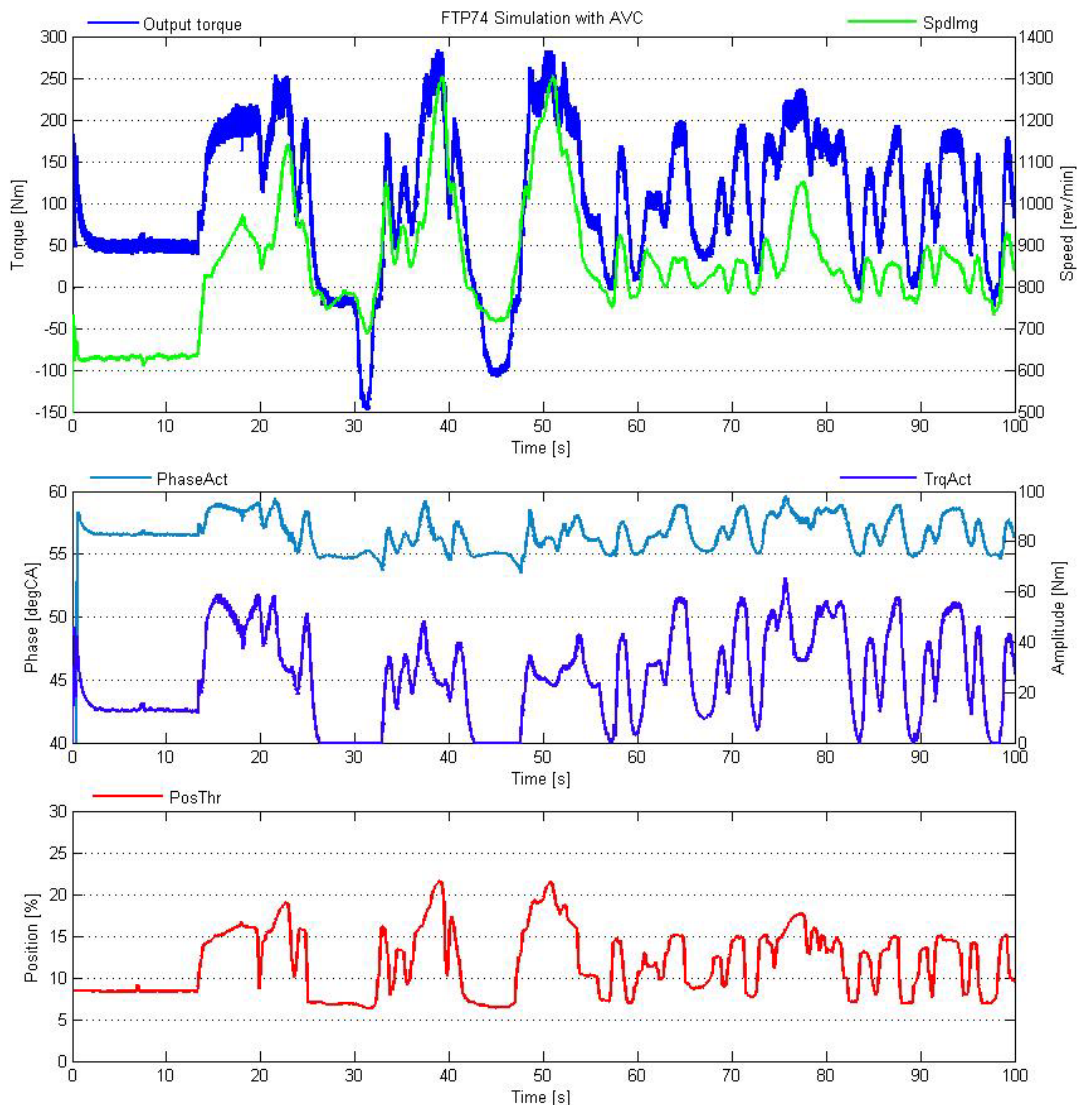
Figure 5.105 – First 100 s of FTP74 city cycle in simulation using throttle position *PosThr* and engine speed *SpdEng* logs from dynamometer tests. The output torque [top, blue] is the combined torque of the engine and IMG at the transmission input shaft. The signal was filtered to attenuated the oscillations and enhance clarity.

5.3.2.3 Calibration sensitivity

The AVC controller models were implemented in the EASIVT vehicle in two separate layers as intended in the simulation stage.

- The high level strategy was compiled for real-time application into a Prodrive Proteus rapid prototype control unit using auto code generation, together with the hybrid functionalities for torque assist and regenerative braking. This controller embeds most of the vehicle control strategy and the IVT high level control. The loop time for this platform is *8 ms*.

- The low level *TrqImg_AVC* formulation from *PosImg*, *TrqAct*, and *PhaseAct* is executed in the PE unit DSP controller at *16 μs* loop-time.

As introduced in Figure 5.70, all control units in the vehicle communicate via CAN bus. The Proteus unit allows on-line calibration of the strategy via CAN Calibration Protocol [CCP] and ATI Vision. The EASIVT vehicle therefore becomes a validation and tuning environment for the various control strategies previously developed in simulation. There are three critical calibration elements to the AVC strategy discussed below: the phase, the amplitude and the idle speed which is also the BSFC IOL minimum speed.

The phase LUT was calibrated using simulation. Once in the vehicle, this part of the strategy was overridden to ensure that appropriate values were used. The phase of the AVC command affects the efficiency of the strategy therefore the calibrated values were offset to observe the effect on the vibration levels at constant amplitude *TrqAct = 100 Nm*. Figure 5.106 shows such test results at 500 rev/min and WOT engine torque. The vibration levels on both sides of the engine mount react in the same way to the phase disturbance, as does the subjective noise assessment in the cabin. The minima observed are within a $2^{\pm 1}$ *degCA* band for each of the 4 steady state operating points tested. The position of the calibrated value inside the crank position band was deemed satisfactory and proved the relatively low sensitivity of the AVC to minor phase disturbance.
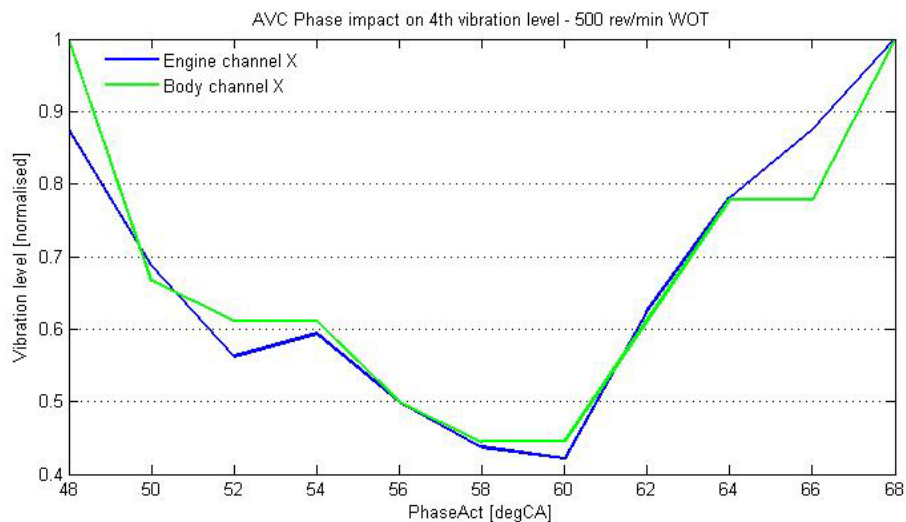
Figure 5.106 – In-Vehicle measurement of vibration levels for different AVC phase [see Section 5.2]. Both sides of the engine mount have minimal 4th order vibration when the AVC phase corrects the engine torque oscillation.

The torque amplitude of the IMG counter-measure is driven by the compromise to be found between acceptable NVH levels associated with the aggressive LSHT operation and the cost in terms of electrical power consumption from the battery. This was investigated [19][77] as part of the overall fuel economy sensitivity analysis.

The initial calibration used in simulation showed poor fuel economy once the amplitude maps were implemented into a backward model simulation routine. The battery stored electrical energy cost was in fact not recovered by the fuel economy gain obtained from LSHT operation. During the EASIVT vehicle calibration phase, 2 iterations were necessary to obtain a satisfactory compromise.

The method established during the NVH study was exploited in the EASIVT vehicle using steady state measurements at constant engine speed and torque, with the additional variable TrqAct. A 4-dimensional 4th order vibration map of the engine was subsequently created and used to generate a calibration recommendation. The AVC amplitude set points were used to interpolate the corresponding vibration levels at a constant engine speed and torque. An overall vibration level ceiling was arbitrarily set to obtain the appropriate TrqAct value at each steady state point. This guaranteed homogeneity and repeatability of the calibration method, whilst changing the 4th order vibration level ceiling would shift the AVC amplitude required and therefore its hybrid cost.

The aforementioned method was applied to limit the engine vibration as recommended by the NVH study with the baseline IVT vehicle. The body vibration map was consequently dropped [split factor *AVC_SPLIT* set to *0*] to focus on one single *AVC_TRQ_Final* LUT. The auto-generated map was manually tuned using the backward simulation information as a means to evaluate the energy cost of the calibration over the drive cycle as seen in Section 5.3.3. The final AVC amplitude map is shown in Figure 5.107.
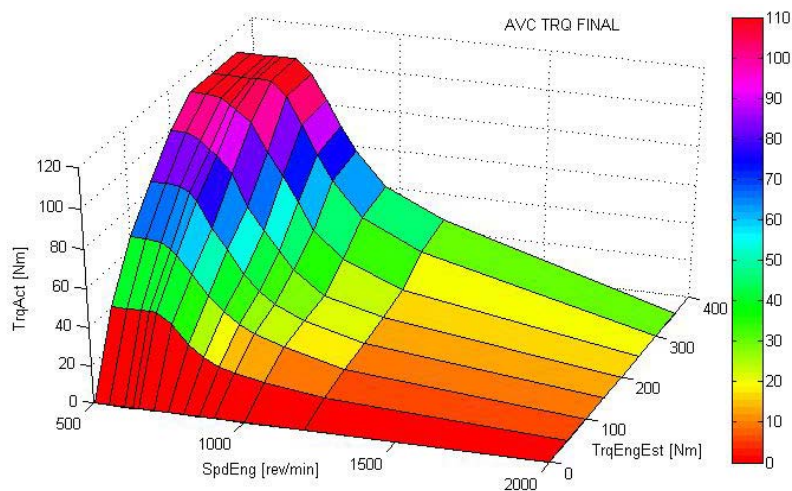
Figure 5.107 – AVC amplitude final calibration map [19]. Only one LUT was retained for the final vehicle calibration. It was tuned using the same NVH equipment as in Section 5.2 and iteration with backward models simulations.

The estimated fuel economy overall benefit from the LSHT operation associated with hybridisation is discussed below.

5.3.3 EASIVT Vehicle LSHT Performance

The AVC calibration was implemented into a backward model simulation routine for fuel economy and battery state of charge estimation in the EASIVT vehicle over the EPA city and highway cycles. This simulation environment [77] based on quasi-static models also integrated the regenerative and torque assist strategies implemented in the hybrid powertrain control [19]. The results are presented in Table 5.14 for the three engine operation strategies previously discussed.

Vehicle Configuration	EASIVT		
Environment	Backward model simulation		
Test weight	2722		kg
Crankshaft inertia	0.5473		kg.m²
FUEL ECONOMY			mpUSg
Drive Cycle	Engine operation strategy		
	Standard	No NVH IOL & AVC ON	No NVH IOL & AVC ON & 520 idle
FTP 75 city cycle	16.98 REF	17.42 -2.60 %	17.95 -5.68 %
HWFET highway cycle	22.21 REF	22.19 +0.1 %	22.21 -0.01 %

Table 5.14 – Fuel economy predictions for EASIVT vehicle from backward model simulations [19][77]. The regenerative braking energy recovered is used to torque assist the engine and AVC in the LSHT region.

Table 5.15 provides a summary of the expected FE benefits of increased LSHT operation without any NVH penalty. The figures are from Table 5.9 and Table 5.14.

FUEL ECONOMY COMPARISON in SIMULATION			mpUSg
Drive Cycle	Configuration		
	Baseline IVT	EASIVT 630 rev/min idle	EASIVT 520 rev/min idle
FTP 75 city cycle	16.96 REF	17.42 -2.71%	17.95 -5.80 %
HWFET highway cycle	22.77 REF	22.19 +2.54%	22.21 +2.43%

Table 5.15 – Fuel economy prediction comparison: EASIVT vs. IVT from backward model simulations [19][77]. Aggressive LSHT operation in EASIVT shows increased FE benefits, but weight and inertia penalty degrades FE in highway cycle when LSHT is not possible.

There are two critical aspects of the LSHT operation: the AVC strategy and the torque assist strategy. The former enables steady state operation where NVH levels are otherwise unacceptable; latter maintains driveability standards with a reduced engine torque margin and increased response lag. Both were at the centre of the calibration exercise performed in the EASIVT vehicle as verified below.

5.3.3.1 NVH reduction effects in LSHT region

The functionality of the AVC was verified in simulation but its NVH performance could only be validated in the vehicle. Therefore the vibration measurement methods established during the baseline IVT investigation were re-conducted with the EASIVT powertrain. The significant improvements offered by the AVC were observable during the calibration tuning carried out in steady state. However, as concluded during the NVH data analysis [Section 5.2], the most representative method for overall NVH performance assessment is the transient data measurement. The results obtained are discussed below.

Figure 5.108 illustrates the 4th order vibration levels measured during a speed transient at *300 Nm* engine torque with AVC deactivated. The vibration levels measured are slightly lower than those of the IVT vehicle [see Figure 5.81]. This is due to the lower Eigen frequency of the IMG [*49.6 Hz,* i.e. 4th order cut-off above *750 rev/min*] compared with the original IVT layout [*76.9 Hz,* i.e. 4th order cut-off above *1135 rev/min*], as also observed in simulation.
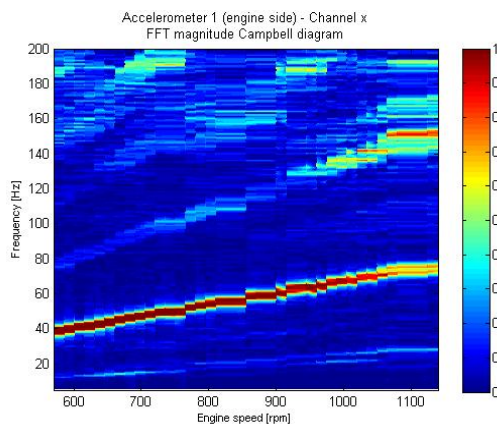
Figure 5.108 – No AVC transient measurement of engine vibration spectrum [normalised]. The 4th order line is clearly visible, showing levels of vibration above *0.019.*
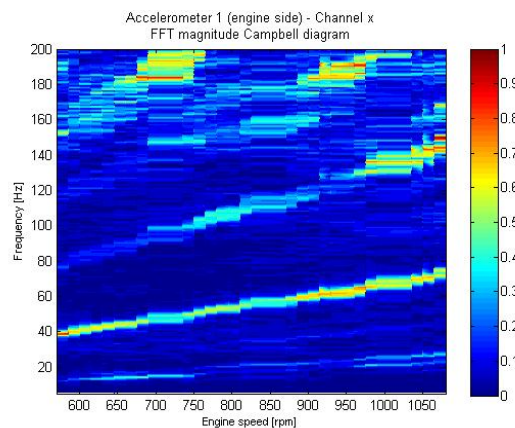
Figure 5.109 – AVC On transient measurement of engine vibration spectrum [normalised]. The 4th order line is significantly attenuated, showing levels of vibration above *0.012.*

Figure 5.109 shows in contrast the vibration levels obtained during the same transient with the AVC activated. The 4th order torque oscillations are kept minimal by the amplitude calibration. Particularly low levels of vibrations are achieved on the 4th order line below *900 rev/min* as recommended during the NVH analysis.

5.3.3.2 Hybrid Control Coordination in Vehicle

The AVC strategy is part of the hybrid control system in the EASIVT vehicle aimed at lowering the vehicle fuel consumption, i.e. torque assist components. These superimposed components of the IMG torque request elaborated by Cacciatori [21] are based on the requirement for improved torque response in LSHT region. The torque assist formulation is decoupled as follows:

- IMG inertial torque component. The inertial component of the engine torque request during transient is the part of the engine output torque which is not reacted by the IVT. The torque differential indeed accelerates the rotating parts of the powertrain and its control ensures accurate delivery of the wheel torque request *TrqWhlReq*. The differential [inertial torque] can also be negative when the engine speed is decreased. The IMG takes over a majority of this torque request in the LSHT region to improve the IOL operation of the engine.

- IMG lag compensation component. The IVT controller accounts for the torque response time of the engine following a change in request. This torque lag is modelled within the control strategy and mostly accounts for manifold filling and emptying effect previously highlighted. The IMG will assist with extra torque to improve the torque response at the transmission input and therefore the driveability performance potential of the powertrain.

In addition to this, a power split component shifts the engine operating torque up or down and transfers the difference onto the IMG request in order to maintain the battery State Of Charge [SOC]. The IMG torque limit therefore raises the necessity for a priority system to prevent saturation or overload. This was included in the top level AVC strategy described previously.

Figure 5.110 shows the various powertrain torque components evolution during a tip-in manoeuvre. As the pedal is depressed, the power demand on the engine is increased and the required engine operating point shifts. The engine is throttled up to the new IOL point, which then varies as the vehicle speed change and the pedal position fluctuates. The large inertial torque required to accelerate engine and IMG is immediately increased causing the IMG to produce both lag compensation and inertial torque. The AVC amplitude demand is initially high because of the low initial engine speed, and then increases with the engine torque. As the speed increases the AVC demand lowers. The effect of the IMG torque boundary is visible on the AVC trace when the IMG torque temporarily reaches *220 Nm* at around *t = 0.75s*.

Figure 5.111 shows the same variables during a launch manoeuvre. All torque values are initially low, with AVC amplitude set around *15 Nm* for the *520 rev/min* idle condition. As the vehicle is accelerated from stand-still, the IMG requests assist the engine in the LSHT region. The effects of the power split component on the engine requested torque are visible, as well as the transmission regime changes [see Appendix A].
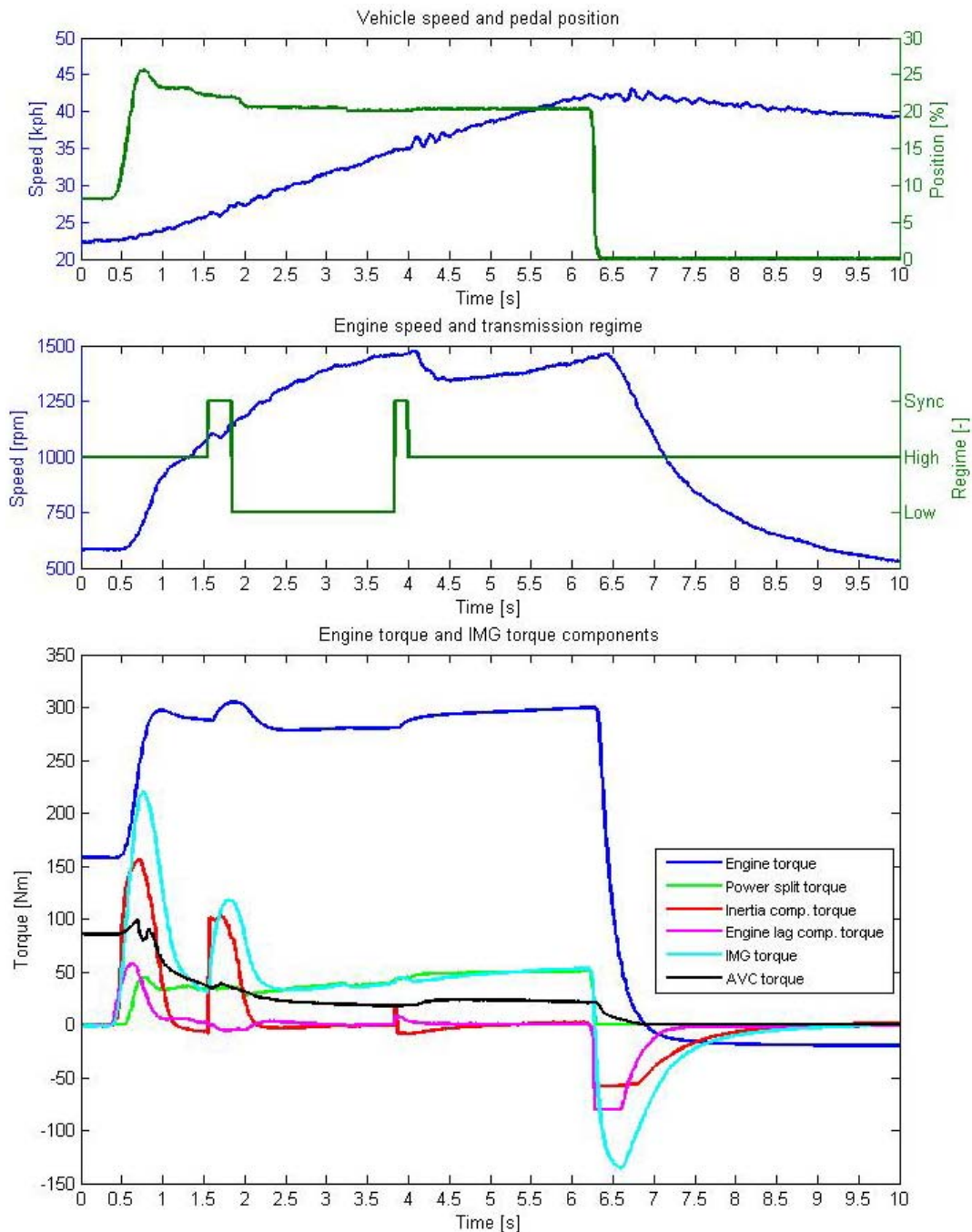
Figure 5.110 – EASIVT vehicle tip-in manoeuvre with all hybrid functions active [19]. The engine is operated in the LSHT region using AVC and torque assist. The AVC amplitude is *90 Nm* in the first *0.5 s* of steady state. When the pedal is depressed to *25 %*, the engine speed is raised with the torque margin and the IMG. On back-out, only the torque assist strategy uses the IMG as generator.
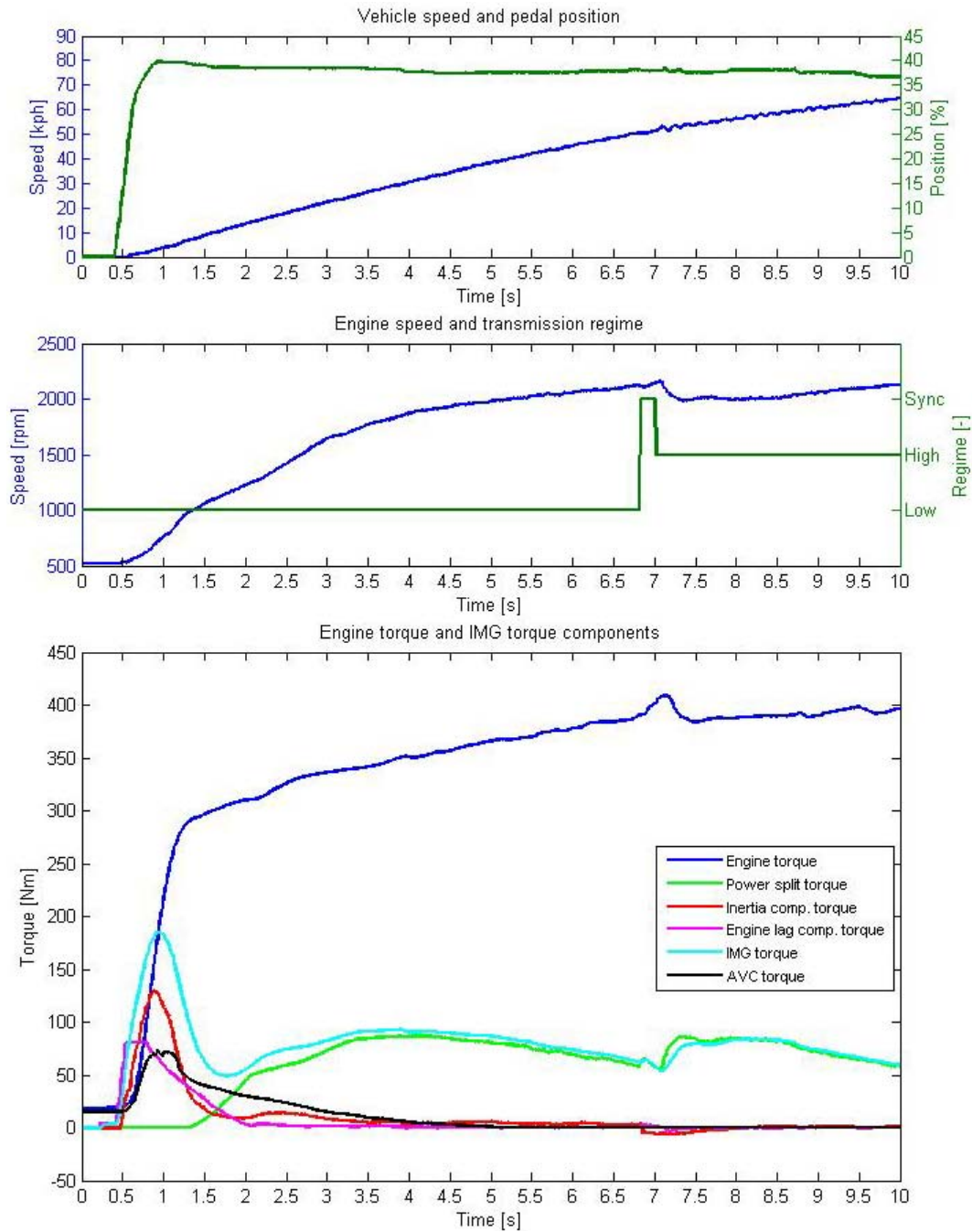
Figure 5.111 – EASIVT vehicle launch manoeuvre with all hybrid functions active [19]. The engine is operated in the LSHT region from *520 rev/min* in the beginning of the transient manoeuvre. The AVC amplitude increases with the raised engine torque, then reduces as the engine speed modes out of LSHT region. The power-split component of the IMG torque request takes over after lag and inertial components reduce.

5.4 Closing Comments

After highlighting the relevance of LSHT engine operation with the IVT powertrain, the requirement for the hybrid EASIVT vehicle were explained. The high overdrive ratios permitted by the IVT can be exploited by a matching prime-mover, i.e. the engine and IMG in this case for the benefit of fuel economy. The engine NVH characteristics originally prevented an non-compromised match within the powertrain. Low speed operation is beneficial to fuel economy but also clearly detrimental to driveability.

An NVH study confirmed the firing frequency torque oscillations to be the source of undesirable noise; the analysis was consequently focussed on setting the requirements for the LSHT vibration reduction strategy. This yielded a method that would be later employed to assess the EASIVT vehicle improvement in that respect. It also created vibration and noise maps which were then used to assess the potential cost of the proposed counter-measure in simulation.

The LSHT region NVH operation issues are addressed in the hybrid powertrain by the development of the AVC strategy. The phase and 4th order frequency control of an additional IMG signal proved successful in the modelling environment established in the previous chapter. The integration of this strategy within the EASIVT powertrain control architecture was carried out in simulation and verified once the vehicle was commissioned. This allowed one single implementation iteration for the auto-compiled AVC controller model.

Finally, the EASIVT vehicle showed the expected performance in driveability. Two hybrid control design & implementation iterations enabled as satisfying strategy to be calibrated in the vehicle. The simulation environment used in this chapter was subsequently qualified, as well as the other platforms used during the EASIVT hybrid control design process.

Chapter 6: V6 TURBO DIESEL ENGINE MODEL

This chapter presents the modelling of the Audi W19 3.0L V6 TDI engine for speed and torque transient simulation in order to investigate Manifold Air Injection [MAI] assist in a CVT powertrain. The CVT here is of the ratio controlled, variable pulley type as detailed in Appendix A. The exercise involves the modelling of the engine and turbocharger in AMESim, and the modelling of the EMS in Simulink as proposed for the gasoline engine case in Chapter 4.

6.1 Requirements

The objectives for this modelling exercise are slightly different from those previously set for the gasoline engine operation in the LSHT region. Combustion torque fluctuations are not included in the scope of this diesel engine investigation. The model will be paired with a CVT and vehicle model to investigate mostly full load transients with the injection of air in the intake manifold. Here the importance is placed upon the engine operating conditions from Table 3.2 that are related to the speed and load transients. The requirements for this V6 turbo Diesel engine model are developed after the description of the engine architecture below.

6.1.1 Engine Description

The Volkswagen – Audi engine was chosen as the basis of the work undertaken to investigate CVT related engine torque response in a diesel engine. This choice was driven by the following considerations:

- A large displacement diesel engine is not a usual match for a CVT in the current personal vehicle market. However, the torque to inertia ratio of the engine is more critical to the CVT transient operation than the inertia alone as explained in Chapter 1. This large displacement engine is often paired with an AT, which is the target market for CVT's.

- ▪ The W19 V6 TDI is a state of the art High-Speed Direct Injection [HSDI] turbocharged engine, with single stage variable geometry turbocharger [Figure 6.112]. Unlike some other large capacity HSDI engines, the W19 does not feature twin-turbocharger layout or dual-stage turbocharging. This reduces the complexity of the charging system to be modelled and reduces the necessary time effort.
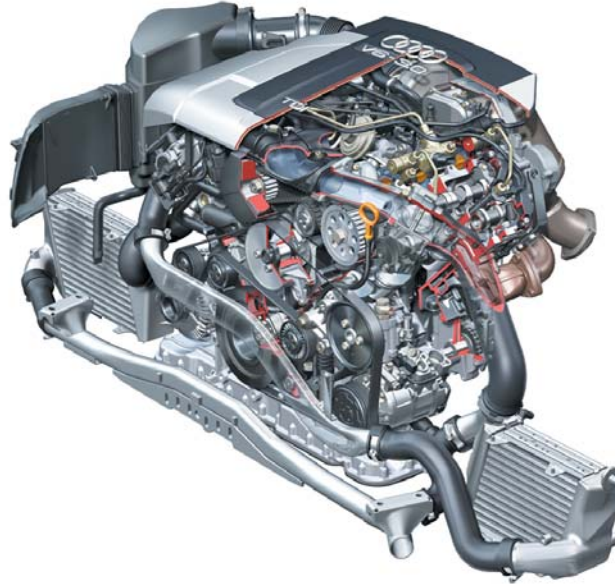
Figure 6.112 – Audi W19 3.0 V6 TDI engine cut-away [A.11]. It features state-of-the-art common rail and piezo injector technology with a single stage variable geometry turbocharger.

Exhaust Gas Recirculation flows from up stream of the turbocharger turbine to down stream of the compressor. EGR is cooled via a heat exchanger with the cooling circuit. The VGT fresh air charge is cooled via two intercoolers.

The requirement for the modelling task is for a realistic engine model that allows carrying out the investigations. Thus there is no specific need to obtain an exact model of the W19 engine as developed in Section 6.1.2.

6.1.2 Operating Conditions

6.1.2.1 Steady State

Constant speed and torque operation of the engine model is not the prime interest of simulation. However, the transients will be characterised by an initial and a final steady state which has to be realistic in order to ensure representative results. A particular effort is therefore required to calibrate the EMS for steady state operation across the speed and load range of the engine. The model thermal efficiency also has to be tuned to allow accurate steady state operation predictions. Less than 5% error against the available experimental data is the target.

6.1.2.2 Turbocharger & EGR Transient

The air-path model and the associated controller for the VNT and the EGR valve are at the core of the simulation exercise. Exhaust transients will be the critical phenomena driving the engine performance with the fuelling strategy during the transient. Therefore the main tasks can be summarized as follows:

- Modelling of the plant to a sufficiently high degree of detail

- Designing the controller in the most realistic way

- Calibrating the associated strategy like a real application

Particular effort will be paid to the VNT controller in both steady state and during transient. The EGR strategy will have a significant influence on the turbocharger operating condition; because it is common practice to shut down the recirculation valve during heavy tip-in to maximize the exhaust back pressure and the intake MAF, hence the EGR strategy calibration will not require the same amount of work as the turbocharger. Its control can be kept rather simple because it will have less influence on the transient predictions. It will not be possible to verify the accuracy of the transient predictions, but the same error levels as for steady state operation should be expected [less than *5 %*].

6.1.2.3 Fuelling Transient

The W19 engine employs a common rail fuelling technology. The rail is a high-pressure bus supplied by a mechanical pump – typically 1600 bar in this application, associated with piezo-injectors controlled by the EMS. The crankshaft driven pump is designed to maintain the highest possible rail pressure across the engine speed range. Therefore the injection pressure can change during the speed transients and is then accounted for by the injection controller. However, injection system models are complex, high frequency hydraulic systems. A well designed fuel system does not impair fuel spray in the cylinder therefore an advanced common rail model is not a direct requirement.

The transient fuelling strategy is a critical function during a transient because:

- the amount of energy in the turbine propelling exhaust gases is a direct consequence of the amount of fuel injected.

- the rate of fuel increase from one cycle to the other in a particular cylinder will influence the level of soot emissions during the transient which is commonly acknowledged as one of the diesel engine limiting factors

Because of the nature of the task to be carried out using the simulation environment, no Rate Of Fuel Increase [ROFI] will be implemented in the controller for the following reasons.

- The turbocharger performance is not compromised because the exhaust gases energy is maximised during the torque transient by unrestricted transient

fuelling. Therefore any gain obtained from the MAI control will come on top of what should be the best possible turbocharger transient.

▪ A ROFI strategy is optimised for smoke limit. Any alteration on the transient air charge management will require a re-calibration of the ROFI for the simulation to be representative. By deliberately not implementing this, the benefits of the MAI strategy will be immediately visible.

6.1.2.4 Powertrain Shifting

The engine speed changes associated with the transient are controlled by the CVT with the load it applies on the crank output shaft. Thus the powertrain shift is an integral part of the simulation and will need to offer consistency and a high level of sensitivity to the engine torque response to quantify the benefits on the vehicle response. The CVT model and its control strategy are consequently to be included in the simulation to help achieve a high level of powertrain control integration as shown in Chapter 2. The CVT and vehicle driveline models are a mean to examine to benefits of the MAI strategy. Low accuracy levels [less than *20 %*] are acceptable provided that repeatability is ensured.
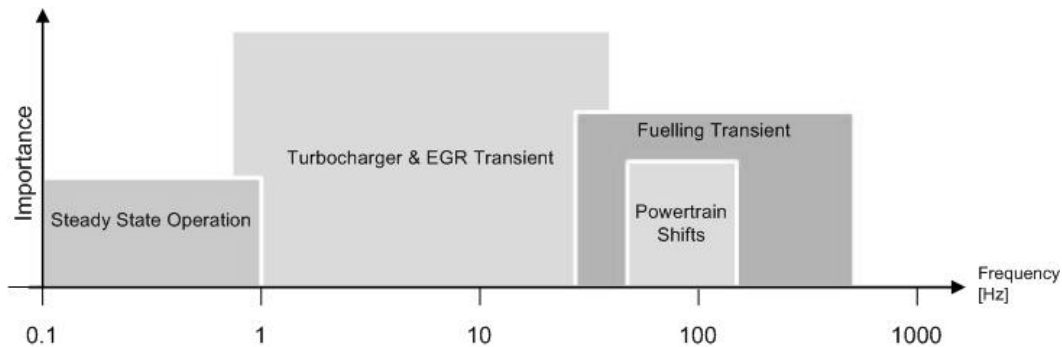
Figure 6.113 – Relative importance of phenomena for V6 diesel engine model established to develop load and transient with MAI. Each frequency band identified previously is represented by a bar which height is arbitrarily set to represent its level of importance in the modelling objectives.

6.2 Available Experimental Data

▪ Full load engine data were available from a confidential source, enabling a high level of model accuracy to be reached without the time expense of data collection.

▪ Full load turbocharger data was available as well as the very critical inertia value of the KKK BV50 turbocharger [$3.10^{-5}\ kg.m^2$].

Figure 6.114 presents the experimental data available for model tuning purposes, in addition to the basic engine dimensions introduced in the next section. Full load torque gives the engine output target to match, but other critical data such as the fuel mass injected per cylinder, the fresh air MAF or the boost pressure proved indispensable to tune the model and calibrate the controller.
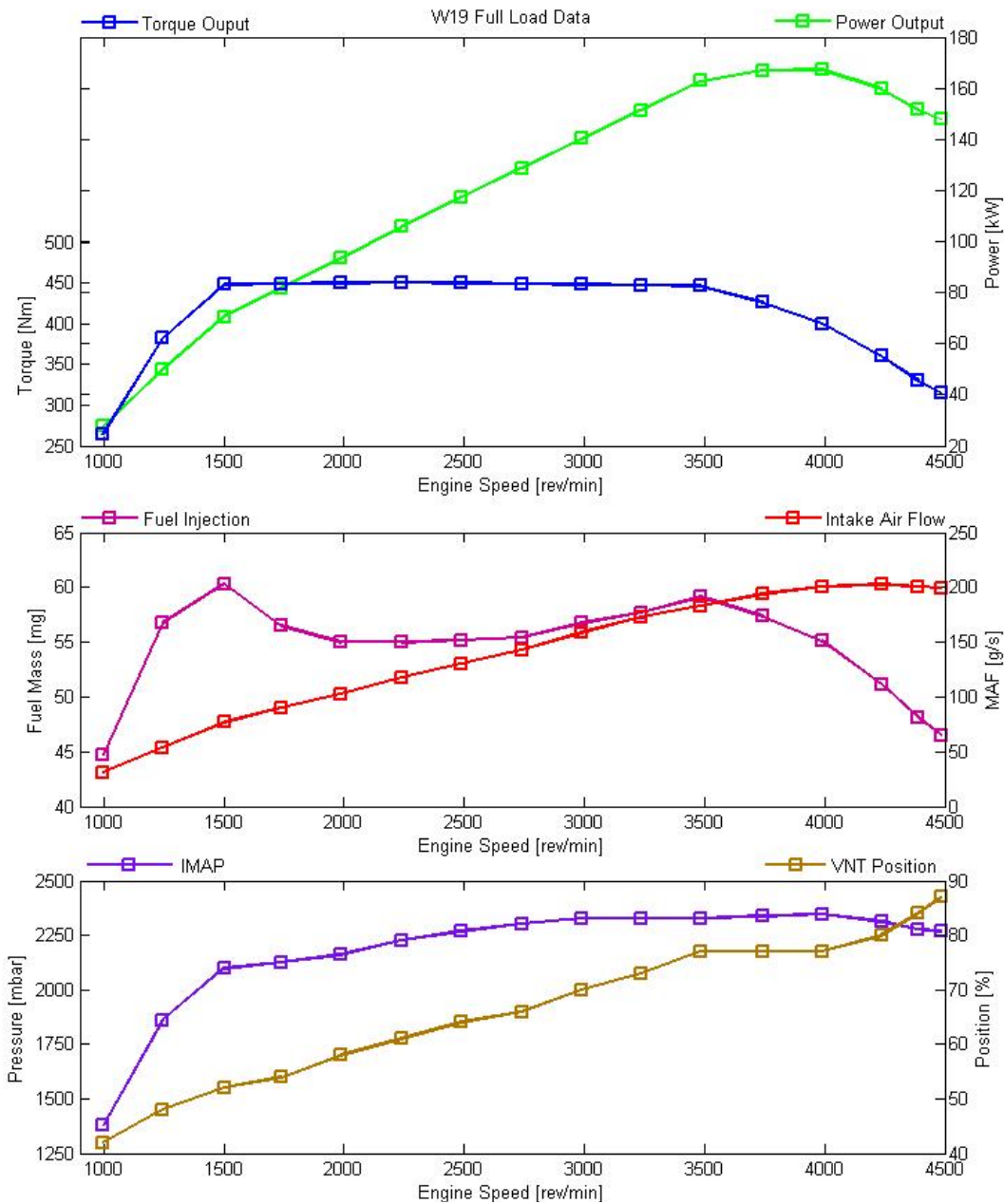
Figure 6.114 – W19 KKK BV50 3.0L V6 TDI engine experimental data. Obtained from engine dynamometer measurements over 16 steady state measurement points, the figures allow calibration of the engine model in full load to match the real-life performance.

6.3 Description

This section describes the model for the engine hardware in AMESim and the associate controller model executed in Simulink. Additional details on the 1D modelling techniques applied in AMESim can be found in Appendix C.

6.3.1 Plant Model

The engine model is based on the work of Rohrbacher [25] under guidance from the author. The principal dimensions of the engine architecture, timing and combustion model parameters are shown in Table 6.16. A single variable geometry turbocharger is blowing through 4 valves per cylinder. The fuelling system has been simplified by removing the common rail on each bank and the high pressure pump. Consequently, the fuelling system is modelled by simple injectors injecting at a constant pressure of *1600 bar* [Figure 6.115]. The multiple injections per stroke that is achieved on the W19 engine by the piezo-technology have also been replaced by a single injection.
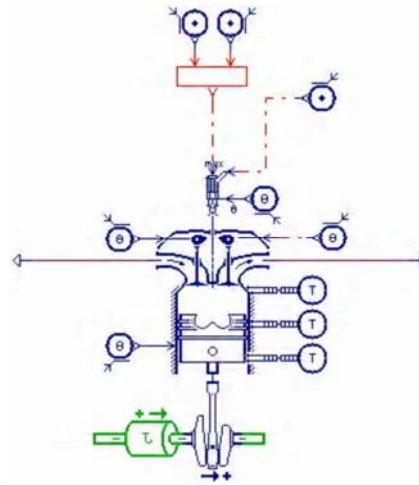
Figure 6.115 – Diesel engine injection, combustion and crankshaft model. Intake, exhaust and turbocharger sub-models are not represented. The injector model interfaces between control variables and the combustion chamber

Simplifications were also made on the intake and exhaust systems as explained below. Nevertheless these simplifications have been managed in order to reduce the computing time whilst keeping the accuracy of the results to an acceptable level. The following sections explain in the further details the modelling work achieved on the various sub-systems of the engine. When real data were not available and when possible, the model parameters were estimated using the AMESim TDI demonstration model parameters.

In Table 6.16, most of the parameters where estimated and then tuned to match the requirements of Section 6.1.2. The cylinder temperatures are from existing, valiudated AMESim engine models. IVO and EVC timings were tuned by Rohrbacher [25]. The timing and parameters of the valvetrain influence the breathing efficiency. The parameters were consequently tuned in full load using the experimental data. A similar approach was adopted to tune the combustion coefficient against the full load torque.

Variable Name	Title	Value	Units
Cyl_block_temp	Cylinder wall temperature	273+260	K
Cyl_head_temp	Cylinder head temperature	273+280	K
Piston_temp	Piston head temperature	273+250	K
IVO	Intake valve opening	-5	degCA
EVC	Exhaust valve closure	+5	degCA
Stoech_AFR	Stoichiometric air fuel ratio	14.6	n/a
Injection_pressure	Injector supply pressure	1600	bar
Injection_temp	Fuel temperature in ramp	273+40	K
Crate	Heat release coefficient	$6.96 \cdot 10^{-3}$	s
Cmode	Heat realease coefficient	450	kJ/kg/deg
Cdiss	Turbulent kinetic energy dissipation coef.	150	Hz

Table 6.16 – Global parameters for Injectors and combustion chambers. The parameters are declared once and applied to all 6 duplicates of the sub-assembly shown in Figure 6.115.

6.3.1.1 Combustion Model

The combustion heat release is calculated by the combustion chamber component according to the extended Chmela [78] equation based model. This model was preferred to the twin-Wiebe [76] model for its more predictive, physical approach which yields better results in transient simulations [Appendix C]. The heat release is calculated with respect to the mass of fuel present in the chamber and the turbulent kinetic energy k which is considered to be only induced by the fuel spray.

Equation 6.13 shows how the rate of heat release is parameterized by the factors C_{rate} and C_{diss}. The latter is not shown here but is present in the calculation of k. The C_{mode} relation between the turbulent kinetic energy and the heat release is defined. These parameters mainly depend on the combustion chamber geometry and fuel air mixing quality. The parameters were taken from the AMESim data base and are shown in Table 6.16.

$$\frac{dQ_{comb}}{dt} = A \cdot C_{mode} \cdot m_f \cdot e^{C_{rate} \frac{\sqrt{k}}{\sqrt[3]{V_{cyl}}}} \qquad A = (1 - X_{BGR})^{\alpha_R}$$

Equation 6.13 – Calculation of the heat release derivative, where k is the turbulent kinetic energy, m_f is the mass of fuel available in the combustion chamber and Q_{comb} is the heat released.

In Equation 6.13, A is a factor that takes into account the effect of the residual exhaust gases on the combustion heat release with X_{BGR} the molar fraction of burned gases in the mixture before the combustion and α_R a constant adjusting the effect of the residual gas on the heat release. This factor A is of main importance when using EGR and turbocharging because of the exhaust back flow; both play a significant role on the engine transient torque.

6.3.1.2 Intake & Turbocharger

The intake system is modelled by pipes, volumes and special components simulating the intercooler and associated heat exchanges. Only straight pipe models have been used. Upstream of the compressor, a pipe of *1m* long is modelling the intake which creates a negative relative pressure at the compressor input. The air filter has not been modelled. The air charge provided by the compressor is cooled by an air to air intercooler. The intercooler is approximated by a special volume that takes into account the pressure drop induced by the system and the heat loss. This heat flux is calculated with respect to the fresh air mass flow going through the intercooler which depends on the vehicle speed and the heat exchanger geometry. The geometry of exchangers was tuned to limit the output air temperature to around *50°C* at the engine maximum power. The cooled air then flows in two intake volumes, one for each bank, which directly feed the cylinder heads. The volume of each manifold is *1.5L* which gives a volume to bank displacement ratio of *1:1*. Figure 6.116 shows the intake and turbocharger sub-assembly.
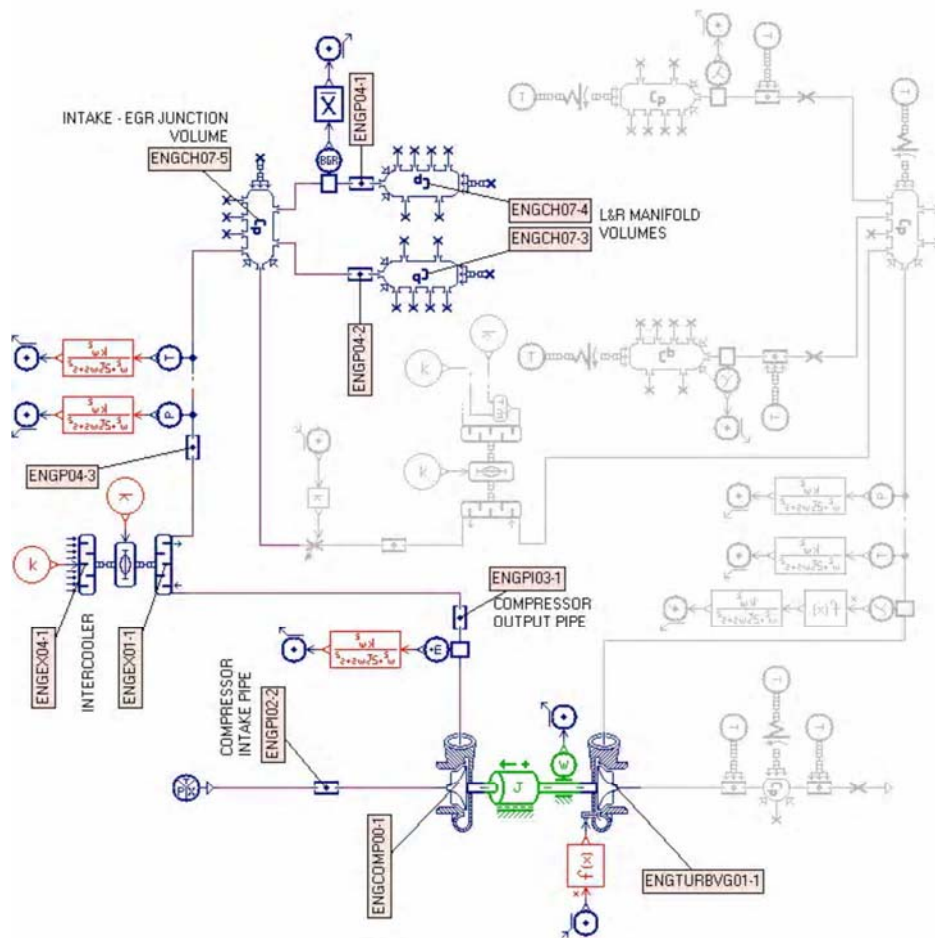
Figure 6.116 – Intake & Turbocharger sub-model assembly. The cylinders [Figure 6.115] are not represented here. Heat exchanges are modelled with cold sources at constant temperature and tuneable radiation, convection or conduction where appropriate.

The turbocharger model is composed of three parts: the compressor, the turbine and the rotary parts inertia [see Figure 6.116]. The later is transferring the turbine power to the compressor and simulates the turbocharger dynamics. A close approximation of the real turbocharger inertia value [$30.10^{-6}kg.m^2$] has been taken. This inertia is an important parameter since it is limiting the turbocharger response during the transient operations. Both compressor and turbine behaviours are characterised by maps as shown in Figure 6.117, defining the turbocharger operating conditions over its speed range.
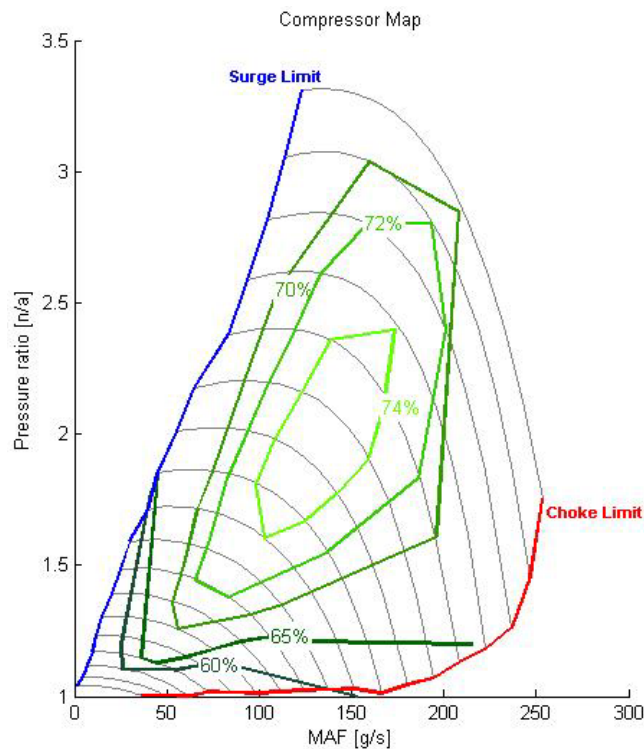
Figure 6.117 – Compressor map implemented in ENGCOMP00-1 [Figure 6.116]**.** Two look-up tables are actually super-imposed here. One gives the pressure ratio across the compressor vs. the corrected MAF at various shaft speeds, the other yields the efficiency value vs. corrected MAF

The turbocharger maps are expressed in term of a temperature corrected mass flow and speed. The VGT map is a combination of layers for different position of the turbine blades. In this particular case, these maps were not available and were derived from demonstration model data in AMESim. The compressor map was tuned to meet the engine performance requirements in a turbocharger matching exercise. Gas thermo-dynamics are taken into account in the model with geometrical considerations allowing prediction of the surge and choke phenomena. Additional model functionalities estimate the exhaust gas back flow. This is of most importance during transient simulations when an increase in the exhaust pressure induces back flow into the cylinders and reduces the engine output torque [63]. Table 6.17 lists the parameters associated with the intake and turbocharger sub-models in Figure 6.116.

Variable Name	Title	Value	Units
Fc [global]	Cut-off frequency for Butterworth filters	10	Hz
ENGPI02-2_pipe_diameter	Compressor intake pipe diameter	80	mm
ENGPI02-2_pipe_length	Compressor intake pipe length	1000	mm
ENGPI03-1_pipe_diameter	Compressor output pipe diameter	80	mm
ENGPI03-1_pipe_length	Compressor output pipe diameter	400	mm
ENGEX01-1_area	Intercooler internal flow equivalent area	600	mm^2
ENGEX01-1_volume	Intercooler internal volume	2	L
ENGEX04-1_area	Intercooler front area	0.03	m^2
ENGP04-3_pipe_diameter	Intercooler output pipe diameter	80	mm
ENGP04-3_pipe_length	Intercooler output pipe length	500	mm
ENGCH07-5_volume	EGR intake junction volume	0.4	L
ENGP04-1&2_pipe_length	Intake run L&R length	20	mm
ENGCH07-3&4_volume	Intake L&R manifold volumes	1.5	L
ENGCOMP00-1_radius	Compressor impeller radius	50	mm
ENGCOMP00-1_surge_coef	Surge coefficient for zero MAF pressure ratio ($Pr_{surge}/Pr_{dm=0}$)	2	n/a
ENGCOMP00-1_choke_coef	Choke coefficient for max MAF ($dmc_{PR=1}/dm_{choke}$)	1.1	n/a
ENGTURBVG01-1_area	Turbine backflow equivalent area	100	mm^2
ENGTURBVG01-1_coefficient	Turbine backflow equivalent flow coefficient	0.72	n/a

Table 6.17 – Local parameters for the intake and turbocharger sub-models. Intake and turbocharger models are parameterized by 1D physical dimensions. The compressor and turbine are characterised by steady state maps [Figure 6.117]

The physical dimensions in Table 6.17 are estimated apart from the compressor and turbine parameters which are taken from an existing AMESim demonstration model of similar nature. It the case of the intercooler, the parameters were tuned to obtain the estimated temperature and pressure drop. The 2nd order low-pass Butterworth filters are set to elimate noise from the controller inputs which would affect the control accuracy. The noise is mostly a 3rd order of engine speed associated with the thermo dynamic effect of each cylinder intake stroke. This is an undesirable input to the controller, but a low cut-off frequency would attenuate the 1st order frequency and consequently degrade the dynamic response of the sensors during the transient. The cut-off frequency for the Butterworth filters was therefore tuned to the maximum value capable of eliminating the cylinder pumping related fluctuations at low engine speed.

6.3.1.3 Exhaust & EGR

The exhaust system has been modelled in the same way as the intake system, using elementary components for pipes and volumes. Two *1.5L* exhaust manifolds are directly fixed onto the cylinder heads and feed the turbocharger turbine via two *500mm* long pipes. The exhaust line downstream of the turbine has been simplified and is only modelled by a pipe filling a *3L* volume which reproduces a silencer; a final pipe of *2m* connects this volume to the ambient condition. The exhaust line aims at defining the turbine downstream pressure. The exhaust gas heat loss is simulated in the exhaust system in order to take into account the loss of energy recoverable by the turbine as well as the exhaust manifold thermal response playing a role in turbocharger lag [79][80].
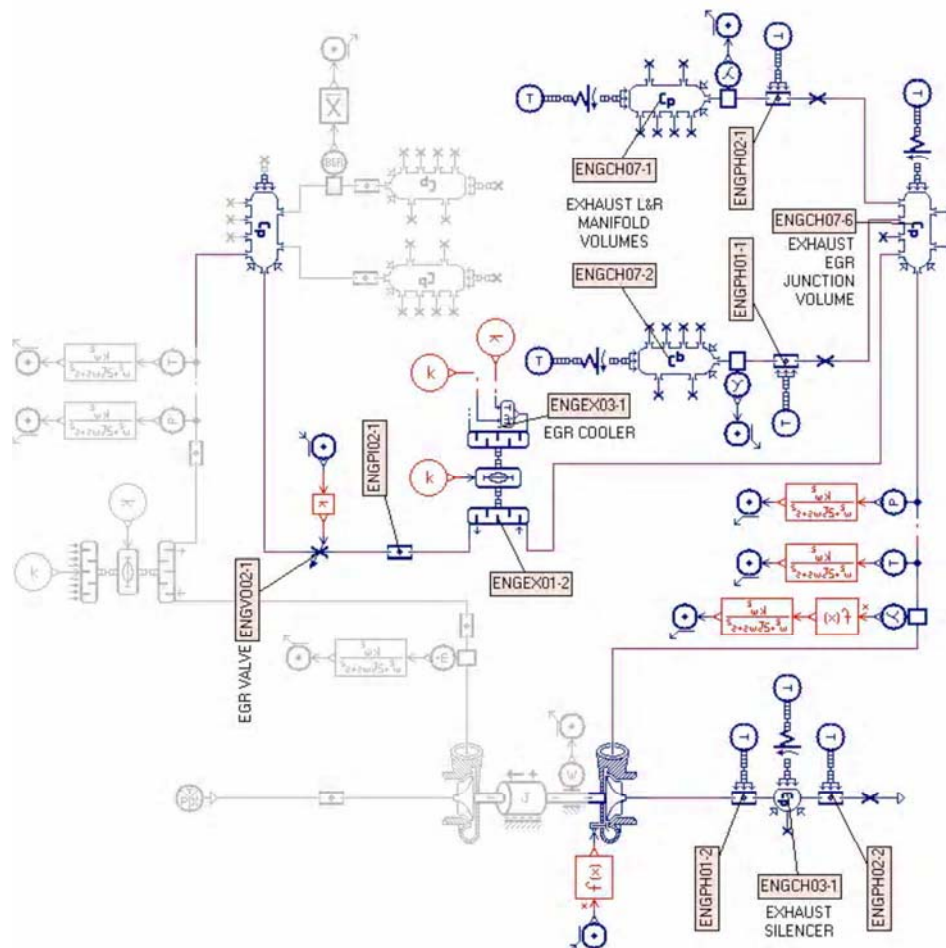
Figure 6.118 – Exhaust & EGR sub-model assembly. The cylinders are again excluded from the diagram for clarity. The EGR intercooler is in the centre, feeding exhaust gases back in the intake. Intake and turbocharger sub-models [Figure 6.117] appear in grey for reference. The exhaust after-treatment system is not modelled.

The EGR system aims at reducing the emission of harmful gases and especially NOx by diluting the intake air charge with recycled exhaust gases and subsequently limiting peak cylinder temperatures. However, the engine output torque can suffer from

the lack of oxygen in the inlet charge. In the model a variable area vane placed just before the turbine input controls the fraction of exhaust gases being re-circulated. These gases are cooled by a water to air intercooler before being injected directly in the intake. The cooling of the re-circulating burned gas limits the increase of the inlet charge temperature and hence limits the breathing efficiency loss. The engine transient torque is affected by the EGR system since even if the valve is closed instantaneously; exhaust gases are still trapped in the intake manifold and the subsequent exhaust manifold pressure increase creates exhaust backflow into the cylinders [63].

Table 6.18 lists the parameters associated with the exhaust and EGR sub-models shown in Figure 6.118. These were set with the same technique as in Section 6.3.1.2.

Variable Name	Title	Value	Units
ENGCH07-1&2_volume	Exhaust L&R manifold volumes	1.5	L
ENGPH01&2-1_pipe_diameter	Exhaust L&R pipe diameter	45	mm
ENGPH01&2-1_pipe_length	Exhaust L&R pipe length	500	mm
ENGCH07-6	EGR exhaust junction volume	0.4	L
ENGEX01-2_area	EGR cooler internal flow equivalent area	300	mm^2
ENGEX01-2_volume	EGR cooler internal volume	0.4	L
ENGEX03-1_heat_value	Engine coolant specific heat_value	1005	J/kg/K
ENGEX03-1_flow	Engine coolant EGR mass flow	0.8	Kg/s
ENGPOI02-1_pipe_diameter	EGR output pipe diameter	25	mm
ENGPOI02-1_pipe_length	EGR output pipe length	700	mm
ENGVO02-1_diameter	EGR valve maximum equivalent diameter	20	mm
ENGVO02-1_inflow_coef	EGR valve maximum inflow coefficient	0.5	n/a
ENGVO02-1_backflow_coef	EGR valve maximum backflow coefficient	0.2	n/a
ENGCOMP00-1_radius	Compressor impeller radius	50	mm
ENGPH01-2_diameter	Turbine output pipe diameter	60	mm
ENGPH01-2_length	Turbine output pipe length	30	mm
ENGCH03-1_volume	Exhaust silencer volume	2	L
ENGCH03-1_area	Exhaust silencer convective exchange area	78000	mm^2
ENGPH02-2_diameter	Exhaust pipe diameter	60	mm
ENGPH02-2_diameter	Exhaust pipe length	1000	mm

Table 6.18 – Local parameters for the exhaust and EGR sub-models. Additionally, all ambient temperature sources used for heat exchanges are between *300* and *345 K* depending on their location in the vehicle.

6.3.1.4 CVT & Driveline Model

During tip-in manoeuvres, the engine is accelerated as quickly as possible to its new target speed, which critically affects the engine torque transient response. This acceleration is proportionally related to the torque balance on the crankshaft. The transmission input torque, i.e. engine load required to produce the wheel torque depends on how much torque is available from the engine during a transient.

For the purpose of simulating the engine load torque, a driveline and vehicle model has been implemented and is illustrated in Figure 6.119. The engine acceleration during a shift is delayed by the engine torque response and the CVT hydraulic response. Because the hydraulic time lag is much smaller than the engine. So the CVT is modelled by a simple variable ratio component that will not account for the actuation lag. This affects the ability of the model to reproduce the high frequency engine acceleration [above 3th order], which is not included in the modelling requirement previously established. The CVT ratio is directly fixed by one input; thus the CVT controller has to define the evolution of the CVT ratio.
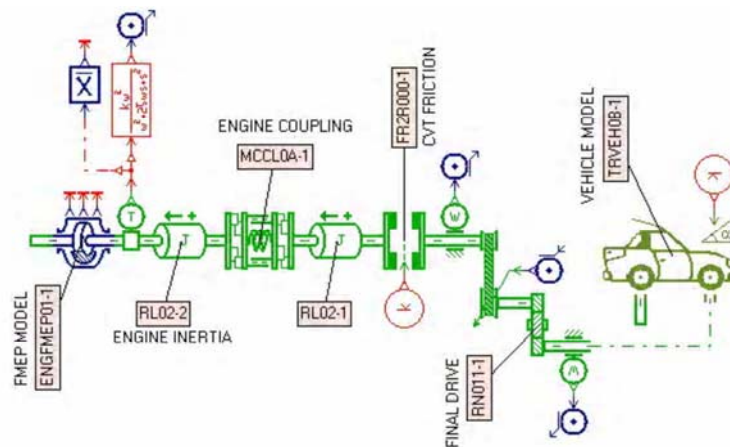
Figure 6.119 – Engine friction, CVT and vehicle models. The engine is not represented. An FMEP model estimates the frictional losses in the engine before torque is transmitted to the CVT via a coupling. The CVT fixed gear set drives the front-wheels of the vehicle longitudinal dynamics model.

The engine friction is modelled by an empirical FMEP model from Patton [81] presented in Equation 6.14. The CVT variator slip is modelled by a clutch-type sub-model limiting the torque through the transmission. A gear set at *85%* efficiency models the differential and final drive ratio as well as the efficiency of the CVT variator. This transmission model is driving a vehicle model which effectively calculates the vehicle longitudinal acceleration and speed from the wheel torque equilibrium. Therefore, the model computes the vehicle resistive torque by adding the rolling resistance, the aerodynamic drag [Equation 6.15] and the slope resistance. The vehicle initial conditions and the initial CVT ratio are finally set to define the initial engine operating point and vehicle speed.

$$FMEP = A + B \cdot N + C \cdot N^2 + D \cdot N^3$$

Equation 6.14 – FMEP model from Patton [81] where A, B, C and D characterize the engine friction and accounts for mechanical, pumping and ancillaries losses. *N* is the engine speed.

$$F_{aero} = \frac{1}{2} \cdot C_x \cdot \rho_{air} \cdot A_{veh} \cdot (V_{veh} + V_{air})^2$$

Equation 6.15 – Aerodynamic force on vehicle as used by sub-model TRV0B-1.

Variable Name	Title	Value	Units
ENGFMEP01-1_displacement	FMEP model cylinder displacement	0.495	L
ENGFMEP01-1_cylinder_no	FMEP model number of cylinders	6	n/a
ENGFMEP01-1_A	FMEP model offset	0.97	bar
ENGFMEP01-1_B	FMEP model linear coefficient	150.10^{-6}	bar / (rev/min)
ENGFMEP01-1_C	FMEP model quadratic coefficient	50.10^{-9}	bar / (rev/min)^2
RL02-2_inertia	Engine lump inertia	0.25	kg.m^2
MCCL0A-1_stiffness	Engine coupling stiffness	22	Nm/deg
MCCL0A-1_damping	Engine coupling damping coefficient	0.22	Nm / (deg/s)
MCCL0A-1_stop	Engine coupling free displacement	±4	deg
RL02-1_inertia	Driveline inertia	0.05	kg.m^2
FR2R000-1_coulomb	CVT maximum Coulomb dynamic torque	1200	Nm
RN011-1_ratio	Final drive ratio	-4	n/a
RN011-1_efficiency	Driveline efficiency	0.85	n/a
TRVEH0B-1_radius	Wheel rolling radius	0.327	m
TRVEH0B-1_radius	Vehicle mass	1.76	t
TRVEH0B-1_A	Rolling resistance	259	N
TRVEH0B-1_B	Rolling viscous friction coefficient	1.727	N / (m/s)
TRVEH0B-1_Cx	Vehicle air drag coefficient	0.3	n/a
TRVEH0B-1_area	Vehicle frontal area	2	m^2

Table 6.19 – Local parameters for the vehicle and driveline sub-models shown in Figure 6.119. The equations for the FMEP model and the vehicle drag force are shown respectively in Equation 6.14 and Equation 6.15

Table 6.19 lists the parameters employed by the various sub-models for the CVT and vehicle. The assembly of the sub-systems presented in the previous paragraphs is shown Figure 6.120, with the interface blocks to Simulink which will be discussed in the following section.
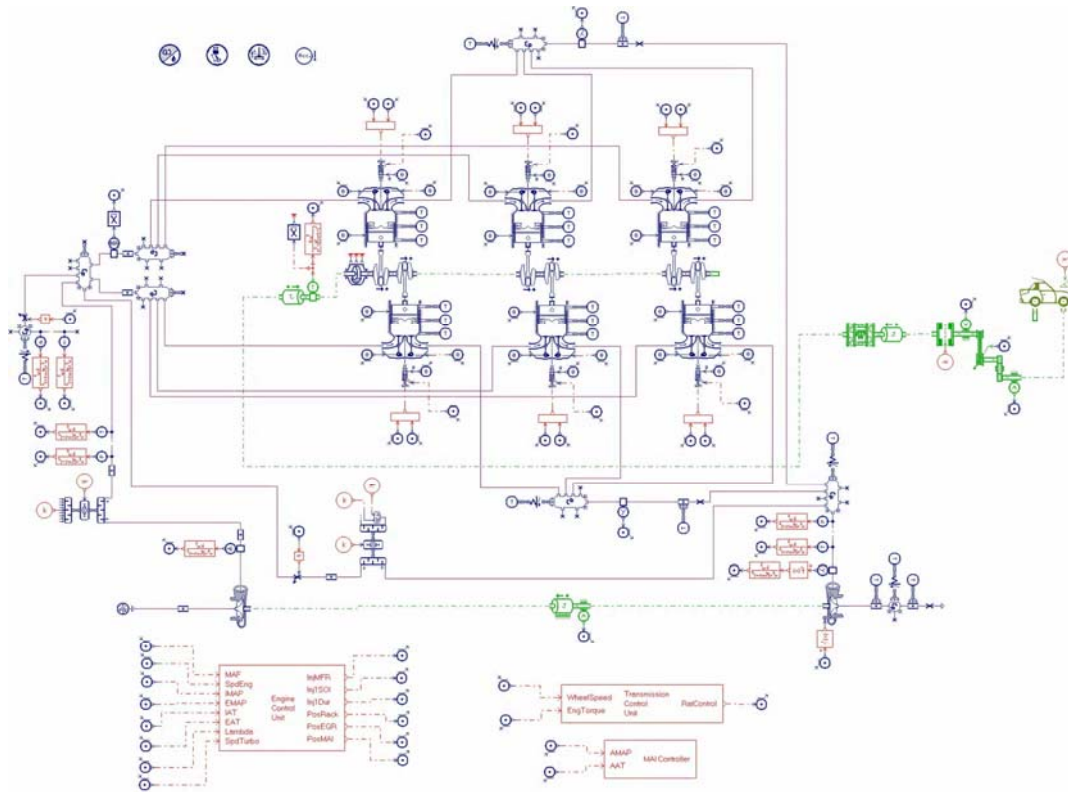
Figure 6.120 – Complete AMESim model of the Audi W19 3.0L V6 TDI. The interface blocks to the controller in Simulink appear at the bottom of the diagram. The CVT and vehicle models detailed above can be found on the right.

6.3.2 Controller Model

The controller for the plant described above is built in Simulink. The AMESim and Simulink solvers were used in a co-simulation hence only exchanging their respective input and outputs through the interface [see Appendix C]. This means that the state variables are not exchanged, but this setup is particularly appropriate for a plant / controller split up. Figure 6.121 presents the engine controller which will be detailed in the following paragraphs. Together with CVT controller, both are run with a trigger at a fixed time step of *1ms*.
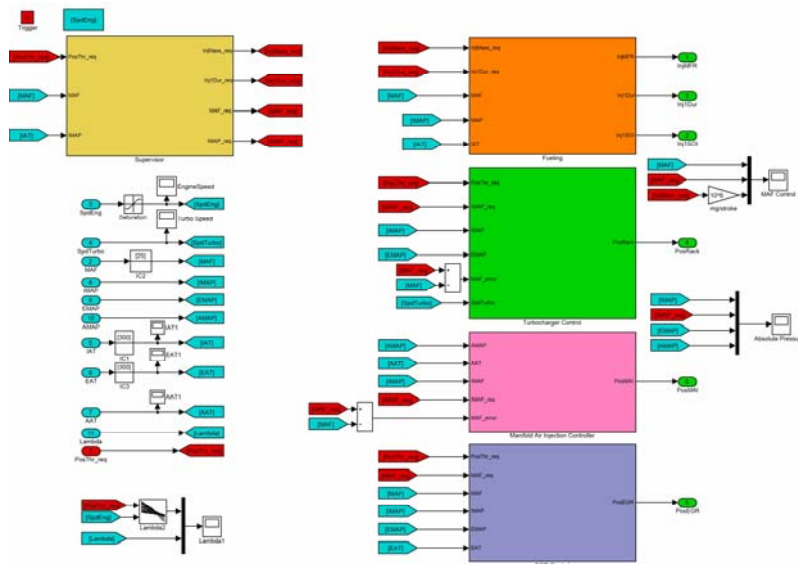
Figure 6.121 – Engine Management System. The supervisory controller at the top left corner sets the targets for each of the EMS sub-functions on the right. Wiring is virtually eliminated by the extensive use of GoTo / From labels.

The engine controller is made of a supervisory block which sets targets for the fuelling, turbocharger and EGR detailed in Sections 6.3.2.1 & 6.3.2.2 below. Calibrated tables fix the required injection mass and duration, air charge MAF and intake pressure [required IMAP]. Those look up tables are based on engine load and speed operating conditions. Each steady state condition defined by a point in the look-up tables was either calibrated for optimised operation or tuned to match the data presented in Section 6.2 above.

The first look-up table to be created is the fuel injection mass shown in Figure 6.122, which reflects the engine external load demand in a similar way to the throttle in an SI engine. This also sets a direct requirement for the intake pressure [IMAP] in order to supply each cylinder with sufficient air charge. A desired lambda table was built from the full load experimental data and commonly used part load AFR. The IMAP look-up table is presented in Figure 6.123. It was calibrated to yield the desired lambda values across speed and load range. At this stage, the EGR calibration influences the output torque even at a fixed *InjMass* and *IMAP*. A certain amount of fresh air has to be

provided in the gas mixture feeding the combustion chamber. For that purpose, the MAF look-up table [Figure 6.124] is calibrated for the same input ranges as the previous two maps.
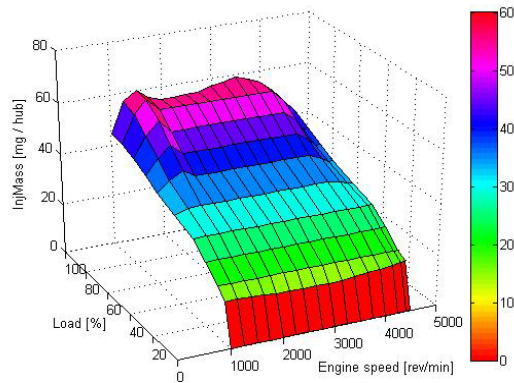
Figure 6.122 – Fuel mass injection look-up table built from fuel load experimental data on down. The amount of fuel injected in each cylinder determines the engine output torque
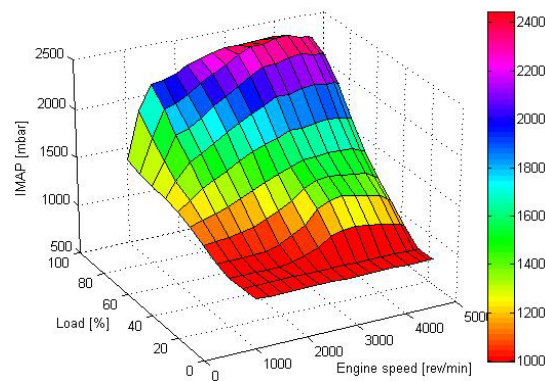
Figure 6.123 – Intake pressure set points. The target boost pressure is used by the turbocharger VNT control
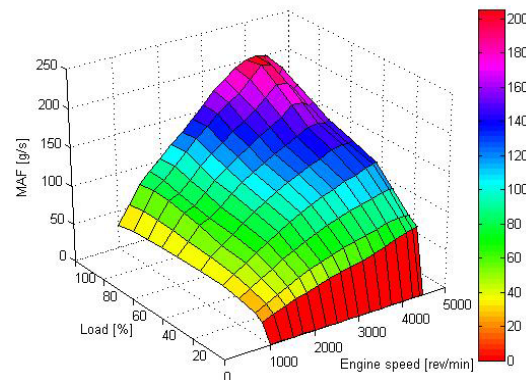
Figure 6.124 – Intake mass air flow target set points. The MAF target value is sent to the EGR controller which regulates the burnt gases recirculation valve opening.

6.3.2.1 Fuelling Strategy

The fuelling strategy simply consists in controlling the injectors opening time and mass flow to spray the required fuel mass per stroke *InjMass_req* from the EMS supervisory block. In the plant model, the mass flow rate during opening is a direct input to the injector.
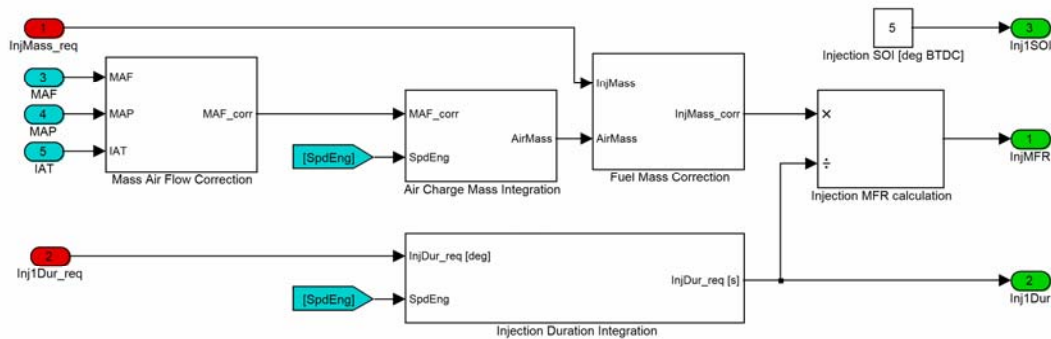
Figure 6.125 – Fuelling control block. The simplest of the EMS sub-functions since it does not involve any feedback loop. The fuel mass per stroke is converted into duration and required mass flow for the injectors. MAF correction and lambda windowing are available features.

The fuel mass requirement is corrected to limit under or over fuelling if the air path control fails to match its targets during a transient. The duration of the single injection *Inj1dur_req* is scheduled across the speed range in order to provide the enough exhaust pressure for the turbine [see next section] whilst keeping the combustion rate and peak pressure to a minimum. The start of injection *Inj1SOI* is set to *5 degCA BTDC* for simplicity.

Consequently the fuelling strategy is a simplified version of the real EMS functions. A multiple injection per stroke strategy is necessary to keep NOx levels down by limiting the ROHR with progressive fuel injection. It is also necessary to maintain the lowest possible peak cylinder pressures. These create undesirable engine vibration levels which contribute to the vehicle NVH. The simplification adopted here helps keeping calibration time down without compromising the ability of the model to faithfully predict torque transient.

6.3.2.2 Turbocharger and EGR Controller Architecture

The control of the variable geometry turbocharger rack and EGR valve during speed and torque transient is the key to good performance and satisfactory emission levels. Their response is very much affected by the exhaust pressure hence making both systems particularly difficult to control. The approach taken is to control the VGT blade position around a calibrated *feed-forward* set point [63]. The intake boost pressure IMAP at the compressor stage the *feed-back* variable of a PI closed-loop control which varies the VGT command around the set-point. The gains are calibrated over the speed and load range from plant response measurements in order to optimise the performance of the PI control.
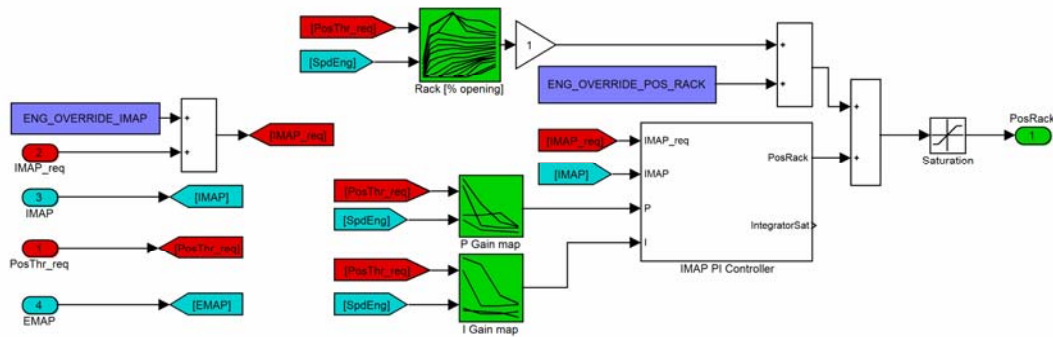
Figure 6.126 – Turbocharger rack controller. The central block is the PI controller for the IMAP. P and I gains are mapped in the smaller green blocks. The output is added to the feed-forward set point. The controller offers the possibility to offset the inputs and the outputs for calibration purposes.

Figure 6.126 shows the turbocharger control architecture with the feed forward set points map [top, in green], PI controller [centre] and associated gain maps [bottom, in green]. The VGT set-points are shown in Figure 6.127. Provision is also made to offset the position and boost pressure set points [in blue] during a simulation to investigate the plant response at a particular operation condition.
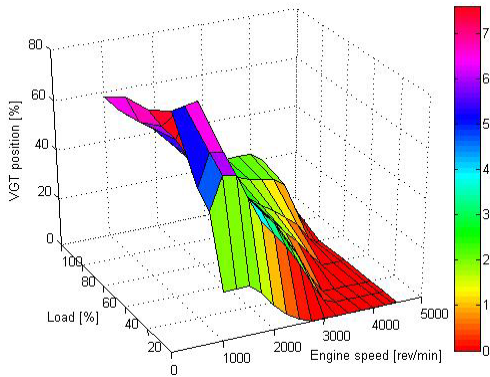
Figure 6.127 – VGT calibrated set points for the feed forward signal in the turbocharger control. Each position is calibrated to be representative of the position of the VGT in steady state.
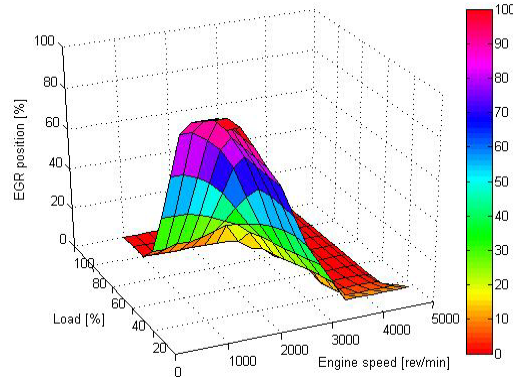
Figure 6.128 – EGR calibrated set points for the feed forward signal in the valve control. Each position is calibrated to be representative of the position of the EGR in steady state.

The EGR control architecture is similar, but uses the fresh air flow *MAF* for a controlled variable. The EGR calibrated set points are shown in Figure 6.128. Simultaneous closed-loop control of the both VGT and EGR is complicated. Early transient simulations highlighted the necessity to couple the two strategies, and in particular the modification of the EGR command depending on the VGT actuation [63]. Therefore the PI control of the EGR was disconnected leaving the feed-forward set point for only command. This would affect the emissions in the low to medium range, but since most transients involved large tip-ins where the EGR set-point is predominant, the simulation results were only mildly affected.

6.3.2.3 CVT Control

The purpose of this study is *not* to investigate the influence of the CVT control strategy on the engine response, but to match the latter to the CVT powertrain requirement. Consequently the transmission controller [Figure 6.129] was kept relatively simple in order to provide a way to reproduce typical driving manoeuvres such as tip-ins.
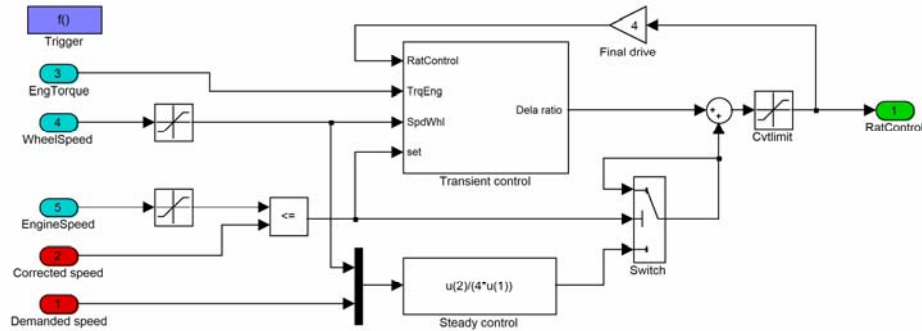
Figure 6.129 – CVT Controller. Transient [top] and steady state [bottom] blocks are alternatively used based on a transient detection function. Interconnection between the two functions ensures continuity.

The CVT control law is based on the ratio derivative control. Jantos [12] demonstrated the need to limit the rate of change of the transmission ratio during speed transients. Large driver tip-ins are associated with a new engine speed request to match the power requirement. This means that extra engine torque is required:

- To accelerate the vehicle.
- To accelerate the engine and transmission input shaft.

If the CVT ratio was decreasing too quickly during the acceleration phase, the vehicle would decelerate as a result of the lack of drive torque. The controller is therefore composed of a steady state block which maintains a desired ratio during cruising for constant engine speed and a transient block [Figure 6.130] which uses engine brake torque as a feed back to optimise the engine acceleration phase.
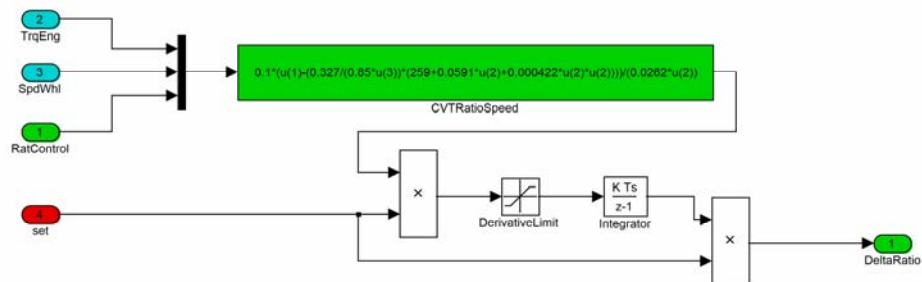
Figure 6.130 – CVT transient control law calculates the maximum rate of change of the CVT ratio so that the wheel torque remains positive during the engine acceleration phase [12].

The transient ratio control law is based on the steady state wheel torque and the engine torque, fed back from the model in this case. Equation 6.16 details the calculation for the maximum CVT ratio derivative during a vehicle tip-in. The CVT controller limits the actual *RatControl* derivative to *40%* of this maximum in order to provide both vehicle *and* engine acceleration. A more elaborate strategy would vary this split factor depending on the aggressiveness of the manoeuvre.

$$\left. \frac{d(RatControl)}{dt} \right|_{MAX} = \frac{TrqEng - \dfrac{TrqWhl}{RatControl \cdot FinalDrive\_ratio \cdot Driveline\_efficiency}}{SpdWhl \cdot FinalDrive\_ratio \cdot Engine\_inertia}$$

Equation 6.16 – Maximal CVT ratio [*RatControl*] derivative [12] to prevent vehicle deceleration during power-on downshift. *TrqWhl* is the resistive torque at the wheel from static, viscous and aerodynamic drag [Equation 6.15].

Consequently during a tip-in manoeuvre, the engine will accelerate to a scheduled speed set point using no more than the available engine torque that builds up as the engine torque request has increased. The advantage of this approach is that any torque response benefits will be directly reflected in the transient profile of the engine speed which makes the most of the available torque margin. This means no particular re-calibration during the MAI investigation stages and a powertrain globally biased towards best performance.

However simplistic the control law may seem, it highlights the benefits an improved engine response. During the calibration phase of a complete powertrain strategy, the compromise to be found between rapid shifts and positive vehicle response would be significantly improved by the larger, faster torque reserve. This ratio derivative control emphasises the engine limited transient performance of the powertrain.

6.4 Performance Analysis

This final section will analyse the behaviour of the model previously described to assess its performance against the full load experimental data and highlight the issues related to CVT operation. A small number of step input tip-in manoeuvres have been chosen to complete this analysis. As stated in the first chapter of this study, the torque response and margin is critical with CVT operation. The most demanding tip-ins below will demonstrate this.

6.4.1 Baseline Engine results

Before looking in detail at the various sub-systems performance during the tip-ins, the complete simulation environment is run in order to validate the behaviour of the system and the full load figures. Figure 6.131 shows a power-on downshift from *1600* rev/min to *3600 rev/min* corresponding to an engine power of *54 kW* to *173 kW*, i.e. full power.

The full load torque at *3600 rev/min* is *460 Nm* compared to *445 Nm* in reality which corresponds to *3.3 %* error. The boost pressure at the same speed is *2400 mbar* in simulation compared to *2320 mbar* experimentally [*3.4 %* error]. The intake mass airflows match perfectly. The levels of accuracy for these variables are below *4 %* from *1500* to *4000 rev/min*, satisfying the requirements for steady state operation of the model.

The air path transients in the exhaust and intake show typical results. The IMAP error between the required and the actual value increases suddenly when the load request increases. This effectively shifts the VGT to a new operating condition at a higher speed. The blades are closed by the PI controller which raises the exhaust pressure [EMAP] and the shaft speed. The MAF on the compressor side subsequently increases from the greater pumping work of both the pistons and the turbocharger.

The effective air fuel ratio reaches a minimum when fuelling levels are not yet matched by the fresh air flow. This is due to the lack of ROFI strategy which would limit the rate of increase of *InjMass_req*. Instead, a first-order filter limits the fuelling command at *40ms* time constant. The air path lag is therefore highlighted, without any consequence to the torque output.
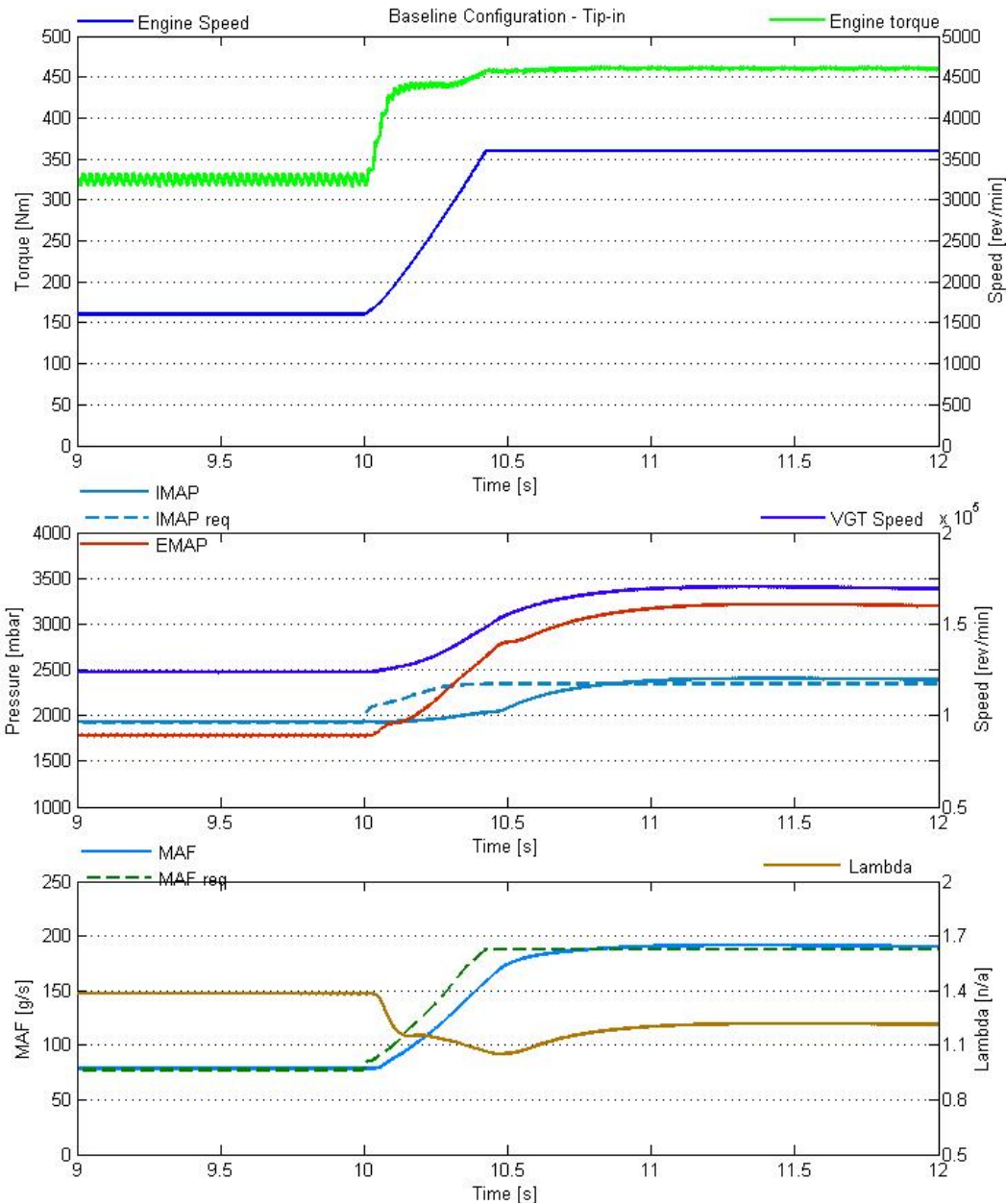
Figure 6.131 – Baseline engine configuration tip-in from *1600 rev/min & 70 %* load to *3600 rev/min & 100 %* load. The torque response enables a new engine speed to be reached with half a second, whilst the turbocharger increases from *125,000* to *170,000 rev/min*. The lower graph shows the air fuel ratio during the manoeuvre staying above stoichiometric.
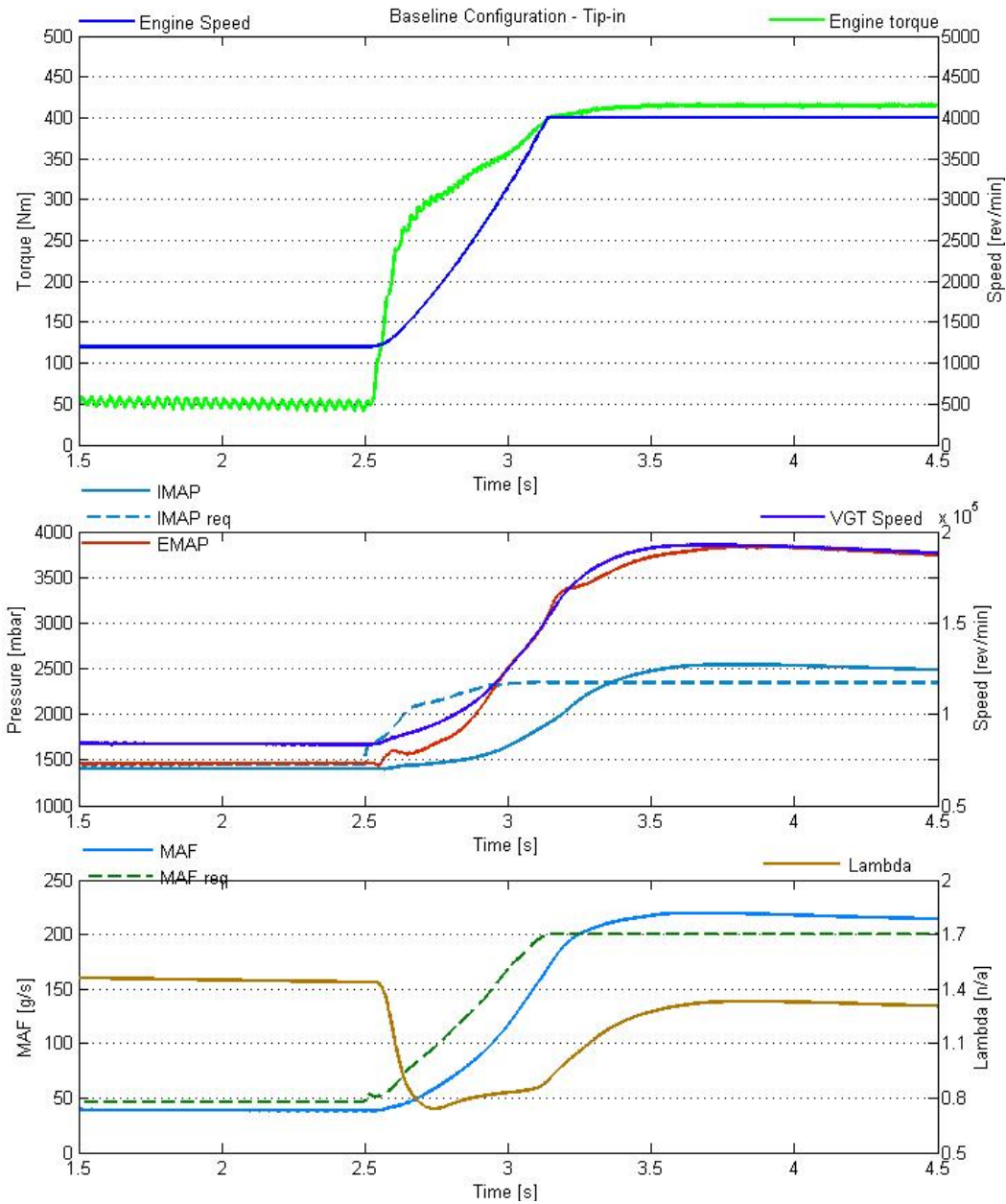
Figure 6.132 – Baseline engine configuration tip-in from *1200 rev/min & 30 %* load to *4000 rev/min & 100 %* load. More aggressive than Figure 6.131, this exhibits a longer torque response and larger error levels for both IMAP and MAF signals. The Lambda value drops below *1* for nearly *0.5 s*.

The manoeuvre presented in Figure 6.132 is a deeper tip-in than Figure 6.131. The initial steady state condition is at *1200 rev/min* and *30 % load*, i.e. *6.3 kW* to full power at *4000 rev/min*, i.e. *176 kW*. From cruising at *50 km/h*, this transient corresponds to a full accelerator pedal input from the driver. This aggressive nonetheless realistic manoeuvre is aimed at revealing any issues related to the torque transient during the engine and vehicle acceleration phase that directly follow the new power request.

The torque response is expectedly much slower than in the previous transient manoeuvre. The IMAP and MAF control performance is degraded, with larger error level reached between target and actual values. Both variables exhibit over shoot after the transient, highlighting the limit of stability of the PI control. Finally the air fuel ratio drops well below stoichiometric during *0.5 s*, with a lowest at *0.76*. Such a fuel mixture would create large amount of particulate matter, i.e. soot.

6.4.2 Sub-systems Evaluation

In this section, both the air path control on one hand and the CVT and vehicle models on the other hand are examined in further detail. The realism of the simulation environment with respect to the initial requirements is highlighted, as well as the short comings of the baseline engine configuration installed in the CVT powertrain

6.4.2.1 Turbocharger Control

The VGT position controller follows the set point calibrated for steady state operation and modulates around this value during the transient to control the IMAP at the required value. Figure 6.133 shows additional VGT controller data related to the first manoeuvre introduced previously in Figure 6.131. The turbocharger speed increases from *125,000* to *170,000 rev/min* from the added power on the shaft by the turbine. The PI controller adjusts the blades position to increase the EMAP for that purpose.
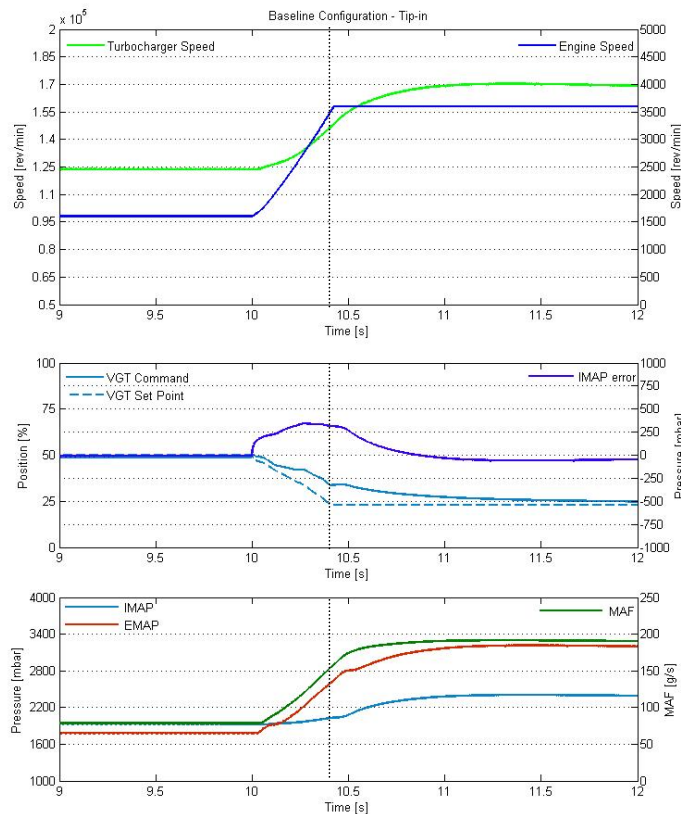
Figure 6.133 – Transient VGT control from *54 kW* to *173 kW* engine power output. The nozzle set point is adjusted from the engine speed and load, while the final command is adjusted around the set point from the IMAP error

The MAF produced at the intake by the compressor follows the same progression until the new engine speed is reached.

At that point, the VGT speed has almost reached its final value and the boost pressure regroups with its target value as the engine pumping work stabilises.

Figure 6.134 shows the VGT lag exposed during the deeper tip-in [Figure 6.132]. The IMAP error created by the larger step in load demand forces the turbine blades to be held around *60 %* by the controller before being slowly re-opened as the EMAP increases. However, this process happens too slowly and results in air fuel mixture largely under stoichiometric as observed in Figure 6.132.
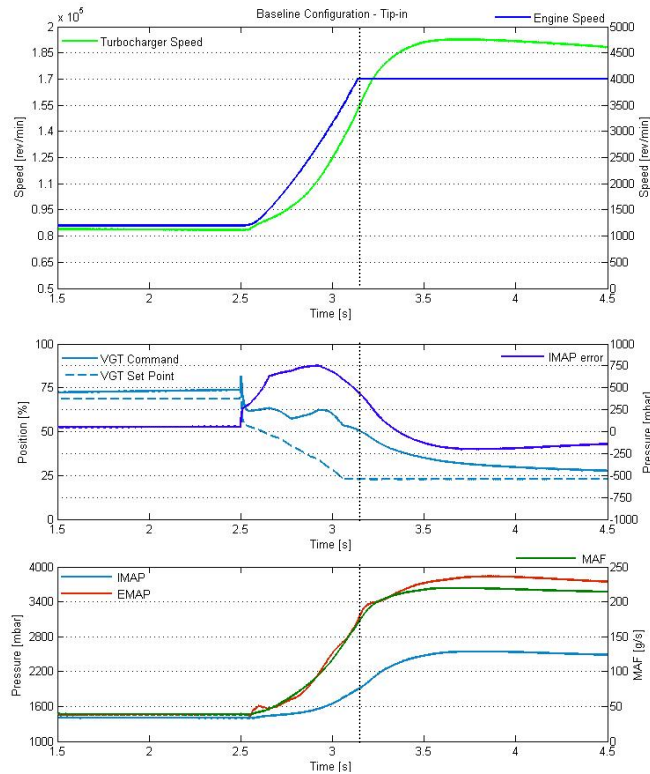
Figure 6.134 – Transient VGT control from *6.3 kW* to *176 kW* engine power output. The nozzle set point is adjusted from the engine speed and load, while the final command is adjusted around the set point from the IMAP error
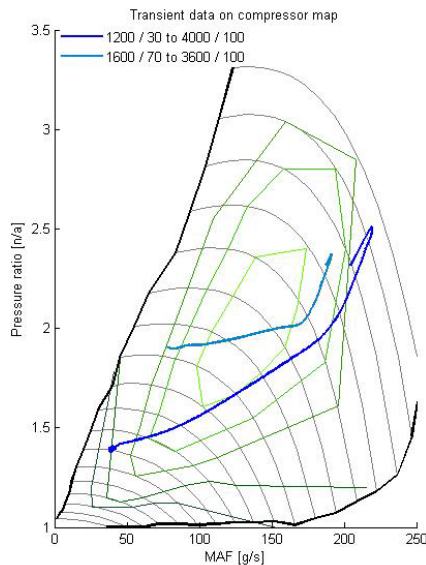
Figure 6.135 –Tip-in comparison of compressor behaviour plotted on speed and efficiency map

Both tip-ins are plotted on top of the compressor map in Figure 6.135. It highlights the satisfying performance of the VGT control during the first tip-in [cyan], the operating condition crossing the best efficiency region. The second tip-in [blue] however shows how the lack of intake pressure compromises the performance in the beginning of the transient, and then overshoots its new steady state condition in the end.

The EGR strategy has little effect on this phenomenon as the valve is rapidly shut down when the load request increases. Fortunately, the cases where turbocharger lag is most critical, e.g. second tip-in are those where exhaust gas recirculation is kept minimal.

6.4.2.2 CVT & Vehicle Models

The baseline powertrain performance is evaluated using the driveline and vehicle model as shown in Figure 6.136. The heavy tip-in illustrated does not involve any rate of fuel increase management which would limit the mass of fuel injected during the engine acceleration phase to prevent the lambda excursion shown previously. Therefore the best torque achievable is used to simultaneously accelerate the vehicle and the engine. Once the new engine speed is reached, the steady state ratio strategy takes over and upshifts progressively to maintain maximum engine speed as the vehicle keeps on accelerating.
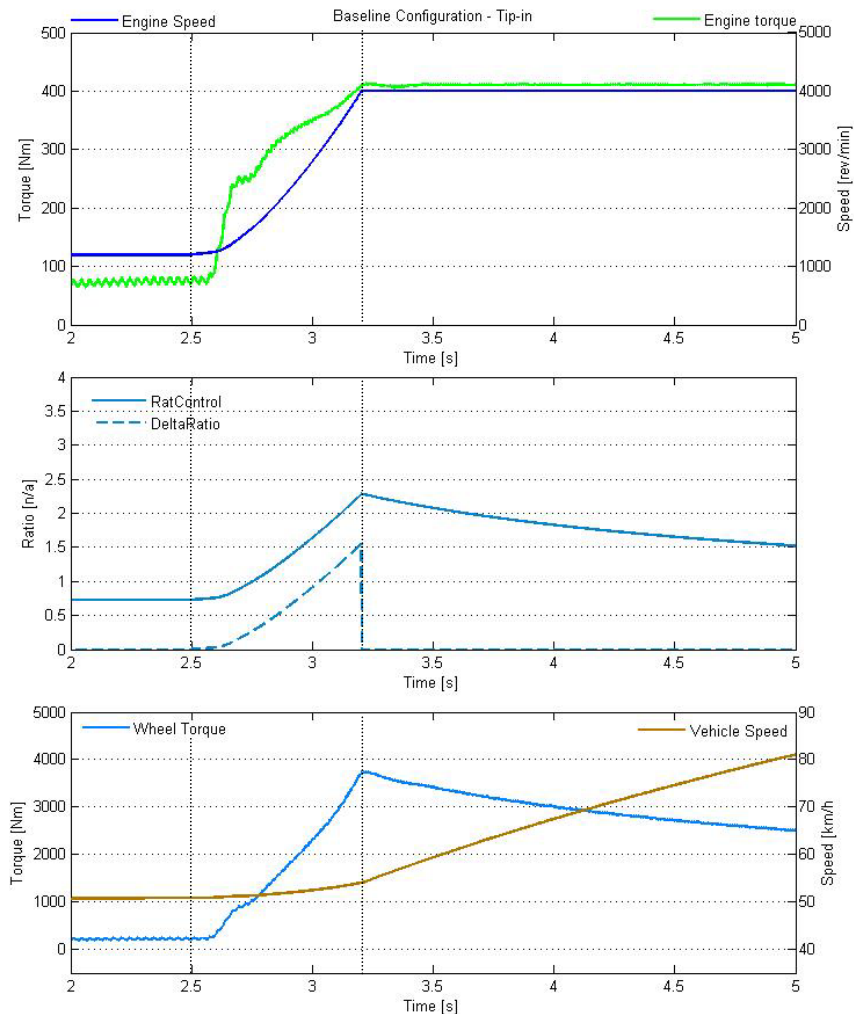
Figure 6.136 – Tip-in transient showing engine torque and speed [top] with wheel torque and vehicle speed [bottom]. The ratio control strategy is illustrated in the centre with the final ratio control to the variator model and the *DeltaRatio* integrated by the transient strategy.

6.5 Closing Comments

A V6 turbo diesel engine model was established within a CVT powertrain model and can be run from the Simulink environment. The level of modeling detail for the engine was driven by the requirements set at the beginning of the chapter. Therefore the engine and its controller in particular are designed to accurately replicate air path transients. The engine simulation was validated against full load data available for the Audi W19.

The simulation of transients made it necessary to model the driveline and vehicle. These are simple sub-models capable of replicating the external load seen by the engine and evaluate its effect on the vehicle longitudinal response. The complete powertrain simulation obtained highlighted issues in the air path response during aggressive transients; these can be attributed to turbocharger lag mainly.

This powertrain model is the starting point for the Manifold Air Injection [MAI] investigations in the next chapter.

Chapter 7: MANIFOLD AIR INJECTION TO IMPROVE TORQUE TRANSIENTS

To compensate for the turbocharger lag and boost the engine transient torque in the conditions identified in the previous chapter, it is proposed to inject air into the intake manifold during tip-in manoeuvres. An air accumulator [82] is used to store pressurized air which is released through a vane controlling the accumulator output mass air flow.

7.1 Design & Modelling

From the initial simulations conducted with the baseline engine, the turbocharger operation suffers a lack of pressure in the intake during the transients. By improving the IMAP during the transient, the following benefits should be obtained in the air path and exhaust system [in logical order].

- Compressor transient operating conditions shifted up from baseline equivalent, resulting in better efficiency and less resistive power on the shaft.

- VGT transient acceleration increased from favourable balance of available exhaust gas energy in turbine stage against pumping work in compressor stage.

- Reduced IMAP error, resulting in less control effort around the VGT position set point.

- Reduced exhaust back pressure [EMAP] at comparable VGT speed from operating the blades closer to feed forward value.

- Less exhaust back flow, therefore better cylinder breathing efficiency and more fresh air intake.

The concept of manifold air injection using an accumulator is investigated in this chapter. The sensitivity of the MAI system performance to the volume and the pressure in the device will be studied to calibrate the control strategy.

7.1.1 Sizing & Filling Considerations

The limiting factor of the system is the mass of air that can be stored which is a function of the accumulator size and the air pressure. As it is better to install the accumulator close to the intake manifold to avoid pressure losses and promote faster system response, the volume has to be packaged under the bonnet. Consequently, the accumulator size has been fixed to *5L*. This is assumed to be the maximum volume that can be fitted in the engine compartment.
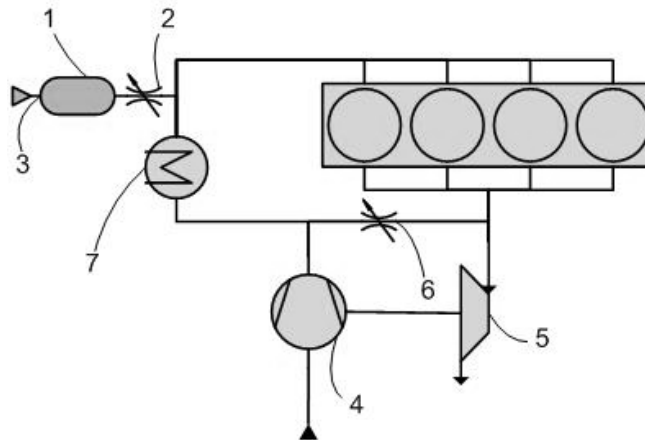
Figure 7.137 – Manifold Air Injection implementation. The accumulator volume ① is installed close to the intake manifold, downstream of the compressor ④ and the intercooler ⑦. A valve ② similar to the EGR valve ⑥ controls the air flow. The charging system ③ is no investigated.

The accumulator initial pressure depends on the air charging system. Two options are available:

- Fill the accumulator directly with the turbocharger extra boost pressure available during back off events. This potentially allows a reduction of MAF overshoot and provides the energy to recharge the accumulator at little cost. The limitation of this concept is that the maximum storage pressure is limited. The presence of EGR gases in the intake chamber also poses limitation to this straight forward filling strategy. It is indeed preferable to store a gas mixture containing mostly fresh air, because EGR gases will be undesirable during the transient.

- Use a disengageable pump driven by the crankshaft in a similar way to a supercharger. During engine braking events for instance [regenerative process] some of the overrun torque can be used to pump air into a second orifice of the accumulator. This has the advantage of preventing the storage of EGR gases inside the MAI chamber

The feeding system has not been modelled during this investigation to focus on the analysis of the potential benefits of the system towards improving the engine torque response during heavy tip-ins. However, initial pressures from *2 to 6 bar* have been tested. The specification and the control strategy for filling the MAI device will depend on the findings in this chapter. The energy requirement to adiabatically compress a volume V_0 at atmospheric condition P_0 into V_{MAI} at P_1 can be calculated from Equation 7.17:

$$U = -\int_{V_0}^{V_{MAI}} P \cdot dV$$

Equation 7.17 – where *U* is the work done during the compression, *P* and *V* are respectively pressure and volume of the initial mass of air during the compression

During an adiabatic process, P and V follow Equation 7.18:

$$P \cdot V^\gamma = P_0 \cdot V_0{}^\gamma = P_1 \cdot V_{MAI}{}^\gamma$$

Equation 7.18 – where *γ = 1.4* for air

Therefore if $P_0 = 1.013 \ 10^5 Pa$, $P_1 = 5 \ 10^5 Pa$, and $V_{MAI} = 0.005m^3$, then $V_0 = 0.0156 \ m^3$. With Equation 7.18, Equation 7.17 can be developed into Equation 7.19:

$$U = -P_1 \cdot V_{MAI}{}^\gamma \left[\frac{V^{1-\gamma}}{\gamma - 1}\right]_{V_0}^{V_{MAI}}$$

Equation 7.19 – with the same notations as in Equation 7.17 and Equation 7.18

So *U = -2289 J*. If the filling time is *5s*, then the power required for the adiabatic compression is *457W*. Because in reallity the compression will not be adiabatic due to energy losses through thermal exchanges, a reasonable estimate of the power required by the filling system is in the region of *1kW*, depending if the mass of air is initially at atmospheric pressure or not.

7.1.2 Manifold Air Injection model

The Manifold Air Injection system is modelled by a volume of *5 L* connected to the intake manifold downstream of the compressor, via a variable area valve as shown in Figure 7.138. The valve has a maximal equivalent diameter of *7 mm*, and the sub-model is of the same type as the EGR valve [*20 mm*].

Thermal exchanges are modelled by a convective exchange and a constant temperature source similarly to the intake and exhaust component described previously. The accumulator output mass air flow is calculated from the pressure ratio across the valve, the temperature inside and the effective area of the valve controlled by the EMS as shown in Equation 7.20.

$$dm = A \cdot C_q \cdot C_m \cdot \frac{P_u}{\sqrt{T_u}}$$

Equation 7.20 – where *A* is the orifice area, C_q is the flow coefficient specific to the geometry, C_m is the flow parameter, P_u and T_u are the upstream state variables [76]
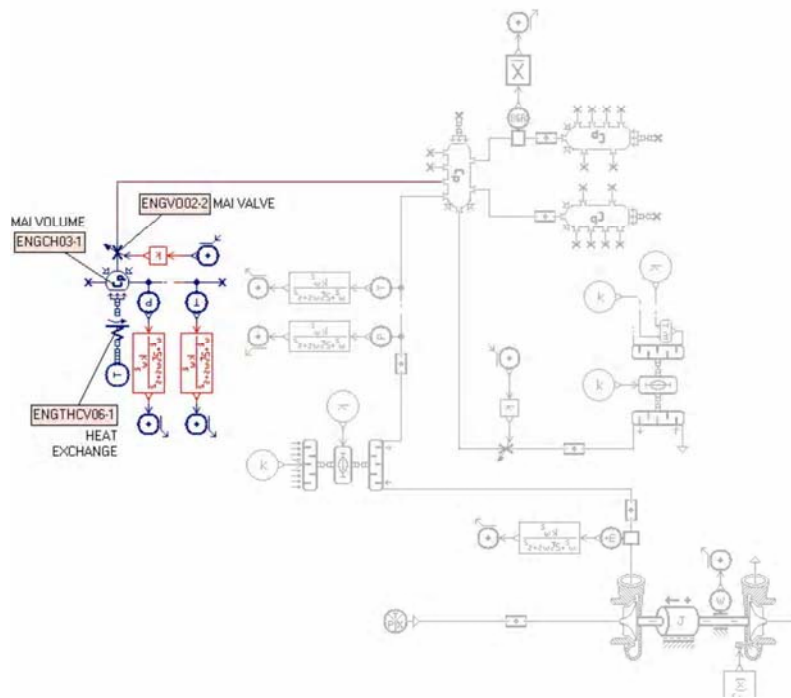
Figure 7.138 – Manifold Air Injection model. This complements Figure 6.116 and shows the intake plenums [right] and the layout of the MAI and the sensors.

The MAI system sub-assembly shown in Figure 7.138 is connected to the intake volume of the existing engine model [see Figure 6.116]. The non-linearity characteristics of the turbocharger and EGR are now also coupled with the air injection. Table 7.20 lists the main parameter implemented in the MAI sub-models. No actuation delay is implemented in the valve model. This is addressed in the controller design.

Variable Name	Title	Value	Units
ENGCH03-1_volume	MAI volume	5	L
ENGCH03-1_ini_pressure	MAI initial condition pressure	5	bar
ENGTHCV06-1_area	MAI convective exchange area	50,000	mm^2
ENGTHCV06-1_coeff	MAI convective exchange coefficient	200	$W/m^2/degC$
ENGVO02-2_diameter	MAI Valve maximum equivalent diameter	7	mm
ENGVO02-2_inflow_coef	MAI valve maximum inflow coefficient	0.72	n/a
ENGVO02-2_backflow_coef	MAI valve maximum backflow coefficient	0.72	n/a

Table 7.20 – Local parameters for the Manifold Air Injection sub-models shown in Figure 7.138. The constant temperature source for the convective thermal exchange model is *320 K*.

7.2 Strategy Development

As stated above, the air path of the engine is a complex system characterized by high non-linearity in the turbocharger response and the EGR system. As a consequence, it is not straight-forward to define the most adequate amplitude and timing of the MAI valve opening.

During the transient, the compromise to find between the amount of air provided respectively by the MAI system and the turbocharger largely involves optimizing the airflow through the compressor:

- Too much air injection pressure would increase the IMAP hence the pressure ratio across the compressor. This would result in the degradation of the compressor efficiency and eventually going into the surge region. The sensitivity of the system to the pressure delivered by the MAI will have to be investigated.

- Too little injection pressure would mean that the volume empties without a significant contribution to the air charge into the engine. This results in a poor performance of the system.

7.2.1 Control Architecture

There are three key components of the MAI valve actuation strategy to resolve:

- When to start opening the valve
- Which opening profile to adopt depending on the transient encountered
- When to close the valve

The IMAP error is an obvious choice to trigger the start of air injection in the intake. This error is indeed immediate after a new engine load demand is set, and its magnitude is in direct relation with the depth of the tip-in. A feed-forward control of the valve opening would require extensive calibration to operate over a range of driving manoeuvre. Moreover, the controller has to be able to react to the improved performance of the compressor. Consequently, the MAF error is used as a control feed-back. Early trials ruled out the IMAP error feed back control because of the following reasons.

- The IMAP error is already PI controlled by the VGT strategy during the tip-in.

- The IMAP does not give a direct indication of the engine air charge during the transient because of the engine pumping effect previously mentioned.

- The MAF error is normally controlled by the EGR strategy, which is rapidly turned off at the beginning of the transient. Therefore there is no interference between the EGR and MAI control efforts.

The controller architecture adopted is presented in Figure 7.139. The MAI valve is closed during steady state operation and then the strategy is latched on when the IMAP error goes above the calibrated threshold value [*ENG_MAI_IMAP_THLD*]. As soon as the large pressure error is detected, the MAF becomes the feed back signal to

the MAI valve controller which effectively regulates the fresh air flow across the compressor. The benefit of using the IMAP error instead of the MAF error is that the boost pressure error builds up almost instantaneously after the tip-in, whereas the MAF error is much more related to the engine speed which increases during the engine acceleration phase.
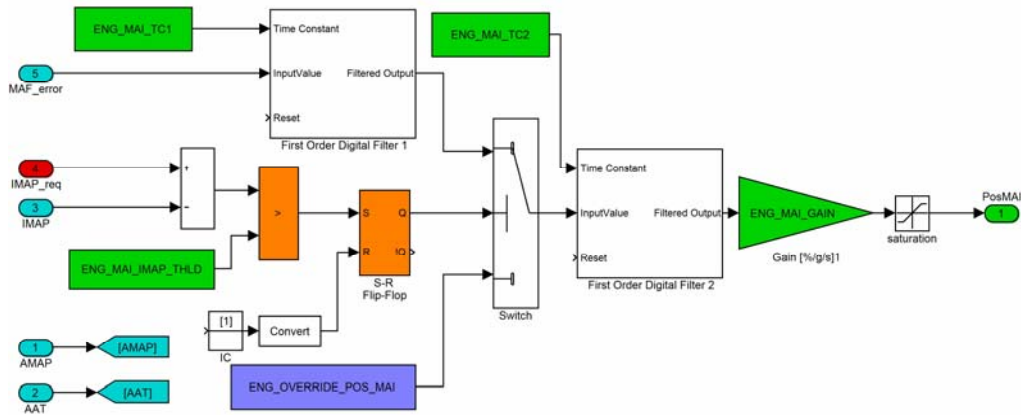
Figure 7.139 – Manifold Air Injection controller. The transient detection blocks [orange] monitors the IMAP error; the filtered MAF error is the input to the feed-forward controller. The MAI valve opening request is filtered to avoid step commands when the strategy triggers.

In the controller illustrated in Figure 7.139, the MAF error is filtered by a first order filter at time constant Tc_1. This eliminates engine speed related fluctuations and their high frequency input to the proportional control. This filtered value varies even during steady state operation as the VGT and EGR strategies have tolerance for small errors. Hence the input to the P gain is again filtered at Tc_2, which should verify the following relation:

$$Tc_2 << Tc_1$$

Equation 7.21 – Desirable relation between the two first order digital filter time constants of the MAI control

Variable Name	Title	Value	Units
ENG_MAI_IMAP_THLD	IMAP error threshold for strategy latching	150	mbar
ENG_MAI_TC1	1st order filter time constant for MAF error	0.1	s
ENG_MAI_TC2	1st order filter time constant for command	0.01	s
ENG_MAI_GAIN	MAI strategy control P gain	2.5	% / (g/s)

Table 7.21 – MAI controller calibration variables. The green blocks in Figure 7.139 can be tuned to optimise the performance of the air injection strategy. The gain and the error feedback filter time constant are critical values which can affect the VGT operating conditions.

Table 7.21 summarizes the calibration variables to tune in the MAI control strategy. This initial strategy which allows investigation of all aspects of the MAI behaviour, as highlighted in the following section. However, it is likely that gain and time constant could be optimised by the use of look-up tables as in the VGT strategy.

7.2.2 Calibration

This section describes the calibration work carried out to optimise the performance of the MAI during a range of mild to heavy tip-ins. The air path critical phenomena are reviewed.

7.2.2.1 Surge Limit

The limit to how much of the MAF error can be compensated for with the MAI is largely due to the turbocharger surge effect as suggested in Figure 7.140. The thick black line on the left hand side of the plot is the surge line beyond which the MAF becomes too low for the compressor to function properly. It is highly undesirable to let the turbocharger reach this very unstable region.
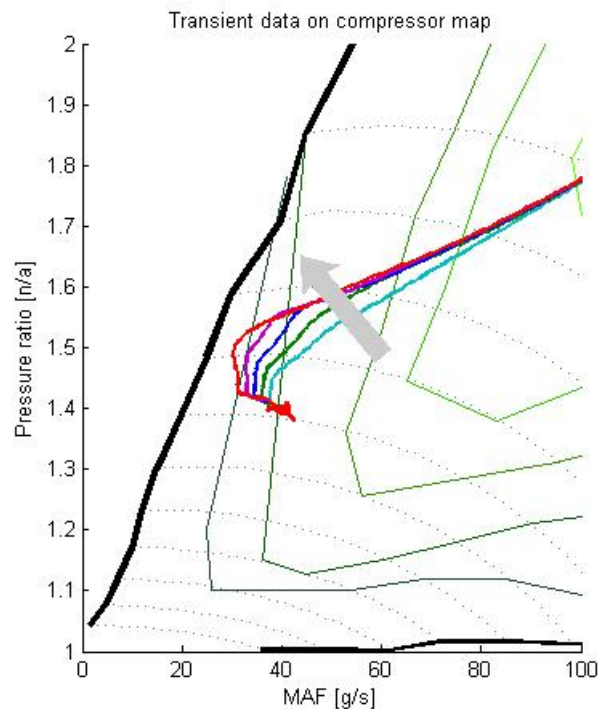
Figure 7.140 – Surge limit on turbocharger operation with MAI. The dotted lines are the turbocharger iso-speed. The thick black line is the surge limit. The arrow indicates increasing P gain.

The direct effect of this phenomenon is that it is not possible to inject a large amount of air early in the transient. A small amount is acceptable, as seen in Figure 7.140 with a number of controller gains investigated. The mass air flow out of the MAI has then to be maintained as the turbocharger accelerates.

7.2.2.2 Feedback MAF Filtering

The time constants *ENG_MAI_TC1* and *ENG_MAI_TC2* respectively for the MAF error filtering and the controller command filtering were calibrated to optimise the IMAP vs. MAF response of the air path during the transient. Because of the cascaded nature of the filter arrangement, there are a number of combinations for Tc_1 and Tc_2 which would provide equivalent results. Therefore the following approach was adopted:

- Tc_1 delays the MAF error feed back to the MAI controller to avoid compressor surge as explained above. Therefore a relatively high value for Tc_1 is required

- Tc_2 filters out the potential valve command steps created by non-zero MAF error when the strategy latches on. Tc_2 can consequently be calibrated aggressively low if surge is avoided with a larger Tc_1 value.
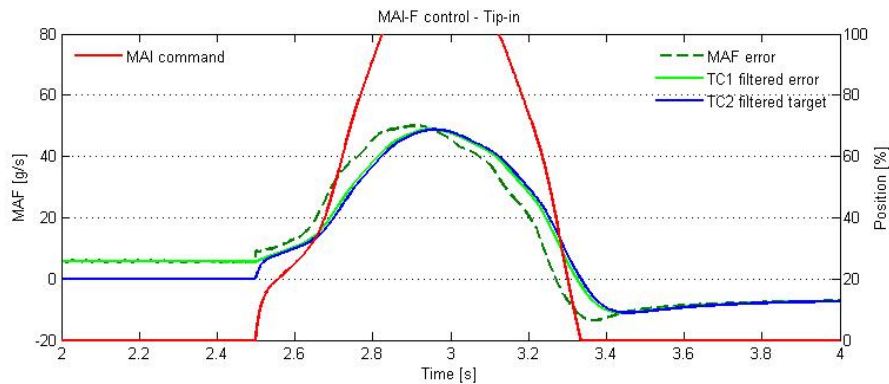
Figure 7.141 – MAI controller internal variables during tip-in. The MAF error [dotted] is filtered [$Tc_1 = 0.1\ s$] into a delayed feed back [light green]. The command [red] is the filtered [$Tc_2 = 0.01\ s$] value of the feedback [blue] multiplied by the gain *ENG_MAI_GAIN*

Figure 7.141 presents the variables involved in the MAI controller at various stages of the proportional feed-back control. By reducing Tc_1 the delay on the feed back is decreased, meaning that the MAI error target [light green] will be closer to the actual error. However, this means that the proportional control will open the valve earlier and can have adverse effect on the compressor operation, as shown in Figure 7.142.

ENG_MAI_TC2 was calibrated to *10 ms* to minimize the controller delay and simulate the MAI valve actuation response.
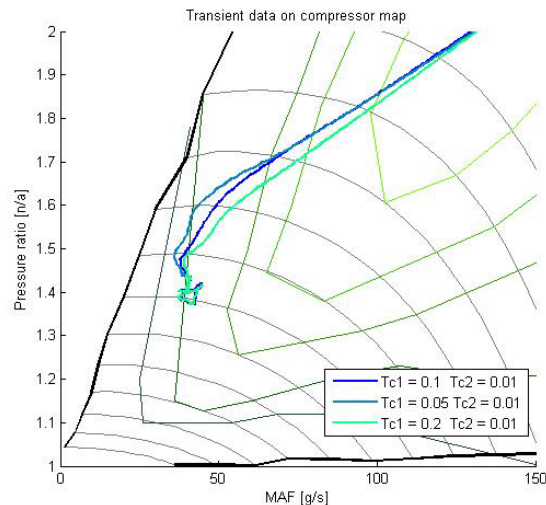
Figure 7.142 – Effect of Tc_1 on the compressor response at the beginning of the transient. Low values create rapid MAI valve

response to MAF error and compressor   blow out.

The various *ENG_MAI_TC1* time constant for the filtering of the VGT MAF error feed back shown in Figure 7.142 confirm the previous explanations. A low time constant [$Tc_1 = 50ms$] provokes a small decrease of the compressor air flow output, associated with a loss of efficiency. A high time constant [$Tc_1 = 200ms$] improves the efficiency in the compressor but the retarded injection means a lower IMAP trace and marginally less torque.
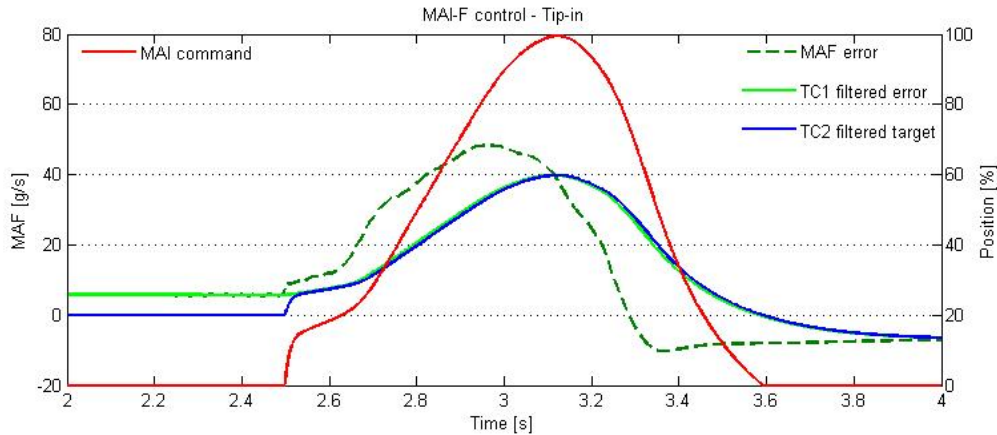
Figure 7.143 – MAI controller internal variables during tip-in with *Tc_1 = 0.2 s*. The MAF error [dotted] is filtered [Tc_1] into a delayed feed back [light green]. The command [red] is the filtered [Tc_2] value of the feedback [blue] multiplied by the gain *ENG_MAI_GAIN*

Figure 7.143 shows how the increase filtering delay affects the valve opening command. The filtered error target is attenuated and the valve hardly reaches the fully opened position. This profile can be compared to Figure 7.141 where the valve is wide opened for *300 ms*. *ENG_MAI_TC1* was subsequently calibrated at *100 ms*.

7.2.2.3 Storage Pressure

The amount of air available in the MAI is also crucial. Not only does it affect the capacity of the system to sustain a long lasting transient, but it also affects the air flow response of the MAI as the pressure ratio across the control valve drops as the volume empties. Figure 7.144 shows the sensitivity of the system to storage pressure for the largest transient [from *1200* to *4000 rev/min* with *30 %* to *100 %* load change].
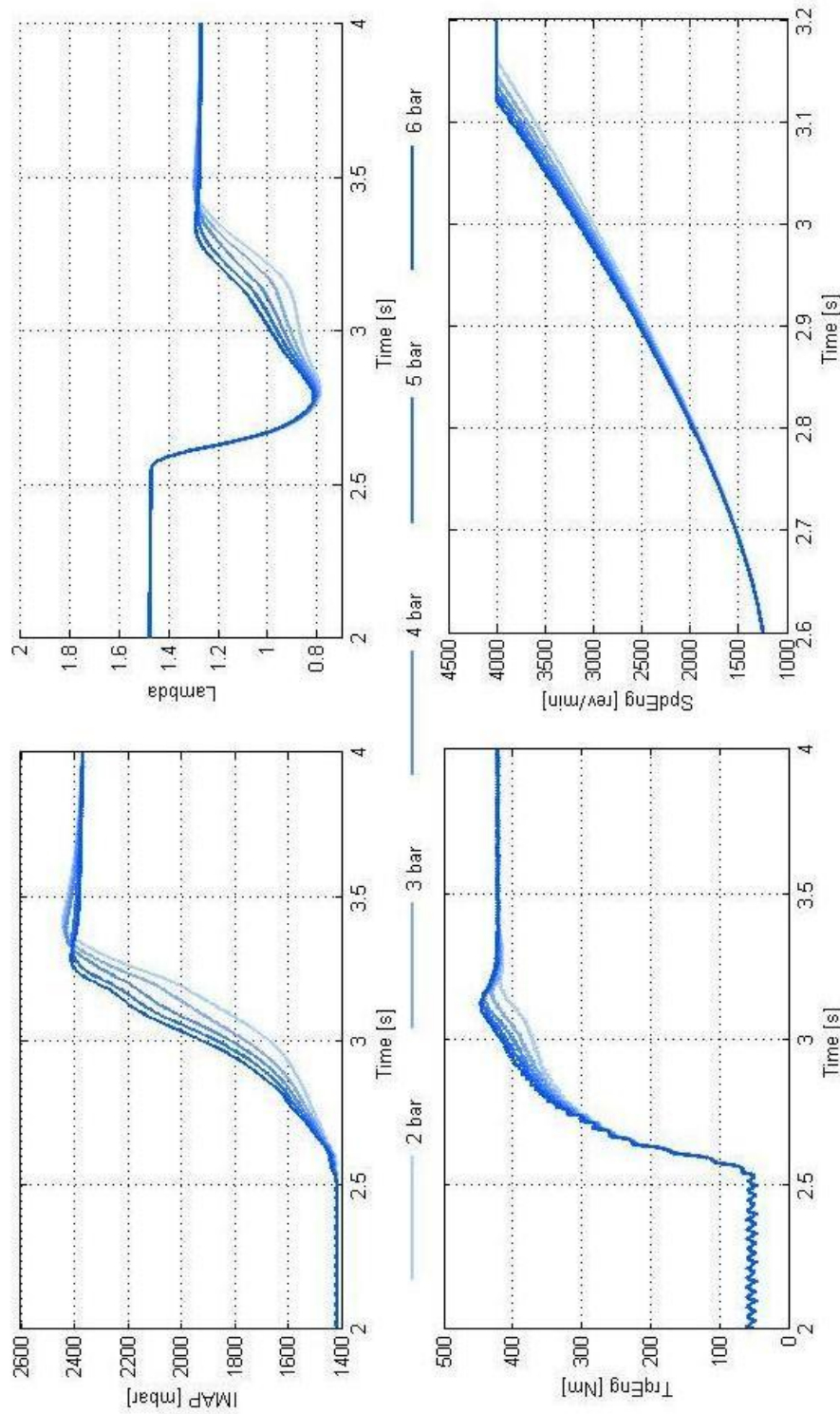
Figure 7.144 – IMAP, Lambda, TrqEng & SpdEng at different MAI filling pressures. All variables monitored here improve with the pressure increase in the MAI. The *2 bar* profiles are extremely close to baseline. *5 bar* seems a good compromise. The improvement from *2 to 6 bar* are: *120 ms* quicker IMAP control – up to *45 Nm* more torque during the transient – time under stoichiometric reduced by *40 %* - *40 ms* quicker engine speed transient.

The mass of air available influences the potential improvement in torque and lambda during the transient as illustrated in Figure 7.144. The differences are further highlighted by the relatively simple control strategy which does not account for the MAI initial conditions, or attempts to regulate the valve opening to maintain a target mass air flow across it as the pressure drops inside the MAI.

The volume pressure sensitivity of the MAI system highlights the potential gains obtained with a high storage pressure, which itself impacts on the requirements for the filling strategy. At *6 bar*, the target IMAP is reached *120 ms* earlier than at *2 bar*, when the initial pressure in the volume is actually lower than the final target IMAP. This means that the valve shuts off before the engine transient is completed.

Engine torque differences of up to *45 Nm* are observed during the transient as well as significantly improved lambda profiles when the total mass of injected air increases with the storage pressure. The engine speed profile optimised by the CVT control law makes the most of the extra available torque in the later part of the transient and the initial MAI pressure can reduce the speed transient phase by up to *40 ms*.

7.2.2.4 Gain Sensitivity

The results presented in Figure 7.145 show that there is an optimum trade off to be found for the choice of the gain in the MAI valve control. On the one hand, it can be noticed that the gain largely affects the rate at which AMAP drops during the boost sequence. On the other hand, the benefits in lambda are not as significant. The VGT appears very sensitive to the rate of MAI valve opening in the early part of the transient when the MAF error builds up and the valve consequently opens. High gain values produce too much MAI air flow which surge the compressor as shown in Figure 7.140.

The overall air charge is however not sensitive to the greater MAI contribution as illustrated by the lambda profile. The IMAP is not reacting either to the MAI gain, therefore confirming that higher gain values only promote earlier air injection and compressor inefficiency. Gain values below *2 % per g/s* offer little contribution to the engine transient performance. A gain below *3 % per g/s* of MAF error was found acceptable for most of the tip-ins simulated with initial AMAP at *5 bar*.
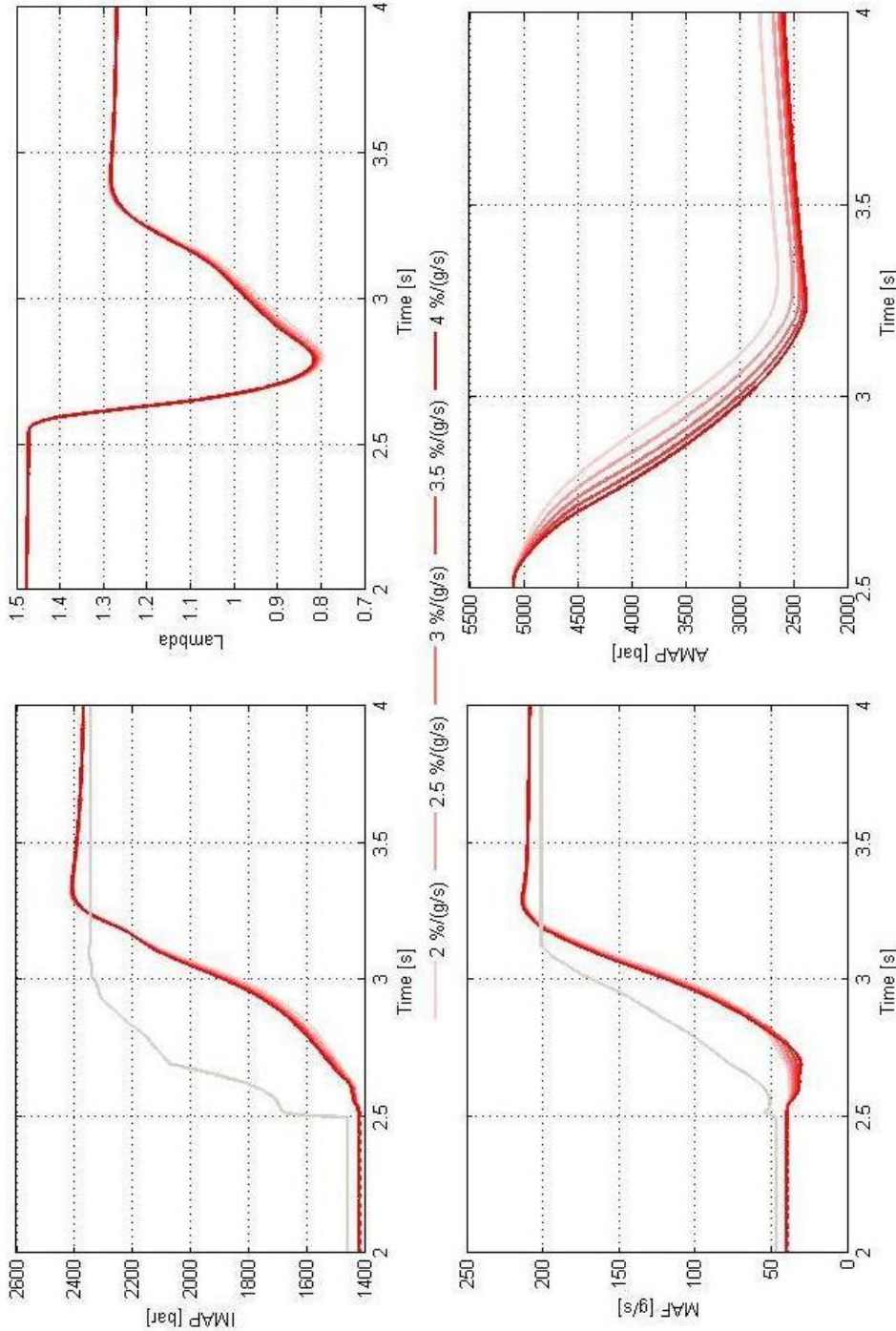
Figure 7.145 – IMAP, Lambda, MAF & AMAP at different proportional gains. The MAI controller gain most influences the AMAP profile and high gain simulations do not show a significant improvement over the low gains. The differences from *2 to 4 %/(g/s)* are: no noticeable IMAP control benefit – up to *12 g/s* less MAF in the early part of the transient – time under stoichiometric unchanged - *150 ms* quicker MAI pressure loss.

7.3 MAI System Performance

7.3.1 Driving Manoeuvres

The Manifold Air Injection is here compared with the baseline simulations, i.e. the same tip-ins without the use of MAI. The benefits of the MAI system can be observed for all tip-ins in Figure 7.146. The transients shown are from *1200 rev/min*, and *30%* engine load [*50 km/h*]. The request is then for *100%* load at *2000, 2500, 3000, 3500 and 4000 rev/min* respectively for tip-in 1,2,3,4 and 5.

Because each transient starts from the same speed and load conditions, the initial change for both IMAP and MAF should be similar. The superimposition on the compressor map [Figure 7.146] of the traces for both baseline and MAI manoeuvres highlights the good repeatability of the simuation.
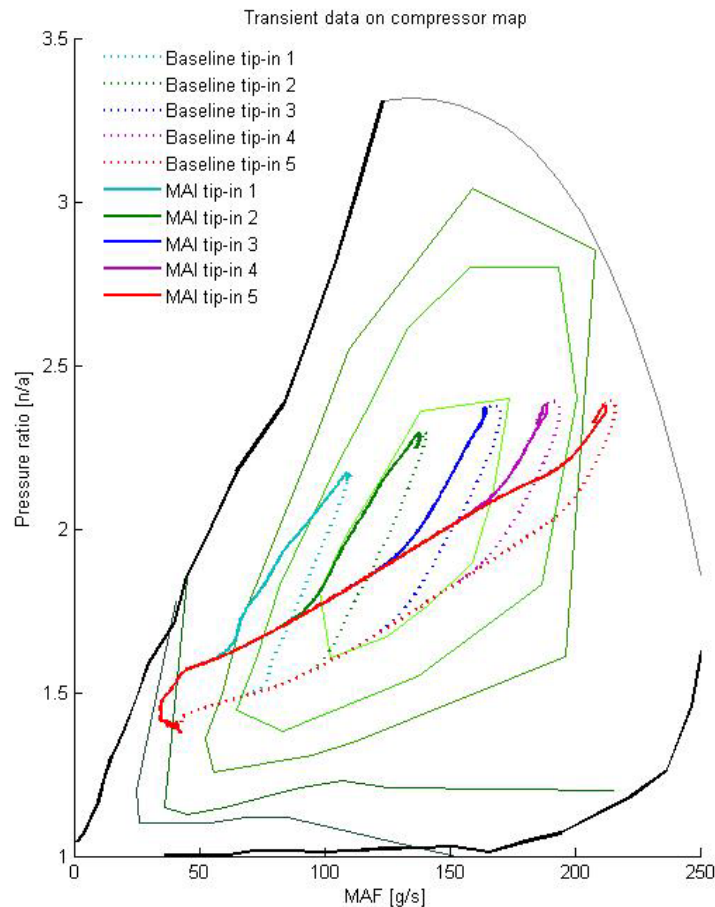
Figure 7.146 – Comparison between baseline and MAI setups. The transients are here represented over the compressor map. The effects of the MAI over both IMAP and MAF profiles are clearly noticeable.

The air path transient affected by the MAI system benefits from the following improvements:

- Increased IMAP throughout each manoeuvre. This increases the engine volumetric efficiency and ultimately produces a leaner mixture.

- Increased efficiency of the compressor operation for the deeper transient manoeuvres. This results in less resitive torque on the VGT shaft, therefore a faster transient.

- Decreased overshoot on final set point. This is due to the smaller IMAP error fed back to the VGT controller.

Figure 7.147 shows the engine torque, speed, lambda value and turbocharger speed for tip-in 1 & 5. Each color on the time history plots corresponds to a manoeuvre and the dotted lines are for the baseline data. The engine torque profiles are shown on the top graph. The torque benefits previously discussed are both on magnitude, with up to *40 Nm* increase for *300 ms* and in response time with more than *150 ms* gained to reach *400 Nm*.

The engine speed response time from one steady state engine operating condition to the other is improved. The full load tip-in 5 benefits the most from the MAI, which confirms the discussions in Section 2.3.2 and 2.3.3 related to the importance of a faster torque response time for CVT. Tip-in 1 is indeed a milder manoeuvre where the response time is comparatively less critical in the way it affects the engine speed controllability.

The bottom two graphs in Figure 7.147 show the lambda and the VGT speed profiles during the same two transients, with and without MAI. For the most aggressive tip-in, the torque benefits mean engine acceleration time is reduced by *12 %* whilst keeping lambda well above the baseline value. The area below stoichiometric in the lambda profile is reduced by up *40 %*. The ROFI strategy would therefore be less compromising on the torque output whilst maintaining the mixture above the transient smoke limit. A Further consequence of the added air is the lesser demand on exhaust after-treatment systems and in particular the Diesel Particulate Filter [DPF]. The VGT speed is quicker by almost *0.1s* in both cases. This further confirms the improvement in VGT transient operation with the MAI system active.
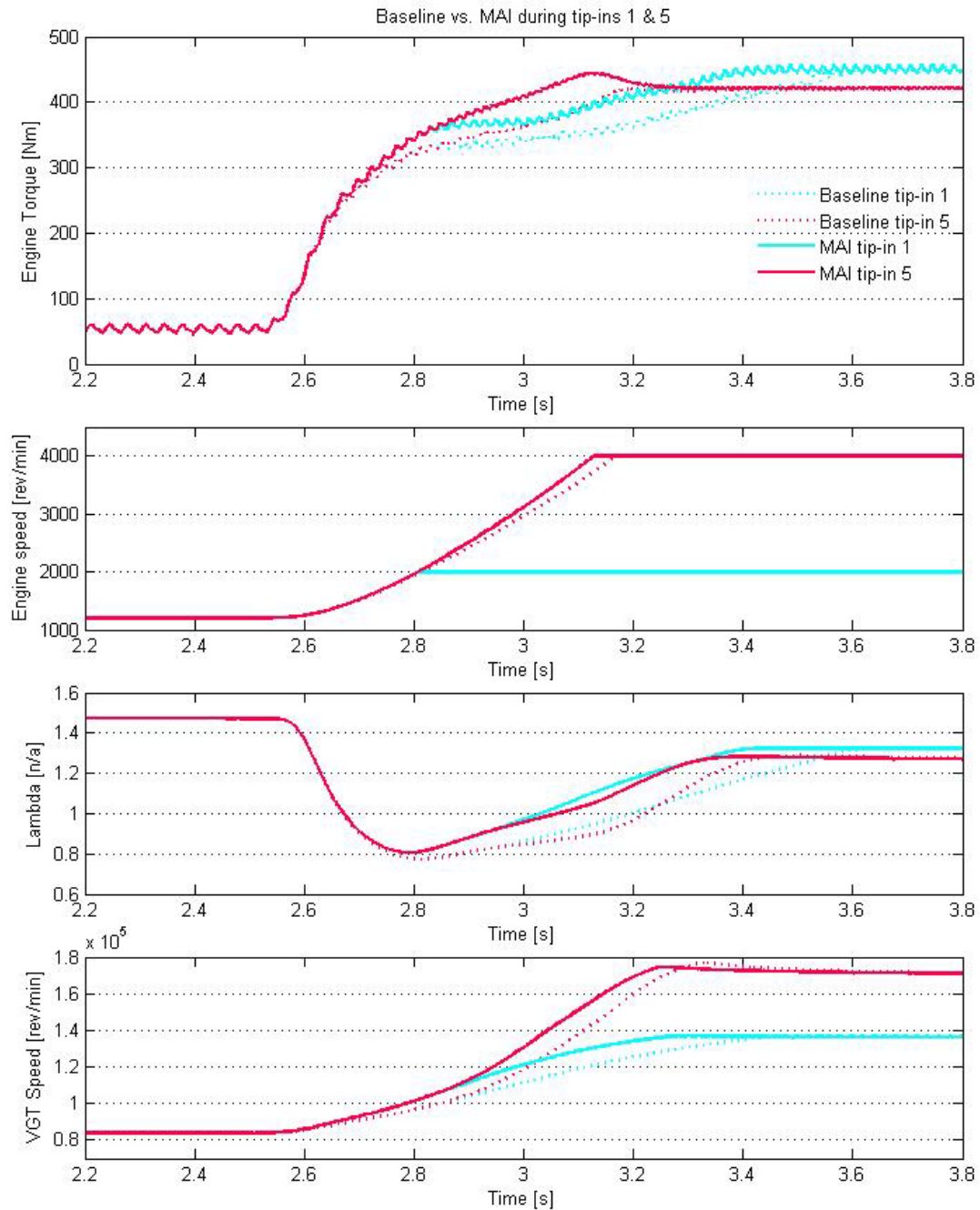
Figure 7.147 – Comparison of baseline vs. MAI for tip-in 1 & 5 shown in Figure 7.146. All crucial engine signals are significantly improved by the air injection during the latter part of the transient. The initial air charge cannot be improved in the same way because of the system response and the compressor surge limitation.

7.3.2 Engine Performance Matching

As introduced in Chapter 2 and confirmed with the improvements summarized above, the CVT benefits from a matched engine response under large transients. This enables a faster engine speed control resulting in quicker vehicle acceleration feel following a step increase in the pedal. The results of this engine matching exercise on the wheel power are illustrated in Figure 7.148.
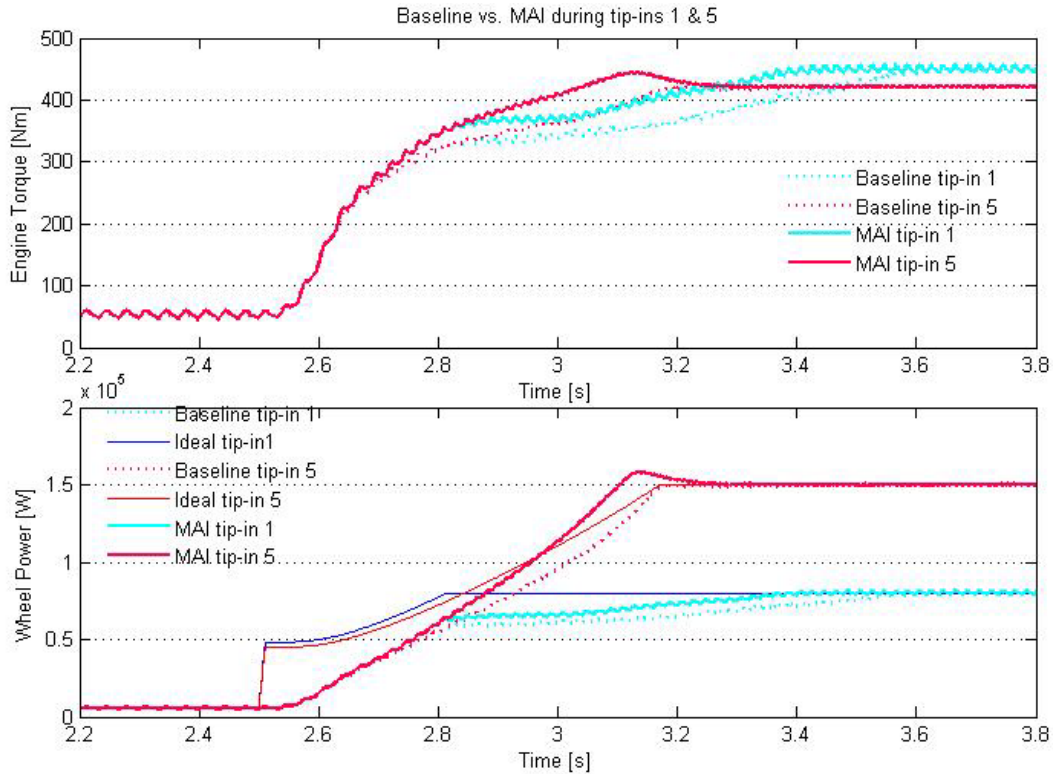
Figure 7.148 – Comparison of baseline vs. MAI for tip-in 1 & 5 shown in Figure 7.146. The wheel power is marginally increase in the small tip-in① more significantly improved in the larger one②. The ideal wheel torque is computed from the actual engine speed, the required engine torque and the CVT efficiency.

As in, the plots in Figure 7.148 are colored differently for tip-in 1 and 2. The engine torque plot on top is carried over from Figure 7.147. The lower graph shows how much wheel power is available at the wheel using the vehicle and driveline model. The smaller weight lines represent the ideal wheel power obtainable if the engine torque response was instantaneous. This does not account for the faster engine speed transient obtainable in such ideal conditions, but it highlights how the instant engine torque deficit influence the wheel response following the change in required power.

As mentioned in Section 7.3.1, the larger speed transient tip-in 5 shows the most significant benefits. The wheel power improvement results in better vehicle response to the driver demand to the CVT transmission. A slight overshoot is observable with tip-in 5 [MAI on] when the actual wheel power crosses the ideal value obtainable with

maximum engine torque at $t = 3s$. However, the wheel power reaches this ideal value almost 0.2s before the baseline configuration. This is combined with improvement on the engine operation itself as previously explained.

The CVT transient control strategy implemented with the model effectively splits the additional torque created by the MAI into the inertial torque and the wheel torque components. The split value was adjusted to *40%* during the CVT controller design as detailed in Section 6.3.2.3. This allows both wheel torque increase *and* engine acceleration to occur simultaneously. By not altering this split value after the calibration of the MAI system, the vehicle acceleration happens quicker and harder during the transient shift of CVT ratio.

7.4 Closing Comments

A complete powertrain model has been setup and exhibited the expected phenomenon when subjected to large speed transients under a tip-in manoeuvre. The issue is related to a starvation of air due to the incapacity of the turbocharger to match the required boost pressure early in the manoeuvre. This resulted in an over rich mixture because the fuelling strategy purposely did not include ROFI limitation. This would compromise the torque rise that is necessary to reach the required engine speed. Therefore the same fuelling strategy could be applied to the CVT matched configuration with MAI and demonstrate the improvement.

After implementing a manifold air injection system in the plant, a controller was built to help improve to exhaust mixture properties and the torque profile during a demanding tip-in. Based on the turbocharger MAF error and triggered by the IMAP error, air was injected directly into the intake manifolds from a pressurized volume.
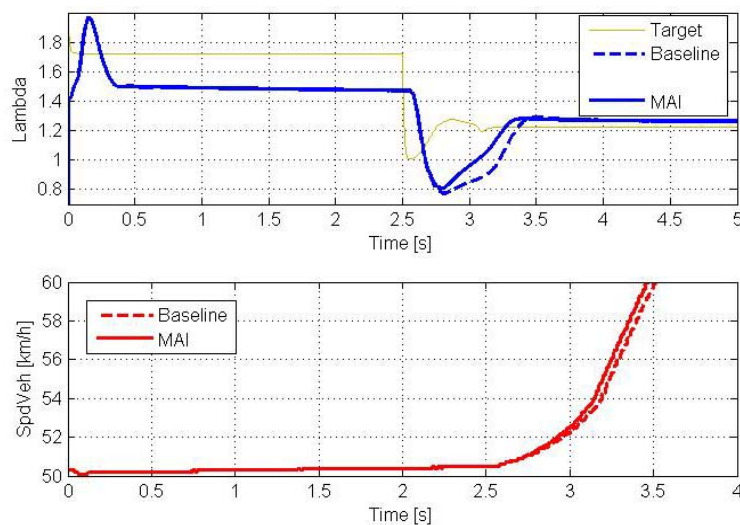
Figure 7.149 – Comparison between Baseline & MAI simulations at 5 bars: the most important improvements are seen with the lambda and the vehicle speed profiles.

The benefits of the device are summed up in Figure 7.149 with the significantly improved lambda profile. The area under the critical value of $\lambda = 1$ is almost halved while the vehicle speed profile shows a small increase in performance. Further work would involve a more advanced coordination of turbocharger, MAI and EGR controllers and an extended range of transient manoeuvre simulations.

Chapter 8: ANALYSIS & DISCUSSIONS

This chapter finally summarizes the research outcomes presented in this document and highlight the achievements of the work. The analysis of the delivered investigations is put in the perspective of the engine characteristics matching exercise and the associated research objectives presented in the first chapter. The ideal characteristics for an internal combustion engine in a CVT powertrain are highlighted in conclusion.

8.1 Research Achievements

The work carried out towards the two investigation paths yielded a number of contributions which are highlighted below. The particular requirements of the CVT powertrain to the engine operation are summarized. The LSHT operation challenges associated with a gasoline engine are discussed; the transient torque performance demand on a diesel engine in a CVT powertrain are also emphasised.

8.1.1 CVT Powertrain Requirements on Engine Operation

The specific need created by the CVT powertrain comes from the engine operation flexibility offered by the transmission as detailed in the first Chapter. Torque at the wheel is produced using the most appropriate speed ratio and therefore the engine effective operation range is extended towards lower speed by the BSFC optimisation strategy. The higher the IOL torque is in the engine map, the lower the engine speed will need to be shifted for an equivalent engine power in steady state. The position of the engine specific IOL with respect to the WOT torque line determines the torque margin used by the CVT control to accelerate the engine in the case of an increased power request. This torque margin is therefore critical to the driveability potential of the CVT powertrain.

When operating in steady state, the CVT powertrain can optimise fuel economy by making use of the maximum overdrive ratio possible that can match the power demand on the IOL. This will interfere with a low speed and high torque region where

the engine can operate efficiently, but with an NVH penalty that is highly undesirable from the driver's perspective. This issue is investigated in a hybrid CVT powertrain with the design and calibration in simulation and the implementation in the vehicle of Active Vibration Control [Section 8.1.2].

For low to medium engine power demand, the optimum speed is below the maximum torque speed and will pose the problem of response to increase power demand from the CVT powertrain. This problem has been investigated with a 3.0L V6 turbo diesel engine simulation with the implementation and control of Manifold Air Injection [Section 8.1.3].

8.1.2 Gasoline Engine LSHT operation

The fuel economy gain from LSHT operation of the V8 engine was demonstrated with backward model simulation using quasi static assumption and small time resolution [77]. The implications of such a strategy are the lower torque margin and the undesirable engine related vibrations.

An instrumented IVT vehicle was used to identify the frequency source of the vibrations and measure the levels of acceleration & noise in the vehicle. This NVH study proved to be an important aspect of an IVT matched engine operation in steady state. Dynamic aspects of LSHT were addressed with the torque assist functionality of the parallel hybrid powertrain.

8.1.2.1 Engine Model

A Ford 5.4l V8 engine was developed in Chapter 4 to replicate the torque oscillations caused by the combustion events. This model was tuned and validated using engine dynamometer data collected for that purpose. The simulation environment was consequently able to predict the torque ripples both in steady state and dynamically.

The engine simulation was validated against real vehicle dynamometer data and coupled to an IMG and PE model. The subsequent platform offers a range of possible applications:

- The LSHT AVC strategy development [Chapter 5]

- The EMS design and optimisation for LSHT operation including sparking strategy, EGR and mixture control [charge dilution], cylinder pressure biased control [see Section 8.2.3].

8.1.2.2 Strategy Implementation Performance in Hybrid Powertrain

The fuel economy predictions using the backward model simulation gave a repeatable way to evaluate the impact of the AVC strategy on fuel economy. A series of 3 full cold start combined EPA cycles were conducted with the EASIVT vehicle before [baseline IVT] and after [EASIVT] the conversion to a hybrid powertrain to evaluate FE benefits and verify the backward model reliability. Warm start cycles were also carried for direct comparison between dynamometer and simulation figures.

Table 8.22 shows a summary of the FE results obtained on the dynamometer and puts them in perspective of the simulation predictions from Chapter 5. The FE gain predicted for the city cycle is confirmed but lower than predicted in simulation. The highway cycle FE impact of the added weight and inertia on the vehicle is worse than expected.

FUEL ECONOMY COMPARISON on VEHICLE DYNAMOMETER			mpUSg
Drive Cycle	Configuration		
	IVT [cold start]	EASIVT [cold start]	EASIVT [warm start]
FTP 75 city cycle	17.39 REF	17.93 -3.10 %	19.53 -12.3 %
HWFET highway cycle	26.02 REF	23.60 +9.27%	24.01 +7.72%

FUEL ECONOMY COMPARISON in SIMULATION			mpUSg
Drive Cycle	Configuration		
	IVT [warm start]	EASIVT [cold start]	EASIVT [warm start]
FTP 75 city cycle	16.96 REF	N/A	17.95 -5.80 %
HWFET highway cycle	22.77 REF	N/A	22.21 +2.43%

Table 8.22 – Fuel economy comparison: EASIVT vs. IVT. The dynamometer figures are the average from 3 complete City and Highway cycles. The simulation predictions are a reminder of the predictions shown in Chapter 5 [Table 5.15]

The FTP75 city cycle fuel economy results obtained on the vehicle dynamometer show a *3.1%* improvement by EASIVT over the baseline IVT vehicle. Both tests are started with an engine soaked in ambient condition overnight and referred to as cold start conditions. A warm start condition is when the test is performed just after a long period of operation, with engine oil and coolant temperatures at their nominal values. The warm start condition is not allowed by the regulations but can be performed to evaluate the impact of engine warm up.

The warm start FE advantage of *9.2%* over cold start test in the city cycle is very significant. This raises the importance of some aspects of LSHT operation that have not been tackled in this study. Engine speed is critical to cold start performance because of the poor mixing and combustion efficiency obtained in cold conditions. The cold start strategy in the baseline vehicle was minimally altered to allow for *520 rev/min* idle in warm conditions. This means that the fully benefits of LSHT operation are only obtained once the vehicle is warm, therefore cold start cycles do not reflect the expected FE improvement [see Section 8.2.3].

In the highway cycle, LSHT operation is not as predominant because of the higher vehicle speed and therefore engine power involved. The weight penalty of the development vehicle and the large cascaded IMG inertia overcomes the benefits of the optimised IOL and hybrid torque assist. Furthermore, the lower regenerative braking energy available in the cycle forces the energy management system to use the power split torque on the IMG to maintain the battery SOC around the target *60 %* value.

Item Description	Sub-description	Average	Median	Var	Comments
Creep [Drive]	Creep speed	6.7	7.0	1.7	Good, satisfying
	Time to get up to speed				Good, acceptable
	Engine NVH				No perceptible engine vibration
Launch Light Pedal	Smoothness / time delay	7.8	8	0.2	Fast reponse
Launch Medium Pedal	Responsiveness / engine delay	7.4	7.5	0.7	Positive feel / good pick-up responsive
Launch Full Pedal	Jerk, acceleration feel	7.4	7.0	0.9	Acceptable response Lack of sustained acceleration
Tip-ins	From 20 km/h – light pedal	7.1	7.0	0.7	Responsive / no delay
	From 20 km/h – medium pedal				OK
	From 20 km/h – full pedal	5.8	6.0	0.6	Slow / bumpy
	From 50 km/h – light pedal	7.5	7.5	0.2	Fine / good response
	From 50 km/h – medium pedal				OK
	From 50 km/h – full pedal	6.2	6.0	1.1	Lack of acceleration / dead time
Brake to rest	From 70 km/h – various pressures	8.2	8	0.4	Very good pedal feel / linearity

Table 8.23– Driveability Appraisal conducted with EASIVT vehicle. Conducted with 9 drivers who have not been involved in the calibration work. The results show good correlation between the drivers assessments and reflects the characteritics sought in the control strategy. The full pedal launch and tip-in manoeuvres highlight the increased weight of the prototype vehicle as well as the limitations caused by the IMG maximum speed.

8.1.2.3 Driveability Evaluation

A driveability appraisal was carried out to evaluate and possibly confirm the longitudinal response improvement observed during the calibration phase of the EASIVT programme. The test were conducted with a reduced number of manoeuvres and the Vehicle Evaluation Rating [VER] scale conventionally used to mark performance, satisfaction index, level of functionality, and more generally most subjective assessments of the driveability performance.

Under the guidance of the author, a set of separate, simple driving inputs were executed and the driver was asked to mark and comment the response felt from the vehicle. No instrumentation or knowledge of the hybrid control strategy was available to the assessor. The results obtained from the 9 drivers of diverse experience showed good levels of correlation between the individual assessments of the various manoeuvre as detailed in Table 8.23.

The LSHT operation related tests showed very satisfying results and confirmed the functionality of the AVC and torque assist strategies. Engine vibration and noise at low speed, creep or idle were low enough to be unnoticed by all drivers. The AVC de-activation was immediately felt. Low and mild pedal input manoeuvres obtained very good feed back, potentially higher than the baseline IVT would. The worse grades were for the largest pedal inputs where the LSHT operation is negligible and the IMG role is reduced due to the higher power speed bands that are in excess of the IMG maximum speed.

8.1.3 Turbo Diesel Transient Torque Assist

The demand for more torque margin associated with BSFC IOL operation of the engine in the CVT powertrain is verified for both diesel and gasoline engine. Although turbocharged diesel engines offer lower BSFC values, they have a slower torque response due to the turbocharger lag as explained in Chapter 2 [Section 2.3.2.3] and verified in Chapter 6. For that reason, a diesel engine model was built and associated to simple CVT and vehicle models to investigate the behaviour of the air flow during the most demanding power-on transients.

8.1.3.1 Engine Model

The engine model was based on the Audi 3.0L V6 TDI engine. The parameters of the sub-models were tuned so that the full load performance could be correlated between available data and simulation results. This yielded accurate prediction of the engine performance in full load. Extensive calibration work was carried out on the VGT control system and a basic EGR strategy was implemented. This allowed optimised power-on transient operation for the plant model which was the basis of the MAI investigation.

Once CVT and vehicle models were implemented, power-on transient manoeuvres could be simulated including engine, CVT and vehicle response. The CVT strategy was designed to make the best use of the torque increase following the accelerator pedal request using an engine torque feedback sensor which would not be

available in a real powertrain for cost reasons. The engine air path subsequently highlighted the lack of available torque associated with turbocharger lag early in the transient manoeuvres.

The phenomenon was particularly critical since no rate of fuel increase limitation was implemented, causing rich mixture during most of the transient. This effectively guarantees that the fuel quantity increase is not affected by the air path lag, therefore highlighting the latter without artificially reducing the engine output. Furthermore, improvements in the fresh air supply will result in better transient AFR and more torque without the need to re-calibrate the ROFI strategy accordingly.

8.1.3.2 Manifold Air Injection Performance

The injection of air in the down-stream flow of the VGT compressor stage was proposed to promote increased fresh air intake following large boost pressure step demand. The sensitivity of such a system with respect to VGT operation and EGR closure strategy is high because of the non-linearity of these sub-systems. It was therefore necessary to optimise the MAI levels for best VGT operation in order to obtain a satisfactory overall behaviour and show relevant benefits.

The MAI system is a pressurized volume of air connected to the intake manifolds via a flow control valve similar to the EGR valve. When required, a controller amount of air passes through the valve and increases the mass of air in the intake. The control strategy is triggered by large step increases in IMAP error which is the feed-back signal to the VNT controller. The opening of MAI valve is proportional to the filtered air flow error, corrected for zero at start of opening.

Simulation runs were performed in a limited number of tip-in manoeuvres to study the sensitivity of the air path to the modification. The results showed how an appropriate coordination of the MAI controller with the transient behaviour of the VGT could improve both mixture properties and torque output. The simple vehicle longitudinal dynamics model illustrated the gains in acceleration profile with MAI compared to the first baseline simulations. The CVT ratio control strategy shifts at a rate that depends on the engine available torque. This torque contributes to the engine acceleration and the wheel torque increase at the same time. So the MAI directly improved the shift time of the CVT *and* the wheel torque. However, the CVT strategy could be modified to use the extra torque from MAI towards the engine acceleration or more wheel torque [see Section 8.2.3]. The former would decrease the shift time and the latter would increase the initial vehicle acceleration.

MAI is a torque assist feature developed in this research effort to match the characteristics of a diesel engine to a CVT powertrain. Other torque assist and boosting technologies were presented in Chapter 2 [Section 2.3.3] that would fulfil a similar role. However, MAI is a simpler, cheaper alternative with similar packaging demands which can be implemented independently of an engine downsizing effort.

8.2 Engine Characteristics Matching Exercise

The conclusions below highlight the research path suggested in the first chapter and followed through this thesis. It leads to a number of ideal engine characteristics recommendations based on the experience and the results above.

8.2.1 Research Work Analysis

Figure 8.150 illustrates the process initiated with the study of the CVT powertrain requirements and finalised in this chapter. It shows how simulation tools were used for the purpose of two separate investigation paths.
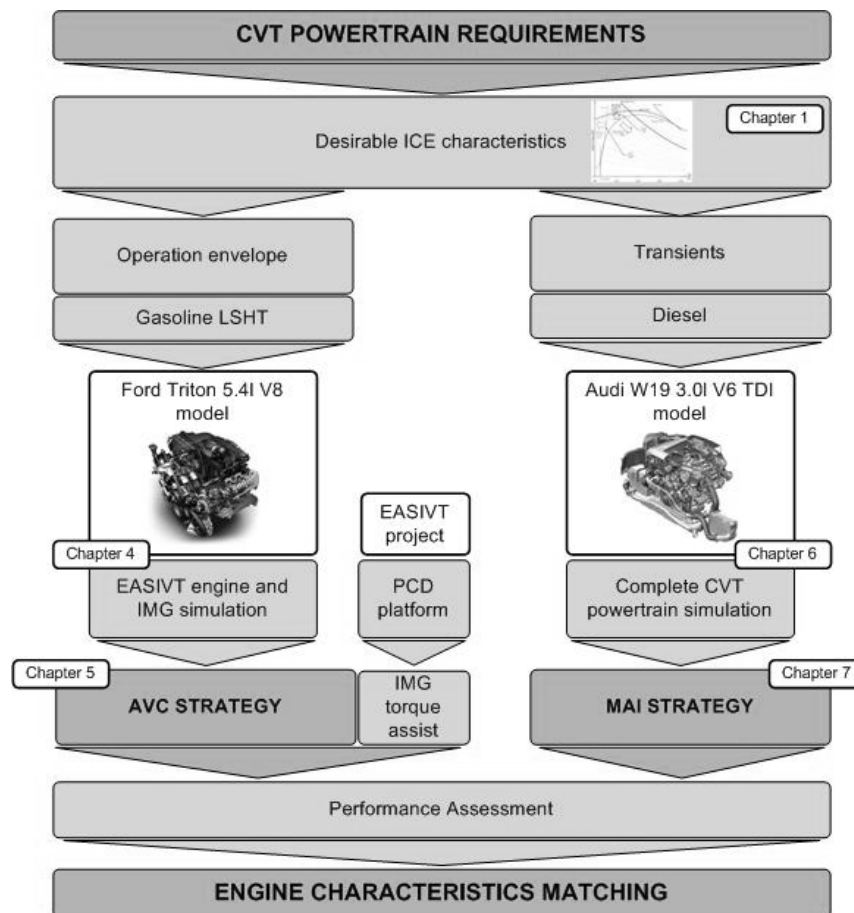
Figure 8.150 – Investigation path summary. The objectives set out in the first chapter lead to the development of two different engine matching strategies.

Both outcomes showed the importance of the operation engine match to the CVT powertrain in terms of fuel economy and driveability. The compromise between these two highly desirable attributes is improved when solutions are provided which allow CVT specific solutions to be implemented in the engine design or control.

The EASIVT project justified this analysis when demonstrating the benefits of a mild hybridisation to the IVT powertrain [*3.1%*]. The drive cycle fuel economy tests and the driveability appraisal confirmed this. Further improvements could be gained with the following developments:

- Increased level of coordination between cold start strategy and LSHT strategies to shift the cold start FE closer to the warm start performance. This involves fuelling and catalyst heat-up strategies.

- Second design iteration on the IMG towards lower inertia and extended speed range based on the findings of EASIVT, as developed by Cacciatori [77]

- Second design iteration on the power electronics to minimise the electrical power losses associated with AVC. Appropriate sizing of the DC link capacity can indeed limit the charge and discharge currents on the battery.

The MAI investigation demonstrates the relevance of torque response improvements of a diesel engine similarly to the IMG torque assist in the gasoline powertrain. The rich mixture excursion area during the heaviest transient was nearly halved. Further investigations should be conducted towards:

- ROFI implementation and calibration for both baseline and MAI engine configuration within the simulation platform

- Upgrading the CVT control with a higher level strategy layer which would fix the engine operating conditions depending on a vehicle speed and a driver demand. This would enable FE optimised operation over a drive-cycle. This work was not carried out because of the time scales involved with the calibration of such a system for both set-ups.

8.2.2 Ideal Engine Set-up for CVT

In the light of the existing engine technologies reviewed in Chapter 1 & 2 and the conclusions above, a number of recommendations can be made for an ideal engine set-up. Diesel and gasoline technologies have both benefited from constant improvements in R&D, therefore no distinctions can really be made as two which of the two suits best the CVT powertrain. The diesel engine often offers better BSFC and CO_2 emissions at comparable weight, but the gasoline engine has better driveability potential for cost effectiveness.

Charge dilution and stratified lean burning are engine operating modes which allow the best BSFC area to be lowered in the gasoline engine map. The response time to WOT from the lower IOL is faster than conventional throttling. This technique implemented in a direct injected and variable valve actuated engine would promote fuel efficiency without compromising the torque margin and response. AVC is an ideal complement to this if the cost of micro hybridisation can be justified. Provided that a VVA system justifies its own cost, new possibilities are offered towards an optimised CVT powertrain. As detailed in Chapter 2 HCCI has significant fuel consumption and emission reduction potential which a CVT can maximise. AVC allows extending the engine operating range towards LSHT region, at speeds where HCCI can be activated.

Diesel engines also have potential for an ideal match in a CVT powertrain. A downsized engine with high boost turbocharger can yield high power density, low inertia and superior efficiency. MAI is ideally suited for high boost VGT because it simplifies the filling strategy by using extra boost pressure during quasi steady state operation. It is therefore an alternative to existing torque assist and boosting devices reviewed in Chapter 2. The driveability detriment of using high boost, larger inertia turbocharger can be addressed with MAI, hence eliminating the need for dual stage air charging layouts. MAI can be controlled by the EMS system upon request from the CVT control strategy.

Although a CVT changes the engine response feel for the driver, it does not necessarily affect the way power is delivered. Indeed a naturally aspirated, gasoline engine CVT powertrain will always have a torque response advantage over turbocharged diesel engine. The extended speed range in gasoline means that power is delivered at higher speed. A turbocharged diesel CVT powertrain reflects other attributes of the engine. These are higher torque at lower speed and a small lag effect. An engine with CVT matched characteristics will still possess the typical attributes of diesel or gasoline technologies. This thesis demonstrates that improvements can be made towards both for the benefit of fuel consumption and driveability. This does not imply that a particular technology has a significant advantage over the other. Ultimately, customers will still seek one or the other depending on personal selection criteria.

8.2.3 Further Work

From the considerations presented above, there are a number of potential extensions to the research presented in this thesis. In the case of a gasoline engine application, the FE benefits of LSHT operation have been demonstrated but also highlighted the short comings of a standard EMS calibration. Based on the simulation environment described in Chapter 4 the following work could be carried out:

- EMS design and optimisation for LSHT using combination with HCCI technology. This involves the development of 1D auto-ignition models and the development of mode transition control.

- Cold start engine and catalyst warm up strategy development using lower engine speed and AVC to maximise FE right after the engine cranking

In the diesel engine application, most of the potential work involves control systems development which includes an extensive calibration effort.

- Add MAI filling strategy to extend the capability of the simulation environment and demonstrate the low energy cost predicted in Section 7.1.1

- Integrate EGR control with MAI strategy and investigate potential advantages of coordinated control similar to VGT and EGR control [see Section 2.3.2.3]

- Demonstrate further benefits with ROFI and CVT supervisory control implementation. This will enable the alteration of the split factor towards shift speed or driving torque at the wheel depending on vehicle speed.

Chapter 9: CONCLUSIONS

To maximise its fuel economy benefits, the CVT powertrain must use the engine at its best specific fuel consumption conditions during steady state operation. This is achieved by ratio or torque control strategies which are calibrated to bias the engine operating conditions towards the most efficient speed and torque for a required power. But vehicle driveability can suffer from this type of calibration because the engine speed is controlled by the CVT using the available torque margin. This available torque reserve can be significantly when best fuel economy is the prime objective of the CVT calibration. Low speed operation under low power conditions is also limited to maintain Noise Vibration and Harshness [NVH] below a driver acceptable level.

The matching of internal combustion engine characteristics consists in finding ways to enhance the compromise found between fuel economy and driveability. This can be achieved by ensuring BSFC operation on the Ideal Operating Line [IOL] is possible in the Low Speed High Torque [LSHT] region, lowering the IOL to increase the torque margin, reducing the torque response lag.

Active Vibration Control [AVC] of the engine combustion frequency torque oscillations reduces the NVH levels perceived by the driver. An AVC strategy was developed in simulation and implemented in a hybrid Infinitely Variable Transmission [IVT] and gasoline engine powertrain. This enabled LSHT operation under low power condition which received good feed-back from a panel of drivers and *3.1%* fuel economy improvement of the FTP75 city cycle.

Manifold Air Injection [MAI] was developed to reduce the torque response lag associated with a turbocharged diesel engine. The system provided faster CVT engine

speed shifts and improved vehicle acceleration. The MAI is a torque assist solution that can be implemented in downsized, high boost turbo diesel engine.

Both methods proved to help fuel consumption in the CVT powertrain by improving the engine operation compromise. The CVT powertrain can meet higher driveability targets without loosing on its fuel economy advantage over other types of transmissions. Gasoline and Diesel technologies both benefit from an engine characteristics matching effort towards the CVT powertrain.

In gasoline applications, Variable Valve Actuation [VVA] and direct injection allow operation in stratified lean-burning and charge dilution modes that are particularly suited to CVT powertrain because of the lowered IOL and the fast response time to maximum torque. AVC can complement this technology to offer extended operating range in LSHT region.

Diesel technology has potential for high efficiency and power density in turbocharged, downsized applications. The increased boost levels in downsized engines are a difficulty for the CVT powertrain because of the subsequent slow torque response. This can be addressed with MAI to improve the torque response characteristic of the downsized diesel engine and potentially replace a dual-stage charging system.

REFERENCES

[1]   **Graham, D. [2002]**, *Meeting the CO2 challenge DEER 2002*, Ricardo plc, slide presentation

[2]   **Guile, C. [2006]**, *An Overview of Future Trends in the Light Duty, On-Highway Transmission Market – The European Story to 2012,* CSM Worldwide, Proceedings of Integrated Powertrain and Driveline Systems Conference, IMechE, London, 2006

[3]   **Kluger, M. A., Long, D. M., [1999],** *An Overview of Current Automatic, Manual, and Contiuously Variasble Transmission Efficiencies and Their Projected Future Improvements,* Southwest Research Institute, SAE 1999-01-1259

[4]   **Burke, M., Briffet, G., Fuller, J., Heumann, H., Newall, J. [2003]**, *Powertrain Efficiency Optimisation of the Torotrak IVT*, Torotrak Development Ltd., SAE 2003-01-0971

[5]   **Singh, J., Berger, K., Mack, P., Piorkowski, P., Hogan, T., Wong, A. [2003]**, *General Motors "VTi" Electronic Continuously Variable Transaxle*, GM Powertrain, SAE 2003-01-0594

[6]   **Lee, Y., Choi, B., Kim, H., Kim, H. [2004]**, *Analysis and Development of CVT Ratio Control by Using of Pressure Control Algorithm*, Hyundai Motor Company, FISITA 2004 World Automotive Congress, Barcelona, 23-27 May 2004, F2004F085

[7]   **Murray, S. [2000]**, *Integrated Control of the Torotrak Powertrain*, Torotrak Development Ltd., Integrated Powertrains and their Control, University of Bath, 19 September 2000

[8]   **Lee, H., Kim, C., Kim, T., Kim, H. [2004]**, *CVT Ratio Control Algorithm by Considering Powertrain Response Lag*, Hyundai R&D & Kia Motor Company & Sungkyunkwan University, SAE 2004-01-1636

[9]   **Deacon, M. [1996]**, *The Control of a Passenger Car Diesel Engine and CVT*, PhD Thesis, Bath University, 1996

[10]   **Wicke, V. [2001]**, *Driveability and Control Aspects of Vehicles with Continuously Variable Transmissions*, PhD Thesis, Bath University, 2001

[11] Dorey, R., Martin, E. [2000], *Vehicle Driveability – Development of an Objective Methodology*, Ricardo Consulting Engineers, SAE 2000-01-1326

[12] Jantos, J. [2001], *Control of the Transmission Ratio Derivative in Passenger Car Powertrain with CVT*, Technical University of Opole, Poland, SAE 2001-01-1159

[13] James, I., Price, D. [1999], *Modelling Techniques Applied to the Development of Torotrak's Series 3 IVT*, Torotrak Development Ltd., CVT'99, Eindhoven, Netherlands, 16-17 September 1999

[14] Burtt, D, James, I. [2004], *Use of System Design Techniques in the Optimization of Integrated Powertrains Incorporating an IVT*, Torotrak Development Ltd., SAE 2004-01-0352

[15] Liu, S., Stepfanopoulou, A. [2002], *Effects of Control Structure on Performance for an Automotive Powertrain with a Continuously Variable Transmission*, IEEE Transactions on Control Systems Technology, Vol. 10, September 2002

[16] Crewe. C. M., Seabrook, J., Brandao, F., Edwards, S. P., [2006], *Novel Techniques for Holistic Powertrain Optimisation – A Hybrid Vehicle Case Study,* Ricardo UK Ltd, Proceedings of Integrated Powertrain and Driveline Systems Conference, IMechE, London, 2006

[17] Brace, C., Gutierez Magana, J. A. [2006], *The Effect of Exhaust After-treatment and Engine Temperature on IOLs for CVT Powertrain,* University of Bath, Proceedings of Integrated Powertrain and Driveline Systems Conference, IMechE, London, 2006

[18] Vaughan, N. D., Maugham, R. D., Brace, C., Murray, S., [2006], *An Engine Control Strategy for Improved Fuel Consumption and CVT Driveability,* Cranfield University, Ricardo Plc, University of Bath, Torotrak Development Ltd, Proceedings of Integrated Powertrain and Driveline Systems Conference, IMechE, London, 2006

[19] Bonnet, B., Cacciatori, E., Vaughan, N. D., Field, M., Wejrzanowski, K., [2006], *Control Development of a Parallel Mild Hybrid SUV with an Infinitely Variable Transmission: Simulation and Vehicle Implementation,* Cranfield University, Torotrak Development Ltd, Newage AVK SEG, FISITA, F2006P401

[20] Cacciatori, E., Bonnet, B., Vaughan, N. D., Burke, M., Price, D., Wejrzanowski, K., [2005], *Regenerative Braking Strategies for a Parallel Hybrid Powertrain with a Torque Controlled IVT*, Cranfield University, Torotrak Development Ltd, Newage AVK SEG, SAE 2005-01-3826

[21] Cacciatori, E., Bonnet, B., Vaughan, N. D., Burke, M., Price, D., Wejrzanowski, K., [2005], *Launch and Driveability Performance Enhancement for a Parallel Hybrid with a Torque Controlled IVT*, Cranfield University, Torotrak Development Ltd, Newage AVK SEG, SAE 2005-01-3831

[22] Sakaguchi, S., Kimura, E., Yamamoto, K., [1999], *Development of an Engine-CVT Integrated Control System,* Honda R&D Co., Ltd., SAE 1999-01-0754

[23] Cacciatori, E., Bonnet, B., Vaughan, N. D., Mebarki, A., Price, D., Burke, M., [2005], *Design Study on a Mild Parallel Hybrid Powertrain for a SUV,* Cranfield University, Torotrak Development Ltd., Newage AVK SEG, JSAE 20055420

[24] Osamura, K., Itoyama, H., Iwano, H., [2001], *Study of an Integrated Diesel Engine – CVT Control Algorithm for Improving Driveability and Exhaust Emission Performance,* Nissan Motor Co., Ltd., SAE 2001-01-3452

[25] Rohrbacher, Y., [2005], *Effect of Air Injection on Turbo Diesel Transient torque Response*, MSc Thesis, Cranfield University, 2005

[26] Field, M., Burke, M. [2005], *Powertrain Control of the Torotrak Infinitely Variable Transmission,* Torotrak Development Ltd., SAE 2005-01-1461

[27] Bohn, C., Cortabarria, A., Härtel, V., Kowalczyk, K. [2002], *Active Control of Engine-Induced Vibrations in Automotive Vehicles using Disturbance Observer Gain Scheduling*, Continental AG, Control Engineering Practice 12, 2004

[28] Grasso, C., Martorelli, M., Petrella, L., Sbarbati, F. [2004], *Powertrain NVH Refinement*, Elasis S.C.p.A., SAE 2004-01-0400

[29] Adamson, S. [2004], *Improved Approaches to the Measurement and Analysis of Torsional Vibration*, Rotec GmbH, SAE 2004-01-1723

[30] Matsuoka, H., Mikasa, T., Nemoto, H. [2004], *NV Countermeasure Technology for a Cylinder-On-Demand Engine – Development of Active Control Engine Mount*, Honda R&D Co., Ltd., SAE 2004-01-0413

[31] Walters, J., Husted, H., Rajashekara, K. [2001], *Comparative Study of Hybrid Powertrain Strategies*, Delphi Automotive Systems, SAE 2001-01-2501

[32] Bonnet, B., Tipner, P., Moreno, R. F., Marco, J., Vaughan, N. D., Kellaway, M., [2006], *In-Vehicle Resting of a 42V Lead-Acid Battery Management System for Mild Hybrid Electric Vehicle,* Cranfield University, Provector Ltd., UK, Presentation to the 10th European Lead Acid Battery Consortium, Athens, 2006

[33] Walters, J., Krefta, R., Gallegos-Lopez, G., Fattic, G., [2004], *Technology Considerations for Belt Alternator Starter Systems,* Delphi Corporation – Energenix Center, SAE 2004-01-0566

[34] Okuda, K., Komatsu, Y., Nakahara, Y., [2006], *Research and Analysis of ISG Belt-drive System for Idling Stop System,* Honda R&D Co., Ltd., SAE 2006-01-1501

[35] Prucka, M. J., [2005], *Development of an Engine Stop / Start at Idle System,* DaimlerChrysler Corp., SAE 2005-01-0069

[36] **Tamai, G., Hoang, T., Taylor, J., Skaggs, C., Downs, B., [2001],** *Saturn Engine Stop-Start with an Automatic Transmission,* General Motors Corp., SAE 2001-01-0326

[37] **Mourelatos, Z. [2000]**, *A Crankshaft System Model for Structural Dynamic Analysis of Internal Combustion Engines*, General Motors R&D, Computers & Structures 79, 2001

[38] **Beuschel, M. Shröder, D. [1999]**, *Identification and Compensation of Combustional Torque Pulsation Using Harmonic Activation Neural Network*, Tecnische univeristät München, EPE '99 Lausanne, 1999

[39] **Fukuo, K., Fujimura, A., Saito, M., Tsunoda, K., Takiguchi, S. [2000]**, *Development of the Ultra-Low-Fuel-Consumption Hybrid Car – Insight*, Honda R&D Co., Ltd., JSAE Review 22, 2001

[40] **Ogawa, H., Matsuki, M., Egushi, T. [2003],** *Development of Powertrain for the Hybrid Automobile – Honda Civic*, Honda R&D Co., Ltd., SAE 2003-01-0083

[41] **Lijima, T., [2006],** *Development of a Hybrid System for the 2006 Compact Sedan,* Honda R&D Co., Ltd., SAE 2006-01-1503

[42] **Aoki, K., Kuroda, S., Kajiwara, S., Sato, H., Yamamoto, Y. [2000]**, *Development of Integrated Motor Assist Hybrid System: Development of the Insight, a Personal Hybrid Coupe*, Honda R&D Co., Ltd., SAE 2000-01-2216

[43] **Davis, R., Lorenz, R. [2003]**, *Engine Torque Ripple Cancellation with an integrated Starter Alternator in a Hybrid Vehicle: Implementation and Control*, IEEE Transactions on Industry Applications, Vol. 39, December 2003

[44] **Badreddine, B., Zaremba, A., Sun, J., Lin, f. [2001]**, *Active damping of Engine Idle Speed Oscillation by Applying Adaptive PID Control*, Ford Motor Company & Wayne State University, SAE 2001-01-0261

[45] **Elsy, D. [2004]**, *IVT Technology – Building on the Fuel Economy Gains Delivered by Hybrids*, Torotrak Development Ltd., Global Powertrain Congress, Ford Conference Centre, Michigan, USA, 28-30 September 2004

[46] **Evans, D., Van Maanen, K. [2003]**, *Electric Machine Powertrain Integration for GM's Hybrid Full-Size Pickup Truck*, GM Powertrain, SAE 2003-01-0084

[47] **Ortmann, W., colvin, D., Fozo, R., Encelewski, M., Kraska, M. [2004]**, *Incorporating an Electrical Machine into the Transmission Control of Ford's Modular Hybrid Transmission*, Ford Motor Company, SAE 2004-01-0069

[48] **Frijlink, P., Schaerlaeckens, W., van den Tillaart, E., de Haas, J. [2001],** *Simulation of a Vehicle With an ICE, CVT, and ISG Powertrain – A Pre-Study for Concept Evaluation and Dimensioning,* PD&E Automotive and TNO Automotive, SAE 2001-01-3453

[49] Heintz, N., Mews, M., Stier, G., Beaumont, A., Noble, A. [2001], *An Approach to Torque-Based Engine Management Systems*, Ricardo GmbH, SAE 2001-01-0269

[50] Gander, H., Loibi, J., Ulm, M. [2000], *Gearbox Integrated Mechatronic Control – A New Approach to Handle Powertrain Complexity*, Siemens AG, SAE 2000-01-1159

[51] Mencher, B., Jessen, H., Kaiser, L., Gerhardt, J. [2001], *Preparing for CARTRONIC – Interface and New Strategies for Torque Coordination and Conversion in a Spark Ignition Engine Management System*, Robert Bosch GmbH, SAE 2001-01-0268

[52] http://www.kistler.co.uk

[53] Müller, R., Hart, M., Krötz, G., Eickhoff, M., Truscott, A., Noble, A., Cavalloni, C., Gnieka, M. [2000], *Combustion Pressure Based Engine Management System*, DaimlerChrysler & Ricardo Consulting Engineers & Kistler AG, SAE 2000-01-0928

[54] Sellnau, M., Matekunas, F., Battiston, P., Chang, C.-F., Lancaster, D. [2000], *Cylinder Pressure Based Engine Control Using Pressure Ratio Management and Low Cost Non-Intrusive Cylinder Pressure Sensors*, Delphi R&D & GM Powertrain, SAE 2000-01-0932

[55] Pierik, R. J., Burkhard, J. F., [2000], *Design and Development of a Mechanical variable Valve Actuation System,* Delphi Automotive Systems, SAE 2000-01-1221

[56] Flierl, R., Kluting, K., [2000], *The Third Generation of Valvetrains – New Fully Variable Valvetrains for Throttle-Free Load Control,* BMW AG, SAE 2000-01-1227

[57] www.bmw.com

[58] Stokes, J., Lake, T. H., Murphy, R. D., Osborne, R. J., Patterson, J., Seabrook, J., [2005], *Gasoline Engine Operation with Twin Mechanical Variable Lift Valvetrain – Stage 1: SI and CAI Combustion with Port Fuel Injection,* Ricardo Plc, SAE 2005-01-0752

[59] Koopmans, L, Ström, H., Lundgren, S., Backlund, O., Denbratt, I. [2003], *Demonstrating a SI-HCCI-SI Mode Change on a Volvo 5-Cylinder Electronic Valve Control Engine*, Volvo Corp. & Chalmers University of Technology, SAE 2003-01-0753

[60] Lancefield, T., [2003], *The influence of Variable Valve Actuation on the Part Load Fuel Economy of a Modern Light-Duty Diesel Engine,* Mechadyne International Ltd, SAE 2003-01-0028

[61] Fessler, H., Genova, M., [2004], *An Electro-Hydraulic "Lost Motion" VVA System for a 3.0 Litre Diesel Engine*, IVECO Motorenforschung AG, SAE 2004-01-3018

[62] **Van Nieuwstadt, M. J., Kolmanovsky, I. V., Moraal, P. E., [2000],** *Coordinated EGR-VGT Control for Diesel Engines: an Experimental Comparison,* Ford Motor Company, SAE 2000-01-0266

[63] **Witejunge, R. S., Hawley, J. G., Vaughan, N. D. [2004]**, *Application of Alternative EGR and VGT Strategies to a Diesel Engine*, University of Bath, SAE 2004-01-0899

[64] **George, S., Morris, G., Dixon, J., Pearce, D., Heslop, G., [2004],** *Optimal Bosst Control of an Electrical Supercharging Application,* Visteon UK, SAE 2004-01-0523

[65] **Kleeberg, H., Tomazic, d., Lang, O., Habermann, K., [2006],** *Future Potential and Development Methods for High Output Turbocharged Direct Injected Gasoline Engines,* FEV Motorentechnik GmbH, SAE 2006-01-0046

[66] **Imagine SA**, AMESim 4.3 User manual

[67] **Li, J. Z., Treusch, C.,Honel, B., Neyrat, S. [2005],** *Simulation of Pressure Pulsations in a Gasoline Engine Injection System and Development of an Effective Damping Technology,* Visteon Corp. & Imagine SA, SAE 2005-01-1149

[68] http://www.ricardo.com/engineeringservices/software.aspx?page=wave

[69] http://www.avl.com

[70] http://www.gtisoft.com/img/broch/broch_gtpower.pdf

[71] http://www.mathworks.com/

[72] **Yeaton, M. [2004],** *Managing the challenges of Automotive Embedded Software Development Using Model-Based Methods for Design and Specification*, The MathWorks, Inc., SAE 2004-01-0720

[73] **Garcia Martinez, O., Kargar, K., [2000],** *Simulation Tool for Transmission and Driveline Systems Design,* Renault, SAE 2000-01-0832

[74] **He, Y., Lin, C., Gangopadhyay, A. [2005],** *Integrated Simulation of the Engine and Control System of a Turbocharged Diesel Engine,* General Motor Corp., Presentation to the GT-Suite Users Conference, November 15, 2005

[75] **He, Y., [2005],** *Development and Validation of A 1D Model of Turbocharged V6 Diesel Engine under Steady-State and Transient Conditions,* General Motors Research and Development, SAE 2005-01-3857

[76] **Imagine SA, Institut Français du Pétrole.** *IFP Engine Library Documentation*

[77] **Cacciatori, E. [2007],** *Advanced Control Concepts for a Hybrid powertrain with Continuously Variable Transmission*, PhD Thesis, Cranfield University, 2007

[78] **Chmela, F. G., Orthaber, G. C., [1999],** *Rate of Heat Release Prediction for Direct Injection Diesel Engines Based on Purely Mixing Controlled Combustion,* AVL List Gmbh, SAE 1999-01-0186

[79] Rakopoulos, E., Adritsakis, D., Hountalas, D. T., [1995], *The Influence of the Exhaust System Unsteady Gas Flow and Insulation on the Performance of a Turbocharged Diesel Engine*, Heat Recovery System and CHP, Vol. 15, No. 1, pp 51-72, Elsevier

[80] Galindo, J., Lujan, J. M., Serrano, J. R., Dolz, V., Guilain, S., [2004], *Design of an Exhaust Manifold to Improve Transient Performance of a High Speed Turbocharged Diesel Engine,* Experimental Thermal and Fluid Science, Elsevier, 2004

[81] Patton, K. J., Nitschke, R. G., Heywood, J. B., [1989], *Development and Evaluation of Performance and Efficiency Model for Spark-Ignition Engines, SAE 890836*

[82] Bonnet, B., Rohrbacher, Y., Vaughan, N. D., [2006], *A Turbocharged Diesel Engine with Intake Air Accumulator to Improve Torque Transients in a CVT Powertrain,* Cranfield University, Proceedings of Integrated Powertrain and Driveline Systems Conference, IMechE, London, 2006

Appendix A: DIFFERENT CVT CONCEPTS

Although gathered under the same acronym, there are a few different CVT concepts and patents. This section aims at clarifying the major differences between existing concepts whether they are currently in production or still under development. Particular attention will be paid to the Torotrak Development Ltd. IVT transmission since it is part of the EASIVT hybrid vehicle powertrain into which the AVC strategy was implemented.

The engineering theories behind the different CVT concepts presented in the following sections are as various as the friction theories, lubrication properties, gear sets theories, hydraulics, etc. Consequently the scope of this technology review is relatively restrictive in order to keep the technical information provided in focus. Thus the mechanical layouts are detailed as much as possible, the engineering compromises made on packaging or functionality are mentioned, the modes of operation subsequently explained. However, belt and chain complicated theories have to be avoided since they are not directly relevant to the present study, lubrication functions are not detailed, nor are the frictional properties of the materials.
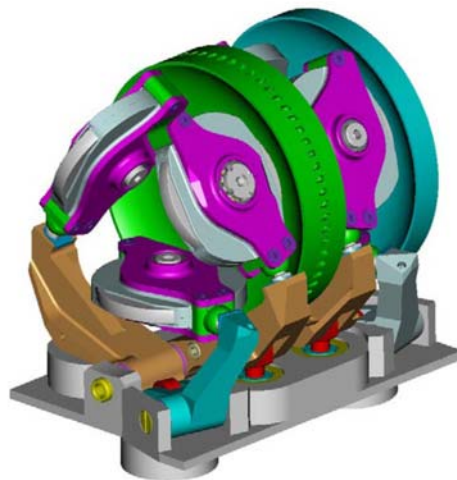
A.1 Full-Toroidal Variator

The first CVT patent goes back as far as the end of the 19th century and was of the toroidal type[A.1][A.2] followed later by its British declination [Hoffman W. D., 1899]. The concept is based on the transmission of torque through a toroidal shaped variator. In 1970, the toroidal CVT technology was licensed by British Leyland to Lucas Aerospace to use in the Harrier Jet Fighter [A.3]. The main disadvantages of the CVT were overcome as advanced technologies progressively got into passenger vehicles during the 1980's and 1990's. Oil manufacturers developed traction fluids for

toroidal transmission that allow better performance and durability. Moreover, the computational power available on-board increased dramatically and it allowed implementing significantly better CVT controllers. Indeed, the lack of ECU power is mainly what prevented this type of transmission to offer a viable alternative to the well established manual transmissions [MT] and 4-speed AT.

Torotrak Development Ltd [A.3] was founded in 1988 in order to develop the concept of a full toroidal variator which rights belonged to its mother company BTG. The purpose of the company is focussed on toroidal CVT now reaching its 3rd development generation called IVT Series III. The transmission is unique in its kind and will therefore be detailed separately in this section.

IVT stands for infinitely variable transmission and apart from a commercial name differentiation it also clarifies its difference with other CVT. The IVT is indeed capable of varying the transmission ratio anywhere between full reverse and full overdrive thanks to its power split layout. This infinite ratio span yields its name to the transmission.

Figure A.151 – The Torotrak full toroidal variator model [A.3]. Input is on the outside [blue] and output on the central disk [green], which separates the two toroidal cavities containing three rollers each [grey].

The core of the transmission is the full toroidal variator invented by Hunt and Hoffman. Figure A.151 shows the basic components of the variator. The two outside disks are clamped on the input shaft visible on the left hand side. The output disks in the middle are stuck together and they rotate around the same axis, i.e. the variator axis. Both input and output disks have matching toroidal surfaces producing two toroidal cavities on each side of the variator.

In each of the cavities is a set of three rollers as seen in Figure A.151. The angle made by the rollers yields the actual ratio of the variator and the symmetrical layout of the device ensures that forces are balanced within the variator. However the load case on each roller requires a reaction force on its support for it to remain in equilibrium as shown in Figure A.152.
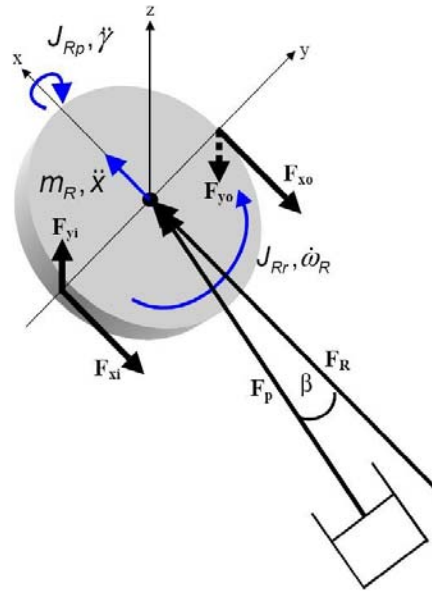
Figure A.152 – Equilibrium forces on the roller [A.4].
Force equilibrium along the x axis is written in Equation
A.22. Moment equilibrium around the z axis is written in
Equation A.23. Moment equilibrium around the x axis is
written in Equation A.24.

The reaction force is provided by hydraulics and its control determines the torque transmitted from one disk to the other. From [A.4], the equilibrium for the roller can be detailed as follows.

$$F_R - F_{xi} - F_{xo} = m_R \cdot \ddot{x}$$

Equation A.22 – Newton's second law projected on the x axis

$$\left(F_{xi} - F_{xo}\right) \cdot r_R = J_{Rr} \cdot \dot{\omega}_R$$

**Equation A.23** – Newton's second law around the z axis

$$\left(F_{yi} + F_{yo}\right) \cdot r_R = J_{Rp} \cdot \dot{\gamma}_R$$

Equation A.24 – Newton's second law around the x axis

Hence it is clear that torque can be transmitted only if F_R is non-zero. When a reaction force is applied then the ratio achieved by the variator depends on the torque ratio as the output power equals the input power – if the friction losses are not taken into account. Additional controlled counter pressure is provided on the outside flanges of the input disks to maintain the assembly together and guaranty adequate contact forces depending on the torque transmitted. An extensive explanation of the full toroidal variator dynamics is published by Fuchs *et al.*[A.5].

A particularity of the toroidal variator is that there is no actual metal to metal contact between the cavities and the rollers. A few tenth of millimetre thick [A.6] oil film under pressure from both sides ensures friction levels to transmit shear forces. This often is referred to as traction drive, ensuring minimum component wear and setting reliability to the highest standard.

Another particularity of the IVT is its low and high regime operating modes. The variator is indeed part of a more complex layout where an epicyclic gear train is used and activated by a couple of hydraulic clutches. This assembly is presented in Figure A.153.

Gear set   Variator

Epicyclic gear   Belt drive   High regime clutch
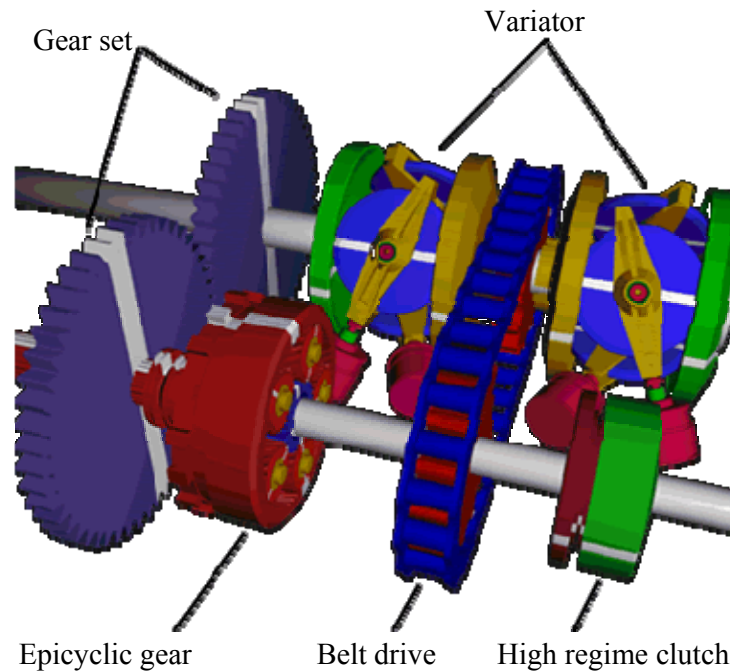
Figure A.153 – The Torotrak IVT Series III core components [A.3].
This stylised but functional representation of the transmission stressed the power recirculation possible between the gear set [left] and the chain [central] via the epicyclic train

The low regime is active when the vehicle is in reverse and during the launch sequence. Power flows from the input shaft through the variator. It is then transmitted to the sun gear of the epicyclic gear via chain drive as seen in Figure A.154. The epicyclic gear train acts virtually as a torque splitter. Some of the power is recycled and fed back from the planet carrier to the transmission input shaft via the low regime clutch and the gear set. The rest goes to the wheel acting as useful power via the annulus of the epicyclic.

The torque split ratio achieved by the epicyclic gear depends on the speed ratio between sun and annulus, i.e. between variator output speed and wheel. So at an appropriate variator torque ratio, the transmission can be controlled so that at a zero vehicle speed, torque is provided at the wheel to hold stationary position without friction being used to achieve this function. This possibility offered by the layout of the transmission and the controller [A.4] gives the IVT an clear edge compared to conventional ATs of clutch fitted CVTs especially under severe gradients or abuse driving.
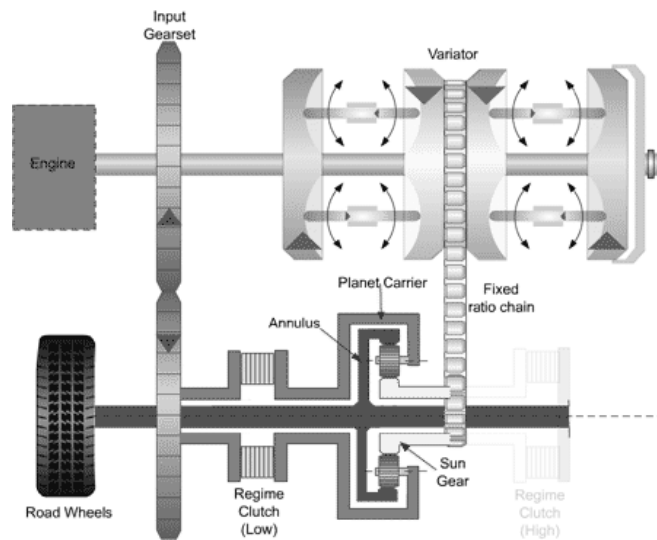

Figure A.154 – Torotrak IVT Series III in low regime [A.3]. Power recycling across the epicyclic is dependant on speed at the sun gear. If it is high, then the wheel will be rotating in reverse. If it's low then there is appoint where it reaches the planet carrier speed [synchronous point]. In the middle speed range, geared neutral is achieved when the wheel is static.

In forward motion there is a point where sun and annulus will be rotating at the same speed. It is called the synchronous point and it is not a fixed as it completely depends on vehicle speed and variator ratio, hence dependant on engine torque and wheel torque. At this point the high regime clutch is engaged while the low regime is disengaged. Consequently torque feed back is no longer happening and the variator ratios are swept back to high overdrive if the vehicle speed keeps increasing.

The low regime operation makes redundant any launch device such as torque converter or a conventional clutch. The trade-off is the relatively low efficiency of the IVT in this mode [4]. Indeed, conveying torque through the variator requires hydraulic power to be supplied in the actuators to provide the necessary reaction force [Figure A.152]. This is relatively inefficient when only a small fraction of this torque is actually going to the wheel and most of it is fed back to the variator input [Figure A.154].

The Series III IVT is still a development version and is only fitted in a number of technology demonstration prototype vehicles. However, a licensing contract exists between Torotrak and Equos to deliver a production ready version of the IVT which beats the best 6-ATs in terms of compactness and weight [A.7][A.8]. See Figure A.155.
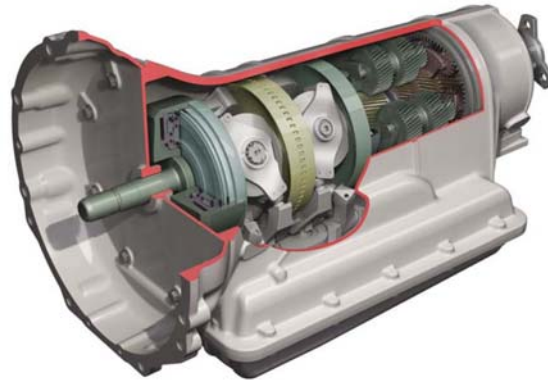
Figure A.155 – Latest development of the Torotrak IVT [A.8]. This production ready axial layout IVT was developed with Koyo and Equos. It is targeted at 6-speed ATs, but it is more compact as well as being lighter.

A.2 Belt & Chain CVTs

Belt type CVTs consist in two pulleys and a belt. Both input and output pulleys are made of two conical shaped flanges moving in and out along their main axis. Controlling the motion of the cones allows controlling the effective radius of one pulley. Therefore varying the diameter of the pulleys in a synchronised manner permits to change the actually speed ratio between the input and the output of the afore mentioned variator.

Most transmission manufacturers now develop and produce belt / chain type CVTs. The German giant ZF recently launched its latest CFT30 [A.9] to be fitted in the Ford 500, the Ford Freestyle and the Mercury Montego. Its earlier CFT23 product [A.10] was first introduced in the 2003 Ford C-Max. The ZF VT1 is installed in various Rover models as well as in BMW's New Mini. Audi and Luk developed the Multitronic transmission which has been around on most Audi models since 2000 [A3, A4 and A6 models]. It is based on a chain type variator developed with LuK [A.11] paired up with a multi-plate clutch for set-off purposes.
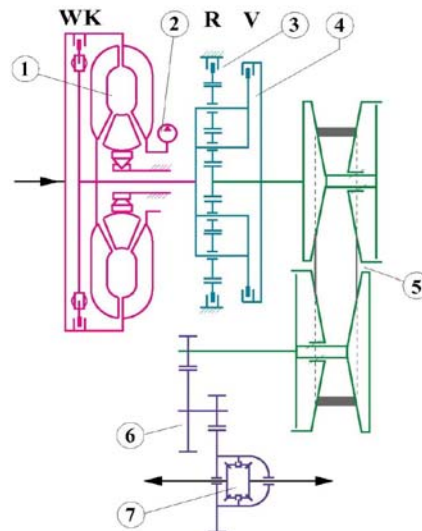

Figure A.156 – ZF's CFT23 CVT – Mechanical layout [A.10]. This schematic representation highlights the torque converter, the epicyclic gear, the belt variator, the final drive and the differential. An increase in pressure at the pulley assuming constant input torque [top shaft] makes the ratio increase, i.e. up-shift

The core of the CFT23 transmission is the pulley / belt variator⑤. Between the engine output shaft and the variator input pulley is a torque converter① similar to ones found on conventional automatics. This device allows boosting the torque coming from the engine together with a slip allowed between its input and output. It is therefore used as a launch [also referred to as set-off] device when the transmission output speed is null, i.e. vehicle at rest.

Then an epicyclic gear set fitted with two clutches achieves the reverse function. When going forward, i.e. "Drive" position, the forward clutch④ is engaged and the power flows from ① to ⑤ bypassing the epicyclic gear. When going backward, i.e. "Reverse" position then the forward clutch is disengaged and the reverse brake is engaged to activate the reversing set③. This means that the variator is used in the same manner whether the vehicle is moving forward or backward. Only the epicyclic speed ratio when in reverse makes the overall achievable transmission ration smaller in this direction.

In some cases, the torque converter is replaced by a conventional clutch, e.g. Audi Multitronic [A.11]. This very much depends on the compromises done by the designers in terms of packaging, cost and driveability. There also exist electrically assisted CVTs for launch manoeuvre where an electrical machine makes up for the absence of torque converter boost effect. This particular arrangement was discussed in Section 2.2.3.

The power is then transferred through the variator via two pulleys. The principle is that by varying the diameters of the two pulleys accordingly, it is possible to vary the ratio over a range determined by the minimum and maximum achievable diameters. Each pulley is made of two separated conical flanges than can slide one relatively to another. A pressure is hydraulically applied to the flanges and holding them together against the chain or the belt in between [see Figure A.157].
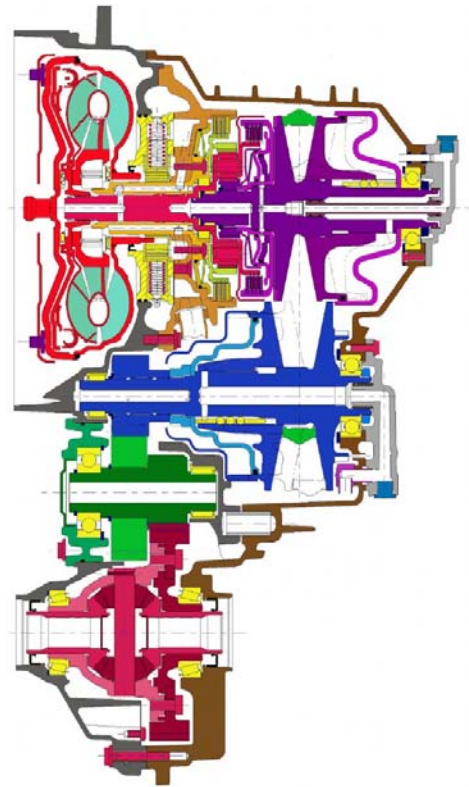

Figure A.157 – ZF CFT23 cross section [A.10]. Typical transverse front wheel drive application of the belt CVT layout. The short length is a real advantage for packaging in medium size vehicles.

The pressure in each of the two pulleys therefore creates a contact pressure on the flanges of the V-shaped belt or chain. The belt is made of endless laminated bands in layers running inserted on both sides of a number of steel elements which are shaped for the pulley's V.

The pulley diameter and subsequent ratio change is achieved by adjusting the pressure and the pressure ratio in both pulleys. The pressure applied by the hydraulic control unit guaranties a sufficient clamping force so that the friction between disks and chain is high enough for power transmission. Then the pressure split between the input pulley and the output pulley will drive the ratio higher or lower. The control of these pressures involves a lot of uncertainties concerning the friction coefficients [oil wear, temperature, mechanical wear]. The HCU also has to complete a lubrication function in the transmission as well as the control of the torque converter and the different clutches.
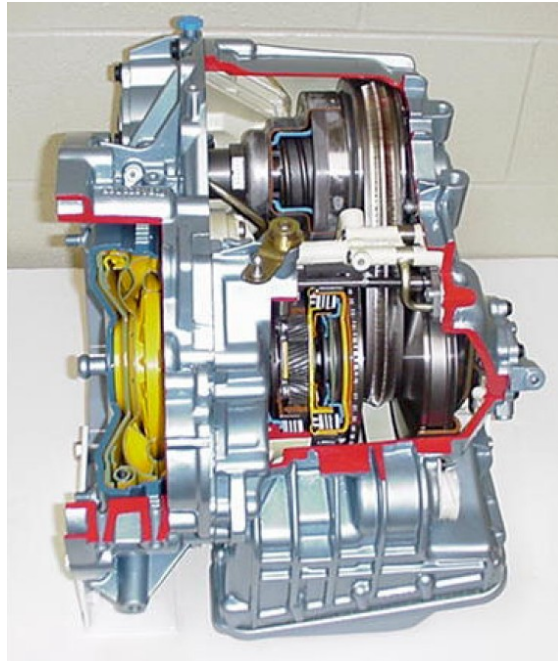
Figure A.158 – ZF's CFT23 [A.10]. The cut-out shows the torque converter [yellow], the hydraulic cylinders in the input and output pulleys, and the epicyclic gear for reverse.

A chain variator is slightly different. The power is transmitted between pulleys and chain in a similar manner, i.e. through contact friction, but the chain is loaded in traction.

The output from the variator generally connects to the transmission output via a final drive gear set and / or a differential depending on the powertrain layout. However, the packaging advantage of the belt CVT is in terms of length and it is particularly suitable for transverse engined, front wheel drive cars in which case the transmission casing will include the differential as well. The convenience of the belt CVT can be seen clearly in Figure A.158. The length of the transmission is particularly short in comparison with a comparable toroidal CVT.

A.3 Half-toroidal CVT

Bearing manufacturer NSK and transmission manufacturer Jatco developed a CVT based on the half-toroidal variator. The development of this unit described by Machida and Murakami [A.12] is based on a 1959 patent by Charles E. Kraus. Half and Full toroidal variator belong to a same family, therefore their architecture is relatively similar. The main difference resides in the shape of the cavities and the rollers support layout as shown in Figure A.159.
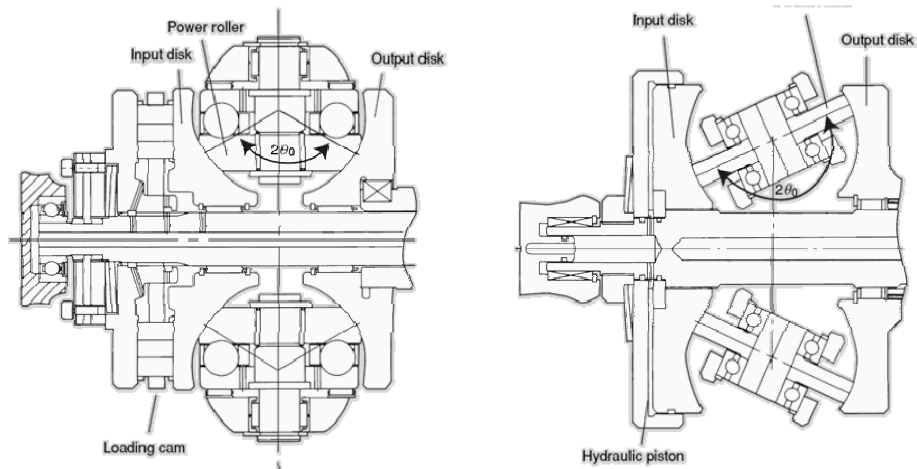
Figure A.159 – Half-toroidal and full-toroidal variator comparison [A.13]. The major difference is in the angle *2θ* formed by the two contact points and the roller centre of rotation. The full toroidal variator has the particularity that *θ=90°* resulting in no axial load produced by contact forces

Like the full-toroidal variator, half toroidal units require a reaction force on the roller support in order to transmit torque. The half-toroidal CVT benefits from a different load case on the rollers which is the main contributor to a theoretically higher efficiency value [A.13]. The Powertoros transmission developed by Jatco and NSK [A.14][A.15] uses a power-split system around the variator itself which is similar to the one described in the previous section.

A.4 References

[A.1] **Murray, S. [2000]**, *Integrated Control of the Torotrak Powertrain*, Torotrak Development Ltd., Integrated Powertrains and their Control, University of Bath, 19 September 2000

[A.2] **Hunt, C. W. [1877]**, US patent No. 197 742

[A.3] **www.torotrak.com**

[A.4] **Brockbank, C., Heumann, H. [2002]**, *Delivery of IVT for a 5 litre SUV: Addressing the Concerns of Geared Neutral*, Torotrak Development Ltd., Innovative Farhzeug-Getriebe C1143, 20-21 March 2002

[A.5] **Fuchs, R., Hasuda, Y., James, I. [2002]**, *Full Toroidal IVT Variator Dynamics*, Koyo Seiko Ltd. & Torotrak Development Ltd., SAE 2002-01-0586

[A.6] **Ono, Y., Goto, M., Yamashita, R., Hasuda, Y., Yasuhara, S., Lee, A., Greenwood, C. [2000]**, *The Durability and Reliability of Variators for Dual-cavity Full-toroidal CVT*, Koyo Seiko Ltd. & Torotrak Development Ltd., SAE 2000-01-0826

[A.7] **Torotrak [2004]**, *Annual Report and Accounts 2004*, Torotrak Plc.

[A.8] **Elsy, D. [2004]**, *IVT Technology – Building on the Fuel Economy Gains Delivered by Hybrids*, Torotrak Development Ltd., Global Powertrain Congress, Ford Conference Centre, Michigan, USA, 28-30 September 2004

[A.9] **Wagner, G., Remmlinger, U., Fisher, M., [2004]**, *CFT30 – A Chain Driven CVT for FWD 6 cylinder application*, ZF GmbH, SAE 2004-01-0648

[A.10] **Mozer, H., Piepenbrink, A., Sommer, S., [2001]**, *The Technology of the ZF CVT – CFT23*, ZF GmbH, SAE 2001-01-0873

[A.11] **http://www.audi.com**

[A.12] **Machida, H., Murakami, Y. [2000]**, *Development of the Powertoros Unit Half toroidal CVT*, NSK R&D, Motion & Control No. 9, October 2000

[A.13] **Imanishi, T., Machida, H. [2001]**, *Development of the Powertoros Unit Half Toroidal CVT (2) Comparison Between Half-Toroidal and Full-Toroidal CVTs,* NSK R&D, Motion & Control No. 10, April 2001

[A.14] **Miyata, S., Machida, H. [2001]**, *Development of the Half Toroidal CVT Powertoros Unit – Development of the Power-Split System*, NSK R&D, Motion & Control No. 11, October 2001

[A.15] **Imanishi, T., Miyata, S. [2003]**, *Development of the Next Generation Half-toroidal CVT*, NSK R&D, Motion & Control No. 14, May 2003

Appendix B: GEAR TRANSMISSION APPLICATIONS FOR TRANSIENT TORQUE CONTROL

It is worth noting that continuously variable transmissions are not the only ones to put new demands on engine management systems. Conventional manuals tended to yield to a new range of automated manual gearboxes, AMTs. This generic term encompasses most transmissions based on helical gears where actuation of the synchronisers and / or the clutch is realised by the controller using electric or hydraulic actuation [Figure B.160]. New standards of shift quality are achieved in this way and AMTs also offer the option for the driver to shift in a sequential manner. The benefits of these developments also lie in the combination of the gears high mechanical efficiency and optimum control, combined with a production cost lower than automatics due to common components with standard manuals [B.1] [B.2].
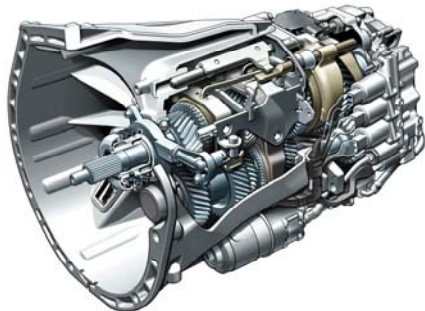
Figure B.160 – Mercedes Sequentronic [B.3] is an automated manual gearbox. Other high profile examples are the BMW SMG II, Alfa Romeo Selespeed, or Ferrari Cambio F1.

Figure B.161 – ZF 6HP26 6-speed automatic transmission [B.4]. In production since 2001, the torque capacity is in excess of 600 Nm within an overall ratio spread of 6.05.

Conventional automatics [Figure B.161] also had a general make over to compensate for relatively low efficiencies due to the torque converter losses. However the driving comfort they provide is much appreciated in the North American market and in Japan so their developers improved them to better the fuel efficiency and increase smoothness. Hence old 4-speed automatics are now replaced by 6-speed transmissions [B.4] [B.5] although the former still represent the biggest market share.

In the following sections, it will be demonstrated how optimum control of new powertrain technologies puts constrains of the engine controller. The demands in term of controllability to the power source, i.e. the engine, are similar to the ones from the CVT controllers.

B.1 Automated Manual Transmissions

Unlike the CVTs which up-shift and down-shift seamlessly and continuously within their ratio span, the automated manual transmissions only have a given number of gear ratios available. Therefore the shifting event is a step change in the transmission speed ratio. It involves a discrete sequence of events where basically one gear set will be disengaged and another one engaged [B.6]. This fundamental difference with consequences on driveability will be discussed in the following paragraphs.

Typically the shifting event consequently involves a wheel power cut-off similar to a driver operated manual shift. However, the AMT offers the possibility for the controller to enhance the jerk under power-on shifting [B.7], i.e. when the vehicle is accelerating. By, again, controlling the engine *and* the transmission in a synchronized manner it is possible to reduce the shifting time, to improve driving comfort, mechanical wear, and reduce fuel consumption when a full automatic mode is featured. The full automatic mode indeed takes control of the shift occurrences as a conventional automatic would do. Most AMTs feature similar shift maps to their AT equivalent, as demonstrated by Wheal *et al.* [B.8] from Ricardo and shown in Figure B.162.
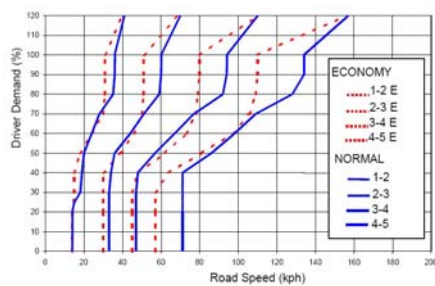
Figure B.162 – Up-shift lines for normal and Economy modes [B.8]. This AMT of a EU market vehicle features a very AT style calibration based on shift maps and two up-shift modes
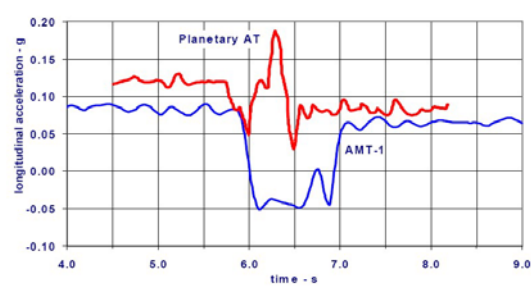
Figure B.163 – Comparison AT and AMT shift profiles [B.8]. Typical difference between AT and AMT is the drive torque loss and overall shifting time.

However, AMT are not capable of power-shifting, i.e. up-shift without loss of drive torque like AT are. The shift profiles, e.g. longitudinal acceleration trace for AMT can be very different from one another depending on the mechanical layout and the controller strategy adopted. Typically the difference with AT is shown in Figure B.163.

B.1.1 Power-On Shift Quality

Wheal *et al.* [B.8] provide a very interesting review of the up-shift qualities for an automated manual gearbox based on a single clutch, single lay shaft concept. They highlight the demands to the engine in torque controllability and emphasise the consequences on the shift feel. An up-shift event can be split into four phases [Figure B.164]:

- Engine torque reduction. The clutch is disengaged and the old gear is deselected during this phase.

- Shift actuation. The new gear is selected

- Torque increase. During this phase the clutch is reengaged with slip control.

- Oscillation period. It largely depends on the driveline dynamics and the clutch control strategy implemented.
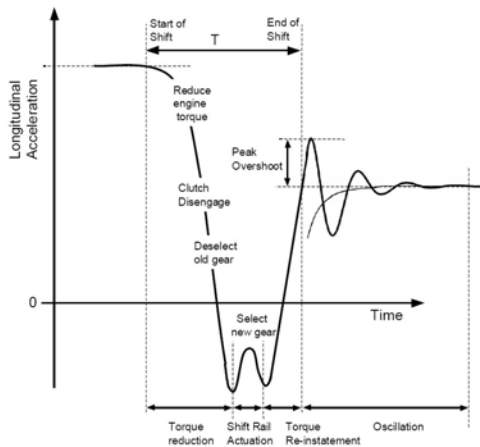

Figure B.164 – Shift profile and event sequence [B.8]. During new gear selection, the vehicle longitudinal deceleration fluctuates as the gear is brought down to synchronised speed.
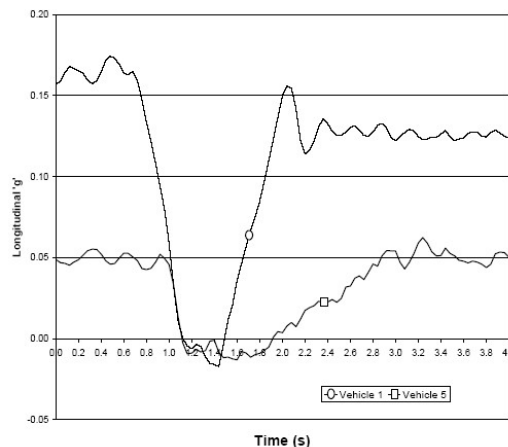
Figure B.165 – Alternative torque Re-Instatement strategies [B.8] for a 1-2 gearshift @ 30% pedal input and 2 different vehicles. Although much longer the up-shift of vehicle 5 was better rated

It is demonstrated that instead of overall shift duration, reduction in post shift oscillations is the main factor for subjective rating. This shows that a clutch engagement strategy that is very aggressive to shorten delays would not provide a satisfactory driveability performance if not integrated with engine torque transient control. Ideally the longitudinal acceleration drops down to the steady acceleration level provided by the next gear ratio as illustrated in Figure B.166. In reality the acceleration becomes negative when drive is lost, jerks as the new gear is selected and then oscillates when torque comes back on clutch reengagement.
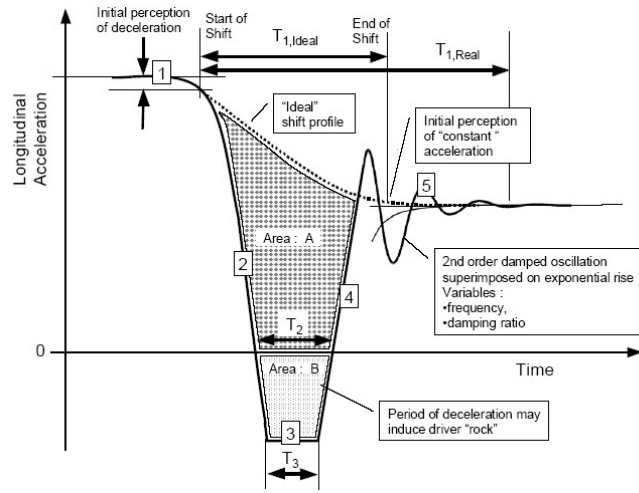
Figure B.166 – Real shift "costs" relative to ideal [B.8].
This diagram defines the shifting time from the initial
perception of deceleration to the initial perception of constant
acceleration

To smoothen the torque oscillations when the clutch is reengaged means
controlling both the clutch slip and the engine torque. Limitations are caused by
uncertainties on static and dynamic friction in the clutch as well as variations with wear
and temperature. Hence direct engine torque and speed control helps keeping these
fluctuations as low as possible as illustrated by Yin *et al.* [B.9] or Wang *et al.* [B.6].

Ultimately, the literature and papers agree on the fact that automated manual
transmissions provide a cost effective solution for improved driver comfort and fuel
economy. However they also agree on the downside which is a poor shift comfort
performance compared to conventional AT [B.8]. The trade off also appear during
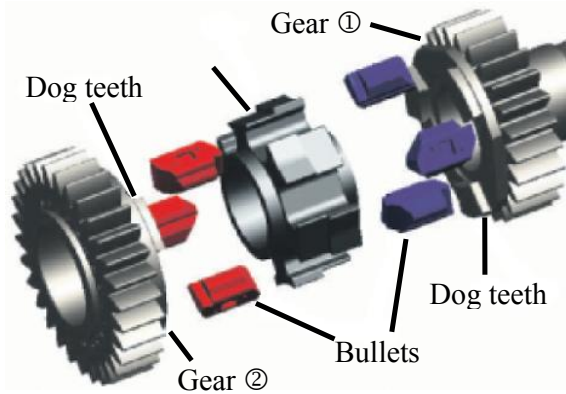launch performance.

The AMT yield significant
benefits for sport driving
orientated vehicles as they shorten
the shift time to a bare minimum
by controlling engine speed to
help synchronizers operation, by
actuating multi-plate wet clutches
for optimum engagement times.
The ultimate example is a formula
one gearbox, which is a
hydraulically actuated sequential
gearbox. However, a more
relevant example is Getrag's SMG
gearbox equipping BMW M series
and illustrated in Figure B.167.

**Figure B.167 – Automated sequential gearbox SMG
[B.10].** With 11 control modes and a launch control
function, this AMT shifts as quickly as *80 ms* in its most
aggressive mode.

B.1.2 The Zeroshift Concept

Zeroshift is a start-up company based in the UK which set off to demonstrate and promote a new gear synchronisation system which can be adapted to a conventional MT architecture. The Zeroshift gear selection mechanism presented in Figure B.169 replaces the traditional multi-cone synchromesh device actuated by the forks. Gears are therefore selected in a similar way to dog gearboxes which are designed to allow gears being engaged without prior synchronisation process. Dog MTs are usually reserved to motorsport applications; they indeed allow a very fast shift procedure by eliminating synchronisation process and engaging the new gear by literally slotting the dog ring into the new gear; this is a rather violent way which would cause unacceptable noise and vehicle bumps at each shit in a road vehicle application.

Figure B.169 – Zeroshift gear selection mechanism [B.11] providing selection of overdrive ratio [red bullet] without de-selection of initial gear. The initial gear is naturally disengaged when the input shaft is synchronised with the final gear [blue bullet]

Figure B.168 – Simplified Zeroshift bullets and hub assembly [B.11]. The bullets slide axially in the hub slots to engage against the dog teeth faces, which are machined at an angle to prevent incidental gear disengagement
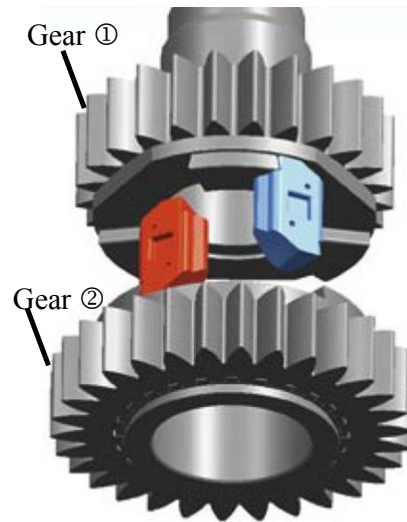
The Zeroshift gear engagement process uses a patented design which replaces the slotted dog ring by a set of "bullets" which slide axially on a hub between two gears as seen in Figure B.168. The hub is rotating with the input shaft through a spline design and the bullets are retained to the hub by a set of springs. The sides of the each gear facing the bullet ring feature dog teeth similar to a dog gearbox design, with an angled face mirroring the bullet shape that prevents any accidental gear disengagement.

The power-on up-shift process from gear 1 to gear 2 can be sequenced as follows:

- Gear 1 is engaged – the blue bullet transmits torque from the input shaft hub to the gear. The red bullet maintains drive on engine overrun, effectively trapping the dog tooth between a red and a blue bullet.

- A shift is initiated – the hub slides toward gear 2. Because the red bullet is not transmitting torque [power-on] it will slide from gear 1 to gear 2, held with the hub by the springs. Meanwhile the blue bullet is stays engaged in gear 1 because of the angled face, effectively stretching its positioning spring

- Gear 2 is engaged – the red bullet hits the dog tooth on gear 2, which rotates slower – causing a rapid deceleration of the input shaft. At that particular time, torque is transmitted by the red bullet to gear 2 with no interruption of drive to the wheels. The blue bullet is outrun by gear 1 and therefore free. It is pulled back to the hub under the spring action.

- The blue bullet secures gear 2 – now positioned on the other side of the dog tooth of gear 2, it plays the same role as the red bullet when in gear 1, securing drive during engine overrun

Power-off downshifts work in much the same way as the power-on up-shift described above, without using the clutch at any time. However, there are a few challenges related to this new concept.

Because the clutch does not intervene in the shifting process, the energy required to accelerate or decelerate the engine and gearbox input shaft during a gear change is not dissipated by clutch slip. This does not happen is traditional MT, because the clutch is disengaged during the gear synchronisation process. Any residual speed mismatch is absorbed by either the clutch or the gear synchronisation mechanism. With a Zeroshift design, the shifts would cause vehicle bumps if no measure was taken to at least reduce the engine output torque for a short period of time.

A second issue concerns the power-off up-shifts and the power-on downshifts. In the both case, the red bullet is transmitting torque initially – making it impossible to disengage it from the gear without respectively a throttle blip and a lift-off.

Finally, both issues of vehicle longitudinal acceleration profile and bullet disengagement require an usual level of interaction between transmission and engine; the former having to send rapid and accurate torque overriding requests to the latter. Simple throttle override is not suitable for the short time periods involved because of the relatively slow response caused by intake dynamics. A direct alteration of spark advance or injection parameters is likely to cause excursions of emission levels at each and every shift. Therefore the Zeroshift gearbox also proves to require a high level of powertrain control integration in order to reach the full benefits of the concept: seamless shift and acceleration performance improvement.

B.2 Dual-Clutch Gearbox

The technology behind the Dual Shift Gearbox [DSG] [B.12] a.k.a. Dual Clutch Transmission [DCT] [B.13] a.k.a. power shift AMT [B.8] is fairly simple and is not new either as it dates back to 1939. However, its control is not straight forward which is why the first production vehicle with this type of transmission only appeared a few years ago. Only recent development of on-board computational power made possible the control of the transmission in a road suitable manner. The DSG gearbox was made famous in the eighties when it was shortly tried on the successful Audi Quattro world rally car. Patents where also held by Porsche [B.14], but the concept was abandoned in the early stages because it proved too difficult to overcome controllability and reliability difficulties.

The principle of the power shift gearbox actually consists in two assembled gearboxes, one for the even gear numbers and one for the odd numbers. Each has its own clutch and they are coupled at the input as well as the output. An example of layout is shown in Figure B.170.
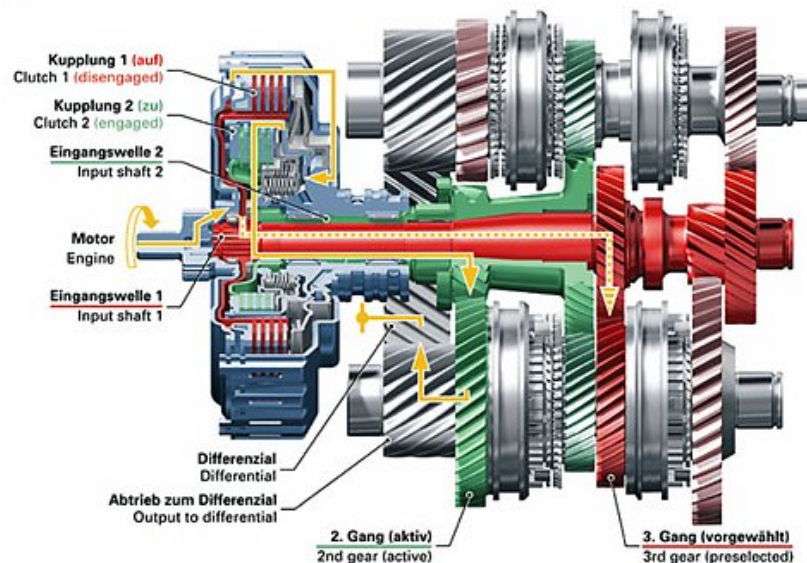
Figure B.170 – Audi DSG gearbox components [B.12]. The green input shaft drives 2nd and 4th at the bottom, 6th on top. The red input shaft drives 3rd and 1st to the bottom output shaft and 5th to the top output shaft. The two output shafts are coupled by a gear stage.

Thanks to its special arrangement the power shift AMT make it possible to shift up or down while changing of "active gearbox", i.e. one clutch is disengaged while the other one is engaged. Concretely, when for example the transmission is set on 3rd gear under acceleration, the controller is free to pre-select 4th gear on the other gearbox [gear synchronized]. Hence a typical upshift or downshift sequence does not involve any synchronization task.
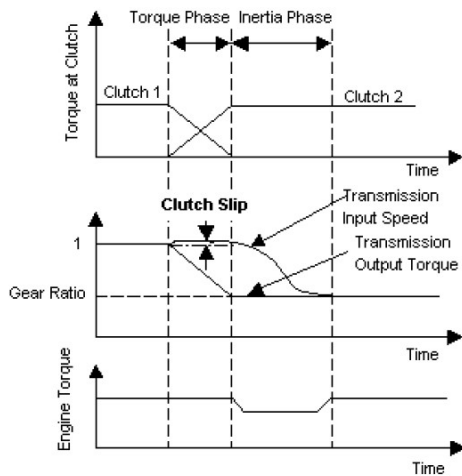
Figure B.171 – Control principle for upshifts [B.13] with control of clutch slip and engine torque

Crolla *et al.* [B.13] detail the opportunities for the control strategy of a DCT and demonstrate how engine torque and clutch slip control can significantly improve the shift quality. Figure B.171 and Figure B.172 illustrate the shift strategies adopted for both power-on upshifts and downshifts. It is explained that indeed power-off upshifts and power-off downshifts can be treated respectably like power-on downshifts and power-on upshifts.

The objective of the clutch to clutch shift strategy presented here is to provide a jerk free gearshift, i.e. with no transmission output torque jerk that would cause vehicle longitudinal acceleration vibrations [B.8]. This problem is avoided in ATs using one-way clutches that automatically disengage if the input torque becomes negative. The mechanical design and the targeted fuel economy benefits in dual shaft gearboxes hence do not allow the use of the clutches for that purpose. The jerk phenomena during an upshift could be caused by:

- Late oncoming clutch engagement implying a drop in the drive torque

- If the oncoming clutch carries too early the full engine torque then the off-going clutch still pressurized produces a large negative torque [drag torque] which once released produces a step rise in output torque.

Crolla *et al.* [B.13] propose a control of the off-going clutch involving a fixed, small amount of slip as shown in Figure B.171. Pressure in the off-going clutch is reduced as the oncoming clutch takes on so as to maintain the reference slip speed. Then during the inertia phase the oncoming clutch is progressively brought to lock with a slight decrease in engine torque.
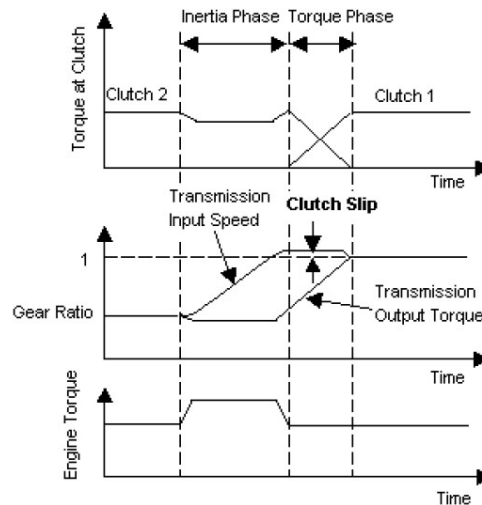

Figure B.172 – Downshift strategy [B.13]. Notice the inertia and torque phases definition.

In this inertia phase torque control while the engine speed is brought down is very important. In past open loop strategies the pressure was increased at the oncoming clutch to achieve the engine speed drop. This causes an increased vehicle jerk when engine inertial energy was transferred to the wheels. It is detrimental to fuel consumption because of unnecessary gearbox actuation energy expense. In the strategy described by Crolla the speed synchronization on each sides of the oncoming clutch is achieved by an engine transient torque control, which comparatively also reduces clutch wear. The details on the engine dynamics subsequent to the "manipulations" in throttle angle and spark advance necessary to achieve this are not discussed here.

The benefits from engine torque control can be pushed even further if during that inertia phase the oncoming clutch pressure is used to close loop control the transmission output torque. This can for example give a desired shift torque profile [e.g. constant torque output in the part-throttle range] or ensure controller robustness under high wear conditions. Very similar demands on engine controllability exist with the downshift strategy.

Figure B.173 illustrates what could be regarded as the most advanced DCT. With 7-speeds and the most demanding specification, the Veyron DCT addresses a number of engineering challenges previously never overcome. With engine torque levels in excess of *1200 Nm*, engine and transmission control coordination is key to reliability.
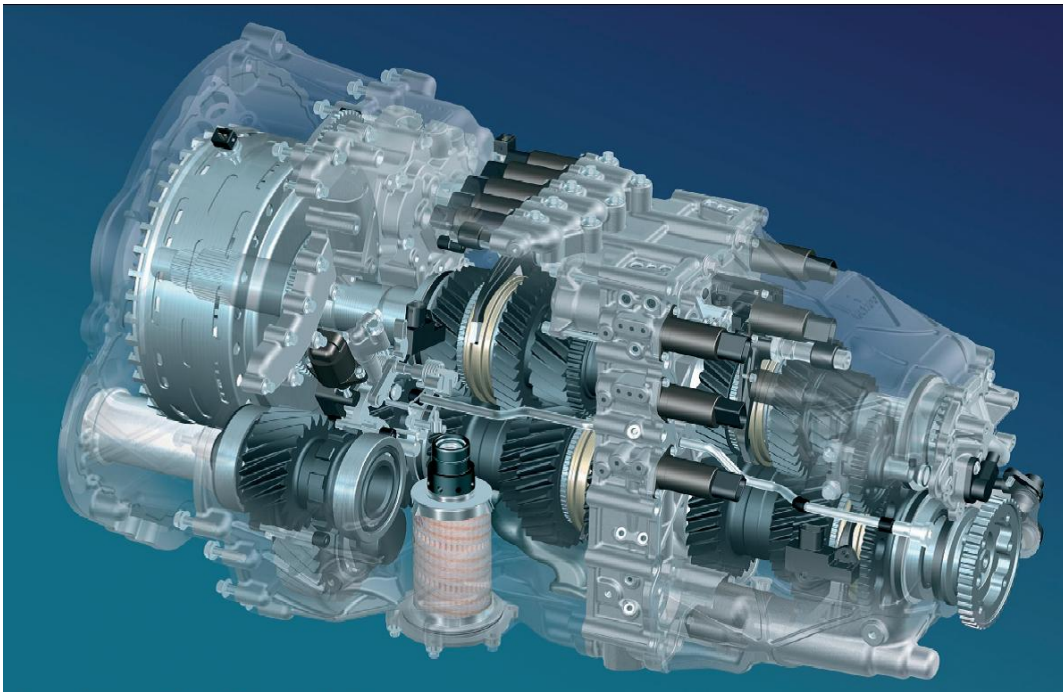
Figure B.173 – Ricardo 7-speed DCT for the Bugatti Veyron [B.15]. Meant to be a technology vitrine for both VW group owned Bugatti and transmission design specialist Ricardo, the Veyron transmission achieves high driveability standards in the most powerful production car ever produced. With engine torque rating in excess of *1200 Nm*, clutch control and shift actuation is critical for the components lifespan, the performance of the vehicle and the safety of the passengers.

B.3 References

[B.1] **Wagner, G. [2001]**, *Application of Transmission Systems for Different Driveline Configurations in Passenger Cars,* ZF Getriebe GmbH, SAE 2001-01-0882

[B.2] **Link, M., Voβ, B., Eggert, E., Nasdal, R. [2001]**, *The Automated Shift Transmission [AST] – Possibilities and Limits in Production-Type Vehicles,* IAV GmbH, SAE 2001-01-0881

[B.3] http://www.mercedes-benz.com

[B.4] **Scherer, H. [2003]**, *ZF 6-Speed Automatic Transmission for Passenger Cars*, ZF Friedrichshafen AG, SAE 2003-01-0596

[B.5] **Greiner, J., Doerr, C., Nauerz, H., Graeve, M. [2004]**, *The New "7G-Tronic" of Mercedes: Innovative Transmission Technology for Better Driving Performance, Comfort and Fuel Economy*, DaimlerChrylser Corporation, SAE 2004-01-0649

[B.6] **Wang, Y., Song, J., Zingkun, L. [2004]**, *Simulation of AMT Autoshift Process Based on Matlab / Simulink / Stateflow*, Tsinghua University, SAE 2004-01-2055

[B.7] **Taguchi, Y., Soga, Y., Mineno, A., Kuzuya, H., Horiuchi, I., Ueda, Y., Miyazaki, T., [2003],** *Development of an Automated Manual Transmission System Based on Robust Design*, Aisin Seiki Co., Ltd, SAE 2003-01-0592

[B.8] **Wheals, J., Crewe, C., Ramsbottom, M., Rook, S., Westby, M. [2002]**, *Automated Manual Transmissions – A European Survey and Proposed Quality Shift Metrics*, Ricardo plc, SAE 2002-1-0929

[B.9] **Yin, X., Tan, J., Lei, Y., Anlin, G. [2004]**, *Combined Control Strategy for Engine Rotate Speed in the Shift Process of Automated Manual Transmission,* Xihua University & Jilin university, SAE 2004-01-0427

[B.10] http://www.mwerks.com

[B.11] www.zeroshift.com

[B.12] www.audi.com

[B.13] **Crolla, D., Goetz, M., Levesley, M. [2004]**, *Integrated Powertrain Control of Gearshifts on Twin Clutch Transmission*, University of Leeds, SAE 2004-01-1637

[B.14] **Flegl, H., Wust, R., Stelter, N., Szofridt, I. [1987]**, *Das Porsche Doppelkupplungs [PDK] Getriebe*, Porsche AG, ATZ Automobiltechnische Zeitschrift Vol. 89, 1987

[B.15] www.imeche.co.uk

Appendix C: 1D MODELLING TECHNIQUES WITH AMESIM AND ENGINE LIBRARY

This Appendix presents the techniques employed to establish the models. It sets the theoretical background necessary to better understand the models description found in Chapter 4. The layout of the simulation environment and assumptions made will be identified and discussed.

C.1 1D Modelling

One dimensional modelling is an approach which consists in describing a local three dimensional phenomenon with one or more governing equations that picture the essence of it. This means that each part of a real life plant has to be split into elements hosting a distinct physical phenomenon. Most of the time, this preliminary task can be done intuitively, and number of examples will be given in this Chapter. The 1D representation is not always a simplification of the more straight forward 3D representation such as one used in computational fluid dynamics [CFD]. It can sometimes simply ignore two of the three dimensions of a problem because they have little or no interaction with the plant to model.

A simple example of this dimension elimination is the planar approach [2D] used for most multi-body mechanical problems. A road map is a two dimensional representation of the real-life environment where the vertical dimension is ignored because it has virtually no interaction with the purpose it serves: helping people travel from A to B.

Figure C.174 and Figure C.175 show simple examples of 1D models for the applications this study has been focusing on. The load and the flow respectively across the spring and through the pipe only go one direction as side effects are assumed to have no influence. Models based on those principles have been successfully established by He [C.2] and Mattarelli *et al.* [C.3] for engines – by Li *et al.* [C.4] and Chiatti *et al.* [C.5] for injection systems – by Lafossas *et al.* [C.6] for Combustion chambers – by Garcia *et al.* [C.7] and Zhang *et al.* [C.8] for powertrains.

Each sub-model in the AMESim libraries for engine, powertrain, hydraulic is made of a set of inputs and / or outputs at the ports which are interconnection points with other sub-models as shown in Figure C.176. Not all 1D sub-models have the simplicity of Figure C.174 and Figure C.175. The variable nozzle turbine shown in Figure C.176 can be used as part of an elaborate turbocharger system model. It has a control port for the angle of the blades, a mechanical port ② that inputs the shaft speed and outputs the torque load on the turbocharger shaft. Port ① and ③ are the thermo-fluid ports where pressure ratio, mass flow and turbine speed are related by a turbine map.

Figure C.174 – Simple 1D model of a spring [C.1] where all side loads are ignored
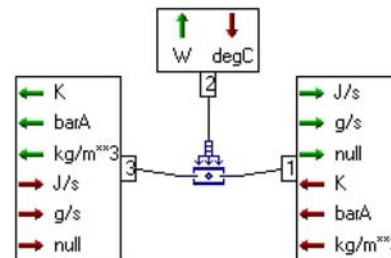
Figure C.175 – 1D model of a pipe [C.9] with heat exchange and gas compositions
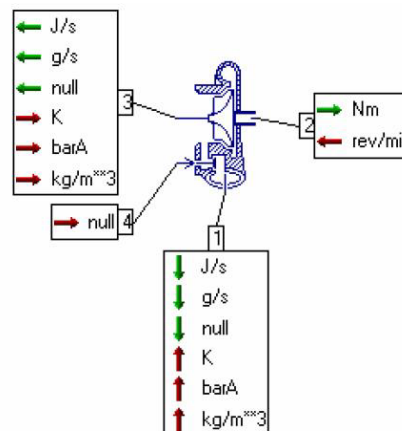
Figure C.176 – Variable Nozzle Turbine sub-model from AMESIM's IFP Engine library [C.9]. Ports 1 and 3 are thermo-fluid ports. Port 2 is a mechanical port and port 4 is a control input

The 1D sub-model approach to the modelling task may appear rather intuitive when components are already available in a library which has been validated. The fact is that validated library component shift the modelling engineer's task from creating robust equations covering all possible configurations towards splitting his system most appropriately and ensure solvability of the model he creates. Indeed, the flow of the variables from one end of the model to another is the responsibility of software user. This requires an adequate overview of the plant to model and an understanding of the causality intrinsic to the system.

C.1.1 Causality Principle

In a one dimensional object oriented modelling environment, causality as introduced in the previous paragraph is a principle that can easily remain unknown to the user of the software. Simulation packages and libraries are designed in such a way that variable flow within the model always remain solvable and the compilers themselves have a certain degree of robustness that allows most simple models to be solved.

However, more complex plants cannot always be modelled completely intuitively by assembling sub-models. They require the user to arrange the elements in a coherent way such as equations can then be solved. Indeed, a causal modelling tool will carry out the calculations in the order defined by the user from the variables flow in the model [C.10]. An interesting definition of causality is given in the AMESim Hydraulic component Design library documentation [C.11] where it is described as the "general principle that the connection can only be made between [...] two sub-models if each supplies the input requirements of the other". In hydraulic or pneumatic systems this means that capacitive components can only be linked together by resistive components; this applies in particular to the air path of an engine model. In mechanical rotational systems, inertias are connected by rotational stiffness elements.

A well designed library allows a skilled user to model virtually any combination by using the appropriate sub-models for each component. There are however alternatives such the Dymola simulation package [C.10] which relieves the user from establishing causality within his model. The solver automatically rearranges the equations prior to a simulation to create a calculation order that is suitable. Zhang *et al*. [C.8] give a particularly good example of the possibilities of Dymola when dealing with a dual shaft AMT model which can be subjected to a number of discontinuities during simulations. Discontinuity handling is explained in the Section C.1.3.

C.1.2 Lumped Parameter Approach

A well tuned 1D plant model can reach accuracy levels that are well beyond the requirements of controller development or design investigation. However, it is important to bear in mind the limitations of such models and the assumptions which were made during the modelling process in order to achieve the necessary performance match. This helps keeping the complexity of the model down as well as the associated simulation run time. This section will describe the general assumptions and limitations of 1D models with particular interests to the sub-models used in this research effort.

The main assumption of the one dimensional modelling technique lays in the lumped parameter approach. Each elementary sub-model has a set of parameters which are indeed the coefficients in the associated ruling equations. Those coefficients do not change with time or space within the sub-model. A lumped parameter is a characteristic value which physical meaning describes a particular behaviour of a sub-model. An example is given below in Figure C.177 with a 1m pipe model closed on one end and supplied at *2 bar* in the other end [C.11]. Three alternative models are presented using basic pipe sub-models. The first alternative is made of one sub-model with a lumped parameter length of 1 m, whereas the other two alternatives are made of smaller length sub-models as specified in Table C.24.
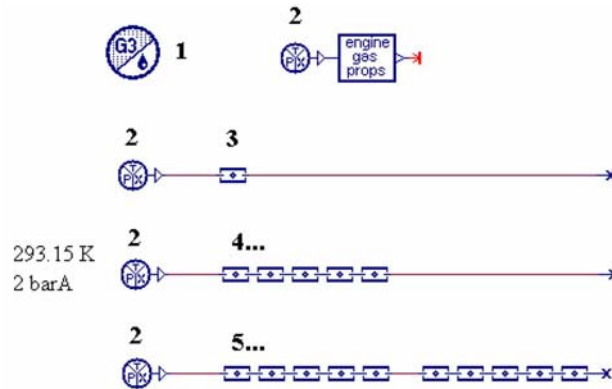

Figure C.177 – Alternative models for a 1m pipe closed in one end
and supplied by a 2 bar pressure source in the other end [C.9].

	Submodel Name and Type		Simulation Parameter
1	ENGMD00	Fluid properties definition	Default values
2	ENGCS001	Constant pressure source	Output pressure = 2 bar
3	ENGPI02	Straight pipe	Length = 1000 mm
4	ENGPI02	Straight pipe	Length = 200 mm
5	ENGPI02	Straight pipe	Length = 100 mm

Table C.24 – Set of parameters for Figure C.177. Items 3, 4 and 5 are alternatives models for a 1m long pipe [C.9]

Because all sub-models are of the same type therefore governed by the same equations, it could be expected that no matter how many small pipe elements are used to make the 1m long pipe, the simulation results would be exactly the same. It is interesting to notice that this is not the case because of the lumped parameter approach. The submodel ENGPI02 used to model the pipe includes resistance, inertia and compressibility effects. Thus combining a greater number of those elements will increase to capability of the model to take wave dynamics into account whereas a single 1m long pipe model will not, as shown in the simulation results presented in Figure C.178.
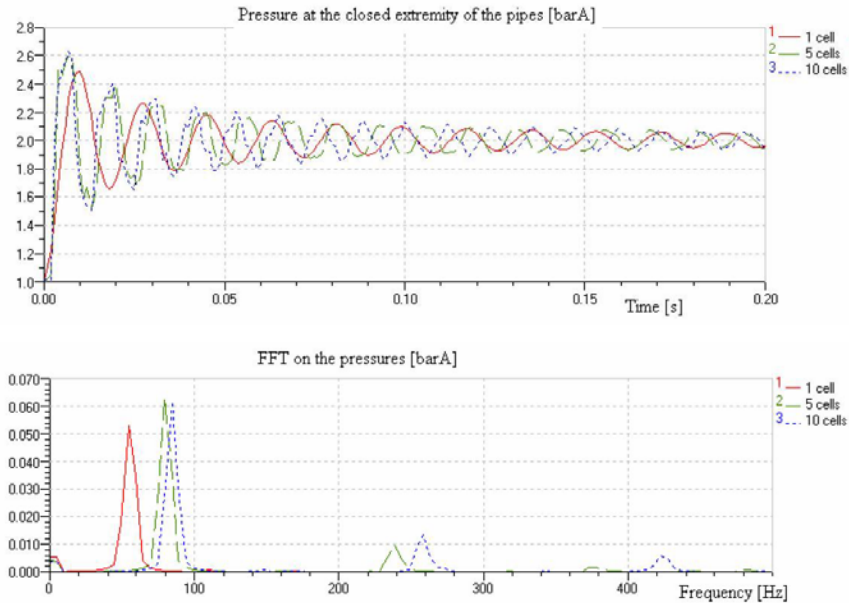
Figure C.178 – Pressure at the closed extremity of the pipe. The more cells in the pipe model, the greater the accuracy of the results by taking into account wave dynamics, otherwise known as the sampling effect [C.9]

The sampling effect subsequently highlighted can play a major role in the number of elements to model the pipe. Such examples exist in other applications such as shafts that are also included in the powertrain models to establish. Depending on the geometry to represent, one submodel might however be enough to satisfyingly reproduce the behaviour of the sub-system in interactions with its environment.

C.1.3 Discontinuities

Another point of potential concern is the way the model handles discontinuities during the simulation. Discontinuities can be defined as an event that is physically and / or numerically violent, i.e. a quantity jumps from one value to another instantaneously [C.12]. There are a number of reasons which can cause discontinuities during a simulation. Some are common and without consequences on the simulation run:

- Aliasing [C.13] due to a communication interval[1] too big for the frequencies in the signal

- Step changes due to modulus functions

Some others can cause the simulation to become very slow, due to the increased numerical stiffness [see definition in Section 3.1]:

- Force step changes due to mode changes, i.e. a different set of equation ruling the local submodel due to a change of conditions. An example of this is friction laws where different equations apply depending on whether or not there is relative motion otherwise known as slip-stick effect.

- Control variables that are limited by saturation functions steps or ramps therefore introducing discontinuous derivatives

- Transitions from laminar to turbulent flow in orifices

- Hysteresis effects

- Valves with characteristics which dramatically change if they are opened or closed

The integration algorithm in simulation software is the core of the simulation process. The equations formed by the submodels are solved in an iterative process which needs to converge at each time step, subsequently yielding the state variables derivatives. The integrations methods are based on the assumption that those derivatives are continuous, therefore handling of discontinuities require the algorithm to reduce the integration time step for convergence to occur.

Effectively, the solver and the submodels in AMESim communicate to ensure that discontinuities are flagged up and dealt with appropriately. It is however recommended to avoid inducing discontinuities in the models unless they actually refer to a real life phenomenon, e.g. gear backlash. Awareness of the intrinsic problems caused by discontinuities is a key to building smooth running simulation environment. Moreover, the possibility to adjust the tolerance requirement on the convergence process helps reducing simulation time at a relatively small cost; but a direct drawback is that discontinuities might be a lot more difficult to handle. The compromise to be

---

[1] In most simulation packages, the communication interval is the time period at which the models variables are sampled. It defines the sampling frequency of the simulation.

found between absolute accuracy of the simulation results, capacity to overcome discontinuities and simulation run times is crucial to success.

C.2 IFP Engine Library

Introduced in Section C.1, IFP Engine [C.9] is an optional library of AMESim components or sub-models that integrates with most other libraries in terms of port compatibility and causality [Section C.1.1]. Although AMESim offers the possibility for the user to develop its own libraries of custom made elements [C.12], IFP Engine offers a range of validated models therefore saving a significant amount of time in development and testing of a custom library. A validated model offers a guaranty that simulation will run successfully in most situation leading to more freedom in the modelling task.
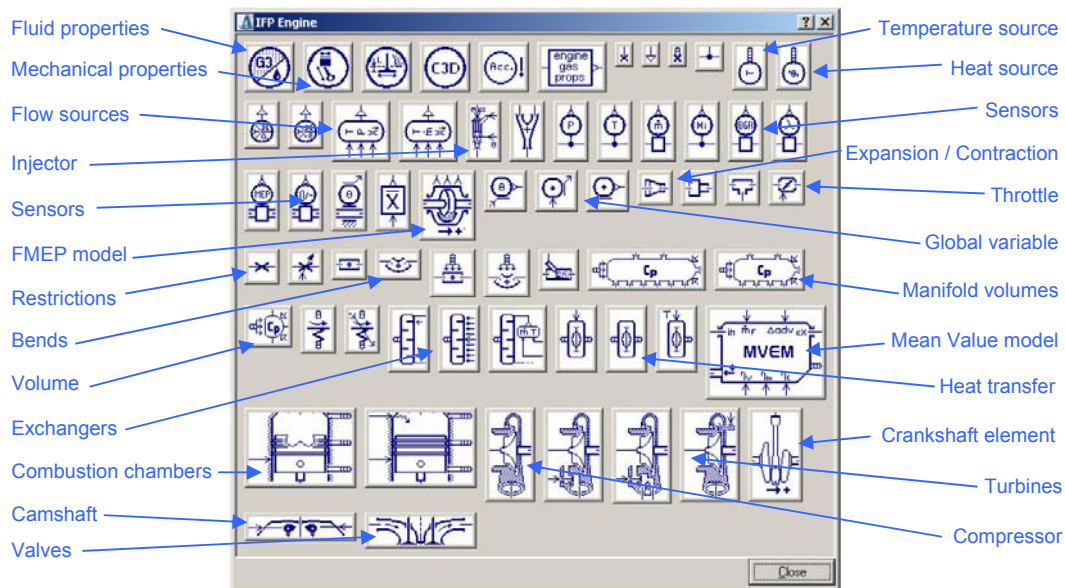
Figure C.179 – Engine Library by IFP [C.9] for AMESim. A large number of submodels covering most engine applications sorted in categories of functionality

The engine library main window is shown and Figure C.179 ; from the environment definition [top-left] to the mechanical interface with the standard library [bottom-right] nearly all aspects of an engine model are covered. This library has been widely used throughout the modelling task which is the subject of this chapter. The most important submodel categories will consequently be introduced below.

C.2.1 Air Path Models

The fundamental approach proposed by most simulation packages to engine air path models is to replace each part or section of the real system by either a volume or a pipe. They form the skeleton of the intake and exhaust model onto with more advanced sub-model can be added, e.g. valves, heat exchanges, turbines, junctions. The following assumptions are taken:

- The flow is always one dimensional [see Section C.1] and the mixture is always homogeneous

- The perfect or semi-perfect gas equation applies

- Intensive variables such as pressure or temperature are average values of the modelled volume, i.e. they are homogeneous enough to validate the lumped modelling approach [see Section C.1.2]

- The kinetic energy of the gases is neglected in chambers

- Only reversible thermodynamic transformations occur in orifice sub-models

- The gas velocity is never supersonic

- The gravity effects can be neglected

For pipes, transient phenomena of compressibility, dissipation and inertia can be taken into account in pipe sub-models. Heat transfers from convection and conductivity can be accounted for in all. Table C.25 shows a list of available pipe sub-models.

Icon	Submodel	Causality	Description
	ENGP00	C	pipe with compressibility effects
	ENGP01	C-R	pipe with compressibility effects & regular pressure drop
	ENGP02	R-C	idem ENGP01 (reversed causality)
	ENGP03	C-R-C	pipe with compressibility effects & regular pressure drop
	ENGP04	R	pipe with only regular pressure drop
	ENGPI01	C-IR	pipe with compressibility effects, inertia & regular pressure drop
	ENGPI02	IR-C	idem ENGPI01 (reversed causality)
	ENGPI03	C-IR-C	pipe with compressibility effects, inertia & regular pressure drop
	ENGPI04	IR	pipe with inertia & regular pressure drop
	ENGPB01	C-R	bended pipe with compressibility effects, regular and singular pressure drops (C-R)
	ENGPB02	R-C	idem ENGPB01 (reversed causality R-C)
	ENGPH01	C-R	pipe with compressibility effects, regular pressure drop and thermal exchanges
	ENGPH02	R-C	idem ENGPH01 (reversed causality)
	ENGPH03	C-R-C	pipe with compressibility effects, regular pressure drop and thermal exchanges
	ENGPBH01	C-R	pipe with compressibility effects, regular and singular pressure drop and thermal exchanges
	ENGPBH02	R-C	idem ENGPBH01 (reversed causality)
	ENGPBH03	C-R-C	pipe with compressibility effects, regular and singular pressure drop and thermal exchanges

Table C.25 – Available pipe submodels. C, R and I stand for compressibility, frictional resistance or dissipation, and inertia effects respectively [C.9]

Three principles apply to the pipe models:

- Mass conservation

$$\frac{\partial \rho}{\partial t} + \frac{\partial \rho u}{\partial x} = q_s$$

Equation C.25 – where ρ is the gas density, u is the gas velocity and q_s is the flow source term [C.9]

- Momentum conservation

$$\frac{\partial \rho u}{\partial t} + \frac{\partial \rho u^2}{\partial x} + \frac{\partial P}{\partial x} = \frac{\partial \tau}{\partial x}$$

Equation C.26 – where P is the gas pressure and $\frac{\partial \tau}{\partial x} = -ff \cdot \frac{u|u|}{2d}$ where ff is the friction factor and d is the pipe diameter [C.9]

- Energy conservation

$$\frac{\partial \rho e}{\partial t} = -P \cdot \frac{\partial u}{\partial x} + R + \Phi + \lambda \cdot \frac{\partial^2 T}{\partial x^2} - h_T \cdot \left(T - T_{out}\right)$$

Equation C.27 – where e is the internal energy, R is the chemical, radiation and phase change over, Φ is the power of the local viscosity forces, λ is the thermal conductivity and h_T is the thermal exchange coefficient [C.9]

Volumes, or chambers, are sub-models were the kinetic energy of the gases it contains is neglected, also known as purely capacitive elements. They are mostly used for causality purposes, i.e. compute pressure and temperatures where a number of pipes are connected. Table C.26 shows a list of available chamber sub-models.

	ENGCH03: volume with 3 flow ports and a thermal port
	ENGCH07: volume with 7 flow ports and a thermal port
	ENGCH09: volume with 9 flow ports and a thermal port
	ENGCHWET01: volume with 2 flow ports and 1 injection port

Table C.26 – Available chamber sub-models [C.9]. Various combinations of ports are possible. The injection chamber is a particular case accounting for vaporisation of the liquid fuel [Section C.2.2]

Three types of gases can be present in the mixture:

- Fresh air   *gas 1*
- Vaporised fuel   *gas 2*
- Burnt fuel   *gas 3*

Pressure and temperature are state variables, hence computed from their derivatives. From the perfect gases relation, the state equation is:

$$P = \rho r T = \left(\sum_i \rho_i r_i\right) \cdot T$$

Equation C.28 – where i is the gas index [C.9]

So the pressure derivative is expressed as:

$$\frac{dP}{dt} = \dot{\rho} r T + \rho \dot{r} T + \rho r \frac{dT}{dt}$$

Equation C.29 – derived from Equation C.28

- Densities are computed from the mass conservation principle:

$$\rho = \frac{\sum_i m_i}{V}$$

Equation C.30 – where m_i is the mass of gas i and V is the total volume in the chamber

$$\dot{\rho} = \sum_i \frac{\dot{m}_i}{V}$$

Equation C.31 – derived from Equation C.30

- The perfect gas constant is calculated from:

$$r = \sum_i x_i r_i \qquad \text{with } x_i = \frac{m_i}{\sum_j m_j}$$

Equation C.32 – where r_i is the gas constant of gas i

$$\dot{r} = \sum_i \dot{x}_i r_i \qquad \text{with } \frac{dx_i}{dt} = \frac{\dot{\rho}_i}{\rho} - \rho_i \frac{\dot{\rho}}{\rho^2}$$

Equation C.33 – derived from Equation C.32

- And the temperature time derivative is calculated from the first principle of thermodynamics:

$$\frac{dT}{dt} = \frac{1}{mC_v}\left[\sum_i \frac{dm_i}{dt}\cdot h_i - \frac{dm}{dt}\int C_v dT + dq - P\frac{dV}{dt} - m\left(\sum_i h_i \frac{dx_i}{dt} - T\frac{dr}{dt}\right)\right]$$

Equation C.34 – where C_v is the specific heat of the mixture, h_i is the enthalpy of gas i, $dq = dq_{comb} + dq_{wall}$ is the energy exchange with the outside, i.e. from combustion or through the walls

Orifices are sub-models where the upstream kinetic energy of the gases is neglected. The flow across the orifice is a function of the input pressure and temperature. The different variants of orifice sub-models are shown in Table C.27.

	ENGPEC01: progressive expansion-contraction
	ENGEC01: sudden expansion-contraction
	ENGTJ01: T-junction
	ENGTHROT01 & 02: throttle valve
	ENGOR01: constant orifice
	ENGVOR01 & 02: modulated orifice

Table C.27 – Available orifice sub-models. Fixed or adjustable, they can represent a number of real-life configurations for pressure drops [C.9]

The mass flow rate *dm* across the orifice is characterised by Equation C.35

$$dm = A \cdot C_q \cdot C_m \cdot \frac{P_u}{\sqrt{T_u}}$$

Equation C.35 – where A is the orifice area, C_q is the flow coefficient specific to the geometry, C_m is the flow parameter (Equation C.36), P_u and T_u are the upstream state variables [C.9]

$$C_m = \begin{cases} \sqrt{\dfrac{2 \cdot \gamma}{r(\gamma - 1)}} \sqrt{\left(\dfrac{P_d}{P_u}\right)^{\frac{2}{\gamma}} - \left(\dfrac{P_d}{P_u}\right)^{\frac{\gamma+1}{\gamma}}} \quad if \left(\dfrac{P_d}{P_u}\right) > P_{cr} \\[2em] \sqrt{\dfrac{\gamma}{r}\left(\dfrac{2}{\gamma + 1}\right)^{\frac{\gamma+1}{\gamma-1}}} \qquad\qquad if \left(\dfrac{P_d}{P_u}\right) \leq P_{cr} \end{cases}$$

Equation C.36 – where P_{cr} is the critical pressure ratio as defined in Equation C.37, [C.9]

$$P_{cr} = \left(\frac{2}{\gamma + 1}\right)^{\frac{\gamma}{\gamma-1}}$$

Equation C.37 – P_{cr} is the critical pressure ratio across the orifice below which the flow is choked at sonic speed [C.9]

C.2.2 Fuelling System

The previous paragraph presented the sub-models available for gas flow. One interfacing chamber between the fuel system models and the pneumatic network was introduced in Table C.26. Together with the three gases, the properties for liquid fuel have to be defined as shown in Figure C.180.
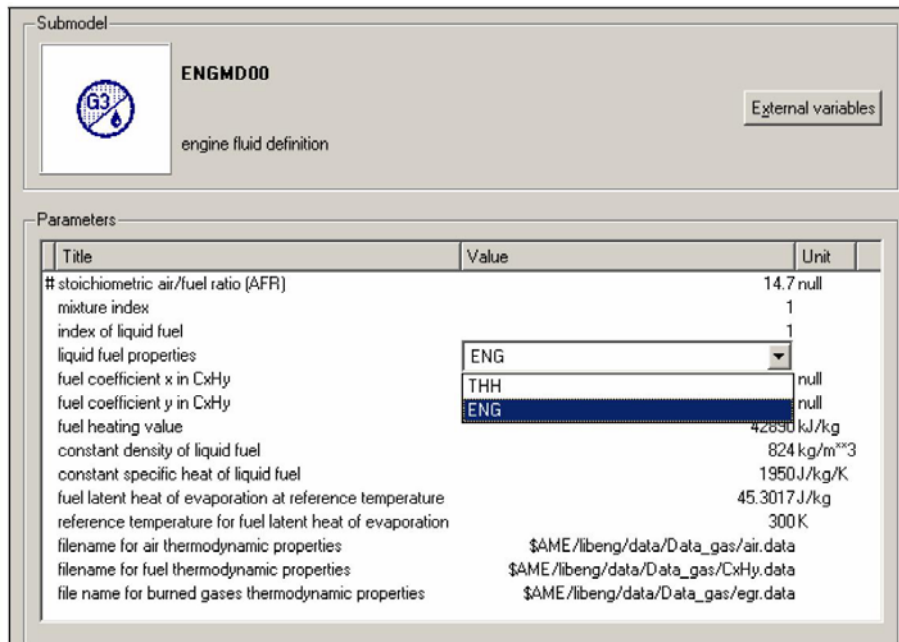
Figure C.180 – Engine fluid definition submodel. This submodel has no connection ports. Its purpose is to define a set of fluid properties for the complete engine model environment
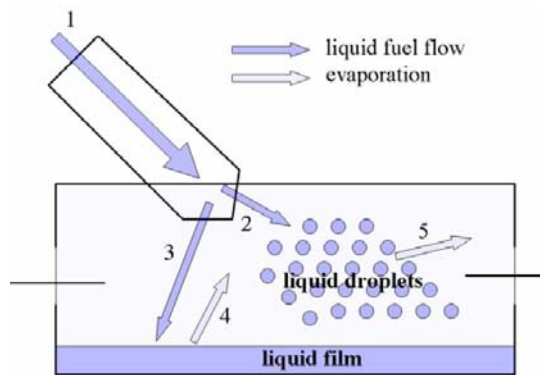
ENGINJ00
The injection rate is defined by:
- A mass flow rate defined in a table (2D) or by an expression, as a function of time and the injection pressure.
- A mass flow rate for closure represented by a line. The slope is defined as a function of the injection pressure and the pulse width is defined as a function of the injection time.

ENGINJ01
The injection rate is defined by an expression or a 2D table, as a function of the time and the injection duration (Tinj).

ENGINJ02
The injection rate is defined in a 3D table, as a function of the time, injection pressure and injection duration (Tinj).

ENGINJ03
The injection rate is assumed to be a trapeze. The injection duration (Tinj) and the Static Flow Rate (SFR) are provided at port 4. The shape of the injection rate is defined in the injector model itself. The user has to set the duration for needle lift and closure.

Table C.28 – Available injector sub-models. The injection rate can be defined by a data file or assumed trapezoidal. Phasing is handled via ports 2 and 3

Figure C.181 – Vaporisation chamber [C.9] for indirect injection, accounting for wall-wetting effect

The main component of the injection system model is the injector introduced in Table C.28. The Engine library is also compatible with the Thermal Hydraulic library, hence offering the possibility to create custom made injector system models for advanced investigation of the injection / combustion interaction. This option was not retained and the Engine library injector was opted for in both direct and indirect injection configuration.

The injector sub-models can be set to inject fuel in the liquid form or already gaseous depending on the most appropriate assumption. For indirect injection configurations if the liquid fuel injection is valid, i.e. most gasoline port injected engine then the injection chamber introduced in Table C.26 can also account for vaporisation effect of the fuel and wall wetting delays. This process is illustrated in Figure C.181.

The fuel evaporation effect is described by a τ-X approach, where τ is the characteristic time constant for fuel evaporation and X is the mass fraction of liquid fuel that is deposited onto the walls during the injector opening.

$$\frac{dm_{vap}}{dt} = \frac{dm_{vap-volume}}{dt} + \frac{dm_{vap-film}}{dt}$$

Equation C.38 – Evolution of the vapour mass of fuel in the injection chamber

$$\frac{dm_{vap-volume}}{dt} = \frac{m_{liq-volume}}{\tau_1} \quad and \quad \frac{dm_{vap-film}}{dt} = \frac{m_{liq-film}}{\tau_2}$$

**Equation C.39** – where $\tau_1 = f(T_{volume})$ and $\tau_2 = g(T_{volume})$

Thus:

$$\frac{dm_{liq-volume}}{dt} = (1-X)\frac{dm_{inj}}{dt} - \frac{dm_{vap-volume}}{dt}$$

Equation C.40 – Evolution of the liquid droplets of fuel in the injection chamber

$$\frac{dm_{liq-film}}{dt} = X\frac{dm_{inj}}{dt} - \frac{dm_{vap-wall}}{dt}$$

Equation C.41 – Evolution of the liquid fuel film on the wall of the injection chamber

A similar modelling technique is employed when the injection chamber is also the combustion chamber, e.g. direct injection. Combustion chamber models will be introduced in Section C.2.3. Advanced fuel injection strategies such as multiple injections can be implemented rather easily by using more than one injector model to replicate the behaviour of one device as demonstrated in Figure C.182. The illustration shows a model for one single real-life injector complete with the control signals listed in Table C.29.
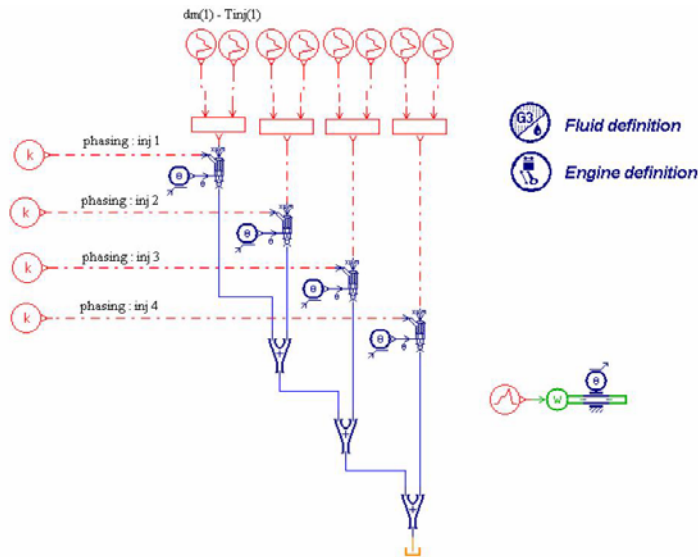
Figure C.182 – Example of a multiple injection system [C.9] using four injectors to model each injection. A dummy crank angle signal created on the right is sent out to the injectors

Control Signal	Comments
Phase angle for Start of Injection [SOI]	After local TDC +360° crank angle
Crankshaft angle	Relative to cylinder 1
Nominal mass flow rate	With wide-open needle
Injection duration	In seconds

Table C.29 – Control Signal for injector model as illustrated in Figure C.182

On the right hand side of Figure C.182, two submodels without ports define the fluid properties [see Figure C.180] and the engine layout required by the submodels presented in the following section.

C.2.3 Engine Block

At the core of the engine block models is the combustion chamber submodel which is an advanced version of the simple chambers described in Section C.2.1. It is an interface element the mechanical submodels of the crankcase, the intake air path, the exhaust system and the fuelling system in the case of direct injection as shown in Figure C.183.
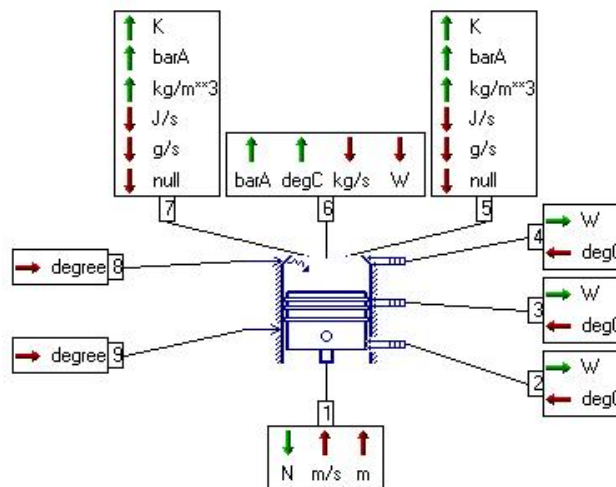
Figure C.183 – Spark ignition engine combustion chamber [C.9]. A total of 9 ports provide interfaces with other physical domains such as thermal exchanges – ports ②, ③ & ④, mechanical – port ①, thermo-fluids – ports ⑤ & ⑦, fuelling – port ⑥, and control signals – ports ⑧ & ⑨

Two main categories of combustion chambers are available to model Otto and Diesel cycles. The submodels for Diesel cycles have the same connection layout as Figure C.183, only with a slightly different icon. A number of different submodels – or set of equations, are indeed available for each type of combustion cycle. They feature

various levels of refinements and computational requirements in order to adapt to the modelling requirements.

The Wiebe law [C.14] is widely used generic model [C.15][C.16]for spark ignition engine combustion based on a reference combustion heat release equation. The instantaneous combustion heat release Q_v is given by Equation C.42:

$$\frac{dQ_v}{d\theta} = Q_{vtot} \frac{A_1}{d_{comb}} \left(1 + f_1\right) \left(\frac{\theta}{d_{comb}}\right)^{f_1} e^{-A_1 \left(\frac{\theta}{d_{comb}}\right)^{(1+f_1)}}$$

Equation C.42 – where d_{comb} is the combustion duration in degree, θ is the crank angle with reference 360º ATDC, Q_{vtot} is the total combustion heat release in Joules, A_1 and f_1 are the Wiebe parameters

Because constant coefficients A_1 and f_1 limit the ability for Wiebe's law to reproduce transients, a number of refinements are available in the engine library. A delay can be implemented between the spark ignition command and the actual start of combustion. It is also possible to define 3D look-up tables defining the coefficients depending on three engine variables among volumetric efficiency, air-fuel ratio, residual gas mass fraction [EGR rate], spark advance and engine speed.

An alternative to the Wiebe model for SI engine is the 1D CFM model by IFP [C.6][C.9] which is a more predictive code. It is based on a two zone approach with a flame propagating from the burned gases zone towards the unburned zone. It actually models the premixed flame combustion that is the main oxidation mechanism in the Otto cycle. The following assumptions are taken [C.6]:

- Homogeneity of the mixture
- Stoichiometric combustion
- Cylindrical combustion chamber
- Pressure is homogeneous within the cylinder

The laminar flame speed is determined from Metghalchi and Keck [C.17] with correlation for gasoline fuel. The progress variable $\tilde{c}$ verifies Equation C.43:

$$\tilde{c} = \frac{m_b}{m} = 1 - \frac{m_u}{m}$$

Equation C.43 – where m_b and m_u are respectively the mass of burned and unburned gases ; the flame layer is assumed infinitely thin [C.6]

The evolution of the kinetic energy starting from intake valve closure [IVC] is the tumble kinetic energy:

$$\frac{dE_k}{dt} = \frac{dE_{k,tumble}}{dt} = \frac{1}{8} \cdot m_{tot} \cdot \omega^2 \cdot \left[n_{tumble} \cdot h^2 \cdot \frac{dn_{tumble}}{dt} + n_{tumble}^2 \cdot h \cdot \frac{dh}{dt} \right]$$

Equation C.44 – where h is the distance between the piston and the cylinder head, $mtot$ is the mass of gas in the cylinder, ω is the engine speed and ntumble is the tumble number which is linearly decreased from IVC to BDC

Then the dissipated kinetic energy is computed from Equation C.45:

$$\frac{dE_{k,diss}}{dt} = \frac{dE_k}{dt} - C_{diss} \cdot E_{k,diss}$$

Equation C.45 – where C_{diss} is the parameter for the destruction of the dissipated kinetic energy [C.9]

The turbulent kinetic energy k is computed from the dissipated kinetic energy:

$$k = C_{turb} \cdot \frac{E_{k,diss}}{m}$$

Equation C.46 – where C_{turb} is the turbulent kinetic energy coefficient [C.9]

Compression ignition engines can be modelled using a adaptation of Wiebe's law, the twin-Wiebe model. Equation C.42 becomes:

$$\frac{dQ_v}{d\theta} = Q_{vtot}\left[Q_{ratio}\frac{A_1}{d_{comb}}\left(1+f_1\right)\left(\frac{\theta}{d_{comb}}\right)^{f_1} e^{-A_1\left(\frac{\theta}{d_{comb}}\right)^{(1+f_1)}} + \left(1-Q_{ratio}\right)\frac{A_2}{d_{comb}}\left(1+f_2\right)\left(\frac{\theta}{d_{comb}}\right)^{f_2} e^{-A_2\left(\frac{\theta}{d_{comb}}\right)^{(1+f_2)}} \right]$$

Equation C.47 – where Q_{ratio} is the parameter that determines the relative importance of premixed and mixing controlled combustion phases [C.9]. A_1, f_1, A_2 and f_2 are the Wiebe parameters

Equation C.47, two Wiebe heat release equations are used respectively for the premixed phase and the mixing controlled combustion phase. Their relative importance is set by the model parameter Q_{ratio} and the submodel does not offer the possibility to use variable Wiebe ratios similar to the SI models. Another limitation to this model is that the fuel injection has to be completed before the start of combustion which is problematic for direct injection application where the injection rate will have a direct effect on the rate of heat release [ROHR].

The Chmela based model [C.18] is more computationally demanding than twin-Wiebe for CI engines but it integrates the injection rate in a similar way to the 1D CFM integrates the tumble kinetic energy. The total kinetic energy is assumed to be provided mainly by the fuel spray:

$$\frac{dE_k}{dt} = \frac{dE_{k,spray}}{dt} = \frac{1}{2} \cdot \left(\frac{1}{n_{nozzle} \cdot \rho_f \cdot S_{nozzle}}\right)^2 \cdot \left(\frac{dm_{inj}}{dt}\right)^3$$

Equation C.48 – where n_{nozzle} is the number of nozzle holes in the injector, S_{nozzle} is the surface of each nozzle hole, ρ_{nozzle} is the fuel density and m_{inj} is the mass of fuel injected

Then the dissipated kinetic energy is computed from Equation C.45. Because the chamber can contain both liquid fuel and gases, Equation C.46 for the turbulent kinetic energy k is slightly modified:

$$k = \frac{E_{k,diss}}{m_{gas}}$$

Equation C.49 – where m_{gas} is the mass of gas only in the cylinder

And the combustion heat release is computed from:

$$\frac{dQ_{comb}}{dt} = C_{mode} \cdot \left(1 - X_{BGR}\right)^{\alpha_R} \cdot m_f \cdot e^{C_{rate}\frac{\sqrt{k}}{\sqrt[3]{V_{cyl}}}}$$

Equation C.50 – where C_{mode} and C_{rate} are parameters defining the evolution of the turbulent variables, α_R defines the effect of the residual burnt gases X_{BGR} on combustion, m_f is the mass of fuel in the chamber

C.3 Controller Implementation

The controller in the simulation environment is in fact a partial or complete model of the electronic module which actually controls the plant in real-life [see Section 3.2]. In a similar way to the plant model, the controller functionalities can be simplified in order to match the level of realism of the plant. This task could be achieved for instance within AMESim to a certain extend, but the Simulink package [C.19] offers a wide range of modelling functionalities which set the standards within the automotive industry for controller development [C.20][C.21].

C.3.1 Controller Modelling with Simulink

Simulink as introduced in Section 3.3 is the graphic user interface which allows time based simulations to be developed using elementary blocks that relate to Matlab functions. Figure C.184 illustrate this approach with an example of a simple controller for CVT transients proposed by Rohrbacher [C.22]. The single output in this case is computed from a combination of simple mathematical operations on the four inputs.
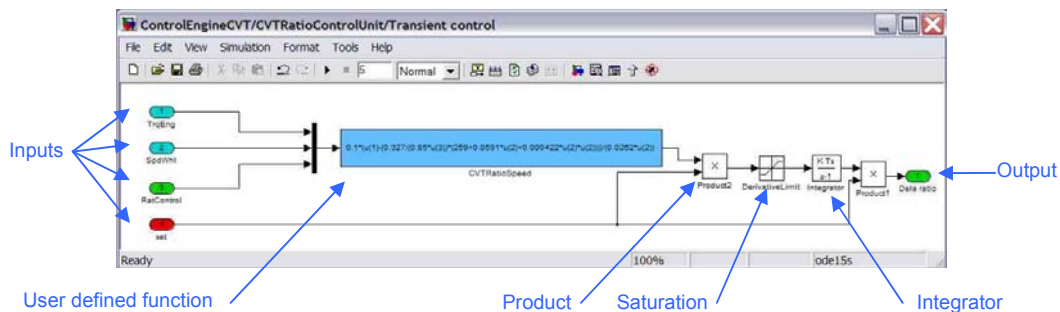
Figure C.184 – Simulink Controller example for CVT transients, made of simple elementary blocks from the Simulink library, including integrator, saturation, product or user defined function [C.22]

Simulink also offers a layer functionality allowing the user to group a set of sub-blocks into one higher level block. This helps conveniently organise a large scale controller by displaying each layer and sub-layer independently. The plant model outputs [e.g. sensors] are then connected to the controller input and vice-versa to form the complete simulation environment.
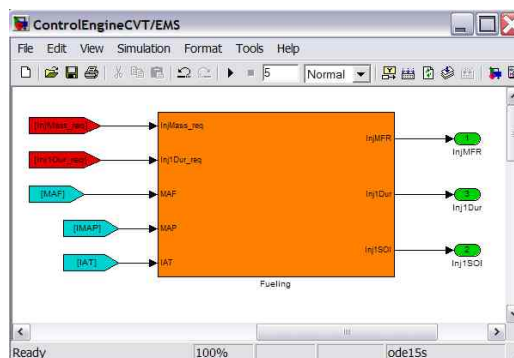

Figure C.185 – Fuelling control block for a diesel engine as part of the complete controller

C.3.2 Co-Simulation Interface

Once both plant and controller models are set up, the solver runs the simulation to compute their behaviour in time as explained in Sections 3.2 and 3.3. In the present case the plant model is written with AMESim and the controller is in Simulink, but only one solver can be used for the simulation. The straight forward approach is to use the Simulink interface in AMESim introduced previously. The AMESim model will therefore be compiled into an S-function [C.19][C.23] and integrated into the Simulink environment. This is effectively an import into Simulink of the AMESim equations describing the plant. The AMESim part of the system receives input variables and state variables to compute state derivatives and output variable. This way, the simulated system is integrated. However, the Simulink solver does not have the same variable step capability as AMESim [Section C.1.3] hence a lot advantages in time, reliability and accuracy are lost in the process.

The alternative to this standard interface is the co-simulation interface in AMESim [C.23]. In this case, only the input and outputs of each side are exchanged; .two solvers are used in this configuration where each software package deals with its own equation. The coupling induced by the state variable exchange is lost, but the advantages of the solvers for their own application are fully used. Figure C.186 summarizes the concept layout for each alternative.
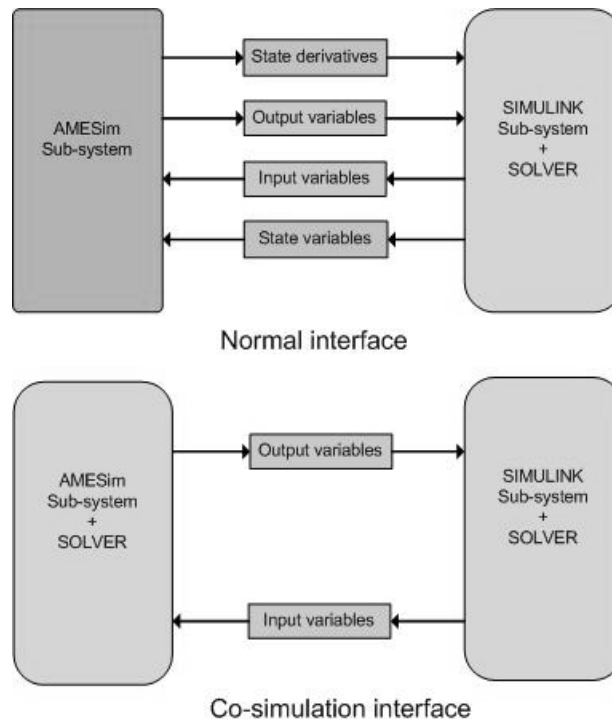
Figure C.186 – Two simulation interfaces for AMESim and Simulink. The co-simulation interface does not exchange states and solves its own subsystems independently

On the one hand, the co-simulation layout [Figure C.186] is particularly recommended for plant / controller splits where only inputs and outputs would be exchanged in real life. The optimized algorithms of AMESim also make simulation times much quicker. A communication time interval is set between AMESim and Simulink at the controller loop time. On the other hand if Simulink includes some of the plant model, the solving can become more problematic and communication intervals will have to e significantly reduced, loosing the quickness advantage of co-simulation whilst compromising the end result accuracy. In the various models introduced in this Thesis, both standard and co-simulation interface were employed depending on the application.

C.4 References

[C.1] **Imagine SA**, AMESim 4.3 User Manual

[C.2] **He, Y., [2005],** *Development and Validation of A 1D Model of Turbocharged V6 Diesel Engine under Steady-State and Transient Conditions,* General Motors Research and Development, SAE 2005-01-3857

[C.3] **Mattarelli, E., Valentini, A., [1998],** *Simulation of a high Performance Turbocharged SI Engine,* University of Modena, SAE 983048

[C.4] **Li, J. Z., Treusch, C.,Honel, B., Neyrat, S. [2005],** *Simulation of Pressure Pulsations in a Gasoline Engine Injection System and Development of an Effective Damping Technology*, Visteon Corp. & Imagine SA, SAE 2005-01-1149

[C.5] **Chiatti, G., Chiavola, O. [2003],** *Modelling High Pressure Injection System and its Effect on Engine Performance*, University Roma Tre, JSAE 20030089

[C.6] **Lafossas, F.-A., Colin, O., Le Berr, F., Menegazzi, P., [2005],** *Application of a New 1D Combustion Model to Gasoline Transient Engine Operation*, Institut Français du Pétrole, SAE 2005-01-2107

[C.7] **Garcia Martinez, O., Kargar, K., [2000],** *Simulation Tool for Transmission and Driveline Systems Design,* Renault, SAE 2000-01-0832

[C.8] **Zhang, Y., Chen, X., Zhang, X., Jiang, H., Tobler, W., [2005],** *Dynamic Modelling and Simulation of a Dual-Clutch Automated Lay-Shaft Transmission,* University of Michigan-Dearborn & Ford Motor Company, Transactions of ASME, Vol. 127, March 2005

[C.9] Imagine SA, Institut Français du Pétrole. *IFP Engine Library Documentation*

[C.10] **www.claytex.com/dymola**

[C.11] **Imagine SA.** Hydraulic Component Design Library Documentation

[C.12] **Imagine SA**, AMESet User manual

[C.13] **National Instruments Corp.** *LabView Analysis Concepts*, User Reference Manual

[C.14] **Wiebe, I. I., [1970],** *Brennhauf und Kreisprozeb von Verbrennungsmotoren,* VEB-Verlag Technik, 1970, Berlin

[C.15] **Lindström, F., Ånsgtröm, H.-E., Kalghatgi, G., Elmqvist Möller, C., [2005],** *An Empiral SI Combustion Model Using Laminar Burning Velocity Correlations,* Sweden Royal Institute of Technology, Shell Global Solutions, GM Powertrain Europe, SAE 2005-01-2106

[C.16] **Hajireza, S., Sundén, B., Mauss, F., [2001],** *Effects of Inhomogeneities in the End Gas Temperature Field on the Auto-ignition in SI Engine,* Lund Institute of Technology, Sweden, SAE 2000-01-0954

[C.17] Metghalchi, M., Keck,. J. C., [1982], *Burning Velocities of Mixtures of Air with Methanol, Iso-octane, Andindolene at High Pressure and Temperature,* Combustion and Flame, Vol. 48, pp 191-210,1982

[C.18] Chmela, F. G., Orthaber, G. C., [1999], *Rate of Heat Release Prediction for Direct Injection Diesel Engines Based on Purely Mixing Controlled Combustion*, AVL List Gmbh, SAE 1999-01-0186

[C.19] www.mathworks.com

[C.20] Dagci, O. H., Brown, A. W., [2006], *Custom Real-Time Interface Blockset Development in Matlab/Simulink for On-Target Rapid Prototyping*, General Motors Corp., SAE 2006-01-0169

[C.21] Cao, C., Shull, D., Himes, E., [2001], *A Model-Based Environment for Production Engine Management System Development,* Delphi Automotive Systems, SAE 2001-01-0554

[C.22] Rohrbacher, Y., [2005], *Effect of Air Injection on Turbo Diesel Transient torque Response, MSc Thesis*, Cranfield University, 2005

[C.23] Imagine SA, AMESim MATLAB / Simulink Interface 4.2 User manual

Executive Producer	**NICHOLAS VAUGHAN**
Special Thanks to	**CLAIRE-MARIE & PATRICK BONNET**
Very Special Effects	**STEPHANIE AUMANN, A.K.A STEFFI**
Steady-Cam	**JEROME CRETET & NICO SERGENT**
Original Sound Track	**SUE BENNETT**
Second Unit Director	**ENRICO CACCIATORI**
Lights	**BAEKHYUN 'HARRY' CHO**
First Assistant	**YANNICK 'ZAXTREM' ROHRBACHER**
Pre-Production Management	**LYNDA MANN**
Production Assistant	**BINNIE HUNT**
Post Production	**CATRIONA ROLFE**
Associate Producer	**DOUG GREENHALGH**
Editing	**MARIN GUENOV**
Studio Scenes	**YOLANDA BONA**
	FRANCINE WATTS
Art Director	**JUSTIN TEW CSA**
Location Scout	**JOSEPHINE 'BIG M' TEW, A.K.A DR. JO**
Costumes	**ANN HECK**
Best Boy	**YANNICK 'CAPTAIN' KERRIOU**
Press Relations	**HAYLEY THOMPSON**
Overseas Crew	**ALEXANDRA & ROMAIN LEBLANC**
As Herself	**DAISY**
Remote Crew #1	**MATTHEW BURKE**
Remote Crew #2	**DAVID PRICE**
Remote Crew #3	**PHIL JORDAN**
Remote Crew #4	**MATT FIELD**
Car Stunts	**PASCO DE PALMA**
Mechanics	**MARK MACDONALD, HOWARD 'H' BERRY**
All Vehicles Courtesy of	**TOROTRAK PLC**
Electricians	**NEWAGE AVK SEG**
Computer Animations	**IMAGINE SA**
Copyrights	**CRANFIELD UNIVERSITY**